



# *Analysis of the magneto-thermo-dynamic behaviour of magnetorheological elastomers*

*A Thesis submitted  
in partial fulfillment of the requirements  
for the degree of*

Doctor  
by Mondragon Unibertsitatea

IKER AGIRRE OLABIDE

Supervised by:  
Dra. María Jesús Elejabarrieta Olabarri

Mondragon Unibertsitatea  
Mechanical and Manufacturing Department

OCTOBER 2017



*Ama, Aita eta Idoiari*



*I will not die an unlived life. I will not  
live in fear of falling or catching fire. I  
choose to inhabit my days, to allow my  
living to open me, to make me less  
afraid, more accessible, to loosen my  
heart until it becomes a wing, a torch,  
a promise. I choose to risk my  
significance; to live so that which came  
to me as a seed goes to the next as a  
blossom and that which came to me as  
a blossom, goes on as fruit.*

Dawna Markova



# Acknowledgements

*Good company in a journey makes the  
way seem shorter*

Izaak Walton

Tesia amaitzear nagoela jabetzen naizen une honetan, atzera begiratu eta pertsona eta erakunde askori eskerrak eman behar ditudalaz ohartzen naiz, horiek denak gabe gaur egun naizenera iristea ezinezkoa izango liratekeelako.

En primer lugar quiero agradecer a mi directora de tesis, Dra. María Jesús Elejabarrieta, por el respaldo y la dedicación mostrada durante todos estos años. Muchas gracias por enseñarme a trabajar con elegancia, y por todas las discusiones, paciencia y apoyo mostrado.

Mila esker Mondragon Unibertsitateari eta Mekanika eta Ekoizpen Industrialia departamentuari tesia bertan egiteko aukera eta baliabideak eskaintzeagatik. Agradecer al Dr. M.Mounir Bou-Ali por ofrecerme la oportunidad de introducirme en el mundo científico y de la investigación. Mila esker Joanes, MR-ko ezagutza guztiak transmititzeagatik eta euki ditudan zalantza denak argintzen laguntzeagatik. Fluidoan mekanika lerroko lankideak ere eskertu nahi ditut azkeneko sei urteetan edozein zalantza argitzeko prest egon direlako.

Tailerreko lakideei, behar izan ditudan pieza guztiak egiteagatik. Idoia Urrutibeascoari laborategiko neurketekin lagundu izanagatik. Gorka Aretxagari utillajeen diseinuan eskeintzako laguntza eta gomendioengatik. Joxemiri euskerazko zalantzak argitzeagatik.

Mondragon Goi Eskola Politeknikoko lankideei beraien laguntza eskaini didatelako, batez ere idazkaritzako, informatikako, liburutegiko eta erosketa saileko lankideei.

Eskerrak eman nahi dizkiot Eusko Jaurlaritzari, Hezkuntza Sailak eskainitako bekari esker tesia hau burutu delako.

I would like to thank Professor Alexander Lion for giving me the opportunity to do a very nice stay at Universität der Bundeswehr München. Thank you for all the support and for letting me being part of the group.

I can not forget the chance Professor Pavel Kuzhir gave me to make an unforgettable stay in the University Côte d'Azur. Thank you very much Pavel for giving

me this opportunity to work in your labs, and all the facilities, support and discussions. It was a pleasure to work with you.

Cikautxo S.Coop.-eri tesi honetan erabili den materiala ahalbidetzeagatik. Bere-ziki, Jose Santos eskertu nahi dut erabili ditugun matrizeen sintesian eskeinitako laguntza guztiagatik.

Azken 3-4 urteak gora-behera askoko urteak izan arren, urte mundialak izan direla esango nuke, bide luze honetan jende ikaragarria ezagutu dudalako eta momentu ahaztezinak bizi ditudalako. Imanol-Unai Unai-Imanol, zuekin pisuan pasatako 3 urteak ahaztezinak dira eta ezin dira hitzen bidez azaldu. Ezin ahaztu gela batetik bestera eginiko ohiuak, erosketak egiteko pasatako momentu ero danak, sukaldatzean egin ditugun mila parreak, RISAS, RISAS Y MAS RISAS. Benetan, mila esker nere bihotzaren barrenetik, zuen alaitasun eta erotasunak edonor laguntzen duelako eta edozein aholku emateko prest zaudetelako. Sois unos cracks!!

Urte hauetan zehar momentu politt asko pasa ditut, eta horien hartean oste-gunetan bizitako pintxopoteak etortzen zaizkit burura. Pintxopoteak juerga bat dirudien arren, haratago dijoan zeozer ere bada. Mila esker Ion, Javi, Gorka eta Joneri, zuek gabe sozaltasun une horiek ez lirakete berdinak izango. Iruditu ez arren zuekin zerbezatxo bat hartzeak eta konta katilu ibiltzea nahikoak dira. Taupa edo Iluntzeko banketetan lasai-lasai jarrita egindako solasaldiak ikaragarriak izan dira, baita Iluntz-Ekaitzeko... ;)

Lankideak baino gehiago lagunak zareten guztioi eskerrik asko! Mila esker Leire, azken finean arreba bat bezelakoa izan zea; zenbat denbora pasa deun MR-ko gauzataz hitzeiten, baino are gehiago beste milaka gaietan hizketan. Eskerrik asko Estela, pisuan zein Alemanian zein eskolan behar izan dudanean laguntza dana eskaini didazulako, bai lankide bai lagun bezela. Maider, zure erotasun puntu horrek edozien alaitzen duelako, baina gehien bat entzuteko eta aholkuak emateko prest zaudelako, eskerrik asko. Eskerrik asko Iruñe, pisuan "orden" pixkat jartzeaz gain nerekin izan dituzun detaile txiki baino politt danengarik. Mila esker Jon, Axi eta Aitor, modu batera edo bestera lagundu izanagatik eta bizi izan ditugun esperientzi, afari eta juerga guztiengatik (Sevilla tiene un color especial!). Erritmo eta buruhauste ezberdinak izan arren bizikletan batera ateratzeko prest egon den Bururi. Eskerrak eman nahi dizkiet Naia, Rita, Badiola, Julen, Endika, Aitor Uli, Arakama, Mikel eta Alexi tesiko gaiak alde batera utzi eta solasaldi bat edukitzeko edozein momentu ona izan delako.

Zenbat ordu pasako nituen fluidoseko laborategian ensaioak egin eta egin... baina luzeak izan arren bertan izandako erosotasuna eta berotasuna eskertu nahiko nuke, bereziki bertan bata besteari laguntzen izan direnei. Oso ondo pasa dugulako, esker mila Miren, Ane, Estela eta Ion.

Nola ez ahaztu modu batera edo bestera musika munduan ezagutu dudan jendeari. Bandako kideei eskerrak eman nahi dizkiet, ensaiatzea gogorra izan arren



kontzertu polittak izan ditugulako. Baina eskerrak, lokaleko atletik kanpora bizi izan ditugun momentuengatik dira. Azkeneko urtea gogor xamarra izan da, baina nola disfrutatu dugun txoznen antolakuntzekin! Eta Salzburgo-Vienara egin genuen bidaia? Ikaragarria eta ahaztezina!! Urte dispertsio handia izan arren kuadrila txiki bat bezela ibili giñelako! Eskerrik asko Andu, Asier (Patxi), Madri eta perkuko kideei. Txarangako kideak ere eskeru nahi ditut, fijo bat izan ez arren zuekin joan naizen denetan asko disfrutatu dudalako!

Bizikleten gainean ordu asko egin ditugu batera, baina maldan gora estutu arren parre artean egiten genituen irteera denak. Mila esker, Ander, Jon, Mikel, Joseba, Julen eta Andoniri. Zenbatetan pasako zitzaigun, hitzeiten hasi eta kon-turatzeko zerbezea eskun. Ez dakizue zenbateaino baloratzen ditudan hizketaldi, konfesio eta parre hoiek.

Esker bereziak eman nahi dizkiet erosketako lista ematen duen betidaniko eta kuadrilako lagun guztie: Mila esker Maik, Axi, Burgui, Eneko, Gordoia, Mendo, Oier, Albi (Maestro birrero), Peru, Guerra, Pedro, Simon, Andoni, Cantero, Txo-txe, Matxin, Xabat eta Anartz. Tesiaren inguruan mila galdera egin dizkidazue, baina gehien egindakoa tesia amaierarena izan da eta une hori lerro hauek amaitzean iritsiko da. Zenbat parre, poteo, afari, juerga, bazkari, bidai... egin ditugun. Ez dakit nola eskertu daitekeen horrelako kuadrila. Ahazteinak dira atzerrira egin-dako bidaiak eta bertan bizitako esperientzia kontagaitz eta kontaezinak.

Azken urteotan Arrasaten, Munichen, Nizan eta munduko edozein txokotan ezagutu dudan jendea ere eskertu nahi dut, modu matera edo bestera euren denbo-ra nerekin konpartitzea erabaki dutelako; mundu honetan esku zabaltasun, alaita-sun eta gogoekin edozein lekutara irits gaitezkeelako, kultura berriak eta jende har-rigarria ezagutu daitekeelako. Eskerrak eman nahi dizkiet Nizako lagun eta pixuki-deei, baina gehien bat Bomber bikoteari.

Lerro hauek ezin ditut amaitu benetan jasan nauten eta tesia dedikatua da-goen hirukoteari. Mila esker AMA, AITA eta IDOIA. Badakit askotan zuek jasan nauzutela egun txar eta txepeletan, eta zuek esker onez niri hitzak atera nahiean ibili zaretela barruan nuena deskargatu nezan. Baina askotan behar nuen gauza bakarra zuen berotasuna izan da. Beti apoilatu nauzute nere erabaki guztietan, zuen gustokoak izan ez arren. Ai Idoia, lerro hauek idaztean malkoz betetzen zaiz-kit begiak. Kanpoan izan zaren bi urteetan faltan bota zaitut, zugabe etxean oso lasai egon arren, zure aholkuak, konta-katilu ibiltzeak edo mandoaz "diskutitzeak" balio asko duelako. Zer esanik ez USA trip bidaia zoragarriaz! Azken lerro haue-tan, Aiton-Amonak, Osaba-Izebak eta Lehengusu-Lehengusinak ere eskertu nahi ditut.

PURA VIDA



# Laburpena

Azken hamarkadetan, bibrazioen aurkako aplikazioen helburu nagusia osagaien bizitza erabilgarria, erosotasuna eta segurtasuna areagotzea izan da. Hala ere, gaur egungo aplikazioek lan-baldintza aldakorretara moldatzeko malgutasuna behar dute. Hori dela eta, material adimenduak gero eta gehiago erabiltzen ari dira industriako sektore ezberdinetan. Material talde honen barruan elastomero magnetoerreologikoak daude, eremu magnetiko baten eraginpean beraien propietateak aldatzen dituztelako.

Tesi doktoral honen helburu nagusia elastomero magnetoerreologikoen propietate magnetotermiko biskoelastikoak aztertzea da, aplikazio industrialetan elastomero magnetoerreologikoen erabilpena areagotu ahal izateko.

Hiru matrize ezberdin eta zortzi partikula-kontzentrazio bolumetrikoko erabili dira elastomero magnetoerreologiko isotropo eta anisotropoak sintetizatzean. Galerafaktorea eta metatze-modulua aztertzen dituen irizpide berria proposatu da sintetizaturiko laginen tarte biskoelastiko lineala definitzeko. Gainera, tarte honen sintesi-eta karakterizazio-aldagaiekiko menpekotasuna aztertu da. Tarte biskoelastiko lineala definitu ostean, sintesi- eta karakterizazio-aldagaien eragina propietate magneto-biskoelastiko linealetan aztertu dira. Horrela, material hauen atenuazio maximoaren aldakuntza definitu da.

Bestalde, konpresio-entsegu magnetodinamiko berria diseinatu eta fabrikatu da, elastomero magnetoerreologikoak frekuentzia altuetan neurtu ahal izateko. Konpresio-entseguaren propietateak neurtzeko prozedura definitu eta gero, elastomero magnetoerreologiko isotropoen konpresio-tarte biskoelastiko lineala aztertu da. Horrela, partikula-kontzentrazioaren, frekuentziaren eta eremu magnetikoaren eragina propietate magnetobiskoelastiko linealetan definitu da.

Azkenik, bi modelo magneto-biskoelastiko berri garatu dira, bata elastomero magnetoerreologiko isotropoetarako eta bestea anisotropoetarako. Bi ereduetan, bilakaera biskoelastikoa aurreikusteko lau parametroko deribatu frakzionarioen ereduak erabili dira. Arrhenius-en ereduak erabiliz tenperaturearen eragina modelatu da, eta proposaturiko eredu biskoelastikoari gehitu zaio. Gainera, proposaturiko ereduko parametro bakoitzean partikula-kontzentrazioak duen eragina aztertu eta modelatu da. Elastomero magnetoerreologiko isotropoetan eremu magnetikoak eragiten duen modulu magnetiko induzitua modelatzeko, dipolo-dipolo interakzioetan oinarritua dagoen ereduak garatu dira. Elastomero magnetoerreologiko anisotropoei dagokienez, eremu magnetikoarekiko menpekotasuna modelatzeko material hauen permeabilitate magnetikoetan oinarritua dagoen ereduak garatu dira. Eredu biskoelastikoa eta eredu magnetikoa elkar-tuz, elastomero magnetoerreologiko anisotropoen bilakaera magnetobiskoelastikoa aurreikusten duen eredu berri bakar bat garatu da.



# Resumen

En las últimas décadas, se han desarrollado múltiples aplicaciones anti-vibratorias con el fin de aumentar la vida útil de los componentes, el confort y la seguridad. La mayor parte de estas aplicaciones utilizan materiales que no se pueden adaptar a unas condiciones de trabajo variables, por lo que surgen como alternativa los materiales inteligentes. Dentro de éste grupo de materiales, se encuentran los elastómeros magnetorreológicos que poseen la capacidad de modificar sus propiedades cuando se aplica un campo magnético externo.

El principal objetivo de ésta tesis es analizar el comportamiento magneto-térmico-dinámico de los elastómeros magnetorreológicos para incrementar su uso en aplicaciones industriales.

Se han sintetizado elastómeros magnetorreológicos isótropos y anisótropos con tres matrices diferentes y ocho concentraciones volumétricas de partículas. Se ha propuesto un nuevo criterio para definir el rango viscoelástico lineal de los elastómeros magnetorreológicos a cortadura analizando el factor de pérdida y el módulo de almacenamiento. Además, se ha estudiado la influencia de las variables de síntesis y de caracterización en el rango viscoelástico lineal, y en las propiedades magneto-viscoelásticas de los elastómeros magnetorreológicos isótropos y anisótropos, lo que ha permitido establecer la máxima atenuación de estos materiales.

Adicionalmente, se ha diseñado e implementado un nuevo ensayo magneto-dinámico de compresión para caracterizar los elastómeros magnetorreológicos a altas frecuencias. En este modo de trabajo se han establecido el límite viscoelástico lineal y las propiedades magneto-viscoelásticas en función de la concentración de partículas, frecuencia y campo magnético.

Por último se han creado dos nuevos modelos magneto-viscoelásticos, uno para elastómeros magnetorreológicos isótropos y otro para anisótropos. Ambos, utilizan un modelo de derivadas fraccionarias de cuatro parámetros para describir el carácter viscoelástico, al que se ha acoplado el modelo de Arrhenius para incluir la temperatura. Cada uno de los parámetros del modelo viscoelástico se ha analizado y modelado en función de la concentración de partículas. En el modelo viscoelástico de elastómeros magnetorreológicos isótropos se ha implementado un nuevo modelo magneto-inducido basado en la interacción dipolo-dipolo para incluir el efecto del campo magnético. En cuanto a los elastómeros magnetorreológicos anisótropos, se ha desarrollado un nuevo modelo para el módulo magneto-inducido a partir de las permeabilidades magnéticas. Este modelo se acopla al efecto viscoelástico dando un único modelo magneto-viscoelástico para elastómeros magnetorreológicos anisótropos.



# Abstract

In the last decades, many anti-vibration applications have been developed to increase the life time of components, the comfort and the security. Most of these applications are based on materials that cannot be adapted to variable working conditions, so that smart materials arise as an alternative. Within these group of materials, magnetorheological elastomers are found whose dynamic properties can be reversibly modified and controlled by an external magnetic field.

The main goal of the presented dissertation was to analyse the magneto-thermodynamic behaviour of magnetorheological elastomers to enhance its use in industrial applications.

Isotropic and anisotropic magnetorheological elastomers samples were synthesised with three different matrices and eight particle contents to study the shear magneto-viscoelastic properties. A new criteria analysing the loss factor and storage modulus was determined to define the shear linear viscoelastic region of magnetorheological elastomers, and the influence of synthesis and characterisation variables in the linear region was studied. Within this linear region, the magneto-viscoelastic properties of isotropic and anisotropic magnetorheological elastomers were studied, and the maximum attenuation variability of these materials was established.

A new magneto-dynamic compression test was designed and manufactured, and the procedure to characterise magnetorheological elastomers at high frequencies in compression mode was implemented. Furthermore, the linear viscoelastic region was defined in these working mode, and the magneto-dynamic properties were analysed as a function of the particle content, the frequency and the magnetic field.

Finally, two new magneto-viscoelastic models were developed, one for isotropic and another one for anisotropic magnetorheological elastomers. In both models, the viscoelastic nature was modelled using a four-parameter fractional derivative model, and the influence of temperature was introduced using the Arrhenius model. Moreover, the influence of particle content in each parameter was analysed and modelled, and a new magneto-induced modulus model based on the dipole-dipole interactions was coupled with the developed models for isotropic magnetorheological elastomers. In respect of anisotropic magnetorheological elastomers, a new magneto-induced modulus model was developed using magnetic permeability components, and it was coupled to the viscoelastic effect in a single magneto-viscoelastic model for anisotropic magnetorheological elastomers.





# Contents

<b>List of Figures</b>	<b>xix</b>
<b>List of Tables</b>	<b>xxiii</b>
<b>Nomenclature</b>	<b>xxv</b>
<b>1 Introduction</b>	<b>1</b>
1.1 Motivation and background . . . . .	2
1.2 Scope of the thesis . . . . .	6
<b>2 Shear magneto-thermo-dynamic characterisation</b>	<b>7</b>
2.1 Introduction . . . . .	8
2.2 Critical review . . . . .	12
2.3 Aims . . . . .	12
2.4 Synthesis . . . . .	13
2.5 Shear test . . . . .	15
2.6 Results . . . . .	18
2.6.1 Linear viscoelastic region . . . . .	18
2.6.2 Magneto-dynamic properties . . . . .	21
2.7 Conclusions . . . . .	24
2.8 Scientific contribution . . . . .	27
<b>3 Compression magneto-dynamic characterisation</b>	<b>55</b>
3.1 Introduction . . . . .	56
3.2 Critical review . . . . .	57
3.3 Aims . . . . .	58
3.4 Synthesis . . . . .	58

3.5	Results . . . . .	59
3.5.1	Technique . . . . .	59
3.5.2	Linear viscoelastic region . . . . .	63
3.5.3	Magneto-dynamic properties . . . . .	64
3.6	Conclusions . . . . .	66
3.7	Scientific contribution . . . . .	67
<b>4</b>	<b>Magneto-viscoelastic modelling</b>	<b>87</b>
4.1	Introduction . . . . .	88
4.2	Critical review . . . . .	92
4.3	Aims . . . . .	94
4.4	Results . . . . .	94
4.4.1	Viscoelastic modelling . . . . .	95
4.4.2	Fillers . . . . .	98
4.4.3	Magneto-induced modulus . . . . .	100
4.4.4	Magneto-viscoelastic modelling . . . . .	102
4.5	Conclusions . . . . .	105
4.6	Scientific contribution . . . . .	107
<b>5</b>	<b>Conclusions and future work</b>	<b>137</b>
5.1	Conclusions . . . . .	138
5.2	Future work . . . . .	141
	<b>References</b>	<b>143</b>

# List of Figures

Figure 2.1	SEM image of the carbonyl-iron powder particles . . . . .	14
Figure 2.2	Sketch of the anisotropic MRE sample vulcanisation device . . . . .	15
Figure 2.3	SEM images of the 15% RTV-SR MRE: (a) isotropic and (b) anisotropic sample . . . . .	15
Figure 2.4	Storage modulus( $G'$ ) (■) and loss factor ( $\tan \delta$ ) (●) versus strain to define the LVE region . . . . .	17
Figure 2.5	Influence of the strain in the (a) storage modulus ( $G'$ ), loss modulus ( $G''$ ) and (c) loss factor ( $\tan \delta$ ) of the 30% isotropic RTV-SR sample as a function of frequency, at 25 °C and 0 kA/m . . . . .	19
Figure 2.6	Influence of the matrix in the LVE limit for the 0% particle content, at 25 °C and 1 Hz . . . . .	19
Figure 2.7	Influence of temperature in the LVE region for the 0% HTV-SR and 0% RTV-SR samples at 1 Hz . . . . .	20
Figure 2.8	Evolution of (a) the storage modulus ( $G'$ ) and (b) the loss factor ( $\tan \delta$ ) of the 10% isotropic RTV-SR as a function of frequency, with temperature ranging from 15 °C to 65 °C and 0 kA/m . . . . .	22
Figure 2.9	Influence of the magnetic field in the (a) storage ( $G'$ ) and (b) loss modulus ( $G''$ ) as a function of frequency for the 30% isotropic RTV-SR sample at 25 °C . . . . .	23

Figure 2.10	Variation of (a) storage ( $G'$ ) and (b) loss modulus ( $G''$ ) of isotropic and anisotropic 15% RTV-SR samples as a function of frequency owing to the magnetic field at 25 °C . . . . .	24
Figure 3.1	Sketch of the vulcanisation of isotropic MREs . . . . .	58
Figure 3.2	Experimental set-up . . . . .	60
Figure 3.3	(a) Dynamic compression test and (b) close-up of the sample holding: (1) electrodynamic shaker, (2) ball joint, (3) uniaxial accelerometer (Brüel & Kjaer 4371), (4) translational oscillatory rod, (5) springs, (6) electromagnet, (7) dynamic force sensor (Dytran IEPE force sensor 1051v2), (8) Mitutoyo ABSOLUTE Digimatic Indicator (linear encoder), (9) sample, (10) static rod, and (11) pre-strain bolt and nut . . . . .	61
Figure 3.4	Stress–strain diagram of an NR 30% isotropic sample for a strain amplitude of 0.2% at 75 Hz, room temperature and 0 kA/m . . . . .	61
Figure 3.5	Stress–strain diagrams at 50 and 200 Hz for a particle content of (a) 0% and (b) 30% isotropic NR samples, at different strain amplitudes, 0 kA/m and room temperature . . . . .	63
Figure 3.6	Stress–strain diagrams for the 15% isotropic NR sample at the studied frequencies, constant strain of 0.3%, 0 kA/m and room temperature . . . . .	64
Figure 3.7	(a) Storage modulus ( $E'$ ) and (b) loss factor ( $\tan \delta$ ) as a function of frequency for all the studied isotropic NR samples, 0 kA/m and room temperature . . . . .	65
Figure 4.1	Sketch of the fractional derivative model . . . . .	95

Figure 4.2	Evolution of the (a) storage modulus ( $G'$ ) and (b) loss factor ( $\tan \delta$ ) of 0%, 10% and 25% isotropic MRE samples as a function of frequency at 25 °C and 0 kA/m . . . . .	96
Figure 4.3	Evolution of the storage modulus ( $G'$ ) and loss factor ( $\tan \delta$ ) as a function of (a) reduced frequency (for -10, 25 and 80 °C), and (b) temperature (for 1, 50 and 100 Hz) for the 0% MRE sample at 0 kA/m	98
Figure 4.4	Experimental data (points) and fractional derivative and particle-matrix model (lines) of (a) storage ( $G'$ ) and (b) loss modulus ( $G''$ ) as a function of frequency at 25 °C and 0 kA/m for isotropic MREs and seven particle contents (0%, 1%, 5%, 10%, 15%, 20% and 25%) . . . . .	100
Figure 4.5	Experimental (points) and numeric data (lines) of (a) longitudinal and (b) transverse components of the magnetic permeability of anisotropic MRE samples (5%, 10%, 15% and 20%) at room temperature as a function of magnetic field density . . . .	102
Figure 4.6	Experimental data (points) and the proposed magneto-viscoelastic model (lines) for the storage modulus ( $G'$ ) of the 10% isotropic MRE sample as a function of frequency at 25 °C and different magnetic field intensities . . . . .	104
Figure 4.7	Experimental data (points) and the proposed magneto-viscoelastic model (lines) for the storage modulus ( $G'$ ) of the 5% anisotropic MRE sample as a function of frequency at 25 °C and different magnetic field intensities (150 and 300 kA/m curves are modelled using experimental data, and the 420 and 560 kA/m curves are the extension of the proposed model) . . . . .	104



# List of Tables

Table 2.1	Summary of the influence of synthesis and working conditions in the LVE region of MREs . . . . .	21
Table 3.1	Mean magnetorheological effect of isotropic MREs	66
Table 4.1	Fitting parameters of a four-parameter fractional derivative model for the seven isotropic MRE samples (0-25%) at 25 °C and 0 kA/m . . . . .	99





# Nomenclature

## List of Abbreviations

BCC	Body-centered cubic
BCT	Body centered tetragonal
CIP	Carbonyl iron powder
CPVC	Critical particle volume concentration
DMA	Dynamic mechanical analysis
FD	Fractional derivative
FEMM	Finite element method magnetics
HTV	High temperature vulcanising
LVE	Linear viscoelasticity
MR	Magnetorheology
MRE	Magnetorheological elastomer
MRF	Magnetorheological fluids
NR	Natural rubber
PDMS	Polydimethylsiloxane
RTV	Room temperature vulcanising
SEM	Scanning electron microscope
SR	Silicone rubber
VSM	Vibrating sample magnetometry
WLF	Williams-Landel-Ferry

## List of Symbols

$A_n, a_n, B_n$	Material parameter
$B$	Magnetic field density
$\mathbf{B}$	Magnetic field density first order tensor
$C$	Elastic part of the viscoelastic branch
$\Delta C$	Magneto-induced modulus variation
$d$	Particle distance
$E^*$	Complex modulus (Compression)
$E'$	Elastic modulus (Compression)
$f$	Frequency
$G^*$	Complex modulus (Shear)

$G_0$	Static modulus (Shear)
$G'$	Storage modulus (Shear)
$G'_0$	Storage modulus in the absence of magnetic field (Shear)
$G'_H$	Elastic modulus at a certain magnetic field (Shear)
$G''$	Loss modulus (Shear)
$G''_0$	Loss modulus in the absence of magnetic field (Shear)
$G''_H$	Loss modulus at a certain magnetic field (Shear)
$H$	Magnetic field intensity
$i$	Imaginary unit
$J_p$	Particle induced polarisation
$K$	Bulk modulus
$R$	Particle radio
$t$	Time
$T$	Temperature
$T_g$	Glass transition temperature
$a$	Fractional order
$a_T$	Shift factor
$\delta$	Phase lag
$\varepsilon$	Strain
$\gamma$	Shear strain
$\varphi$	Volumetric particle content
$\mu_0$	Vacuum magnetic permeability
$\mu_1$	Relative magnetic permeability of a medium
$\mu_{  }$	Longitudinal magnetic permeability component
$\mu_{\perp}$	Transverse magnetic permeability component
$\rho$	Density
$\sigma$	Stress
$\tau$	Shear stress
	Relaxation time
$\omega$	Angular frequency

*The journey is what brings us happiness not the destination*

Dan Millman

# 1

## Introduction

## 1.1 Motivation and background

In the last decades, many anti-vibration applications have been developed to increase the life time of components, the comfort and the security. Most of these applications are based on materials that cannot be adapted to variable working conditions, so that smart materials arise as an alternative. Within these group of materials, magnetorheological elastomers are found whose dynamic properties can be reversibly modified and controlled by an external magnetic field.

Smart materials are those materials which can vary their properties depending on an external effect, such as piezoelectric materials, shape memory alloys, temperature-responsive polymers, ferrofluids, etc. In 1948, [Rabinow \(1948\)](#) found that some materials modify their properties when an external magnetic field was applied, and they recovered their initial properties when the field was removed. This property variability due to an external magnetic field is called magnetorheological (MR) effect. There are three type of MR materials according to the main media—magnetorheological fluids (MRF), magnetorheological gels (MRG) and magnetorheological elastomers (MREs).

In the last three decades, the main studied topics have been the magnetorheological fluids. These materials consist of magnetisable particles suspended in a non-magnetic fluid media. MRFs operate within a post-yield continuous shear or flow regime ([López-López et al. 2012](#)). When a magnetic field is applied to MRFs, particles are aligned and characterised by the yield stress. Nevertheless, MRFs show drawbacks such as particle sedimentation, environmental pollution due to leaks, and problems to keep the fluid in the application device ([Ginder et al. 2002](#)).

In order to overcome the drawbacks of the MRFs, the fluid media have been substituted by a polymeric matrix. These materials are named as magnetorheological elastomers (MREs). MREs always operate in the pre-yield regime ([Carlson and Jolly 2000](#)).

The MREs have been used in applications such as isolators ([Ladipo et al. 2016](#); [Sun et al. 2015](#)), seismic isolator ([Yu and Yang 2012](#)), seat isolators ([Li et al. 2012](#)) and dumpers ([Tu et al. 2014](#)). During the designing and prototyping of these applications, the dynamic properties of these materials and its dependency with the

synthesis and working conditions have to be known. Furthermore, appropriate constitutive models are supportive for the design of MRE applications.

Dynamic characterisations of MREs have been performed using oscillatory movements, as tensile, compression or shear movements. The shear movement can be rotational or linear, and the magnetic field is perpendicular to the movement. In the literature, most of the works have studied the shear mode because there are commercial equipment developed for magnetorheological characterisations. However, in tensile and compression tests the movement is linear and the magnetic field is parallel to mechanical strain [Varga et al. \(2006\)](#).

The most important property of MRE materials is the variability of the dynamic properties depending on the applied magnetic field. These variability have been studied analysing the storage modulus variation with an external magnetic field, and have been measured with the relative MR effect, also known as MR effect. That effect was defined as the ratio between the change in its storage modulus with and without magnetic field and the storage modulus without magnetic field ([Chen et al. 2008a](#)).

Within the synthesis variables the most significant components are the main matrix, particle content and pre-structure process. The MR effect is dependent on the matrix and it is larger using a softer matrix ([Yang et al. 2015](#)), although natural rubber is used due to its good dynamic properties. Therefore, an equilibrium have to be obtained between the dynamic properties and the MR effect. The particle content is also a determinant synthesis parameter—a larger content increases the dynamic properties of MREs ([Wang et al. 2011](#)) and improve the MR effect ([Lokander and Stenberg 2003b](#)). During the cross linking or vulcanisation process, the magnetic field aligns the particles in chains obtaining chain-like structures once the elastomer is vulcanised. Those MRE samples are considered as anisotropic MREs ([Ju et al. 2015](#)), and those which are synthesised without any magnetic field are named isotropic MREs ([Bellucci et al. 2016](#)). The dynamic properties ([Lu et al. 2012](#)) and the MR effect are larger for anisotropic MREs ([Schubert and Harrison 2015](#)).

The dynamic properties of MRE are also dependent on the characterisation variables. As many viscoelastic materials, MREs can be modelled by the complex modulus when they are working in the linear viscoelastic region ([Jones 2001](#)). At

low strains, the behaviour is independent of strain, but at higher strains the behaviour is non-linear. This behaviour is known in the literature as the Payne effect (Payne 1962). In general, the dynamic properties and the MR effect are increased with frequency (Li et al. 2010), temperature (Wang et al. 2011) and magnetic field (Carlson and Jolly 2000). Furthermore, the MR effect is larger within the linear region (Jung et al. 2016; Lokander and Stenberg 2003a; Schubert and Harrison 2015).

During the prototyping of the MRE applications, finite element simulations, which are based on appropriate constitutive models, are also supportive. The predominant behaviour of MREs is the viscoelastic one owing to the nature of the matrix. However, the influence of the particle content, the particle-matrix interaction and the external magnetic field in the viscoelastic properties have to be analysed and modelled.

The modelling of the viscoelasticity of these materials have been done by different constitutive models, as classical differential models and fractional derivative models. One of the classical differential model used in MREs was the standard linear model (Chen and Jerrams 2011; Han et al. 2012), also known as Zener model (Zener 1948). The Boltzmann differential model have also been used in the modelling of the viscoelastic behaviour of MREs (Behrooz et al. 2014; Liao et al. 2013).

In order to avoid the addition of many material parameters, fractional derivative models can be used containing less material parameters and with a physical interpretation (Pritz 1996), and are very useful to model the dynamic behaviour. Therefore, fractional derivative models have been used to study the viscoelastic behaviour of MREs (Guo et al. 2014; Zhu et al. 2013).

The viscoelastic behaviour of MREs is modified due to the embedded particles during the vulcanisation process (Lu et al. 2012). That is why, the interaction between the filler (particle) and the matrix have been modelled (Guth 1945; Leng et al. 2013).

In the literature, the dipole-dipole interaction model proposed by Jolly et al. (1996a) to model the magnetic field influence in the MRE properties is the most used one. Furthermore, Davis (1999) extended this model to take into account the interaction of all particles of a chain. The variation of the modulus due to the

magnetic field have also been modelled using an effective permeability of MREs (Dong et al. 2013; Leng et al. 2013).

With this brief frame, the present thesis aims to analyse the magneto-thermo-dynamic behaviour of MREs. The present dissertation has been developed as a compendium of scientific publications and it is presented as an academic thesis format. The current thesis comprises five chapters including the first one for the introduction and the fifth one for the conclusions. The three central chapters (*Shear magneto-thermo-dynamic characterisation*, *Compression magneto-dynamic characterisation*, and *Magneto-viscoelastic modelling*) provides a brief summary of the publications to which they are associated.

Chapter 2, *Shear magneto-thermo-dynamic characterisation*, summarises the synthesis process and the shear characterisation tests of isotropic and anisotropic MREs, and the influence of synthesis and characterisation variables in the magneto-viscoelastic properties of MREs are analysed. A criteria to define the linear viscoelastic region of MREs is proposed analysing the loss factor and the storage modulus. Furthermore, the influence of synthesis (matrix, volumetric particle content and pre-structure) and characterisation variables (frequency, temperature and magnetic field) in the LVE region are analysed. From that analysis, a strain amplitude is determined to study the shear magneto-viscoelastic properties of isotropic and anisotropic MREs.

Chapter 3, *Compression magneto-dynamic characterisation*, is focused on a new compression test for a wide frequency range, and the linear region in compression mode to study the magneto-dynamic properties of isotropic MREs is analysed. A new compression test (design, manufacture and procedure) is proposed to characterise MREs at high frequencies, up to 200 Hz. The LVE region is analysed in compression mode and the influence of particle content and frequency is studied. Furthermore, the linear compression magneto-dynamic properties are analysed at high frequencies.

Chapter 4, *Magneto-viscoelastic modelling*, presents two magneto-viscoelastic models, one for isotropic MREs and another on for anisotropic MREs, including the influence of frequency, temperature, particle-matrix interaction and magnetic field. The viscoelastic behaviour of isotropic MREs is modelled using a four-parameter fractional derivative model, and the influence of temperature is cou-

pled using the Arrhenius model. The evolution of each parameter is studied as a function of the particle content for isotropic MREs. A magneto-induced modulus (modulus owing to an external magnetic field) model based on the dipole-dipole interaction is proposed to predict the influence of the magnetic field. Furthermore, the viscoelastic, the particle-matrix and the magneto-induced modulus models are coupled in a single three-dimensional magneto-viscoelastic model. In respect of anisotropic MREs, the viscoelastic behaviour is modelled with a four-parameter fractional derivative model, and a magneto-induced modulus model is developed adapting the [López-López et al. \(2012\)](#) model and introducing experimental magnetic permeability components for anisotropic MREs. Both models, are coupled in a single magneto-viscoelastic model.

## 1.2 Scope of the thesis

The main goal of the present dissertation was to analyse the magneto-thermodynamic behaviour of magnetorheological elastomers. In order to meet this main goal, the study comprise the following specific objectives:

- Implement an experimental shear procedure to analyse the shear magneto-thermo-dynamic properties of isotropic and anisotropic MREs within the linear viscoelastic region.
- Develop an experimental compression technique to analyse the compression magneto-viscoelastic properties of isotropic MREs within the linear viscoelastic region.
- Develop two magneto-viscoelastic models to predict the shear magneto-viscoelastic behaviour of isotropic and anisotropic MREs in a wide range of working conditions.



*Opportunities don't happen, you create them*

Chris Grosser

# 2

## Shear magneto-thermo-dynamic characterisation

- I. Agirre-Olabide, J. Berasategui, M.J. Elejabarrieta, and M.M. Bou-Ali. 2014. Characterization of the linear viscoelastic region of magnetorheological elastomers. *J. Intell. Mater. Syst. Struct.*, 25(16):2074-2081. doi: 10.1177/1045389X13517310
- I. Agirre-Olabide, M.J. Elejabarrieta, and M.M. Bou-Ali. 2015. Matrix dependence of the linear viscoelastic region in magnetorheological elastomers. *J. Intell. Mater. Syst. Struct.*, 26(14):1880-1886. doi: 10.1177/1045389X15580658
- I. Agirre-Olabide, and M.J. Elejabarrieta. 2017. Effect of synthesis variables on viscoelastic properties of elastomers filled with carbonyl iron powder. *J. Polym. Res.*, 24(9):139. doi: 10.1007/s10965-017-1299-z

This chapter aims therefore to synthesise isotropic and anisotropic MREs, and analyse the shear magneto-thermo-dynamic properties of MREs within the linear viscoelastic region. To that end, a synthesis procedure is determined for each matrix. Subsequently, a standard method is defined to determine the linear viscoelastic region of MREs, and the influence of synthesis and characterisation parameters in the linear region are analysed. Finally, the magneto-viscoelastic properties of MREs are studied within the linear viscoelastic region.

## 2.1 Introduction

Magnetorheological elastomers (MREs) are classified as smart materials whose dynamic properties can be reversibly modified and controlled by an external magnetic field. These materials consist of magnetisable particles embedded in a polymeric matrix.

The MREs are used in applications such as isolators ([Liao et al. 2012](#)), seismic isolator ([Yu and Yang 2012](#)), seat isolators ([Li et al. 2012](#)) and dumpers ([Tu et al. 2014](#)). However, the dynamic properties of these materials have to be determined to obtain the adequate design of the products. Hence, the dependence of synthesis and characterisation variables on the dynamic properties of MREs have to be determined.

The shear dynamic characterisations of MREs are performed by oscillatory movements, which can be rotational or linear, and the external magnetic field is perpendicular to the movement. The double lap shear test have widely been used in the literature and was adapted to dynamic machines ([Behrooz et al. 2014](#); [Danas et al. 2012](#); [Jolly et al. 1996b](#); [Norouzi et al. 2016](#)) and electrodynamic shakers ([Blom and Kari 2005](#); [Lejon and Kari 2013](#); [Yang et al. 2015](#)). Dynamic mechanical analysers (DMA) have also been used to characterise MREs ([Lu et al. 2012](#); [Pickering et al. 2015](#); [Raa Khimi and Pickering 2016](#); [Wang et al. 2015](#)). According to rotational movements, in the literature the most used machines are the rheometers, which are equipped with a magnetorheological device ([Feng et al. 2015](#); [Gao and Wang 2016](#); [Li and Nakano 2013](#); [Stepanov et al. 2007](#); [Yunus et al. 2016](#)).

As many viscoelastic, materials MREs can be modelled by the complex modu-

lus when they are working in the linear viscoelastic (LVE) region (Jones 2001). At low strains, the behaviour is independent of the strain, while at higher strains the behaviour is non-linear, which is known in the literature as the Payne effect (Payne 1962). Within the LVE region, for a given harmonic shear strain ( $\gamma$ ), the shear stress ( $\tau$ ) will also be harmonic with a phase lag ( $\delta$ ) respect to the shear strain (equations 2.1 and 2.2).

$$\gamma(t) = \gamma_{\max} \cdot e^{i\omega t} \quad (2.1)$$

$$\tau(t) = \tau_{\max} \cdot e^{i(\omega t + \delta)} \quad (2.2)$$

where  $\gamma_{\max}$  is the amplitude of the shear strain,  $\tau_{\max}$  is the shear stress amplitude,  $t$  is time, and  $\omega$  is the angular frequency. Both are used to obtain the shear complex modulus ( $G^*$ ),

$$G^* = \frac{\tau(t)}{\gamma(t)} = \frac{\tau_{\max} \cdot e^{i(\omega t + \delta)}}{\gamma_{\max} \cdot e^{i\omega t}} = \frac{\tau_{\max}}{\gamma_{\max}} (\cos \delta + i \sin \delta). \quad (2.3)$$

The shear complex modulus consists of a real part, storage modulus ( $G'$ ), and an imaginary part, loss modulus ( $G''$ ).

$$G' = \frac{\tau_{\max}}{\gamma_{\max}} \cos \delta \quad (2.4)$$

$$G'' = \frac{\tau_{\max}}{\gamma_{\max}} \sin \delta \quad (2.5)$$

The loss factor ( $\tan \delta$ ) is the relation between the loss modulus and the storage modulus (Equation 2.6).

$$\tan \delta = \frac{G''}{G'} \quad (2.6)$$

The property variation of MRE materials owing to an external magnetic field, is larger in the low strain region or within the LVE region (Jung et al. 2016; Lokander and Stenberg 2003a; Schubert and Harrison 2015). Therefore, the linear region has to be determined to maximise the property variability. The linear viscoelastic region is defined by the LVE limit, which is determined at the point where the

$G'$  and  $G''$  become dependent on the strain. Tian et al. (2013a) analysed the LVE region of isotropic MREs, for which they used stress–strain curves and also storage modulus–strain curves. To determine the LVE region, Gordaninejad et al. (2012); Ju et al. (2012) and Qiao et al. (2012) defined a linear elastic deformation at 1% of strain, because at high strains the shear modulus become dependent on strain.

In the literature, few studies have analysed the influence of synthesis and characterisation variables on the LVE region. Tian et al. (2013a) concluded that particle content decreases the LVE region of the MRE materials. Bellan and Bossis (2002) showed that for MREs with large particle content, the Payne effect becomes larger. The influence of temperature in the LVE limit of polymers is rarely studied, although it was determined that the strain limit increases with a decrease in the polymer stiffness (Airey and Rahimzadeh 2004). Nevertheless, the LVE region of some polymers decreases with the increment of temperature (Arenz 1998; Leblanc 2012). Moreover, Starkova and Aniskevich (2007) proposed that the LVE region of polymers is wider with a higher transition temperature.

Magneto-viscoelastic properties are dependent on synthesis and characterisation variables. One of the most important properties of MRE materials is the variability of the dynamic properties depending on the applied magnetic field, and it is measured with the relative MR effect, also known as MR effect. That effect is defined as the ratio between the change in its storage modulus with and without magnetic field and the storage modulus without magnetic field (Chen et al. 2008a),

$$\text{MR effect} = \frac{G'_H - G'_0}{G'_0} \times 100 \quad (2.7)$$

where  $G'_H$  is the storage modulus at a certain magnetic field and  $G'_0$  is the storage modulus in the absence of a magnetic field.

Within the synthesis variables, the decisive components are the main matrix, particle content and pre-structure process (vulcanisation of isotropic or anisotropic samples). The mechanical performance was improved replacing the silicone rubber (SR) by natural rubber (NR) (Chen et al. 2007a). Chen et al. (2008b) studied the damping properties of MRE elastomers based on different matrices. The MR effect is dependent on the matrix and it is larger using a softer matrix (Lokander and Stenberg 2003b; Yang et al. 2015). Therefore, an equilibrium has to be

obtained between the dynamic properties and the magneto-induced modulus.

Particle content is a key parameter to determine the dynamic mechanical properties of MREs under the same characterisation conditions (Hu et al. 2005). Both storage modulus and loss factor increase with the particle content (Fan et al. 2011; Wang et al. 2011; Zhu et al. 2013). The MR effect of MREs is also influenced by the particle content; specifically, the effect is higher with a larger volumetric particle content (Ge et al. 2013; Gordaninejad et al. 2012; Lokander and Stenberg 2003b; Ubaidillah et al. 2016b).

Embedded particles can be randomly distributed or aligned in chains. Isotropic MREs are cured without the influence of a magnetic field. On the other hand, chains are obtained by applying an external magnetic field during the pre-structure process; samples with oriented chains are called anisotropic MREs. Anisotropic samples show higher MR effect than isotropic ones (Schubert and Harrison 2015). While dynamic properties are larger for anisotropic samples (Lu et al. 2012), the loss factor decreases when an external magnetic field is applied to the MRE during characterisation (Sun et al. 2008).

The dynamic properties of MRE are also dependent on characterisation variables as strain, frequency, temperature and magnetic field. The MR effect is larger within the linear region (Jung et al. 2016; Lokander and Stenberg 2003a; Schubert and Harrison 2015). Moreover, dynamic properties increases with the frequency (Li et al. 2010) and the MR effect is increased with temperature (Wang et al. 2011). When a larger magnetic field is applied, the magneto-induced modulus and the MR effect are increased (Carlson and Jolly 2000).

In this chapter, isotropic and anisotropic MREs are synthesised for different matrices. The characterisation of the synthesised samples is performed with a rheometer equipped with a magnetorheological device. A standard procedure is proposed to define the linear viscoelastic region of MREs, which analyses the storage modulus and the loss factor. The influence of synthesis (matrix, particle content and pre-structure) and characterisation variables (frequency, temperature and external magnetic field) are studied to determine the LVE region and the shear magneto-thermo-dynamic properties. All these results were published in the papers attached in the section 2.8. scientific contribution.

## 2.2 Critical review

From the reviewed bibliography it can be concluded that there is a lack of a criteria to determine systematically the LVE region of viscoelastic materials, and how the synthesis and characterisation variables influence the linear region in shear mode. In the literature, the LVE region was defined analysing the storage modulus, while the loss factor have not been studied.

Moreover, it is observed that some synthesis variables as particle content modify the LVE limit (Tian et al. 2013a). Airey and Rahimzadeh (2004) concluded that the strain limit is increased when the polymer stiffness increases. However, the influence of the matrix and the pre-structure have not been studied for MREs.

Characterisation variables also influence the LVE region, which is decreased for some polymers with the increment of temperature (Arenz 1998; Leblanc 2012). Nevertheless, the influences of frequency and magnetic field have not been analysed in shear mode.

According to magneto-viscoelastic properties, synthesis and characterisation variables have to be analysed to obtain the larger MR effect. While the MR effect is larger in the LVE region (Jung et al. 2016; Lokander and Stenberg 2003a; Schubert and Harrison 2015), there are few works analysing the influence of synthesis and characterisation variables in its properties within the LVE region.

In this chapter, therefore, a standard procedure is developed to define the LVE region analysing storage modulus and loss factor. The influence of synthesis (matrix, particle content, and pre-structure) and characterisation variables (frequency, temperature, and external magnetic field) in the LVE region are studied. The shear magneto-viscoelastic properties are analysed within the LVE region, and the influence of synthesis and characterisation variables are studied.

## 2.3 Aims

The goal of this chapter is to implement an experimental shear procedure to analyse the shear magneto-thermo-dynamic properties of isotropic and anisotropic MREs

within the linear viscoelastic region. The specific objectives are:

- Define a procedure to analyse the LVE region of any rubber material.
- Analyse the influence of synthesis and characterisation variables in the LVE region of MREs.
- Analyse the magneto-thermo-dynamic properties of MREs to maximise the MR effect.

## 2.4 Synthesis

In this chapter, isotropic and anisotropic MREs filled with ferromagnetic particles were synthesised using three different matrices, and eight particle contents were analysed.

The synthesised matrices were a natural rubber (NR), a high temperature vulcanising silicone rubber (HTV-SR), and a room temperature vulcanising silicone rubber (RTV-SR). The NR and HTV-SR were vulcanised at 180 °C and RTV-SR was vulcanised at room temperature. RTV-SR is a polydimethylsiloxane (PDMS) based rubber and has two components: the main matrix WACKER Elastosil® M 4644 A and the vulcaniser WACKER Elastosil® M 4644 B mixed in 10:1 ratio.

For synthesising the MREs, CIP was used as ferromagnetic iron particle; it had a spherical shape and average size of  $1.25 \pm 0.55 \mu\text{m}$ . The shape and the size of the particles was analysed using a scanning electron microscope (SEM) image (Figure 2.1). The image was obtained by a SEM working in low vacuum conditions and microanalysis, JEOL JSM 5600 LV, and with a voltage acceleration of 15 kV. These particles were provided by BASF. The volumetric contents studied in this chapter were: 0%, 1%, 5% 10%, 15%, 20%, 25% and 30%.

Lokander and Stenberg (2003a) defined the maximum particle content when all particles are in contact one to each other, and the voids between them is replaced by rubber. This content is defined as the critical particle volume concentration (CPVC),

$$CPVC = \frac{100 \times \rho_{\text{app}}}{\rho_{\text{Fe}}} \quad (2.8)$$

where  $\rho_{\text{app}}$  is the apparent density of the filler, and  $\rho_{\text{Fe}}$  is the material density of the filler, 2400 and 7800 kg/m<sup>3</sup> respectively. Therefore, the CPVC for the particles used in this thesis is 30.76% and the synthesised maximum content was 30%.

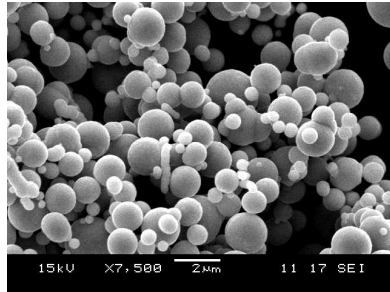


**Figure 2.1** SEM image of the carbonyl-iron powder particles

The synthesis process was the same for NR and HTV-SR (NE-9340) matrices because of the vulcanisation temperature and solid state of the raw material. For the mixing process, a two-roll mixing mill was used, and the particles were added gradually. A homogenous mixture was poured into a 1 mm thick mould, and the mould was then placed in an oven at 180 °C under a hydraulic pressure of 200 bar.

The RTV-SR matrix had two components, and vulcanisation began when both were mixed. The main matrix (Elastosil® M 4644 A) and the particles were mixed by hand, and vacuum cycles were applied for 30 min to extract air bubbles generated during mixing. Then, the vulcaniser was added, and vacuum cycles were again applied to remove air bubbles. Finally, the homogenous mixture was poured into a 1 mm thick mould.

For the RTV-SR matrix, two pre-structure conditions were studied: pre-structure without a magnetic field (isotropic MRE) and with a magnetic field (anisotropic MRE). During pre-structuring, a magnetic field was applied in the thickness direction (Figure 2.2) to obtain a chain alignment of the particles in the direction perpendicular to the characterisation shear strain (Varga et al. 2006). The magnetic field density was  $130 \pm 10$  mT measured by the Gaussimeter FH-54.

To guarantee the particle distribution (isotropic and anisotropic MREs), images were obtained using a Nova NanoSEM 450 scanning electron microscope (SEM) working under low vacuum conditions with a voltage acceleration of 18 kV. Figure 2.3 shows SEM images of the 15% RTV-SR MRE sample: in Figure 2.3(a),



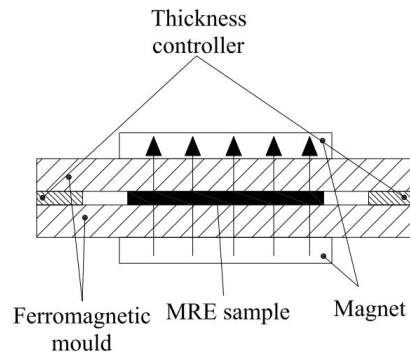


**Figure 2.2** Sketch of the anisotropic MRE sample vulcanisation device

a homogeneous particle distribution can be seen (isotropic MRE), and in Figure 2.3(b), the particles are aligned perpendicular to the surface in the direction of the applied external magnetic field during vulcanisation (anisotropic MRE). While in Figure 2.1 the particles were agglomerated, after synthesising isotropic samples (Figure 2.3(a)) particle agglomerations were not seen in isotropic MREs and they were randomly distributed.

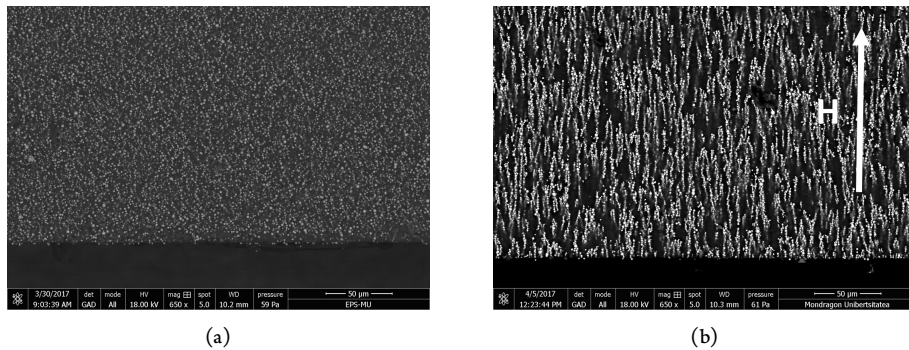


**Figure 2.3** SEM images of the 15% RTV-SR MRE: (a) isotropic and (b) anisotropic sample

## 2.5 Shear test

The shear dynamic characterisations of MREs are performed by oscillatory movements, which can be rotational or linear, and the external magnetic field is per-

pendicular to the movement. The double lap shear test have widely been used in the literature and have been adapted to dynamic machines (Behrooz et al. 2014; Norouzi et al. 2016) and electrodynamic shakers (Lejon and Kari 2013; Yang et al. 2015). Dynamic mechanical analyser have also been used to characterise MREs (Raa Khimi and Pickering 2016; Wang et al. 2015). According to rotational movements, in the literature the most used machines are the rheometers, which are equipped with a magnetorheological device (Gao and Wang 2016; Yunus et al. 2016).

In this chapter, characterisations were performed using an Anton Paar Physica MCR 501 rheometer equipped with a MRD 70/1T magnetorheological cell, and a parallel plate configuration was used. One of the plates had a serrated surface, and its diameter was 20 mm (PP20/MRD /TI/P2). The tested samples had a diameter of 20 mm and a thickness of 1 mm, and for each vulcanised material three samples were studied.

The analysed frequency range was 1–40 Hz, and the studied temperature range was 15–65 °C controlled using a Julabo F-25 water-based heating/cooling system. To avoid sliding between the samples and the plates, and to increase the MR effect, a normal force of 5 N was defined (Dong et al. 2012). The magnetic field goes from the minimum intensity of 0 kA/m to a maximum of 616 kA/m. After each characterisation, a demagnetization cycle was applied. In the samples, the possible magnetisation was tested, and it was seen that the magnetisation was minimum because the measured field was below  $15 \pm 8 \mu\text{T}$ .

Two different tests were performed: strain sweep tests and frequency sweep tests. Strains sweep test were used to determine the LVE region variation owing to matrix, particle content, pre-structure of the samples, frequency, external characterisation magnetic field and temperature. Once the LVE region was defined, frequency sweep tests were performed to analyse the magneto-viscoelastic properties of isotropic and anisotropic MREs.

Within the linear region, the storage modulus and the loss factor are constant (Nashif et al. 1985). Gordaninejad et al. (2012) defined a limit when the stress–strain relation becomes non-linear at 1% of strain. Moreover, Wereley et al. (2006) define the LVE limit for magnetorheological fluids (MRF) at the point where the storage modulus deviates 10% from the plateau value.

In this thesis, it is the first time the loss factor and the storage modulus are separately analysed to define the LVE region in shear mode. For this purpose, a straight line is approached for each ( $G'$  and  $\tan \delta$ ), and the LVE limit is defined at the point where the experimental data deviates 10% from the approached straight line (Figure 2.4).

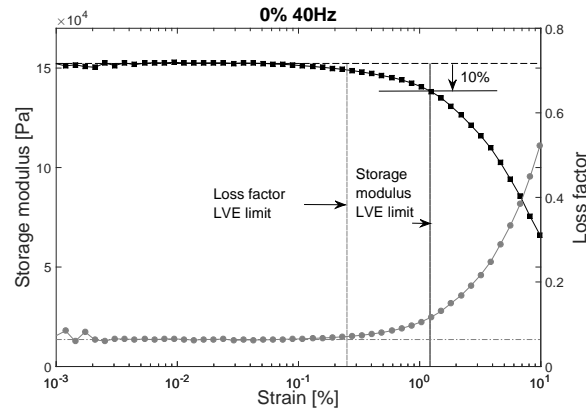


**Figure 2.4** Storage modulus( $G'$ ) (■) and loss factor ( $\tan \delta$ ) (●) versus strain to define the LVE region

To perform LVE region characterisation, 50 points were defined from 0.001% to 10% logarithmically spaced, and at each point measurements were made for 5 seconds. This logarithmic scale allows covering a wider range of deformations. These tests were made at two frequencies which limit the interest frequency band, 1 and 40 Hz.

After the LVE region was defined, frequency sweep tests were performed at a strain which guarantees that all results were in the LVE region. A linear distribution of 40 frequencies between 1 and 40 Hz was applied. The measurement period for each point was 5 seconds, and three magnetic fields were analysed within the range of 0–616.7 kA/m. The studied temperatures ranged from 15 °C to 65 °C, with an increment of 10 °C, and were controlled using a Julabo F-25 water-based heating/cooling system.

## 2.6 Results

In this section, a summary of the results presented in the three papers, to which the chapter refers and include it in sec 2.8., are shown. In [Agirre-Olabide et al. \(2014\)](#) the criteria to determine the LVE region was defined, and the influence of synthesis and characterisation variables in the RTV-SR matrix was studied. Furthermore, in [Agirre-Olabide et al. \(2015\)](#) three matrices were analysed, and the variation of the LVE was studied as a function of synthesis and characterisation variables. Using the LVE region defined in [Agirre-Olabide et al. \(2014; 2015\)](#), in [Agirre-Olabide and Elejabarrieta \(2017\)](#) the shear magneto-viscoelastic properties were studied.

In this summary, the influence of synthesis (matrix, particle content and pre-structure) and characterisation variables (frequency, temperature and magnetic field) in the LVE region are shown, and the linear magneto-thermo-dynamic properties in shear mode are studied as a function of matrix, particle content, pre-structure, frequency, temperature and magnetic field.

### 2.6.1 Linear viscoelastic region

A summary of the results published in ([Agirre-Olabide et al. 2014; 2015](#)) about the analysis of the LVE region of MREs are presented in this subsection.

The influence of the strain in the viscoelastic properties of elastomeric materials is called the Payne effect ([Payne 1962](#)); with an increase in strain, the storage modulus ( $G'$ ) decreases and the loss modulus ( $G''$ ) increases. At low strains (LVE region), the magnetorheological effect is larger ([Jung et al. 2016; Lokander and Stenberg 2003a; Schubert and Harrison 2015](#)) and the properties remain constant; however, at higher strains, the viscoelastic properties depends on the applied amplitude. Figure 2.5 shows the mentioned influence for the RTV-SR matrix with 30% particle content.

In Figure 2.4, can be seen that the LVE limit defined by the loss factor is more restrictive than the LVE region determined by the storage modulus. That is why, all the results shown in this section are related to the loss factor analysis. Nevertheless, the LVE region of the storage modulus is also analysed because in the literature it is the analysed variable to study the linear viscoelasticity. All the LVE limits of the

## 2. Shear magneto-thermo-dynamic characterisation

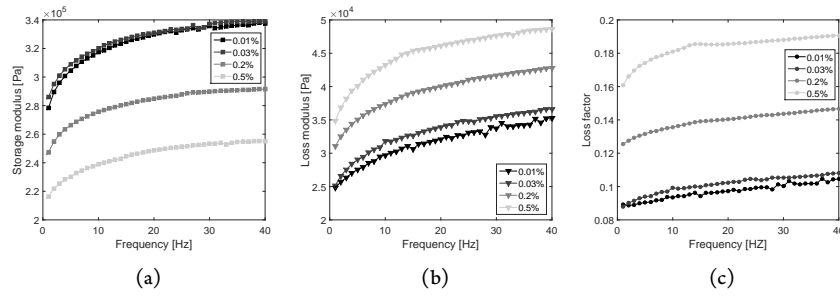


**Figure 2.5** Influence of the strain in the (a) storage modulus ( $G'$ ), loss modulus ( $G''$ ) and (c) loss factor ( $\tan \delta$ ) of the 30% isotropic RTV-SR sample as a function of frequency, at 25 °C and 0 kA/m

analysed variables are shown in Table 1, Table 2 and Table 3 of [Agirre-Olabide et al. \(2015\)](#) in sec. 2.8.

First, the synthesis parameters, i.e. matrix, particle content and pre-structure are analysed. The influence of the matrix is shown in the Figure 2.6, where three matrices are analysed without particles. HTV-SR is the matrix that has the lowest LVE region defined by the loss factor, while the RTV-SR matrix has the largest LVE limit. That is why the softer the matrix, the larger the LVE region.

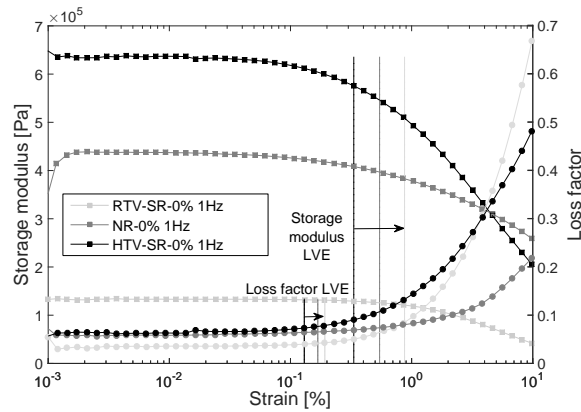


**Figure 2.6** Influence of the matrix in the LVE limit for the 0% particle content, at 25 °C and 1 Hz

The particle content has a large influence in the LVE region. When the particle content is increased, the LVE limit defined by the loss factor is decreased. Moreover, this behaviour is also seen for all the matrices analysed in this thesis (Table 1, Table 2 and Table 3 [Agirre-Olabide et al. \(2015\)](#)). However, the influence of par-

ticle content is dependent on the matrix. When the matrix is softer the influence of particles is greater, hence in this case the influence on the RTV-SR is larger than on the HTV-SR.

The particle distribution is also a variable that has to be taken into account, because anisotropic MREs have the tendency to decrease the LVE region. When the loss factor is analysed at the same particle volume fraction, the anisotropic samples have lower LVE region (Table 1 Agirre-Olabide et al. (2014)).

Characterisation variables such as frequency, magnetic field and temperature also determine the LVE region of each sample. When the frequency is increased, the LVE strain limit defined by the loss factor is also increased; therefore, the increment of frequency increases the LVE region. For the NR and RTV-SR samples and all working conditions (Table 1, Table 2 and Table 3 Agirre-Olabide et al. (2015)) the LVE limit is also increased with the increment of frequency.

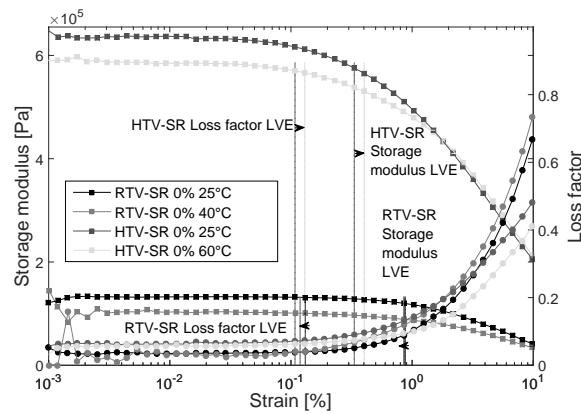


**Figure 2.7** Influence of temperature in the LVE region for the 0% HTV-SR and 0% RTV-SR samples at 1 Hz

The influence of temperature in the LVE region depends on the matrix. Figure 2.7 analyses the influence of temperature. HTV-SR and RTV-SR matrices are analysed without particle content, and two different behaviours can be seen. The loss factor determined that the LVE limit increases for HTV-SR with temperature, whereas RTV-SR sample LVE region is reduced. The reason for this behaviour could be explained by the transition temperature ( $T_g$ ). The matrices studied in this study are working in the rubbery region when the temperature is increased (over the transition temperature (Jones 2001)) because the storage modulus and

the loss factor decrease with the temperature. Therefore, the RTV-SR samples have the higher  $T_g$ , and it is proposed that samples are working close to the  $T_g$  when the temperature is increased. That is why the LVE region is decreased.

The external magnetic field depends on the matrix. Thus, NR and HTV-SR increase the LVE region with increments of the magnetic field. However, the influence on the LVE limit of the RTV-SR samples is not evident.

As a summary of the LVE limits determined by the loss factor, the influence of the synthesis and characterisation variables are shown in Table 2.1.

**Table 2.1** Summary of the influence of synthesis and working conditions in the LVE region of MREs

LVE	RTV-SR	HTV-SR	NR
Particle content	↓	↓	↓
Frequency	↑	↑	↑
External magnetic field	~	↑	↑
Temperature	↓	↑	↑

## 2.6.2 Magneto-dynamic properties

A summary of the results published in [Agirre-Olabide and Elejabarrieta \(2017\)](#) about the analysis of the shear magneto-thermo-dynamic properties are presented in this subsection. Magneto-viscoelastic properties are studied as a function of matrix, particle content, frequency, temperature and external magnetic field.

MRE material are working in the rubbery region because the storage modulus and loss factor increase with frequency (Figure 2.8). Furthermore, when the matrix is stiffer, the energy dissipation is larger. However, the loss factor of softer matrices is more sensitive to frequency.

When the particles are embedded in a matrix, new interactions are created between particles and matrix; consequently, a mechanical reinforcement is created which increases the storage modulus owing to the formation of a physically bonded filler network and to strong polymer-filler couplings ([Aloui and Klüppel 2015](#); [Phewthongin et al. 2006](#)). The energy dissipation also increases with the particle content owing to increased friction between particles ([Ju et al. 2015](#); [Shuib](#)

et al. 2015). The influence of particle content in the loss factor is dependent on the matrix, and the larger influence occurs for the softer matrix. The loss factor of the RTV-SR and NR increases with particle content owing to the particle friction, while the frequency dependence is reduced for the maximum particle content NR samples.

As an example, in Figure 2.8 the influence of temperature (from 15 °C to 65 °C) in the frequency band from 1 to 40 Hz is shown for the 10% RTV-SR sample. The storage modulus and loss factor decrease with the increment of temperature for all the studied samples; this represents the inverse of the frequency effect.

The influence of temperature depends on the particle content. Within the studied temperature ranges, its influence on the storage modulus is larger with the particle content, whereas the influence on the loss factor is decreased. At high particle content levels, the influence of temperature in storage modulus is larger than the frequency one. On the other hand, the loss factor of the studied samples is more sensitive to frequency than to temperature.

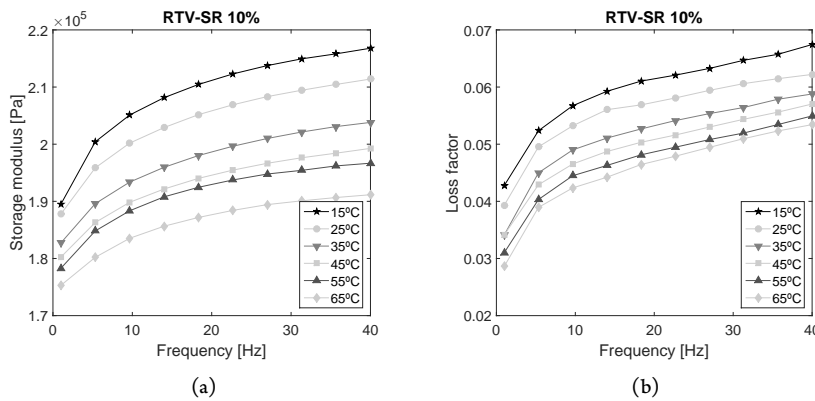


**Figure 2.8** Evolution of (a) the storage modulus ( $G'$ ) and (b) the loss factor ( $\tan \delta$ ) of the 10% isotropic RTV-SR as a function of frequency, with temperature ranging from 15 °C to 65 °C and 0 kA/m

These properties can be modified by applying an external magnetic field. As an example, Figure 2.9 shows the 30% RTV-SR sample. The viscoelastic properties are modified, and the influence on the storage modulus is larger than that on the loss modulus. However, the influence of the magnetic field is completely dependent on the matrix. In the literature, the influence of the magnetic field is studied



by the magnetorheological (MR) effect (equation 2.1). The MR effect increases with particle content but it is more sensitive for the softer matrix, RTV-SR. These results are in agreement with those reported by [Shuib et al. \(2015\)](#) and [Jung et al. \(2016\)](#).

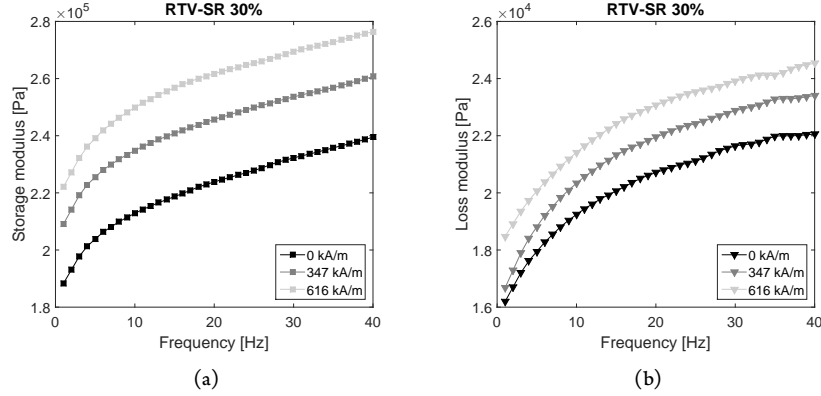


**Figure 2.9** Influence of the magnetic field in the (a) storage ( $G'$ ) and (b) loss modulus ( $G''$ ) as a function of frequency for the 30% isotropic RTV-SR sample at 25 °C

MREs are widely applied as vibration isolators. Therefore, the variation of dissipated energy or loss modulus is studied. The loss modulus MR effect, analogously to the MR effect, is defined as

$$\text{Loss modulus MR effect} = \frac{G''_{\text{H}} - G''_0}{G''_0} \times 100 \quad (2.9)$$

where  $G''_{\text{H}}$  is the loss modulus at a certain magnetic field, and  $G''_0$  is the loss modulus in the absence of a magnetic field. The measurement of the different matrices under the same characterisation conditions indicate that the MR effect and loss modulus MR effect are larger for a softer matrix, which is in agreement with literature ([Yang et al. 2015](#)). To maximise the MR effect and the loss modulus MR effect, RTV-SR-based anisotropic MRE samples were synthesised.

The dynamic properties are modified when a rubber matrix filled with soft magnetic particles is vulcanised under a magnetic field ([Lu et al. 2012](#); [Schubert and Harrison 2015](#)). Both storage and loss modulus increase with particle content and frequency for the anisotropic sample. Particle chains are created in the MRE sample, and consequently, the interaction forces between particles increase, in

turn increasing the storage and loss modulus (Figure 2.10) (Ju et al. 2015). However, the maximum influence of the pre-structure process is seen in the MR effect and loss modulus MR effect. The influence of the magnetic field is larger for anisotropic samples than for isotropic ones (Figure 2.10). The particle interaction magnetic forces are larger for anisotropic samples because particles are aligned, and consequently, the distance between particles decreases. As the particles come closer, the energy dissipation increases owing to the slipping of the particles. The maximum MR effect of 30% and loss modulus MR effect of 21% was obtained with the 30% anisotropic RTV-SR sample.

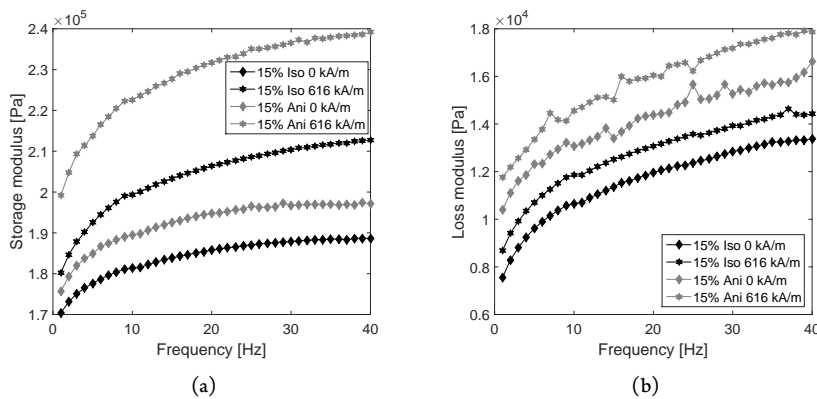


**Figure 2.10** Variation of (a) storage ( $G'$ ) and (b) loss modulus ( $G''$ ) of isotropic and anisotropic 15% RTV-SR samples as a function of frequency owing to the magnetic field at 25 °C

## 2.7 Conclusions

In this chapter, MRE samples were synthesised and characterised under the same conditions. Three matrices, eight volumetric particle contents, and two pre-structures were synthesised, and SEM images validated the mixing and vulcanising process. The linear viscoelastic region was determined and the influence of synthesis and characterisation variables was studied. Using a strain amplitude within the LVE region, the shear magneto-thermo-dynamic properties were analysed.

A new standard procedure to determine the LVE region of MREs was defined, which included the analysis of storage modulus and loss factor. Besides, with that

procedure, the influence of synthesis (matrix, particle content and pre-structure) and characterisation parameters (frequency, temperature and magnetic field) in the shear LVE region was studied. From the storage modulus and loss factor analysis, it was observed that the most restrictive dynamic property to define the LVE region was the loss factor.

The matrix is a key synthesis parameter to determine the LVE limit of the MRE. The softer the matrix, the larger the LVE region of the MRE. Moreover, the LVE region was reduced with the increment of particle content.

Characterisation variables also determined the LVE region of MREs. Frequency increased the LVE region of the MREs in all the analysed working conditions. Furthermore, the magnetic field and the temperature influence depended on the matrix.

The shear magneto-viscoelastic properties of the synthesised MREs were obtained in the LVE region. The storage and loss modulus increased with frequency, while decreased with temperature; this is a typical behaviour of viscoelastic material within the rubbery region.

The storage and loss modulus increased with the particle content for all the studied matrices in shear mode. However, the influence on each matrix was different. At high particle content levels, the influence of temperature in storage modulus was larger than that of frequency. On the other hand, the loss factor of the studied samples was more sensitive to frequency than to temperature.

The MR effect was dependent on the viscoelastic nature of the matrix. Larger MR effects occurs when the matrix was softer. In this chapter, RTV-SR was the softer matrix, and it showed maximum storage and loss modulus MR effect. Therefore, the influence of particle content and external magnetic field in the storage and loss modulus were completely dependent on the matrix.

To maximise the storage and loss modulus MR effect, anisotropic MREs were synthesised with the softer matrix (RTV-SR). Anisotropic samples showed a larger shear storage and loss modulus than isotropic ones. Both were increased when a magnetic field was applied owing to larger particle-particle interaction forces, 30% MR effect and 21% loss modulus MR effect.



## 2.8 Scientific contribution

# Characterization of the linear viscoelastic region of magnetorheological elastomers

*I. Agirre-Olabide, J. Berasategui, M.J. Elejabarrieta and M.M. Bou-Ali*

Mechanical and Manufacturing Department, Mondragon Unibertsitatea, Loramendi 4,  
20500 Arrasate-Mondragon, Spain

Journal of Intelligent Material Systems and Structures


2014 vol. **25**(16) pag. 2074-2081

DOI: 10.1177/1045389X13517310

IF-JCR: 2.072 J. Rank-JCR: 84/260

## Characterization of the linear viscoelastic region of magnetorheological elastomers

Iker Agirre-Olabide, Joanes Berasategui, Maria J Elejabarrieta and M Mounir Bou-Ali

Journal of Intelligent Material Systems and Structures  
2014, Vol. 25(16) 2074–2081  
© The Author(s) 2014  
Reprints and permissions:  
sagepub.co.uk/journalsPermissions.nav  
DOI: 10.1177/1045389X13517310  
jim.sagepub.com  


### Abstract

The linear viscoelastic behaviour of magnetorheological elastomers is analysed in this work according to their formulation and working conditions. This study comprised both the synthesis of different magnetorheological elastomers and the strain and frequency sweep characterization under different magnetic fields and temperatures. The characterization was performed by a Physica MCR 501 rheometer from Anton Paar, equipped with a magnetorheologic cell 70/IT MRD. In the synthesis with a given elastomeric matrix, samples with different magnetic particle content are studied with two types of curing conditions: under the action of a magnetic field (anisotropic magnetorheological elastomers) and without a magnetic field (isotropic magnetorheological elastomers). The working conditions are excitation frequency, temperature and the applied external magnetic field. In this work, a new procedure to determine the linear viscoelastic behaviour is proposed; the loss factor is analysed in addition to analysing the storage modulus to determine the linear viscoelastic region of each sample. The results show that high temperatures and magnetorheological elastomers with higher volume fraction of magnetic particles restrict the linear viscoelastic behaviour of magnetorheological elastomers.

### Keywords

Magnetorheological elastomers, viscoelasticity, linear viscoelastic region, complex shear modulus, loss factor

### Introduction

Magnetorheological elastomers (MREs) are classified as smart materials whose dynamic properties can be reversibly modified and controlled by an external magnetic field. These materials consist of magnetizable particles embedded in a polymeric matrix. The behaviour of MREs is similar to that of magnetorheological fluids (MRFs); whereas MRFs work over the pre-yield regime, MREs work under the named post-yield regime (Carlson and Jolly, 2000).

Magnetizable suspended particles can be homogeneously dispersed in the matrix or aligned in chains. Chain-like structures are obtained by the application of an external magnetic field during the cross-linking processes due to the field-induced interactions created between the particles and are called anisotropic MREs. However, elastomers are called isotropic MREs when they are cured without the influence of an external magnetic field (Li et al., 2008; Varga et al., 2006).

The magneto-dynamic characterization of MREs has been made by dynamic mechanical studies applying oscillating forces. Most of the testing use the double lap shear technique, where a MRE layer is adhesively bonded between three metallic plates (Shen et al., 2004;

Wang et al., 2011). This applied the magnetic field in the perpendicular direction of the shear stress or in the parallel direction of the aligned particle chains. The magnetic field is applied by an electromagnet. Nevertheless, new characterization techniques are used in rheometers, which apply a rotational shear stress instead of applying a linear shear stress. This test has been used to analyse the particle chain orientations, creep and recovery behaviour of MREs, and the influence of external magnetic field on the MRE properties (Boczkowska et al., 2012; Li et al., 2010a).

In the literature, many constitutive models have been developed to predict the behaviour of the MREs at different testing conditions (Li et al., 2010a) and different interactions between the components of MREs (Galipeau and Ponte Castañeda, 2013; Leng et al.,

Mechanical and Manufacturing Department, Mondragon Unibertsitatea, Arrasate-Mondragon, Spain

### Corresponding author:

Maria J Elejabarrieta, Mechanical and Manufacturing Department, Mondragon Unibertsitatea, 20500 Arrasate-Mondragon, Spain.  
Email: mjelejabarrieta@mondragon.edu

2013; Ponte Castañeda and Galipeau, 2011; Shen et al., 2004).

Many materials, such as fluids and polymers, show viscoelastic behaviour. MRFs also show viscoelastic behaviour, and these can be modelled by a complex modulus (Wereley et al., 2006), but the characterization is valid only if the complex modulus is measured within the linear viscoelastic (LVE) region. The elastic limit yield stress is defined as the point at which the storage modulus deviates significantly from the plateau value in the LVE range.

However, Laun et al. (2010) defined a LVE region for low-strain amplitudes. MRF response is predominantly elastic in the small-amplitude region, and at large shear amplitudes, the predominant response is viscous.

Similar to MRFs, MREs work at the LVE region at low deformations. Li et al. (2010b) developed a four-parameter model to describe the performance of the MREs. Besides, a rheological model is defined to predict the dynamic behaviour of MREs, which models the viscoelasticity of the polymer, magnetic field-induced properties and interfacial slippage between matrix and particles (Chen and Jerrams, 2011). To determine the LVE region, Gordaninejad et al. (2012) defined a linear elastic deformation at 1% of strain, because at high strains, MRE has a nonlinear behaviour due to the nonlinear behaviour of the compression and shear modulus.

The aim of this work is to study the LVE region limit for MREs in different compositions, pre-structure and working conditions. Besides, the influence of the synthesis and the characterization variables in the LVE limit, such as particle content, the particle structure (isotropic and anisotropic), frequency, external magnetic field and temperature is studied for the first time. Oscillatory tests are used to obtain the dynamic properties of the MREs, and the viscoelastic behaviour is modelled by the dynamic complex modulus (Jones, 2001). In the literature, the storage modulus was analysed to determine the LVE limit; this work defines a new procedure to analyse both the loss factor and the storage modulus to determine the LVE region of each sample under the mentioned conditions.

### MRE synthesis

In this study, the MRE samples are compounded by a paramagnetic matrix, a vulcanizer and ferromagnetic particles. The matrix used is the silicone WACKER ELASTOSIL® M 4644 A and the vulcanizer WACKER ELASTOSIL® M 4644 B, both are mixed in the ratio 10:1 respectively.

Spherical carbonyl-iron powder particles are embedded in the matrix with an average particle size of  $1.25 \pm 0.55 \mu\text{m}$  (Figure 1). The carbonyl-iron particles

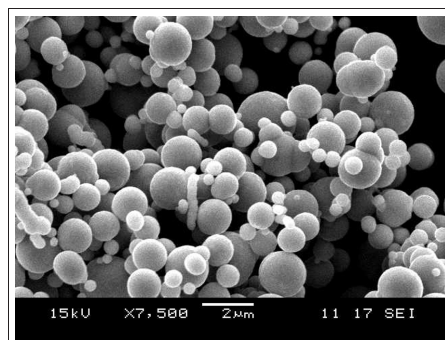


**Figure 1.** SEM image of the carbonyl-iron powder particles. SEM: scanning electron microscope.

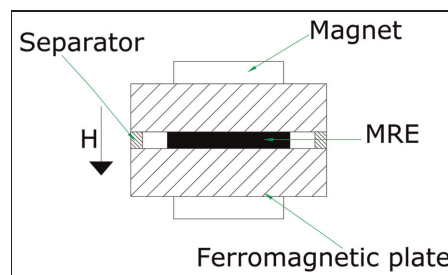


**Figure 2.** Sketch of the anisotropic pre-structure device. MRE: magnetorheological elastomer.

are supplied by BASF, the chemical company, Germany.

The synthesis process consists of blending the particles and the matrix. After all, vacuum cycles are applied to the homogeneous mixture for 30 min. Subsequently, the vulcanizer is added, and the vacuum cycles are repeated at the same conditions. The cycle quantity varies with the particle volume fraction.

In this work, two pre-structure conditions are studied: under an external magnetic field (anisotropic MRE) and without its influence (isotropic MRE).

Anisotropic samples have been pre-structured by a device where neodymium magnets are applied (Figure 2). The device guarantees a homogeneous magnetic flux because of the ferromagnetic plates. The mentioned field is applied along the thickness of the sample (Varga et al., 2006). The intensity of the field during the pre-structure is  $0.13 \pm 0.01 \text{ T}$  and is measured by a Gaussmeter FH-54.

The maximum volume fraction of particles is estimated at 30% from equation (1), known as critical particle volume concentration (CPVC), which is

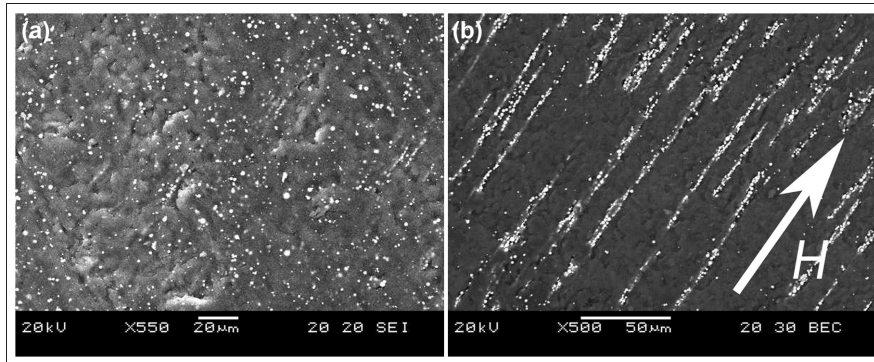


**Figure 3.** SEM images of MREs with carbonyl-iron particles: (a) isotropic MRE and (b) anisotropic MRE. White arrows indicate magnetic field direction.  
SEM: scanning electron microscope; MRE: magnetorheological elastomer.

independent of the type of matrix (Lokander and Stenberg, 2003)

$$CPVC = \frac{100 \times \rho_{app}}{\rho_{Fe}} \quad (1)$$

where  $\rho_{app}$  is the apparent density of the carbonyl-iron powder particles, the ratio between the volume (including the voids or pores which may contain) and its real weight, and  $\rho_{Fe}$  is the density of the iron, 2400 and 7800 kg/m<sup>3</sup>, respectively.

Three particle volume fractions are synthesized: minimum of 0%, maximum of 30% and an intermediate one of 10%. Two pre-structure conditions are used to obtain isotropic and anisotropic samples.

The nomenclature used in this work to define each sample is as follows: first of all, the particle content is defined and after this the pre-structure, for example, 10%\_0.13T, which means that the sample has 10% of carbonyl-iron powder particles and the pre-structure condition was 0.13 T of constant magnetic field.

Finally, scanning electron microscope (SEM) images are used to guarantee the homogeneous particle distribution for isotropic samples and the particle chain structures for anisotropic MREs. The images are obtained by a SEM of low vacuum and microanalysis, JEOL JSM 5600 LV, and with a voltage acceleration of 20 kV. Figure 3(a) shows an isotropic MRE sample where the particle distribution is homogeneous, and in Figure 3(b), the particle chain structure is observed, aligned in the magnetic field direction.

### MRE characterization

Viscoelastic materials, similar to MREs, could work within the LVE region or at the non-LVE region (Jones, 2001). This work studies the LVE region

variations due to the particle content, frequency, external magnetic field, the pre-structure of the samples and the temperature. The rheological test used to define the LVE region was a strain sweep using oscillatory rheometry. Once the LVE region limit is defined, the dynamic properties of the MREs are studied within the linear region and in the nonlinear region to show the influence of the LVE limit on the dynamic properties.

The results in this study were obtained using an Anton Paar Physica MCR 501 rheometer equipped with the MRD 70/1T magnetorheological cell and the parallel disc configuration. The parallel disc diameter was 20 mm (PP20/MRD/TI/P2). The magnetic field goes from the minimum intensity of 0 kA/m to a maximum of 616.7 kA/m. After each characterization, a demagnetization cycle was applied.

The frequency range goes from 1 to 40 Hz, and the temperatures analysed were 25 °C, 30 °C and 40 °C controlled with water-based heating/cooling system Julabo F-25. Moreover, a 3 N constant normal force was applied to avoid slipping between the sample and the plates.

Strain sweep tests control the applied strain to the sample and measure the shear stress at a constant frequency. Assuming that the analysed MRE samples had a linear behaviour, the strain is harmonic (equation (2)), and the stress is also harmonic but with a given phase difference with respect to the strain (equation (3))

$$\gamma(t) = \gamma_{max} \cdot e^{j\omega t} \quad (2)$$

$$\tau(t) = \tau_{max} \cdot e^{j(\omega t + \delta)} \quad (3)$$

where  $\gamma_{max}$  is the amplitude of the shear strain,  $\tau_{max}$  is the amplitude of the shear stress and the constant  $\delta$  is



the phase difference between the strain and stress. Both are used to obtain the shear complex modulus

$$G^* = \frac{\tau(t)}{\gamma(t)} = \frac{\tau_{\max} \cdot e^{j(\omega t + \delta)}}{\gamma_{\max} \cdot e^{j\omega t}} = \frac{\tau_{\max}}{\gamma_{\max}} (\cos \delta + j \sin \delta) \quad (4)$$

The shear complex modulus consists of a real part, the storage modulus or the rigidity ( $G'$ ), and an imaginary part, loss modulus or the energy dissipation ( $G''$ )

$$G' = \frac{\tau_{\max}}{\gamma_{\max}} \cos \delta \quad (5)$$

$$G'' = \frac{\tau_{\max}}{\gamma_{\max}} \sin \delta \quad (6)$$

The loss factor ( $\tan \delta$ ) is the relation between the loss modulus and the storage modulus (equation (7))

$$\tan \delta = \frac{G''}{G'} \quad (7)$$

At the LVE region, the storage modulus and the loss factor are independent of the strain (Figure 4) (Nashif et al., 1985). Wereley et al. (2006) determined the elastic limit yield stress for MRF as the point where the storage modulus deviates 10% from the plateau value. Laun et al. (2010) develop a MRF model taking into account the storage and the loss modulus at the linear and nonlinear regions.

In this work, both the storage modulus and the loss factor deviation are studied to define the LVE region. First of all, a criterion to define the LVE region of the storage modulus and the loss factor is established. A straight line with a null slope is defined by the method of the least squares for both the storage modulus and the loss factor. Next, the limit of the LVE region is defined as the point where the storage modulus and the loss factor deviate 10% from the approximated straight line according to Wereley et al. (2006) (Figure 4).

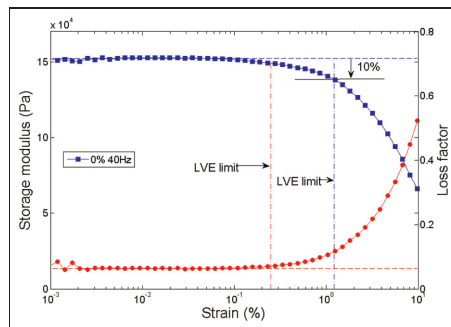


Figure 4. Storage modulus (■) and loss factor (●) versus strain to define the LVE region. LVE: linear viscoelastic.

To perform LVE region characterization, 50 points are defined from 0.001% to 10% logarithmically spaced, and at each point, measurements were made for 5 s. This logarithmic scale allows covering a wider range of deformations. These tests were made at two frequencies which limit the interest frequency band, 1 and 40 Hz.

Once the LVE region is defined, the dynamic properties of MREs are studied using the frequency sweep tests. There were 40 points measured from 1 to 40 Hz linearly spaced, and each point was measured for 5 s. As an example, the characterized sample was 30%\_0.13T at a constant temperature of 25 °C, and two strain amplitudes were analysed within the LVE region and a strain amplitude in the nonlinear region, even if a LVE behaviour is assumed in the nonlinear zone to define the storage modulus and loss factor.

## Results

The LVE region depends on the particle volume fraction, pre-structure, frequency, external magnetic field and temperature. First of all, an experimental inherent error is defined by the experimental strain sweep test and the sample type. This way, the repeatability of the test is shown in Figure 5, where the storage modulus and the loss factor are represented for the 0% sample at a frequency of 40 Hz. The storage modulus has a 3% relative error, and the loss factor has a 5% relative error.

After the relative error of the test is defined, the LVE region of the specimens is analysed as a function of the particle content, pre-structure, frequency, external magnetic field and temperature. The more representative LVE limit of the storage modulus and the loss factor for all the samples as a function of the analysed variables is given in the Table 1 at 25 °C, 30 °C and 40 °C.

The LVE region defined by the loss factor is more restrictive than the region defined by the storage

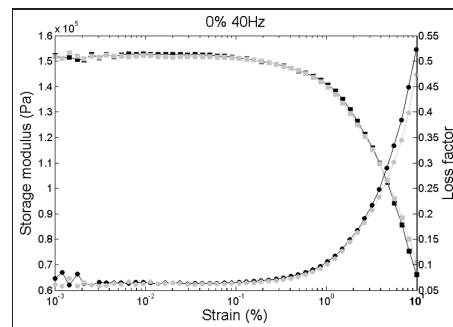


Figure 5. Repeatability of the 0%\_0T sample at 40 Hz. Storage modulus (■) and the loss factor (●) versus strain.

Table 1. LVE regions of the storage modulus and loss factor as a function of the synthesis, frequency, magnetic field and temperature.

Storage modulus	25°C						30°C						40°C					
	Sample		0 kA/m		616.7 kA/m		Sample		0 kA/m		616.7 kA/m		Sample		0 kA/m		616.7 kA/m	
	1 Hz	40 Hz	1 Hz	40 Hz	1 Hz	40 Hz	1 Hz	40 Hz	1 Hz	40 Hz	1 Hz	40 Hz	1 Hz	40 Hz	1 Hz	40 Hz	1 Hz	40 Hz
Storage modulus	0%_0T	1.220	0.874	0.524	0.640	0.833	0.879	0%_0T	0.833	0.879	0.511	0.427	0.560	0%_0T	0.850	1.141	0.331	0.412
	10%_0T	0.485	0.524	0.524	0.640	0.419	0.511	10%_0T	0.419	0.511	0.427	0.560	10%_0T	0.454	0.561	0.331	0.412	
	10%_0.13T	0.430	0.436	0.530	0.396	0.390	0.434	10%_0.13T	0.390	0.434	0.470	0.389	10%_0.13T	0.333	0.350	0.340	0.374	
	30%_0T	0.157	0.148	0.189	0.190	0.158	0.155	30%_0T	0.158	0.155	0.162	0.163	30%_0T	0.208	0.153	0.156	0.186	
Loss factor	0%_0T	0.108	0.100	0.125	0.105	0.121	0.121	0%_0T	0.121	0.121	0.132	0.115	0%_0.13T	0.112	0.095	0.112	0.096	
	10%_0T	0.112	0.251	0.086	0.146	0.131	0.153	10%_0T	0.131	0.153	0.087	0.116	10%_0T	0.138	0.184	0.040	0.116	
	10%_0.13T	0.106	0.165	0.086	0.118	0.072	0.212	10%_0.13T	0.072	0.212	0.050	0.150	10%_0.13T	0.058	0.114	0.049	0.150	
	30%_0T	0.074	0.088	0.075	0.063	0.076	0.088	30%_0T	0.076	0.088	0.064	0.074	30%_0T	0.069	0.080	0.064	0.074	
LVE: linear viscoelastic.	0%_0T	0.076	0.067	0.091	0.062	0.057	0.078	0%_0.13T	0.057	0.078	0.051	0.056	0%_0.13T	0.057	0.054	0.029	0.042	
	10%_0T	0.112	0.251	0.086	0.146	0.131	0.153	10%_0T	0.131	0.153	0.087	0.116	10%_0T	0.138	0.184	0.040	0.116	
	10%_0.13T	0.106	0.165	0.086	0.118	0.072	0.212	10%_0.13T	0.072	0.212	0.050	0.150	10%_0.13T	0.058	0.114	0.049	0.150	
	30%_0T	0.074	0.088	0.075	0.063	0.076	0.088	30%_0T	0.076	0.088	0.064	0.074	30%_0T	0.069	0.080	0.064	0.074	

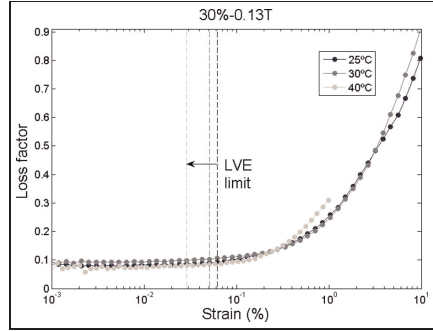


Figure 6. Influence of the temperature on the loss factor LVE limit of the 30%\_0.13T sample. LVE: linear viscoelastic.

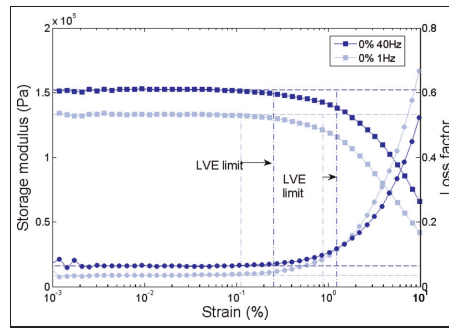
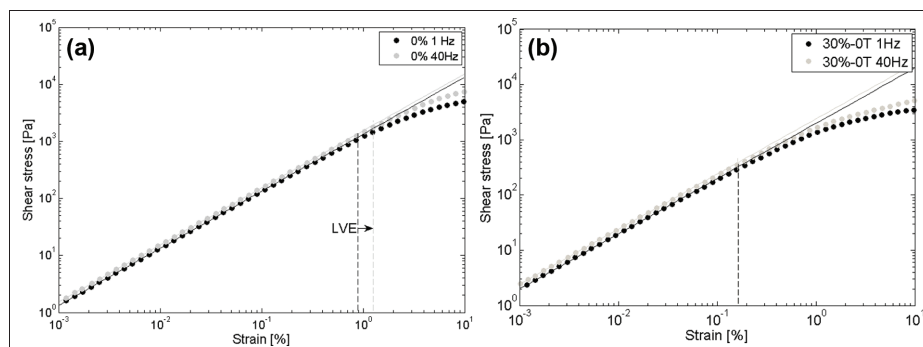


Figure 7. LVE region limit increment due to the frequency for the 0%\_0T sample storage modulus (■) and the loss factor (●) versus strain. LVE: linear viscoelastic.

modulus (Figure 4). However, the storage modulus LVE region is also analysed. The LVE region is reduced with the increment of the particle content independent of the frequency, external magnetic field and pre-structure for both the storage modulus and the loss factor (Table 1). As Phewthongin et al. (2006) said, the matrix (chlorinated polyethylene/natural rubber matrix) is reinforced by the particles (silica particles) due to the physical interactions between particle and matrix, and therefore, the LVE region is reduced. The temperature is another variable that limits the LVE region, because the temperature increase reduced the LVE region (Figure 6). That decrease is a typical behaviour of an elastomeric matrix (Jones, 2001).

Table 1 shows the LVE regions of the storage modulus and loss factor as a function of the synthesis, frequency, magnetic field and temperature. Figure 7 shows the increment of the LVE region when the frequency is



**Figure 8.** Shear stress–strain diagrams at 1 and 40 Hz for the (a) 0%<sub>0T</sub> sample and (b) 30%<sub>0T</sub> sample. LVE: linear viscoelastic.

raised up (Nashif et al., 1985). Isotropic MRE sample shows that tendency, but for anisotropic MREs, it is not a predominant trend.

The LVE limit can also be obtained from the stress–strain diagrams. For it, the same criterion defined previously is used, and to define the linear function parameters, the least-squares method is performed. In Figure 8(a), the shear stress–strain diagram of the 0%<sub>0T</sub> sample is shown, where the LVE region is broader with the increment of the frequency. However, in Figure 8(b), the stress–strain diagram of the 30%<sub>0T</sub> sample, the influence of the frequency is not appreciated. Therefore, the particle content increment reduces the LVE limit, which can be seen in Figure 8, and diminishes the influence of the frequency. The LVE limits defined in the strain–stress diagram are similar to the LVE limits defined by the storage modulus in Table 1.

The pre-structure is also a variable that has to be taken into account, because anisotropic MRE has the tendency to decrease the LVE. When the loss factor is observed at the same particle volume fraction, the anisotropic samples have lower LVE region (Table 1).

Finally, the external magnetic field tends to reduce the LVE region. Table 1 shows that the limit of the LVE region is limited by the maximum volume fraction of anisotropic sample when it works at the maximum temperature under magnetic field and at the lowest frequency.

Once the LVE region is defined, a frequency sweep test is done to determine the importance of the LVE region limit. As an example, the 30%<sub>0.13T</sub> sample is tested at 25 °C, so that the LVE region limit is 0.06 which is defined in Table 1. Therefore, the strain amplitude used is 0.01% and 0.05% within the LVE region, and 0.1% and 1% in the nonlinear region, assuming a viscoelastic behaviour for the storage modulus and the

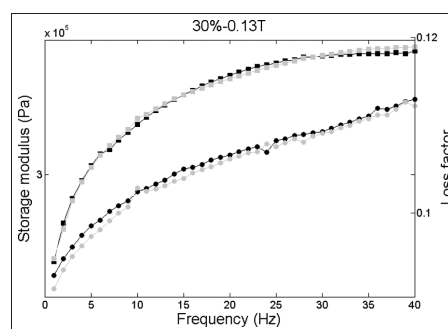
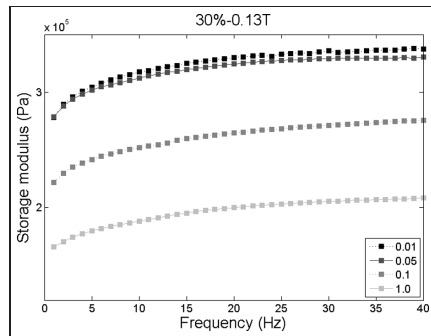


**Figure 9.** Repeatability of the frequency sweep test for the 30%<sub>0.13T</sub> sample. Storage modulus (■) and the loss factor (●) versus frequency at 0.05% strain amplitude.

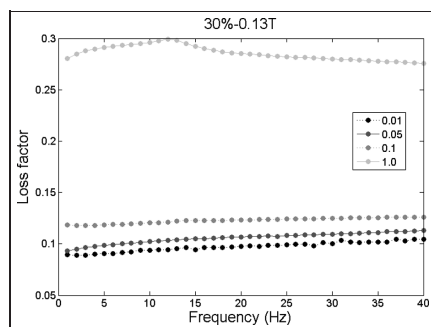
loss factor. The repeatability is analysed (Figure 9) where the error is less than 1% for the storage modulus and less than 2% for the loss factor.

Figure 10 shows that within the LVE region, the storage modulus is linear, and there is a variation of 2% at all the frequency ranges when the strain amplitudes are lower than the LVE limit, which is in accordance with Gordaninejad et al. (2012). However, when the strain amplitude is out of the LVE region, the storage modulus decreases 23% with the increment of the strain from 0.05% to 0.1%. The rigidity reduction is 63% when the strain increases from 0.05% to 1.0%, which is in accordance with the reports by Popp et al. (2010) in the nonlinear region.

The loss factor also varies with the strain amplitude (Figure 11). When the amplitude is within the LVE region, the variation is of 8%. Nonetheless, an amplitude higher than the LVE region limit increases the loss



**Figure 10.** Influence of the LVE on the storage modulus of the 30%-0.13T sample.  
LVE: linear viscoelastic.



**Figure 11.** Influence of the LVE on the loss factor of the 30%-0.13T sample.  
LVE: linear viscoelastic.

factor to 15% with an amplitude of 0.1%. On the other hand, an increment of 63% is observed in the loss factor when the strain amplitude is 1.0%.

## Conclusion

A new standard procedure to determine the LVE region of MREs has been defined, which includes the analysis of the storage modulus and the loss factor. Besides, with that procedure, the influence of the composition and pre-structure, and the test parameters on the LVE is studied. From the storage modulus and loss factor analysis, it is observed that the most restrictive dynamic property to define the LVE region is the loss factor. Independently of the frequency, external magnetic field and the pre-structure, the LVE region is reduced with the increment of the particle volume fraction and the

temperature. The dynamic properties of the MREs are independent of the strain in the strain range lower than the limit established by the LVE. Hence, the LVE region limit has to be defined to predict the linear behaviour of the MREs.

## Declaration of conflicting interests

The authors declare that there is no conflict of interests.

## Funding

The authors gratefully acknowledge the finance obtained from the Department of Education of the Basque Government, for the Project ACTIMAT, UE2013-09 and IT557-10, and the finance obtained from the Spanish Government for the project Non-Orientated Fundamental Investigation DPI2012-36366.

## References

- Boczkowska A, Awietjan SF, Pietrzko S, et al. (2012) Mechanical properties of magnetorheological elastomers under shear deformation. *Composites Part B: Engineering* 43(2): 636–640.
- Carlson JD and Jolly MR (2000) MR fluid, foam and elastomer devices. *Mechatronics* 10(4): 555–569.
- Chen L and Jerrams S (2011) A rheological model of the dynamic behavior of magnetorheological elastomers. *Journal of Applied Physics* 110(1): 013513.
- Galipeau E and Ponte Castañeda PP (2013) A finite-strain constitutive model for magnetorheological elastomers: magnetic torques and fiber rotations. *Journal of the Mechanics and Physics of Solids* 61(4): 1065–1090.
- Gordaninejad F, Wang X and Mysore P (2012) Behavior of thick magnetorheological elastomers. *Journal of Intelligent Material Systems and Structures* 23(9): 1033–1039.
- Jones DIG (2001) *Handbook of Viscoelastic Vibration Damping*. Chichester: John Wiley & Sons.
- Laun HM, Gabriel C and Kieburg Ch (2010) Magnetorheological fluid in oscillatory shear and parameterization with regard to MR device properties. *Journal of Intelligent Material Systems and Structures* 21(15): 1479–1489.
- Leng D, Sun L, Sun J, et al. (2013) *Derivation of Stiffness Matrix in Constitutive Modeling of Magnetorheological Elastomer*. Bristol: IOP Publishing Ltd.
- Li J, Gong X, Xu Z, et al. (2008) The effect of pre-structure process on magnetorheological elastomer performance. *International Journal of Materials Research* 99(12): 1358–1364.
- Li WH, Zhou Y, Tain TF, et al. (2010a) Creep and recovery behaviors of magnetorheological elastomers. *Frontiers of Mechanical Engineering in China* 5(3): 341–346.
- Li WH, Zhou Y and Tian TF (2010b) Viscoelastic properties of MR elastomers under harmonic loading. *Rheologica Acta* 49(7): 733–740.
- Lokander M and Stenberg B (2003) Performance of isotropic magnetorheological rubber materials. *Polymer Testing* 22(3): 245–251.
- Nashif AD, Jones DIG and Henderson JP (1985) *Vibration Damping*. New York: John Wiley & Sons.

- Phewthongin N, Saeoui P and Sirisinha C (2006) Rheological behavior of CPE/NR blends filled with precipitated silica. *Journal of Applied Polymer Science* 100(4): 2565–2571.
- Ponte Castañeda P and Galipeau E (2011) Homogenization-based constitutive models for magnetorheological elastomers at finite strain. *Journal of the Mechanics and Physics of Solids* 59(2): 194–215.
- Popp KM, Zhang XZ, Li WH, et al. (2010) MRE properties under shear and squeeze modes and applications. *Journal of Intelligent Material Systems and Structures* 21(15): 1471–1477.
- Shen Y, Golnaraghi MF and Heppler GR (2004) Experimental research and modeling of magnetorheological elastomers. *Journal of Intelligent Material Systems and Structures* 15(1): 27–35.
- Varga Z, Filipcsei G and Zrinyi M (2006) Magnetic field sensitive functional elastomers with tuneable elastic modulus. *Polymer* 47(1): 227–233.
- Wang X, Ge HY and Liu HS (2011) Study on epoxy based magnetorheological elastomers. *Advanced Materials Research* 306–307: 852–856.
- Wereley NM, Chaudhuri A, Yoo J-H, et al. (2006) Bidisperse magnetorheological fluids using Fe particles at nanometer and micron scale. *Journal of Intelligent Material Systems and Structures* 17(5): 393–401.



# Matrix dependence of the linear viscoelastic region in magnetorheological elastomers

*I. Agirre-Olabide, M.J. Elejabarrieta and M.M. Bou-Ali*

Mechanical and Manufacturing Department, Mondragon Unibertsitatea, Loramendi 4,  
20500 Arrasate-Mondragon, Spain

Journal of Intelligent Material Systems and Structures

2015 vol. **26**(14) pag. 1880-1886

DOI: 10.1177/1045389X15580658

IF-JCR: 1.975 J. Rank-JCR: 105/271

## Matrix dependence of the linear viscoelastic region in magnetorheological elastomers

Journal of Intelligent Material Systems and Structures  
2015, Vol. 26(14) 1880–1886  
© The Author(s) 2015  
Reprints and permissions:  
sagepub.co.uk/journalsPermissions.nav  
DOI: 10.1177/1045389X15580658  
jim.sagepub.com  


Iker Agirre-Olabide, Maria Jesus Elejabarrieta and M Mounir Bou-Ali

### Abstract

The aim of this work is to study the linear viscoelastic region limit of isotropic magnetorheological elastomers at different compositions and working conditions. Regarding the synthesis process, the matrix and the particle content are analysed. The analysed matrixes are a natural rubber, a silicone rubber and ELASTOSIL<sup>®</sup> silicone, and three particle contents are synthesised. The influence of the characterisation variables on the linear viscoelastic limit, that is, frequency, external magnetic field and temperature, is also analysed. Strain sweep tests are used to determine the dynamic complex modulus. The loss factor and the storage modulus are analysed to define the linear viscoelastic limit of each isotropic magnetorheological elastomer sample in all the working conditions. The results show that the linear viscoelastic region of the magnetorheological elastomers is defined by the loss factor. Moreover, the volumetric particle content reduces and frequency increases the linear viscoelastic region of all the matrixes, whereas the external magnetic field and the temperature influences are matrix dependent.

### Keywords

Magnetorheological elastomers, matrix, viscoelasticity, linear viscoelastic, complex shear modulus

### Introduction

Magnetorheological elastomers (MREs) are considered as smart materials because they have the ability to vary their dynamic properties when a magnetic field is applied, due to the particles embedded in the matrix. The MR effect is the variation of the storage modulus, when an external magnetic field is applied (Lokander and Stenberg, 2003a; Yu et al., 2012). This effect is influenced by the matrix because a softer matrix has a larger MR effect (Popp et al., 2008). Furthermore, the effect is larger for samples with larger particle content up to a limit of around 30% volumetric content, depending on the particle size (Gong et al., 2007; Lokander and Stenberg, 2003a). Temperature and strain are also decisive for the dynamic properties of MREs (Lokander and Stenberg, 2003a; Zhang et al., 2011). The MR effect is dependent on strain and thus larger at small strain amplitudes (Lokander and Stenberg, 2003a).

The characterisation of MREs is performed by oscillatory movements, such as shear or compression movements. The shear movement can be rotational or linear where the external magnetic field is perpendicular to the movement. These techniques have been used to determine the properties of the MREs and the influence of

pre-structure, creep and recovery, and external magnetic field (Boczkowska et al., 2012; Li et al., 2010).

The viscoelastic behaviour of MREs can be described by the complex modulus in the frequency domain (Wereley et al., 2006). The complex modulus is valid for the linear viscoelastic (LVE) region, which is defined by the LVE limit. The limit is determined at the point where the  $G'$  and  $G''$  become dependent on the strain. Tian et al. (2013) analysed the LVE region of isotropic MREs, for which they used stress–strain curves and also storage modulus–strain curves. They conclude that particle content decreases the LVE region of the MRE materials. When the storage modulus is dependent on strain, it decreases with the increment of strain, a behaviour called the Payne effect (Payne, 1962). Bellan and Bossis (2002) showed that for MRE with large particle content, the Payne effect becomes larger.

Mechanical and Manufacturing Department, Mondragon Unibertsitatea, Arrasate-Mondragon, Spain

### Corresponding author:

Maria Jesus Elejabarrieta, Mechanical and Manufacturing Department, Mondragon Unibertsitatea, Loramendi 4, 20500 Arrasate-Mondragon, Spain.

Email: mjelejabarrieta@mondragon.edu



The LVE region of MRE isotropic samples is reduced with the increment of the external magnetic field (Tian et al., 2013). To determine the LVE region, Gordaninejad et al. (2012) defined a linear elastic deformation at 1% of strain, because at high strains, MRE has a non-linear behaviour due to the non-linear behaviour of the compression and shear modulus. Moreover, Agirre-Olabide et al. (2014) defined the LVE region of a silicone rubber MRE at 0.029%, which is determined by the loss factor.

Due to the importance of the LVE region, the LVE region of three different elastomers with three volumetric particle contents in different working conditions is analysed in this work. The matrixes analysed are a natural rubber and two silicone rubber containing Carbonyl Iron Powder (CIP) spherical particles with an average particle size of  $1.25 \pm 0.55 \mu\text{m}$ . One of the silicones is based on two components, the matrix and the vulcaniser, and vulcanises at room temperature; the other is vulcanised at high temperature. The analysed synthesis variables are the matrix and the particle content, and the characterisation variables are frequency, external magnetic field and temperature. An oscillatory rotational shear test is performed to define the LVE region of each sample in all working conditions. The viscoelastic behaviour of isotropic MREs is modelled by the dynamic complex modulus (Jones, 2001), and the loss factor is analysed to define the LVE limit; furthermore, the storage modulus is also analysed in relation to the work published in the literature.

### Isotropic MRE synthesis

The three different isotropic matrixes analysed in this work are two types of silicone rubber and a natural rubber. The difference between the types of silicone rubber lies in the degrees of softness and also the vulcanisation process. One of the types of silicone rubber is the silicone WACKER ELASTOSIL® M 4644 A and the vulcaniser WACKER ELASTOSIL® M 4644 B, mixed to a ratio of 10:1, respectively, which vulcanises at room temperature. The vulcanisation of the other silicone rubber, NE-9340, and the natural rubber takes place at a high temperature, 180°C.

The particles embedded in the matrix are spherical CIP particles. The average particle size is  $1.25 \pm 0.55 \mu\text{m}$  and particles are supplied by BASF, The Chemical Company.

The synthesis process also depends on the matrix. The process of the silicone rubber that vulcanises at room temperature, ELASTOSIL, is considered next. First, the particles and the main matrix are mixed and vacuum cycles are subsequently applied for 30 min to remove the air bubbles generated during the mixing. After this, the vulcaniser is mixed and again vacuum

cycles are applied for 30 min to remove the air bubbles. The number of cycles depends on the particle content. Then, the mixture is poured into a 1-mm-thick mould to obtain a sample of 1-mm thickness, and after 12 h, the samples are vulcanised.

On the other hand, the mixing process for silicone rubber and natural rubber is different. For the mixture, a two-roll mixing mill is used, and the particle content is added gently to guarantee a homogeneous mix. Then the mixture is poured into a 1-mm-thick mould and is placed in an oven at 180°C and with a compression pressure of 200 bar for 10 min.

The maximum particle content analysed in this work is 30% volumetric content and is defined by the critical particle volume concentration (CPVC) criterion (Lokander and Stenberg, 2003b). This criterion is independent of the matrix. Three volumetric particle contents are synthesised in this work for each matrix. The maximum particle content is 30% and the minimum is 0% for the three matrixes. An intermediate particle content of 10% is also defined for the ELASTOSIL matrix and 15% for silicone and natural rubber.

### MRE characterisation

MRE materials could work within the LVE region or at the non-linear region as viscoelastic materials (Jones, 2001). The results of this study were obtained using an Anton Paar Physica MCR 501 rheometer equipped with the MRD 70/IT magnetorheological cell and the parallel disc configuration. The parallel disc diameter was 20 mm (PP20/MRD/TI/P2). The magnetic field intensities range from the minimum of 0 kA/m to the maximum of 616.7 kA/m. After each test, demagnetisation cycles are applied to guarantee the same initial conditions for each test. The analysed frequencies are 0 and 40 Hz. One of the assumptions in the LVE theory is that the inertia forces of the sample are negligible in the oscillatory shear deformation. According to Ferry (1980), the inertia force will be small if the density  $\rho$  is small compared with  $G'/h^2\nu^2$ , where  $h$  is the thickness of the sample and  $\nu$  is the oscillatory frequency in hertz. This criterion is equivalent to saying that the sample thickness is small compared with the wavelength of a shear wave propagated through the medium (1)

$$\rho \ll \frac{G'}{h^2\nu^2} \quad (1)$$

Therefore, in this work, the thickness of the sample is 1 mm and the highest frequency is 40 Hz. Moreover, the more critical situation would be the sample which has the lowest storage modulus; hence, the studied situation is the ELASTOSIL sample at 40 Hz and 40°C with a storage modulus of 110,000 Pa. The density of the samples is 1070 Kg/m<sup>3</sup>

$$1070 \text{ kg/m}^3 \ll \frac{110,000}{0.001^2 40^2} = 6875,000 \text{ kg/m}^3 \quad (2)$$

From equation (2), we concluded that the inertia forces are negligible.

Temperatures are 25°C for all samples, 40°C for the ELASTOSIL and 60°C for the silicone and natural rubber. These are controlled with a water-based heating/cooling system Julabo F-25. To avoid slipping between the samples and the plates and to increase the MR effect (Dong et al., 2012), a normal force of 3 N is defined.

When the test is running, the controlled parameter is the strain, and consequently, the shear stress is measured at a constant frequency. The strain sweep test is performed to determine the LVE limit of each sample and conditions. For the strain sweep test, a logarithmic slope is defined and ranges from 0.001% to 10%; 50 points are measured and for each point, 5 s are measured.

However, to determine the limit of each sample and condition, the shear dynamic complex modulus has to be defined. Assuming that the behaviour of the analysed MRE is linear, the strain is harmonic, and consequently, the stress is also harmonic, but with a given phase difference (3). Both are used to obtain the shear dynamic complex modulus ( $G^*$ ) (Ferry, 1980)

$$G^* = \frac{\tau_{\max} \cdot e^{j(\omega t + \delta)}}{\gamma_{\max} \cdot e^{j\omega t}} = \frac{\tau_{\max}}{\gamma_{\max}} (\cos \delta + j \sin \delta) \quad (3)$$

where  $\gamma_{\max}$  is the amplitude of the shear strain,  $\tau_{\max}$  is the amplitude of shear stress and  $\delta$  is the phase difference between the strain and stress. The shear complex modulus is composed of a real part or storage modulus ( $G'$ ) and an imaginary part or loss modulus ( $G''$ ). The relation between both is the loss factor ( $\tan \delta$ ).

Once the complex modulus is defined, the LVE limit is defined. Within the linear region, the storage modulus and the loss factor are constant (Nashif et al., 1985). Gordaninejad et al. (2012) defined a limit when the strain–stress relation becomes non-linear at 1% of strain. Moreover, Wereley et al. (2006) define the LVE limit for magnetorheological fluids (MRFs) at the point where the storage modulus deviates 10% from the plateau value. However, Laun et al. (2010) analysed the storage and the loss modulus to define the linear and non-linear regions of the magnetorheological models for the MRF.

In this work, the loss factor and the storage modulus are analysed (Agirre-Olabide et al., 2014). For this purpose, a straight line is approached for each ( $G'$  and  $\tan \delta$ ), and the LVE limit is defined at the point where the experimental data deviate 10% from the approached straight line (Mezger, 2006) (Figure 1). In all the figures of this work, the same criterion is used to define the storage modulus (■) and the loss factor (●).

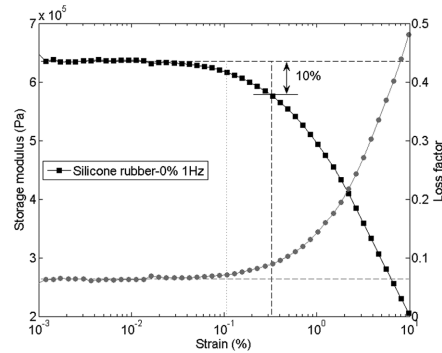


Figure 1. LVE criterion for the silicone rubber without particles and at 1 Hz.

## Results

The LVE region is dependent on the synthesis and the working conditions, such as matrix, particle content, frequency, the external magnetic field and temperature. The loss factor and the storage modulus of each sample at all working conditions are analysed.

In Figure 1, it can be seen that the LVE limit defined by the loss factor is more restrictive than the LVE region determined by the storage modulus. That is why all the results shown in this work are related to the loss factor analysis. Nevertheless, the LVE region of the storage modulus is also analysed because in the literature it is the analysed variable to study linear viscoelasticity. All the LVE limits in all the analysed variables are shown in Tables 1 to 3.

First, the synthesis parameters, that is, the matrix and the particle content, are analysed. The influence of the matrix is shown in Figure 2, where the three matrixes are analysed without particles. Silicone rubber is the matrix that has the lowest LVE region defined by the loss factor, while the ELASTOSIL matrix has the largest LVE limit. The same conclusion is obtained from the storage modulus analysis. That is why the softer the matrix, the larger the LVE region.

Figure 3 shows the influence of the particle content; as an example, natural rubber and three particle contents are shown. The particle content has a large influence on the LVE region. When the particle content is increased, the LVE limit defined by the loss factor is decreased. Moreover, this behaviour is also seen for all the matrixes analysed in this work (Tables 1 to 3). From the storage modulus analysis, the LVE region is also decreased with an increment of particle content. These results are in accordance with those shown by Li and Nakano (2013). The decrease of the LVE region is explained by the reinforcement experienced by the

**Table 1.** LVE strain limits of the ELASTOSIL matrix for all analysed working conditions.

25°C					40°C				
Sample	0 kA/m		616.7 kA/m		Sample	0 kA/m		616.7 kA/m	
	1 Hz	40 Hz	1 Hz	40 Hz		1 Hz	40 Hz	1 Hz	40 Hz
<i>Storage modulus</i>									
0%	0.874	1.220	–	–	0%	0.850	1.141	–	–
10%	0.485	0.524	0.524	0.640	10%	0.454	0.561	0.331	0.412
30%	0.157	0.148	0.189	0.190	30%	0.208	0.153	0.156	0.186
<i>Loss factor</i>									
0%	0.131	0.251	–	–	0%	0.119	0.184	–	–
10%	0.106	0.165	0.086	0.146	10%	0.060	0.099	0.040	0.116
30%	0.074	0.088	0.075	0.063	30%	0.069	0.080	0.064	0.074

LVE: linear viscoelastic.

**Table 2.** LVE strain limits of the natural rubber matrix for all analysed working conditions.

25°C					60°C				
Sample	0 kA/m		616.7 kA/m		Sample	0 kA/m		616.7 kA/m	
	1 Hz	40 Hz	1 Hz	40 Hz		1 Hz	40 Hz	1 Hz	40 Hz
<i>Storage modulus</i>									
0%	0.529	0.484	–	–	0%	1.899	1.774	–	–
15%	0.225	0.243	0.290	0.272	15%	0.590	0.482	0.619	0.587
30%	0.126	0.139	0.138	0.167	30%	0.185	0.158	0.196	0.188
<i>Loss factor</i>									
0%	0.169	0.179	–	–	0%	0.256	0.398	–	–
15%	0.094	0.094	0.118	0.114	15%	0.127	0.175	0.158	0.231
30%	0.045	0.051	0.059	0.058	30%	0.074	0.074	0.080	0.080

LVE: linear viscoelastic.

**Table 3.** LVE strain limits of the silicone rubber matrix for all analysed working conditions.

25°C					60°C				
Sample	0 kA/m		616.7 kA/m		Sample	0 kA/m		616.7 kA/m	
	1 Hz	40 Hz	1 Hz	40 Hz		1 Hz	40 Hz	1 Hz	40 Hz
<i>Storage modulus</i>									
0%	0.333	0.405	–	–	0%	0.402	0.489	–	–
15%	0.190	0.231	0.229	0.279	15%	0.190	0.231	0.229	0.231
30%	0.130	0.133	0.157	0.191	30%	0.157	0.159	0.157	0.191
<i>Loss factor</i>									
0%	0.108	0.131	–	–	0%	0.130	0.158	–	–
15%	0.074	0.075	0.089	0.090	15%	0.074	0.075	0.089	0.090
30%	0.042	0.051	0.061	0.075	30%	0.051	0.062	0.074	0.062

LVE: linear viscoelastic.

matrix when particles are embedded in a matrix due to physical interactions (Phewthongin et al., 2006). However, the influence of the particle content is dependent on the matrix. When the matrix is softer, the influence of the particles is greater; hence, in this case, the influence on the ELASTOSIL is larger than that on the silicone rubber.

The characterisation variables such as frequency, magnetic field and temperature also determine the LVE region of each sample. The frequency analysis is shown in Figure 4, where the 15% particle content silicone rubber sample is analysed as an example. When the frequency is increased, the LVE strain limit defined by the loss factor is also increased; therefore, the increment of

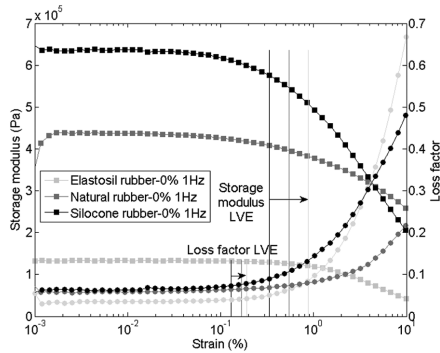


Figure 2. Influence of the matrix on the LVE limit.

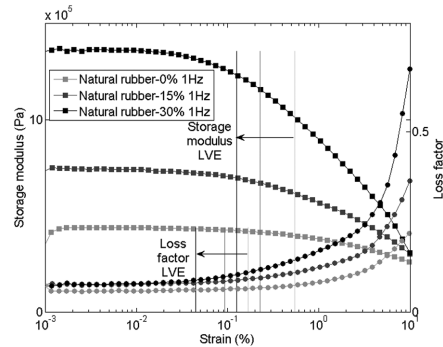


Figure 3. Influence of particle content on the LVE region for the natural rubber samples.

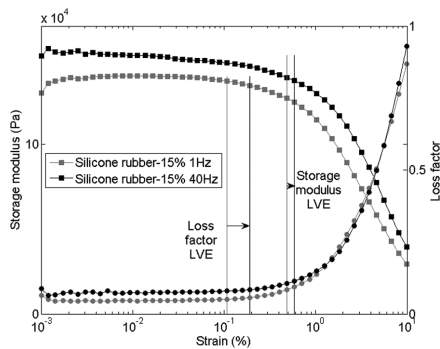


Figure 4. Influence of frequency on the LVE region for the 15% silicone rubber sample.

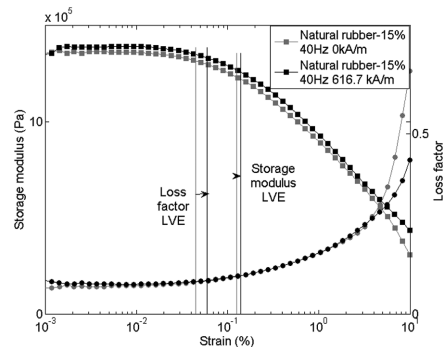


Figure 5. Influence of the external magnetic field on the LVE region for the 15% natural rubber sample.

the frequency increases the LVE region. For the natural rubber and ELASTOSIL samples and all the working conditions (Tables 1 to 3), the LVE limit is also increased with the increment of frequency (Nashif et al., 1985). Moreover, the same behaviour is seen at the LVE limit defined by the storage modulus.

Unlike the previously analysed variables, the external magnetic field depends on the matrix. Thus, natural rubber and silicone rubber increase the LVE region with increments of the magnetic field. As an example, in Figure 5, the 15% particle content natural rubber sample is shown. But the influence on the LVE limit of the ELASTOSIL samples is not evident. Furthermore, the external magnetic field effect is similar for the loss factor and the storage modulus.

The influence of temperature is also analysed and depends on the matrix. Figure 6 analyses the influence of temperature and matrix. Silicone rubber and

ELASTOSIL matrixes are analysed without particle content. In Figure 6, two different behaviours can be seen. The loss factor defined that the LVE limit increases for silicone rubber with temperature, whereas ELASTOSIL sample LVE region is reduced. The influence of temperature on the LVE limit is rarely studied, although it is determined that the strain limit is increased with a decrease in stiffness (Airey and Rahimzadeh, 2004), as for the silicone and natural rubber analysed in this work. Nevertheless, the LVE region of some polymers is decreased with the increment of the temperature (Arenz, 1999; Leblanc, 2012), such as the ELASTOSIL sample (Figure 6). The reason for this behaviour could be explained by the transition temperature ( $T_g$ ). The matrixes studied in this study are working in the rubbery region when the temperature is increased, over the transition temperature (Jones,

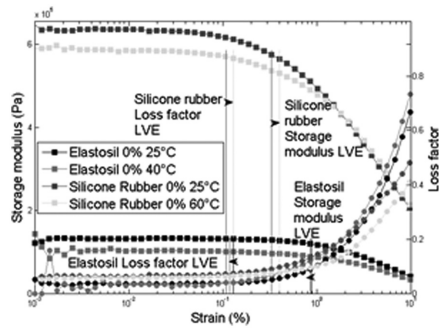


Figure 6. Influence of temperature on the LVE region for the 0% silicone rubber sample and for the 0% ELASTOSIL sample at 1 Hz.

2001), because the storage modulus and the loss factor decrease with the temperature. Moreover, Starkova and Aniskevich (2007) proposed that the LVE region is wider with a higher transition temperature. Therefore, the ELASTOSIL samples have the higher  $T_g$ , and it is proposed that samples are working close to the  $T_g$  when the temperature is increased. That is why the LVE region is decreased.

Moreover, the combination of particle content and frequency is analysed. However, to analyse the combination, a stress-strain diagram is used. A first-order polynomial function is approach to the Figure 7(a) curves, and then the LVE limit is determined at the point where the shear stress deviates 10% from the approach function. In Figure 7(a) and (b), the silicone rubber samples are used with a logarithmic and linear scale, respectively. The increment of frequency increases the LVE region. However, when frequency and particle content are combined, the increment of frequency is reduced. Figure 7(b) shows that the increment of frequency is larger when particle content is smaller. The values of the LVE strain limits determined by these diagrams are similar to LVE limits determined by the storage modulus because the influence of the storage modulus on the dynamic complex modulus is larger than the loss modulus or the imaginary part.

As a summary of the LVE limits determined by the loss factor, the influence of the synthesis and characterisation variables is shown in Table 4.

**Conclusion**

The LVE region limit has to be defined to predict the linear behaviour of the MRE. The LVE region of the MRE materials is defined by the loss factor, because it is more restrictive than the limit defined by the storage modulus.

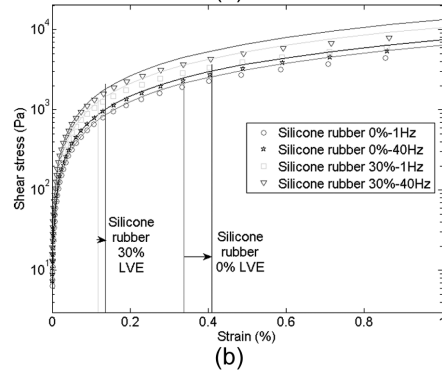
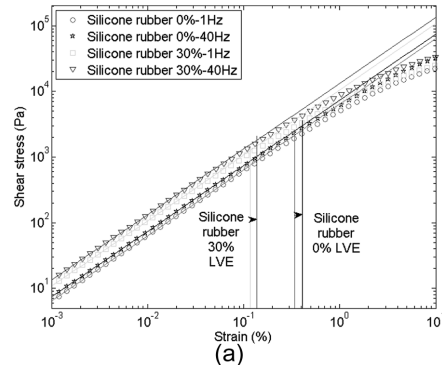


Figure 7. Influence of particle content and frequency on the LVE region: (a) logarithmic scale and (b) linear x-axis scale.

Table 4. Summary of the influence of synthesis and working conditions on the LVE region of MRE.

LVE	ELASTOSIL	Silicone rubber	Natural rubber
Particle content	↓	↓	↓
Frequency	↑	↑	↑
External magnetic field	~	↑	↑
Temperature	↓	↑	↑

LVE: linear viscoelastic; MRE: magnetorheological elastomer.

The matrix is a determinant synthesis parameter to determine the LVE limit of the MRE. The softer the matrix, the larger the LVE region of the MRE. However, the contribution of particle content in the LVE region depends on the matrix and working conditions. Furthermore, an increment in the particle content decreases the LVE limit.

The characterisation variables also determine the LVE region of the MRE. The frequency increases the LVE region of the MRE in all analysed working

conditions. Furthermore, the magnetic field and the temperature influence depend on the matrix.

#### Declaration of conflicting interests

The authors declared no potential conflicts of interest with respect to the research, authorship and/or publication of this article.

#### Funding

This study received financial support from the Department of Education of the Basque Government for the Project ACTIMAT, Research Group program IT557-10 and MAGNETOBUSH (UE2013-09) and also received the financial support from the Spanish Government for the project AVISUINT (DPI 2012-36366).

#### References

- Agirre-Olabide I, Berasategui J, Elejabarrieta MJ, et al. (2014) Characterization of the linear viscoelastic region of magnetorheological elastomers. *Journal of Intelligent Material Systems and Structures* 25(16): 2074–2081.
- Airey Gordon D and Rahimzadeh Behzad (2004) Combined bituminous binder and mixture linear rheological properties. *Construction and Building Materials* 18(7): 535–548.
- Arenz RJ (1999) Nonlinear shear behavior of poly(vinyl acetate) material. *Mechanics of Time-Dependent Materials* 2(4): 287–305.
- Bellan C and Bossis G (2002) *Field Dependence of Viscoelastic Properties of MR Elastomers*. Singapore: World Scientific.
- Boczkowska A, Awietjan SF, Pietrzko S, et al. (2012) Mechanical properties of magnetorheological elastomers under shear deformation. *Composites Part B: Engineering* 43(2): 636–640.
- Dong X, Ma N, Qi M, et al. (2012) The pressure-dependent MR effect of magnetorheological elastomers. *Smart Materials & Structures* 21(7): 075014 (5 pp.).
- Ferry JD (1980) *Viscoelastic Properties of Polymers*. New York: John Wiley & Sons.
- Gong XL, Chen L and Li JF (2007) *Study of Utilizable Magnetorheological Elastomers*. Lake Tahoe, NV: World Scientific Publishing Co. Pte Ltd.
- Gordaninejad F, Wang X and Mysore P (2012) Behavior of thick magnetorheological elastomers. *Journal of Intelligent Material Systems and Structures* 23(9): 1033–1039.
- Jones DIG (2001) *Handbook of Viscoelastic Vibration Damping*. Chichester: John Wiley & Sons.
- Laun HM, Gabriel C and Kieburg Ch (2010) Magnetorheological fluid in oscillatory shear and parameterization with regard to MR device properties. *Journal of Intelligent Material Systems and Structures* 21(15): 1479–1489.
- Leblanc JL (2012) Effect of temperature on dynamic rheological properties of uncured rubber materials in both the linear and the nonlinear viscoelastic domains. *Journal of Applied Polymer Science* 126(2): 408–422.
- Li WH and Nakano M (2013) Fabrication and characterization of PDMS based magnetorheological elastomers. *Smart Materials & Structures* 22(5): 055035.
- Li WH, Zhou Y, Tian T, et al. (2010) Creep and recovery behaviors of magnetorheological elastomers. *Frontiers of Mechanical Engineering in China* 5(3): 341–346.
- Lokander M and Stenberg B (2003a) Improving the magnetorheological effect in isotropic magnetorheological rubber materials. *Polymer Testing* 22(6): 677–680.
- Lokander M and Stenberg B (2003b) Performance of isotropic magnetorheological rubber materials. *Polymer Testing* 22(3): 245–251.
- Mezger TG (2006) *The Rheology Handbook: For Users of Rotational and Oscillatory Rheometers*. Hannover: Vincentz Network.
- Nashif AD, Jones DIG and Henderson JP (1985) *Vibration Damping*. New York: John Wiley & Sons.
- Payne AR (1962) The dynamic properties of carbon-black loaded natural rubber vulcanizates. Part 1. *Journal of Applied Polymer Science* 6: 53–57.
- Phewthongin N, Saeoui P and Sirisinha C (2006) Rheological behavior of CPE/NR blends filled with precipitated silica. *Journal of Applied Polymer Science* 100(4): 2565–2571.
- Popp K, Kosasih PB, Zhang XZ, et al. (2008) *Fabrication and Characterization of MR Elastomers with High MR Effects*. Daejeon, Republic of Korea: International Institute of Acoustics and Vibrations.
- Starkova O and Aniskevich A (2007) Limits of linear viscoelastic behavior of polymers. *Mechanics of Time-Dependent Materials* 11(2): 111–126.
- Tian TF, Zhang XZ, Li WH, et al. (2013) *Study of PDMS Based Magnetorheological Elastomers*. Ankara, Turkey: Institute of Physics Publishing.
- Wereley NM, Chaudhuri A, Yoo J-H, et al. (2006) Bidisperse magnetorheological fluids using Fe particles at nanometer and micron scale. *Journal of Intelligent Material Systems and Structures* 17(5): 393–401.
- Yu M, Ju B, Fu J, et al. (2012) Influence of composition of carbonyl iron particles on dynamic mechanical properties of magnetorheological elastomers. *Journal of Magnetism and Magnetic Materials* 324(13): 2147–2152.
- Zhang W, Gong X, Xuan S, et al. (2011) Temperature-dependent mechanical properties and model of magnetorheological elastomers. *Industrial and Engineering Chemistry Research* 50(11): 6704–6712.

Effect of synthesis variables on viscoelastic  
properties of elastomers filled with carbonyl iron  
powder

*I. Agirre-Olabide and M.J. Elejabarrieta*

Mechanical and Manufacturing Department, Mondragon Unibertsitatea, Loramendi 4,  
20500 Arrasate-Mondragon, Spain

Journal of Polymer Research

2017 vol. **24**(9) pag. 139

DOI: 10.1007/s10965-017-1299-z

IF-JCR: 1.615 J. Rank-JCR: 40/86



## Effect of synthesis variables on viscoelastic properties of elastomers filled with carbonyl iron powder

Iker Agirre-Olabide<sup>1</sup> · María Jesús Elejabarrieta<sup>1</sup> Received: 30 January 2017 / Accepted: 31 July 2017  
© Springer Science+Business Media B.V. 2017

**Abstract** This work studies the influence of synthesis variables on the lineal viscoelastic properties of elastomers filled with soft magnetic particles. Three matrices [natural rubber (NR), high-temperature vulcanising silicone rubber (HTV-SR), and room-temperature vulcanising (RTV-SR)] and three volumetric particle contents (0%, 15%, and 30%) were studied. Anisotropic samples were synthesised with a softer matrix to obtain a larger magnetorheological (MR) effect, and the variation of their properties under an external magnetic field was examined. All samples were characterised within the lineal viscoelastic (LVE) region using a rheometer, because the MR effect is larger within this region. The influence of the matrix, particle content, and pre-structure on the viscoelastic properties of the synthesised samples was studied. The storage and loss modulus increased with the frequency owing to the viscoelastic behaviour of an elastomer in the rubbery phase. Both moduli also increased with the filler content. The influence of the filler is dependent on the matrix, and the maximum variation was seen in the NR-based samples. However, the maximum MR effect was seen in the samples with a softer matrix, and the effect was enhanced in the anisotropic samples. In this work, the MR effect on the loss modulus was studied, and the tendencies were found to be similar to those of the storage modulus. The main contribution of this work is that all dynamic behaviour results were comparable because all synthesis variables and characterisation conditions were identical. Therefore, how the particle content, frequency, and magnetic field affects each matrix can be studied.

**Keywords** smart polymers · magnetorheological elastomer · synthesis · lineal viscoelasticity · dynamic properties

### Introduction

Elastomers filled with magnetic particles, also called magnetorheological elastomers (MREs), are classified as smart materials because their properties vary under an external magnetic field. One of the ratios used to measure the variability of the properties is the magnetorheological (MR) effect; it is defined as the ratio of the difference in storage modulus with and without a magnetic field to the storage modulus without a magnetic field, as defined in Eq. (1) [1].

$$MR \text{ effect} = \frac{G_1 - G_0}{G_0}, \quad (1)$$

where  $G_0$  is the rigidity without the magnetic field and  $G_1$ , the rigidity under a magnetic field during characterisation. The MR effect is dependent on synthesis variables such as the matrix, particle content, and pre-structure.

Chen et al. [2] studied the influence of the matrix in the mechanical properties using a natural rubber (NR) and a silicone rubber (SR). The mechanical performance improved replacing the SR with NR. Chen et al. [3] studied the damping properties of MRE elastomers based on different matrices. A low damping ratio matrix leads to a low damping ratio MRE. Lokander and Stenberg [4] studied SR-based MRE samples and concluded that a larger MR effect is obtained with a softer matrix.

Previous studies used soft or hard magnetic particles as the filler material. When hard magnetic materials are used in MRE samples, magnetic nonlinear behaviour is obtained owing to the nature of the material [5]. Furthermore, energy

✉ María Jesús Elejabarrieta  
mjelejabarrieta@mondragon.edu

<sup>1</sup> Mechanical and Manufacturing Department, Mondragon Unibertsitatea, 20500 Arrasate-Mondragon, Spain



dissipation increases when using hard magnetic materials owing to the rotation of the particles [6]. However, previous studies used soft magnetic particles for the reversibility of properties in the absence of a magnetic field [7–9].

Particle content is a key parameter to determine the dynamic mechanical properties of MREs under the same characterisation conditions [10]. Both the storage modulus and the loss factor increase with the particle content [11–13]. The MR effect of MREs is also influenced by the particle concentration; specifically, the effect is higher with larger volumetric particle content [12, 14–16].

Embedded particles can be randomly distributed or aligned in chains. Isotropic MREs are cured without the influence of a magnetic field. On the other hand, chains are obtained by applying an external magnetic field during the pre-structure process; samples with oriented chains are called anisotropic MRE. Anisotropic samples show higher MR effect than isotropic ones [17].

Li et al. [18] and Zhu et al. [13] mentioned that the initial and dynamic mechanical storage modulus of MREs increase with the magnetic field during the pre-structure process. Nonetheless, this modulus increases until the saturation of the MR effect. However, the loss factor decreases when an external magnetic field is applied to the MRE during characterisation [19].

The viscoelastic properties of the materials are also dependent on the characterisation conditions. Strain is one of the most important properties owing to the Payne effect [20]. In the lineal region at low strains, this behaviour is independent of the strain, and the time-dependent stress and strain can be expressed in a sinusoidal form [21]. However, at higher strains, the behaviour is nonlinear. Lokander and Stenberg [14] show that the MR effect of isotropic MREs decreases with the strain amplitude, whereas the damping ratio increases [3].

Gordaninejad et al. [15], Ju et al. [12], and Qiao et al. [22] defined the lineal viscoelastic limit at a strain of 1%. Qiao et al. [22] analysed the lineal viscoelastic behaviour of MREs and determined that the limit decreases with an increase in the external magnetic field. Agirre-Olabide et al. [23, 24] determined the lineal viscoelastic (LVE) region by analysing the loss factor which guarantees lineal dynamic characterisation at room temperature. This region was analysed as a function of the matrix, particle content, pre-structure, frequency, temperature, and external magnetic field.

In this work, the influence of synthesis and characterisation variables on the viscoelastic properties of MREs are analysed under the same characterisation conditions. In previous works, we determined the LVE region under different conditions and for different samples [23, 24]; in this study, those regions were used to study the dynamic behaviour and maximise the MR effect of MREs. The studied synthesis variables were the matrix and particle content, and the influence of the pre-structure

was analysed using a softer matrix. Three matrices were vulcanised: NR, room-temperature vulcanising silicone rubber (RTV-SR), and high-temperature vulcanising silicone rubber (HTV-SR); all matrices were filled with soft magnetic particles. The analysed characterisation variables were frequency and magnetic field. To study the energy dissipation due to the magnetic field, the loss modulus MR effect was defined. The main contribution of this work is that the influence of the particle content, frequency, and magnetic field in each matrix can be compared because the characterisation conditions for all samples were identical.

## Experimental

Isotropic elastomers filled with soft magnetic particles were synthesised using three different matrices; for the anisotropic sample, the softer matrix was used. As a soft magnetic filler, carbonyl iron powder (CIP) particles were used, and three particle contents were studied. Characterisation was performed using a rheometer equipped with a magnetorheological device for the magnetic field, and all frequency sweep tests were performed within the LVE region.

## Material

In this study, three rubber materials were used: NR, HTV-SR, and RTV-SR. NR and HTV-SR were vulcanised at 180 °C and HTV-SR was vulcanised at room temperature. HTV-SR had two components: the main matrix WACKER Elastosil® M 4644 A and the vulcaniser WACKER Elastosil® M 4644 B mixed in 10:1 ratio.

For synthesising the MREs, CIP was used as the ferromagnetic iron particle; it had a spherical shape and average size of  $1.25 \pm 0.55 \mu\text{m}$ . The shape and the size of the particles was analysed using scanning electron microscope (SEM) image (Fig. 1). The image was obtained by a SEM working in low vacuum and microanalysis, JEOL JSM 5600 LV, and with a voltage acceleration of 15 kV. These particles were provided by BASF. Three volumetric concentrations were used:

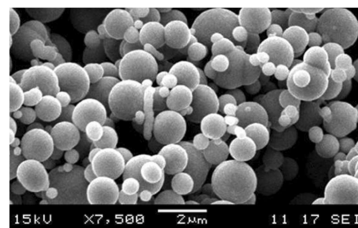


**Fig. 1** SEM image of carbonyl iron powder particles

without particles (0%), intermediate concentration (15%), and maximum concentration (30%).

Lokander and Stenberg [14] defined the maximum particle content when all particles are in contact one to each other and the voids between them is replaced by rubber. This content is defined as the critical particle volume concentration (CPVC),

$$CPVC = \frac{100 \times \rho_{app}}{\rho_{Fe}}, \quad (2)$$

where  $\rho_{app}$  is the apparent density of the filler and  $\rho_{Fe}$  is the material density of the filler 2400 and 7800 respectively. Therefore, the CPVC for the particles used in this work is 30.76% and the maximum content synthesized was 30%.

#### Preparation of isotropic and anisotropic samples

The synthesis process is the same for NR and HTV-SR (NE-9340) matrices because of the vulcanisation temperature and solid state of the raw material. For the mixing process, a two-roll mixing mill was used, and the particles were added gradually. A homogenous mixture was poured into a 1-mm-thick mould, and the mould was then placed in an oven at 180 °C under compression pressure of 200 bar.

The RTV-SR matrix had two components, and vulcanisation began when both were mixed. This matrix (Elastosil® M 4644 A) and the particles were mixed by hand, and vacuum cycles were applied for 30 min to extract air bubbles generated during mixing. Then, the vulcaniser was added, and vacuum cycles were again applied to remove air bubbles. Finally, the homogenous mixture was poured into a 1-mm-thick mould.

For the RTV-SR matrix, two pre-structure conditions were studied: pre-structure without a magnetic field (isotropic MRE) [23] and with a magnetic field (anisotropic MRE) [24]. During pre-structuring, a magnetic field was applied in the thickness direction to obtain a chain alignment of the particles in the direction perpendicular to the characterisation shear strain [17]. The magnetic field density was  $0.13 \pm 0.01$  T as measured by the Gaussimeter FH-54.

To guarantee that the synthesised samples were isotropic and anisotropic MRE samples, images were obtained using a Nova NanoSEM 450 scanning electron microscope (SEM) working under low vacuum conditions with an acceleration voltage of 18 kV. Figure 2 shows SEM images of the 15% MRE sample: in Fig. 2a, a homogeneous particle distribution can be seen (isotropic MRE), and in Fig. 2b, the particles are aligned perpendicular to the surface in the direction of the applied external magnetic field during vulcanisation (anisotropic MRE). While in Fig. 1 the particles are agglomerated, after synthesising isotropic samples (Fig. 2a) particle agglomerations were not seen in isotropic MREs and they were randomly distributed.

#### Characterisation

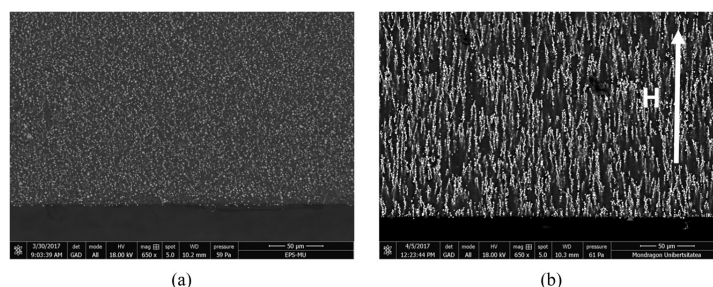
This work studies the dynamic behaviour of MREs within the LVE region. For this purpose, dynamic frequency sweep tests were performed to determine the lineal dynamic properties of the analysed MRE.

Characterisation was performed using an Anton Paar Physica MCR 501 rheometer equipped with a MRD 70/1 T magnetorheological cell, and a parallel plate configuration was used. One of the plates had a serrated surface, and its diameter was 20 mm (PP20/MRD/T1/P2). The tested samples had a diameter of 20 mm and thickness of 1 mm, and for each vulcanised material, three samples were studied.

The frequency range of 1–40 Hz was analysed, and all tests were performed at a temperature of 25 °C controlled using the Julabo F-25 water-based heating/cooling system. To avoid sliding between the samples and the plates and to increase the MR effect, a normal force of 5 N was defined [25].

Three external magnetic fields were studied: minimum of 0 kA/m, intermediate of 347 kA/m, and maximum of 616 kA/m. In the samples, the possible magnetisation was tested, and it was seen that the magnetisation was minimum because the measured field was below  $15 \pm 8$   $\mu$ T.

**Fig. 2** SEM images of 15% RTV-SR MRE: (a) isotropic and (b) anisotropic samples



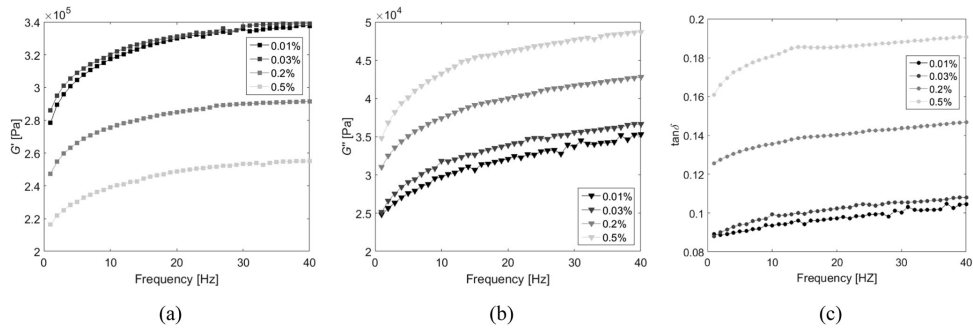


**Fig. 3** Influence of strain on the (a) storage modulus ( $G'$ ), (b) loss modulus ( $G''$ ) and (c) loss factor ( $\tan \delta$ ) of the 30% isotropic RTV-SR sample as a function of frequency

Frequency sweep tests were performed within the LVE region at a strain of 0.01%, as defined in our previous works [23, 24].

As the samples were tested in the lineal region, the viscoelastic behaviour can be modelled by the complex shear modulus ( $G^*$ ), which is independent of the strain. The complex shear modulus is defined by the shear strain and shear stress. Owing to the lineal behaviour, the applied shear strain is harmonic, and consequently, the shear stress is also harmonic [26]. From the relationship between the two, the dynamic shear modulus is defined as

$$G^* = \frac{\tau(t)}{\gamma(t)} = \frac{\tau_{\max} e^{j(\omega t + \delta)}}{\gamma_{\max} e^{j\omega t}} = \frac{\tau_{\max}}{\gamma_{\max}} (\cos \delta + j \sin \delta) \quad (3)$$

where  $\gamma_{\max}$  is the amplitude of the shear strain;  $\tau_{\max}$ , the amplitude of the shear stress;  $\delta$ , the phase difference between the strain and the stress; and  $\omega$ , the frequency (unit: rad/s). The complex shear modulus is compounded by a real part, or the storage modulus ( $G'$ ), and an imaginary part, or the loss modulus ( $G''$ ).

For the frequency sweep test, a lineal distribution of 40 frequencies between 1 and 40 Hz was applied. The measurement period for each point was 5 s, and three magnetic fields were analysed within the range of 0–616.7 kA/m.

**Results and discussion**

The viscoelastic behaviour of the MRE materials is due to the elastomeric matrix. Therefore, the influence of the matrix, particles, and magnetic field was studied. Moreover, the softer matrix (RTV-SR) was used to study the influence of the magnetic field during vulcanisation.

The influence of strain on the viscoelastic properties of elastomeric materials is called the Payne effect [20]; with an increase in strain, the storage modulus ( $G'$ ) decreases and the loss modulus ( $G''$ ) increases. At low strains (LVE region), the magnetorheological effect is larger [14] and the properties remain constant; however, at higher strains, the viscoelastic

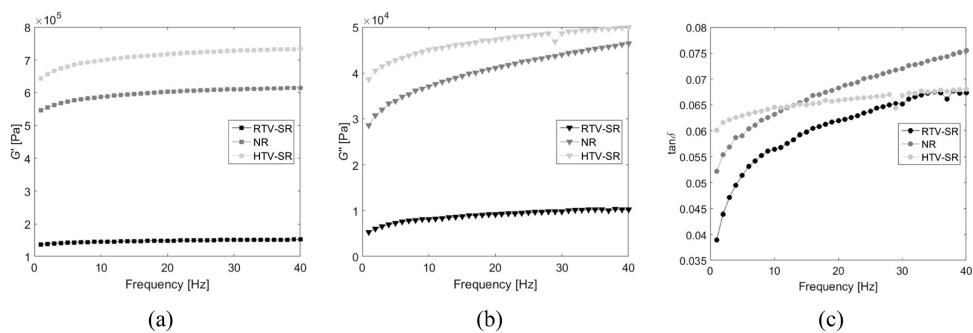


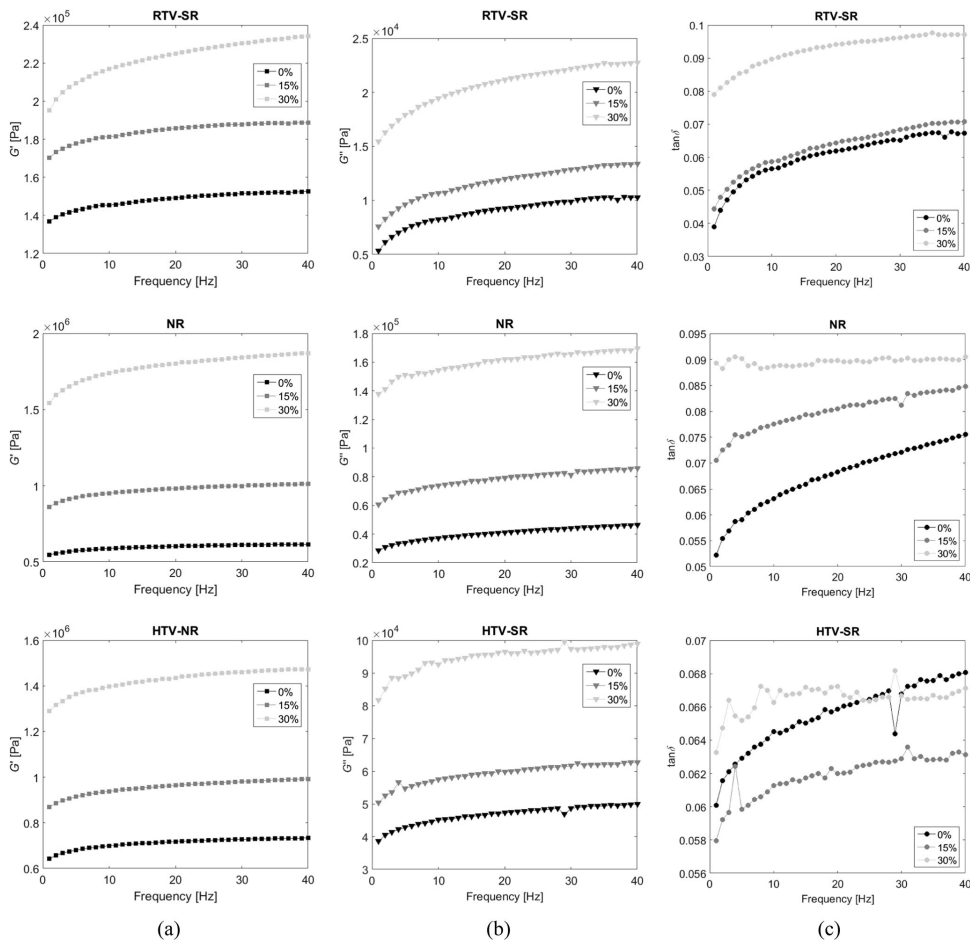
**Fig. 4** Influence of the matrix (RTV-SR, NR and HTV-SR) on the (a) storage modulus ( $G'$ ), (b) loss modulus ( $G''$ ) and (c) loss factor ( $\tan \delta$ ) as a function of frequency

properties depends on the applied amplitude. Figure 3 shows the mentioned influence for the RTV-SR matrix with 30% particle content; the behaviour of loss modulus and loss factor are similar (Fig. 3). Therefore, in this work, we focused on the LVE region and used a strain of 0.01% [24] because the magnetorheological effect is larger [27] and the properties are independent of the strain.

Figure 4 shows the influence of the matrix on the dynamic properties in the studied cases. The increase due to frequency is the typical behaviour of a viscoelastic material within the

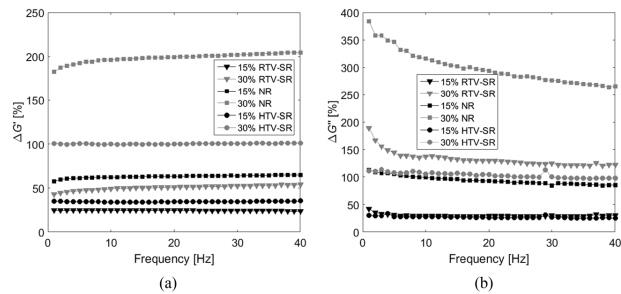
rubbery region [28]. It is also seen that when the matrix is stiffer, the energy dissipation is larger. At low frequencies, the loss factor is larger for the HTV-SR sample, while the influence of the frequency is larger for softer matrices.

Figure 5 shows the influence of the particle content on the viscoelastic properties for each matrix. When the particles are embedded in a matrix, new interactions are created between the particles and the matrix; consequently, a mechanical reinforcement is created that increases the storage modulus owing to the formation of a physically bonded filler network and to



**Fig. 5** Influence of the particle content on the (a) storage modulus ( $G'$ ), (b) loss modulus ( $G''$ ) and (c) loss factor ( $\tan \delta$ ) as a function of frequency for different matrices (RTV-SR, NR and HTV-SR)

**Fig. 6** Variation of (a) storage ( $G'$ ) and (b) loss modulus ( $G''$ ) with the addition of soft magnetic fillers in different matrices



strong polymer-filler couplings [29, 30]. The energy dissipation also increases with the particle content owing to increased friction between particles [31, 32]. The influence of particle content in the loss factor is dependent on the matrix, the larger influence occurs for the softer matrix. The loss factor of RTV-SR increases with the particle content and the highest energy dissipation is given with the higher particle content owing to the particle friction. For the NR samples, it is also increased, while the frequency dependence is reduced for the maximum particle content. However, the influence of the particle content in loss factor for HTV-SR samples is different; it increases with the particle content while with the addition of 15%

particle content it decreased. This can be explained by the energy dissipation mechanism. The pure elastic part of the matrix consist of long polymer chains and the viscoelastic part on short chains [33]. Therefore, when particles are added the short chain might be broken and consequently the loss factor is decreased. Figure 5 indicates that by increasing the particle content up to the maximum defined by the critical particle volume concentration (CPVC) higher rigidity and energy dissipation can be obtained [14].

However, the influence of the particle content is completely dependent on the matrix. Figure 6 shows the increase of the storage and loss moduli with the addition of CIP particles

**Fig. 7** Influence of the magnetic field on the (a) storage ( $G'$ ) and (b) loss modulus ( $G''$ ) as a function of the frequency for the 30% HTV-SR and RTV-SR samples

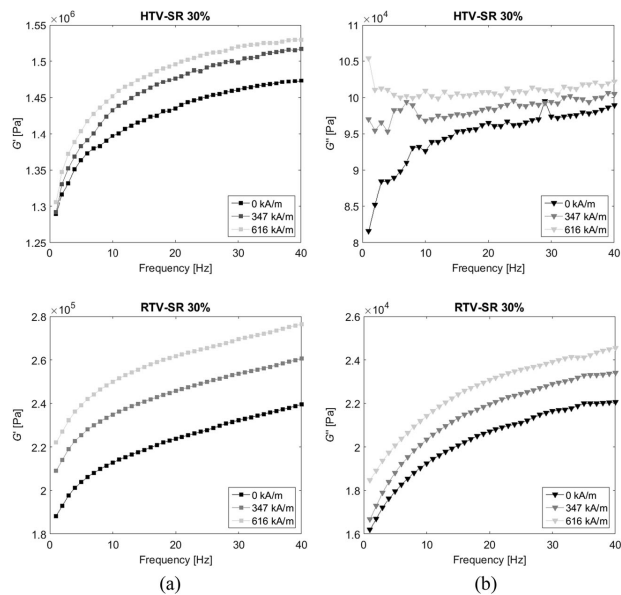


**Table 1** Maximum mean MR effect for (a) storage and (b) loss modulus for different matrices and particle contents

	RTV-SR	NR	HTV-SR
(a) MR effect: Storage modulus ( $G'$ )			
15%	10.78 ± 1.7	6.42 ± 0.27	2.53 ± 0.52
30%	16.66 ± 0.79	9.31 ± 0.69	4.79 ± 0.59
(b) MR effect: Loss modulus ( $G''$ )			
15%	9.66 ± 1.62	6.11 ± 1.15	5.55 ± 1.06
30%	11.29 ± 0.91	7.39 ± 1.9	8.11 ± 1.12

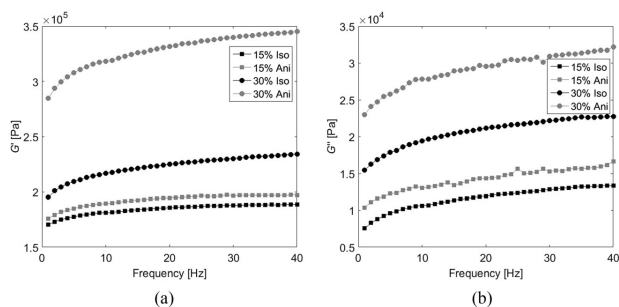
relative to the 0% samples. In all cases, the storage modulus increased and loss modulus decreased with frequency. The largest increase in viscoelastic properties is seen in the NR matrix (maximum of 200% for  $G'$  and 300% for  $G''$  with 30% particle content), and the smallest increase is seen in the RTV-SR matrix (maximum of 50% for  $G'$  and 140% for  $G''$  with 30% particle content). HTV-SR shows the same maximum increase of 100% for both  $G'$  and  $G''$ .

These properties can be modified by applying an external magnetic field. As an example, Fig. 7 shows the 30% HTV-SR and 30% RTV-SR samples. The viscoelastic properties are modified, and the influence on the storage modulus is larger than that on the loss modulus. However, the influence of the magnetic field is completely dependent on the matrix. The magnetorheological effect increases with the particle content. These results are in agreement with those reported by Raa Khimi et al. and Jung et al. [31, 34].

MREs are widely applied as vibration isolators. Therefore, the variation of dissipated energy or loss modulus is studied. The loss modulus MR effect, analogously to the MR effect, is defined as

$$\text{Loss modulus MR effect} = \frac{G''_1 - G''_0}{G''_0}, \quad (4)$$

**Fig. 8** (a) Storage ( $G'$ ) and (b) loss modulus ( $G''$ ) of isotropic and anisotropic RTV-SR samples as a function of frequency and different particle contents



where  $G''_0$  is the loss modulus without any magnetic field and  $G''_1$ , the loss modulus in the presence of a magnetic field. In Table 1, the mean maximum MR effects are shown for the storage and loss modulus. The influence of the magnetic field on the loss factor is not remarkable because the increase of storage and loss modulus with magnetic field are similar (Table 1). The loss modulus MR effect is lower than the MR effect for RTV-SR and NR and higher for HTV-SR. The measurement of the different matrices under the same characterisation conditions indicated that the MR effect and loss modulus MR effect were larger for a softer matrix, which was in agreement with literature [35]. Therefore, depending on the application of these materials, a softer matrix or high-attenuation matrix must be used; for example, a high-attenuation matrix should be used for vibration isolators.

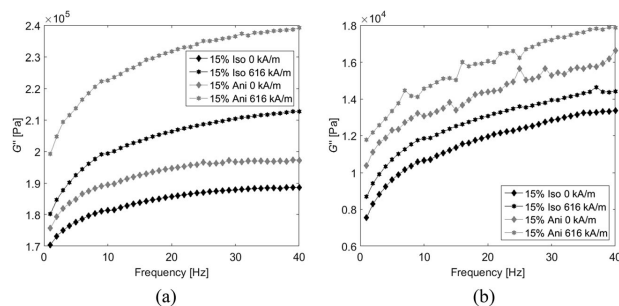
The MR effect increases with the particle content but it is more sensitive for the softer matrix, RTV-SR. To obtain a larger MR effect, RTV-SR-based anisotropic MRE samples were synthesised.

The dynamic properties are modified when a rubber matrix filled with soft magnetic particles is vulcanised under a magnetic field [27, 36]. This influence can be seen in Fig. 8, where both the storage and loss modulus increase with the particle content and frequency for the anisotropic sample. Particle chains are created in the MRE sample, and consequently, the interaction forces between particles increase, in turn increasing the storage modulus [32].

The increase for the maximum particle content is larger because all particles are almost in contact with each other. The microstructure is similar to the three-dimensional lattice of iron particles [37], and larger energy dissipation occurs owing to interfacial slipping [31, 32]. However, the maximum influence of the pre-structure process is seen in the MR effect.

As an example of the influence of the magnetic field, 15% isotropic and anisotropic samples are shown in Fig. 9. The influence of the magnetic field is larger for anisotropic samples than for isotropic ones. The particle interaction magnetic forces are larger for anisotropic samples because particles are

**Fig. 9** Variation of (a) storage ( $G'$ ) and (b) loss modulus ( $G''$ ) of isotropic and anisotropic 15% RTV-SR samples as a function of frequency owing to the magnetic field



aligned, and consequently, the distance between particles decreases. As the particles come closer, the energy dissipation increases owing to the slipping of the particles. In Table 2, the maximum mean MR effects are shown.

### Conclusions

In this work, the synthesis and characterisation effects were analysed under the same characterisation conditions.

Three different matrices were synthesised with soft magnetic fillers and characterised under the same conditions within the LVE region. The storage and loss modulus increased with the frequency; this is a typical behaviour of viscoelastic material within the rubbery region.

The storage and loss modulus increased with the particle content for all the studied matrices. However, the influence on each matrix was different. The NR matrix showed the maximum increase of 200% for storage modulus and 300% for loss modulus with 30% particle content. The HTV-SR showed the same increase of 100% for both the storage and the loss modulus with 30% particle content.

The MR effect is dependent on the viscoelastic nature of the matrix. Larger MR effects occur when the matrix is softer. In this work, RTV-SR was the softer matrix, and it showed maximum storage modulus MR effect of 16% and loss modulus MR effect of 11%.

**Table 2** Maximum mean MR effect for (a) storage and (b) loss modulus for isotropic and anisotropic RTV-SR samples

	Isotropic	Anisotropic
(a) MR effect: Storage modulus ( $G'$ )		
15%	10.78 ± 1.7	18.70 ± 1.83
30%	16.66 ± 0.79	25.46 ± 1.43
(b) MR effect: Loss modulus ( $G''$ )		
15%	9.66 ± 1.62	20.55 ± 1.54
30%	11.29 ± 0.91	21.46 ± 1.25

Therefore, the influence of the particle content and external magnetic field on the storage and loss modulus are completely dependent on the matrix. To obtain a larger MR effect, anisotropic MREs were synthesised with a softer matrix. Anisotropic samples show a larger storage and loss modulus compared to the isotropic ones. The distance between particles is closer owing to vulcanisation under a magnetic field. As the particles are closer, the energy dissipation increases owing to the slipping of the particles. When a magnetic field is applied, the particle-particle interaction forces are larger; this increased the MR effect to 30% for the anisotropic sample with maximum particle content. The loss modulus MR effect for the same sample also increased by up to 21%.

**Acknowledgements** The authors gratefully acknowledge the financial support from the Department of Education of the Basque Government for the Research Predoc Grant PRE\_2014\_1\_284, AVISANI (PI-2016-1-0026), ACTIMAT, IT009-16 and the AVISANI (DPI2015-71198-R) research project from the Spanish government.

### References

- Chen L, Gong XL, Li WH (2008) Effect of carbon black on the mechanical performances of magnetorheological elastomers. *Polym Test* 27:340–345. doi:10.1016/j.polymertesting.2007.12.003
- Chen L, Gong X, Jiang W, Yao J, Deng H, Li W (2007) Investigation on magnetorheological elastomers based on natural rubber. *J Mater Sci* 42:5483–5489. doi:10.1007/s10853-006-0975-x
- Chen L, Gong X, Li W (2008) Damping of Magnetorheological Elastomers. *Chinese J Chem Phys* 21:581–585. doi:10.1088/1674-0068/21/06/581-585
- Lokander M, Stenberg B (2003) Improving the magnetorheological effect in isotropic magnetorheological rubber materials. *Polym Test* 22:677–680. doi:10.1016/S0142-9418(02)00175-7
- Stepanov GV, Chertovich AV, Kramarenko EY (2012) Magnetorheological and deformation properties of magnetically controlled elastomers with hard magnetic filler. *J Magn Magn Mater* 324:3448–3451. doi:10.1016/j.jmmm.2012.02.062
- Yu M, Qi S, Fu J, Zhu M (2015) A high-damping magnetorheological elastomer with bi-directional magnetic-control

- modulus for potential application in seismology. *Appl Phys Lett* 107:111901. doi:10.1063/1.4931127
7. Ivaneyko D, Toshchevikov VP, Saphiannikova M, Heinrich G (2011) Magneto-sensitive elastomers in a homogeneous magnetic field: A regular rectangular lattice model. *Macromol Theory Simul* 20:411–424. doi:10.1002/mats.201100018
  8. Melenev P, Raikher Y, Stepanov G, Rusakov V, Polygalova L (2011) Modeling of the Field-Induced Plasticity of Soft Magnetic Elastomers. *J Intell Mater Syst Struct* 22:531–538. doi:10.1177/1045389X11403819
  9. Gong X, Fan Y, Xuan S, Xu Y, Peng C (2012) Control of the damping properties of magnetorheological elastomers by using polycaprolactone as a temperature-controlling component. *Ind Eng Chem Res* 51:6395–6403. doi:10.1021/ie300317b
  10. Hu Y, Wang YL, Gong XL, Gong XQ, Zhang XZ, Jiang WQ, Zhang PQ, Chen ZY (2005) New magnetorheological elastomers based on polyurethane/Si-rubber hybrid. *Polym Test* 24:324–329. doi:10.1016/j.polymertesting.2004.11.003
  11. Fan Y, Gong X, Xuan S, Zhang W, Zheng J, Jiang W (2011) Interfacial friction damping properties in magnetorheological elastomers. *Smart Mater Struct* 20:35007. doi:10.1088/0964-1726/20/3/035007
  12. Ju BX, Yu M, Fu J, Yang Q, Liu XQ, Zheng X (2012) A novel porous magnetorheological elastomer: preparation and evaluation. *Smart Mater Struct* 21:35001. doi:10.1088/0964-1726/21/3/035001
  13. Zhu J-T, Xu Z-D, Guo Y-Q (2012) Magneto-viscoelasticity parametric model of an MR elastomer vibration mitigation device. *Smart Mater Struct* 21:75034. doi:10.1088/0964-1726/21/7/075034
  14. Lokander M, Stenberg B (2003) Performance of isotropic magnetorheological rubber materials. *Polym Test* 22:245–251. doi:10.1016/S0142-9418(02)00043-0
  15. Gordaninejad F, Wang X, Mysore P (2012) Behavior of thick magnetorheological elastomers. *J Intell Mater Syst Struct* 23:1033–1039. doi:10.1177/1045389X12448286
  16. Ge L, Gong X, Fan Y, Xuan S (2013) Preparation and mechanical properties of the magnetorheological elastomer based on natural rubber/rosin glycerin hybrid matrix. *Smart Mater Struct* 22:115029. doi:10.1088/0964-1726/22/11/115029
  17. Varga Z, Filipcsei G, Zrinyi M (2006) Magnetic field sensitive functional elastomers with tuneable elastic modulus. *Polymer (Guildf)* 47:227–233. doi:10.1016/j.polymer.2005.10.139
  18. Li J, Gong X, Xu Z, Jiang W (2008) The effect of pre-structure process on magnetorheological elastomer performance. *Int J Mater Res* 99:1358–1364. doi:10.3139/146.101775
  19. Sun TL, Gong XL, Jiang WQ, Li JF, Xu ZB, Li WH (2008) Study on the damping properties of magnetorheological elastomers based on cis-polybutadiene rubber. *Polym Test* 27:520–526. doi:10.1016/j.polymertesting.2008.02.008
  20. Payne AR (1962) The dynamic properties of carbon black-loaded natural rubber vulcanizates. Part I *J Appl Polym Sci* 6:57–63. doi:10.1002/app.1962.070061906
  21. Ferry JD (1980) *Viscoelastic Properties of Polymers*, 3rd edn. Wiley, New York
  22. Qiao X, Lu X, Li W, Chen J, Gong X, Yang T, Li W, Sun K, Chen X (2012) Microstructure and magnetorheological properties of the thermoplastic magnetorheological elastomer composites containing modified carbonyl iron particles and poly(styrene-*b*-ethylene-ethylene-propylene-*b*-styrene) matrix. *Smart Mater Struct* 21:115028. doi:10.1088/0964-1726/21/11/115028
  23. Agirre-Olabide I, Berasategui J, Elejabarrieta MJ, Bou-Ali MM (2014) Characterization of the linear viscoelastic region of magnetorheological elastomers. *J Intell Mater Syst Struct* 25:2074–2081. doi:10.1177/1045389X13517310
  24. Agirre-Olabide I, Elejabarrieta MJ, Bou-Ali MM (2015) Matrix dependence of the linear viscoelastic region in magnetorheological elastomers. *J Intell Mater Syst Struct* 26:1880–1886. doi:10.1177/1045389X15580658
  25. Dong X, Ma N, Qi M, Li J, Chen R, Ou J (2012) The pressure-dependent MR effect of magnetorheological elastomers. *Smart Mater Struct* 21:75014. doi:10.1088/0964-1726/21/7/075014
  26. Jones DIG (2001) *Handbook of viscoelastic vibration damping*. John Wiley & Sons Ltd, Chichester
  27. Schubert G, Harrison P (2015) Large-strain behaviour of Magneto-Rheological Elastomers tested under uniaxial compression and tension, and pure shear deformations. *Polym Test* 42:122–134. doi:10.1016/j.polymertesting.2015.01.008
  28. Nashif AD, Jones DIG, Henderson JP (1985) *Vibration damping*. John Wiley & Sons, New York
  29. Phewthongin N, Saecoui P, Sirisinha C (2006) Rheological behavior of CPE/NR blends filled with precipitated silica. *J Appl Polym Sci* 100:2565–2571. doi:10.1002/app.22550
  30. Aloui S, Klüppel M (2015) Magneto-rheological response of elastomer composites with hybrid-magnetic fillers. *Smart Mater Struct* 24:25016. doi:10.1088/0964-1726/24/2/025016
  31. Raa Khimi S, Pickering KL, Mace BR (2015) Dynamic properties of magnetorheological elastomers based on iron sand and natural rubber. *J Appl Polym Sci* 132:41506. doi:10.1002/app.41506
  32. Ju B, Tang R, Zhang D, Yang B, Yu M, Liao C (2015) Temperature-dependent dynamic mechanical properties of magnetorheological elastomers under magnetic field. *J Magn Magn Mater* 374:283–288. doi:10.1016/j.jmmm.2014.08.012
  33. Han Y, Zhang Z, Faidley LE, Hong W (2012) Microstructure-based modeling of magneto-rheological elastomers. *Proc SPIE, Behavior and Mechanics of Multifunctional Materials and Composites*, 8342:83421B. doi:10.1117/12.925492
  34. Jung HS, Kwon SH, Choi HJ, Jung JH, Kim YG (2016) Magnetic carbonyl iron/natural rubber composite elastomer and its magnetorheology. *Compos Struct* 136:106–112. doi:10.1016/j.compstruct.2015.10.008
  35. Yang C, Fu J, Yu M, Zheng X, Ju B (2015) A new magnetorheological elastomer isolator in shear-compression mixed mode. *J Intell Mater Syst Struct* 26:1290–1300. doi:10.1177/1045389X14541492
  36. Lu X, Qiao X, Watanabe H, Gong X, Yang T, Li W, Sun K, Li M, Yang K, Xie H, Yin Q, Wang D, Chen X (2012) Mechanical and structural investigation of isotropic and anisotropic thermoplastic magnetorheological elastomer composites based on poly(styrene-*b*-ethylene-co-butylene-*b*-styrene) (SEBS). *Rheol Acta* 51:37–50. doi:10.1007/s00397-011-0582-x
  37. Boczkowska A, Awietjan SF, Wroblewski R (2007) Microstructure–property relationships of urethane magnetorheological elastomers. *Smart Mater Struct* 16:1924–1930. doi:10.1088/0964-1726/16/5/049



*Follow an old path and you find the expected. Blaze a new trail and you have an adventure.*

Kelsey

# 3

## Compression magneto-dynamic characterisation

- I. Agirre-Olabide, and M.J. Elejabarrieta. 2017. A new magneto-dynamic compression technique for magnetorheological elastomers at high frequencies. *Composites Part B*, *submitted*

In this chapter, a new magneto-dynamic compression technique is designed and manufactured to measure magneto-viscoelastic properties of magnetorheological elastomers (MREs) at high frequencies. Isotropic MREs filled with carbonyl iron powder are synthesised. A standard procedure is defined to calculate the viscoelastic compression properties of MREs using stress–strain diagrams. Furthermore, the LVE region for MREs in compression mode is defined, and the influence of synthesis and characterisation variables are analysed. Finally, the compression magneto-viscoelastic properties of isotropic MREs within the linear region are analysed at high frequencies.

## 3.1 Introduction

MREs have been used in many applications, and some of them are working in compression mode, such as in isolators ([Kavlicoglu et al. 2011](#); [Komatsuzaki et al. 2016](#); [Ladipo et al. 2016](#); [Lerner and Cunefare 2008](#); [Sun et al. 2015](#); [Yang et al. 2015](#)). Therefore, the viscoelastic properties of these materials have to be characterised in compression mode.

In compression tests, [Varga et al. \(2006\)](#) concluded that the variation of storage modulus was larger when the mechanical stress and applied magnetic field were parallel. Therefore, to characterise the MREs in compression mode, the equipment were modified to apply an external magnetic field. For that purpose, two solutions have been developed, one using permanent magnets (500 mT) ([Hiptmair et al. 2015](#); [Vatandoost et al. 2017](#); [Yang et al. 2015](#)) and the other using electromagnets (1T) ([Kallio et al. 2007](#); [Li and Sun 2013](#); [Ubaidillah et al. 2016b](#)).

According to characterisation devices, universal testing machines ([Kallio et al. 2007](#)), fatigue machines ([Norouzi et al. 2016](#); [Ubaidillah et al. 2016b](#)) and dynamic mechanical analysers ([Li and Sun 2013](#)) have been adapted to characterise MREs. However, the maximum characterisation frequency was 25 Hz. To characterise MRE materials at higher frequencies, electrodynamic shakers were used. [Yang et al. \(2015\)](#) characterised MREs in compression mode up to 30 Hz. Nevertheless, in shear mode larger frequencies up to 1 kHz have been characterised using an electrodynamic shaker [Kari and Blom \(2005\)](#).

In the literature, MRE properties were measured in shear mode, and consequently the LVE region was analysed in that mode, which was determined at the point when viscoelastic properties deviates 10% (Agirre-Olabide et al. 2014; Bonhome-Espinosa et al. 2017; Ubaidillah et al. 2016a; Wereley et al. 2006). The shear LVE region decreases with particle content and becomes larger with frequency (Agirre-Olabide et al. 2015), while magnetic field does not restrict the LVE region (Agirre-Olabide et al. 2015; Ubaidillah et al. 2016a; Yang et al. 2017).

## 3.2 Critical review

The characterisation of viscoelastic properties in compression mode is important owing to MRE applications (Komatsuzaki et al. 2016; Ladipo et al. 2016; Sun et al. 2015; Yang et al. 2015). However, in the literature the larger characterised frequency in compression mode have been 30 Hz for MREs. Furthermore, the LVE region was not defined for MREs in compression mode. To characterise the magneto-dynamic properties in compression mode, the magnetic field have to be parallel to the mechanical stress (Varga et al. 2006).

In this chapter, a new magneto-dynamic compression technique to characterise MREs at high frequencies is developed. The LVE region for MREs in compression mode is defined and subsequently the influence of synthesis and characterisation variables in the linear region are analysed. The compression magneto-viscoelastic properties of isotropic MREs within the linear region are measured at high frequencies. Using an electrodynamic shaker, frequencies from 50 to 200 Hz are characterised, and a magnetic field parallel to the mechanical stress is obtained with an electromagnet. A standard procedure is defined to calculate the viscoelastic properties of MREs using stress–strain diagrams. Two tests are employed, a strain sweep test to define the LVE region of isotropic MREs in compression mode as a function of particle content and frequency and, using that limit, a frequency sweep test to analyse magneto-viscoelastic properties in the linear region.

### 3.3 Aims

The goal of this chapter is to develop an experimental compression technique to analyse the compression magneto-viscoelastic properties of isotropic MREs within the linear viscoelastic region. The specific objectives are:

- Synthesise compression MRE samples
- Define a new procedure to determine the compression magneto-viscoelastic properties of MREs
- Analyse the influence of synthesis and characterisation variables in the LVE region of MREs in compression mode.
- Analyse the magneto-viscoelastic properties of MREs.

### 3.4 Synthesis

In this chapter, isotropic compression MRE samples are synthesised with three particle contents based on a natural rubber (NR) matrix.

The isotropic MREs contained carbonyl iron powder (CIP) as the filler and natural rubber as the matrix. The CIP particles were spherical with an average size of  $1.25 \pm 0.55 \mu\text{m}$ . The particles were supplied by BASF, The Chemical Company.

The mixing of particles and the matrix was done with a two-roll mixing mill; particles were added gently to guarantee a homogeneous mix. The mixture was

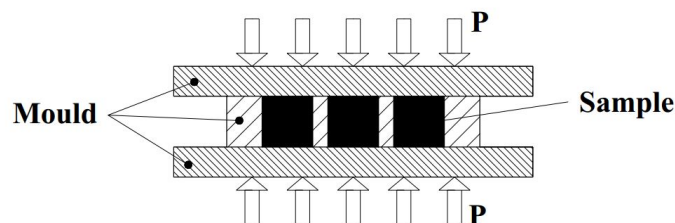


**Figure 3.1** Sketch of the vulcanisation of isotropic MREs

poured into a 10 mm thick mould (Figure 3.1), and placed in an oven at 180 °C with a hydraulic pressure of 200 bar for 10 min (indicated with a P in Figure 3.1). The samples were  $10 \pm 0.1$  mm in diameter and  $10 \pm 0.05$  mm high. The particles were randomly distributed, resulting in homogeneous and isotropic MREs. Three volumetric particle contents were studied in this chapter—0%, 15% and 30%.

## 3.5 Results

In this section, the results obtained in the paper shown in sec. 3.7. are resumed. A compression technique to characterise MREs at high frequency was developed. A standard procedure was defined to calculate the viscoelastic properties of MREs using stress–strain diagrams. Two characterisation tests were defined: strain sweep tests were performed to define the LVE region of isotropic MREs in compression mode as a function of particle content and frequency, and using that limit, frequency sweep tests to analyse magneto-viscoelastic properties in the linear region at high frequencies.

### 3.5.1 Technique

A new magneto-dynamic compression test device was designed and manufactured (which was fixed to an electrodynamic shaker) to characterise MREs at high frequencies. The magneto-dynamic response was obtained in the frequency range of 50–200 Hz. The test is detailed in Figure 3.2.

The proposed test was an open-loop test in which a sinusoidal signal was introduced and the output signal was measured. The OROS (OR763) analyser consists of two output channels and four input channels. The frequency and the level of the generated signal were defined using the analyser (A). The analyser (A) generated a sinusoidal signal at a certain frequency that was sent to the electrodynamic shaker (B). The shaker (B) applied a sinusoidal displacement to the testing device, which was measured using an accelerometer (C). The response of the system was measured with a force sensor (D), and the magnetic field density applied to the testing device was regulated with a DC power supply (E). The data acquisition for accel-

eration and force signals was accomplished using the analyser (A).

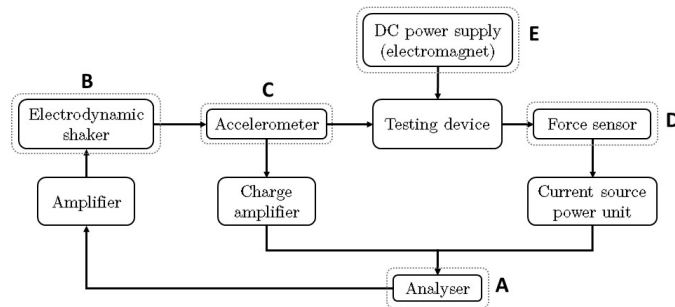


**Figure 3.2** Experimental set-up

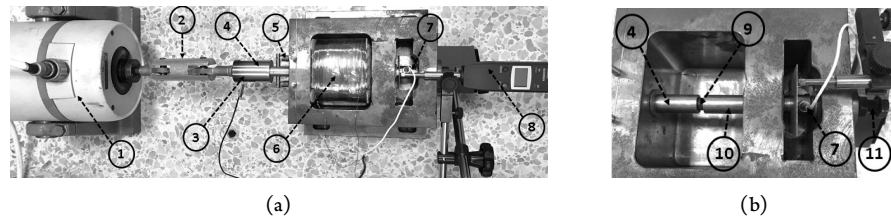
Once the overall view of the proposed technique is defined, the details of each element, the characterisation procedure and the data processing are explained.

Figure 3.3(a) shows a photo of the whole testing device and Figure 3.3 (b) shows a close-up of the sample. A sinusoidal signal was sent to a Ling V406 electrodynamic shaker (1), which applied a sinusoidal movement at a defined frequency and level conditions. The connection between the testing device and the shaker was done via a ball joint (2), which only transmitted a linear displacement to the device. The next element was the translational oscillatory rod (4), which had an accelerometer (Brüel & Kjaer 4371) (3) to measure the input acceleration introduced to the system. That oscillation was applied to the sample (9) and the response was transmitted through the static rod (10), and it was measured using a Dytran IEPE force sensor 1051v2 (7). The magnetic field was applied with an electromagnet with 2700 turns in the coil (6).

Once the sample was placed between the translational oscillatory and static rods, the desired pre-strain was applied with the bolt (11) and measured using a Mitutoyo ABSOLUTE Digimatic Indicator (linear encoder) (8). The accuracy of the encoder was 0.01 mm. The contact between the static and oscillatory rods was guaranteed due to springs (5).

The two measured signals, the input acceleration and output force, were harmonic and were measured in the time domain. In all studied cases and from both signals, 10 oscillations were measured after the first 10 periods had passed; a mean oscillation was obtained for each signal. Next, a sine function was fitted to the mean acceleration using the least square method and was integrated two times to

### 3. Compression magneto-dynamic characterisation



**Figure 3.3** (a) Dynamic compression test and (b) close-up of the sample holding: (1) electrodynamic shaker, (2) ball joint, (3) uniaxial accelerometer (Brüel & Kjaer 4371), (4) translational oscillatory rod, (5) springs, (6) electromagnet, (7) dynamic force sensor (Dytran IEPE force sensor 1051v2), (8) Mitutoyo ABSOLUTE Digimatic Indicator (linear encoder), (9) sample, (10) static rod, and (11) pre-strain bolt and nut

obtain the oscillatory displacement. At least 50 periods and 125 points per period were measured, and consequently the resolution was different for each frequency.

The stress was determined from the force signal and the cross-section of the sample, and the strain was determined from the displacement, sample's height and pre-strain measured with the linear encoder. As an example, an NR sample was measured at 75 Hz. The stress–strain diagram of the test is shown in Figure 3.4.

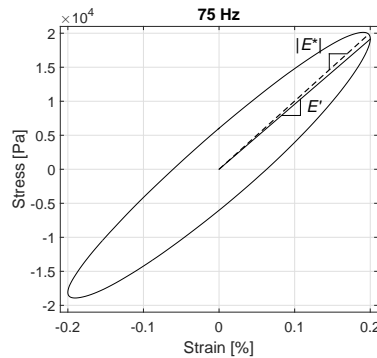


**Figure 3.4** Stress–strain diagram of an NR 30% isotropic sample for a strain amplitude of 0.2% at 75 Hz, room temperature and 0 kA/m

According to Lakes (2009), the complex ( $E^*$ ) and storage modulus ( $E'$ ) and

the loss factor ( $\tan \delta$ ) can be obtained from a stress–strain diagram,

$$|E^*| = \frac{\sigma_{\max}}{\varepsilon_{\max}}, \quad (3.1)$$

$$E' = \frac{\sigma_{\varepsilon_{\max}}}{\varepsilon_{\max}}, \text{ and} \quad (3.2)$$

$$\tan \delta = \frac{\varepsilon_{\sigma=0}}{\varepsilon_{\sigma_{\max}}}, \quad (3.3)$$

where  $\sigma_{\max}$  is the maximum stress,  $\varepsilon_{\max}$  is the maximum strain,  $\sigma_{\varepsilon_{\max}}$  is the stress at the maximum strain,  $\varepsilon_{\sigma=0}$  is the strain when the stress is equal to 0 and  $\varepsilon_{\sigma_{\max}}$  is the strain at the maximum stress.

Two characterisation tests were performed, a strain sweep test to define the LVE region of isotropic MREs in compression mode and a frequency sweep test to study the magneto-viscoelastic properties within the LVE and at high frequencies.

The linear viscoelastic LVE region has to be defined to guarantee the largest MR effect, which is the largest storage modulus variation (Jung et al. 2016; Lokander and Stenberg 2003b; Schubert and Harrison 2015). The LVE region was identified by performing strain sweep tests. When the response is linear, the stress–strain curve shape is elliptical (Nashif et al. 1985; Poojary and Gangadharan 2017). The LVE region is determined when the storage modulus deviates 10% (Agirre-Olabide et al. 2014; Bonhome-Espinosa et al. 2017; Ubaidillah et al. 2016a; Wereley et al. 2006). In shear mode and for NR, the LVE region decreases with particle content and low frequencies (Agirre-Olabide et al. 2015), while the magnetic field does not restrict the region (Agirre-Olabide et al. 2015; Ubaidillah et al. 2016a; Yang et al. 2017). Therefore, the studied frequencies were 50, 75, 100, 150 and 200 Hz, and 5 strain amplitudes were analysed for each frequency. The influence of the magnetic field was not studied because the most restrictive case is in the absence of the field.

Next, the LVE region was identified, a strain that guarantees the region was defined and oscillatory tests were performed; the studied frequencies were 50, 75, 100, 150 and 200 Hz. To obtain an adjustable magnetic field, an electromagnet with 2700 turns in the coil was designed, and three currents were applied—0.5, 1 and 1.4 A. Using Finite Element Method Magnetics (FEMM) software simulations, the mentioned currents (0.5, 1 and 1.4 A) were simulated and the results



showed that the magnetic field densities applied to the samples were 30, 60 and 85 mT, respectively.

### 3.5.2 Linear viscoelastic region

To study the LVE region, stress–strain diagrams were studied. In the stress–strain diagrams of Figure 3.5, ellipses at 50 and 200 Hz are shown for 0% and 30% MRE samples. Within the linear region, increasing the strain amplitude causes ellipses to become larger and wider, and the shape does not change. It can also be seen that the stress is larger with particle content and frequency. Furthermore, the elliptical shape disappears with strain amplitude for the lower frequency and higher particle content.

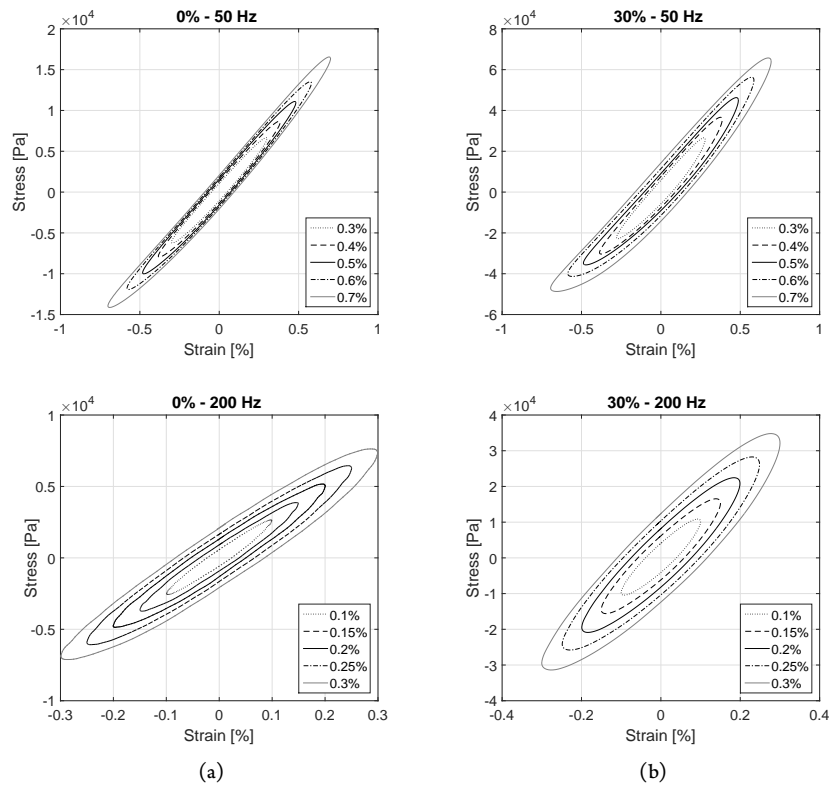


**Figure 3.5** Stress–strain diagrams at 50 and 200 Hz for a particle content of (a) 0% and (b) 30% isotropic NR samples, at different strain amplitudes, 0 kA/m and room temperature

The LVE region decreases with the particle content and increases with fre-

quency. These results are in accordance with the literature for shear mode (Agirre-Olabide et al. 2014; 2015). Therefore, the LVE region is determined by the 30% sample at a frequency of 50 Hz. Taking into account experimental points of the 30% MRE, the 10% deviation occurs between 0.5 and 0.3% strains. The strain that guarantees the LVE region is therefore 0.3%. Comparing these results with the tendencies shown in the literature for the LVE region in shear mode (Agirre-Olabide et al. 2015), the influence of particle content and frequency are the same, while the LVE region is larger in compression mode.

### 3.5.3 Magneto-dynamic properties

Frequency sweep tests were performed to analyse the influence of particle content, frequency and magnetic field on the storage modulus of isotropic MREs based on NR within the LVE region. In Figure 3.6, the influence of frequency is shown for the 15% sample. The elliptical shape remains constant, and the stress is larger with increasing frequency. Furthermore, the ellipse rotates with frequency.

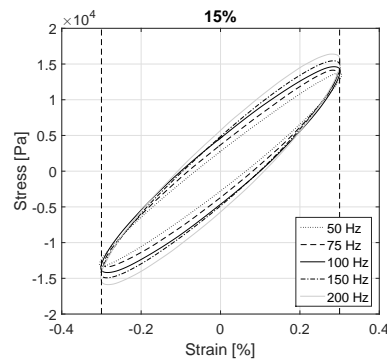


**Figure 3.6** Stress–strain diagrams for the 15% isotropic NR sample at the studied frequencies, constant strain of 0.3%, 0 kA/m and room temperature

In Figure 3.7, the influence of particle content and frequency on the viscoelastic compression properties of isotropic MREs are shown. A maximum 16% increase of the storage modulus for the 30% sample is seen, increasing frequency from 50 to 200 Hz (Figure 3.7(a)). However, the larger frequency influence is seen from 50 to 100 Hz. The particle influence is larger; a 75% increase can be obtained by increasing the particle content from 0% to 30% due to filler reinforcement phenomena (Aloui and Klüppel 2015). These tendencies are in agreement

with the literature for the compression mode (Kallio et al. 2007; Ubaidillah et al. 2016b).

The loss factor also increases with frequency, but the tendency is not so clear (Figure 3.7(b)), which is in accordance with the literature (Kallio et al. 2007; Ubaidillah et al. 2016b). The influence of particle content seems to increase the loss factor, comparing all contents with the 0% sample. However, comparing the 15% and 30% contents, the loss factor decreases. This can be explained by the damping mechanism. When particles are introduced, internal particle friction and interfacial damping between the particles and the matrix are generated, and added to the damping due to the polymer chains (Ju et al. 2015; Khimi and Pickering 2015; Pickering et al. 2015; Shuib et al. 2015). However, when the particle content is close to the maximum, the polymer chains are smaller and the predominant damping is due to particle friction. This is why the loss factor decreases at high particle contents.

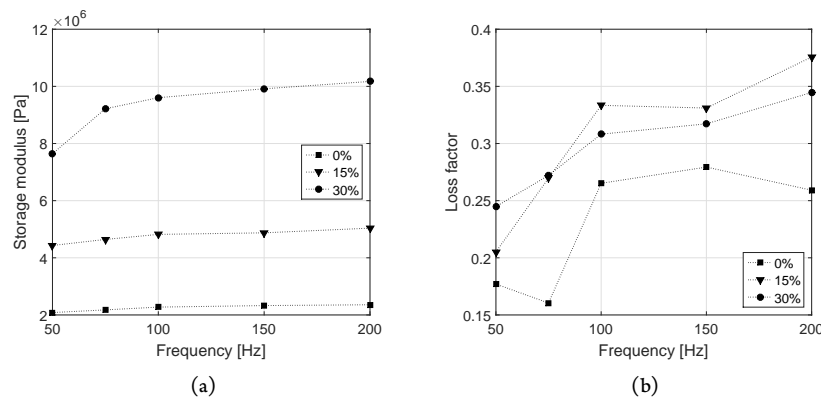


**Figure 3.7** (a) Storage modulus ( $E'$ ) and (b) loss factor ( $\tan \delta$ ) as a function of frequency for all the studied isotropic NR samples, 0 kA/m and room temperature

The storage modulus increases with the magnetic field, and the MR effect values are shown in Table 3.1. The larger MR effect occurs with higher particle content and magnetic field density. However, there are not as large as in the literature (Jung et al. 2016; Kallio et al. 2007; Schubert and Harrison 2015; Ubaidillah et al. 2016b; Yunus et al. 2016) due to the low magnetic fields studied in this work. Hence, a larger magnetic field will increase the MR effect. Comparing the compression results with our previous work (Agirre-Olabide and Elejabarrieta 2017),

which investigates the magneto-dynamic properties in shear mode, it can be seen that the MR effect is larger in compression mode.

**Table 3.1** Mean magnetorheological effect of isotropic MREs

Particle content	Frequency [Hz]		
	30 mT	60 mT	85 mT
15%	$1.07 \pm 0.73$	$2.76 \pm 0.81$	$4.03 \pm 0.72$
30%	$3.31 \pm 0.47$	$6.89 \pm 1.01$	$8.75 \pm 2.07$

## 3.6 Conclusions

In this chapter, a new magneto-dynamic compression technique was developed to characterise MREs at high frequencies. To the best of the author's knowledge, it is the first time the LVE region was determined in compression mode for MREs. This chapter has analysed the influence of synthesis and characterisation variables on the LVE region, and compression magneto-viscoelastic properties from 50 to 200 Hz were characterised within the LVE region.

Using strain sweep tests, the linear viscoelastic region was determined for isotropic MREs in compression mode. The LVE region was defined by the storage modulus when the discrepancy was larger than 10%. The LVE region increased with frequency and decreased with particle content. Hence, it was determined by the 30% sample at 50 Hz. However, the LVE region in compression mode was larger than in shear mode.

Magneto-viscoelastic properties were analysed using frequency sweep tests. The storage modulus and the loss factor increased with particle content and frequency. The largest storage modulus increase of 75% occurred with the particle content, while an increment of 16% was generated with frequency. The damping of MREs was also increased with particle content.

The variation of the storage modulus due to magnetic field increased with particle content and magnetic field up to 8%. The MR effect was larger in compression mode than in shear mode.

### 3.7 Scientific contribution

## A new magneto-dynamic compression technique for magnetorheological elastomers at high frequencies

*I. Agirre-Olabide and M.J. Elejabarrieta*

Mechanical and Manufacturing Department, Mondragon Unibertsitatea, Loramendi 4,  
20500 Arrasate-Mondragon, Spain

Composites Part B: Engineering

Status: 2017 *submitted*

## A new magneto-dynamic compression technique for magnetorheological elastomers at high frequencies

Iker Agirre-Olabide, María Jesús Elejabarrieta

*Mech. & Manuf. Dept., Mondragon Unibertsitatea, 20500 Arrasate-Mondragon, Spain*

---

### Abstract

A new magneto-dynamic compression technique was designed and manufactured to measure the magneto-viscoelastic properties of magnetorheological elastomers (MREs) at high frequencies. Isotropic MREs filled with carbonyl iron powder were synthesised, and three volumetric particle contents were studied—0%, 15% and 30%. Viscoelastic properties were calculated using stress-strain diagrams for each frequency and strain amplitude condition. The linear viscoelastic (LVE) region in compression mode was defined for MREs, and the influence of synthesis and characterisation variables in this region was analysed. Moreover, the compression magneto-viscoelastic properties were measured up to 200 Hz in the LVE region. Two types of tests were performed to characterise isotropic MREs in compression mode, a strain-sweep test to define the LVE region and a frequency-sweep test to study the magneto-viscoelastic properties in the LVE and at frequencies. The LVE region was determined at 0.3% by the higher particle content sample and at the lower frequency. Within the LVE region, the storage modulus and the loss factor increased with frequency and particle content, while the loss factor decreased with the maximum particle content due to the predominant damping mechanism. The compression magnetorheological (MR) effect increases with particle content and magnetic field density.

*Keywords:* Magnetorheological elastomers; Dynamic compression test; Linear viscoelastic region; Magnetic field.

---

### 1. Introduction

During the last two decades interest in smart materials has grown. Magnetorheological elastomers (MREs) are classified as smart materials due to the variability of their properties with the application of an external magnetic field. This characteristic is the result of ferromagnetic particles embedded in the polymeric matrix.

MREs can be clustered based on filler particle distribution. When the particles are randomly

---

*Email address:* [mjelejabarrieta@mondragon.edu](mailto:mjelejabarrieta@mondragon.edu) (María Jesús Elejabarrieta)

distributed MREs are isotropic, and when the particles are aligned in a certain direction the MREs are anisotropic [1, 2].

MREs normally operate in the pre-yield regime and are characterised by the field-dependent modulus [3] — the variation of storage modulus owing to a magnetic field is called magnetorheological (MR) effect. That effect is larger at low strain levels or within the linear viscoelastic (LVE) region [4–6], where viscoelastic properties are independent of strain. In literature, MRE properties were measured in shear mode, and consequently the LVE region was analysed in that mode, which was determined at the point when viscoelastic properties deviates 10% [7–10]. The LVE region decreases with particle content and becomes larger with frequency [11], while magnetic field does not restrict the LVE region [9, 11, 12].

MREs are used in many applications and some of them are working in compression mode, such in isolators [13–18]. Therefore, the viscoelastic properties of these materials have to be characterised in compression mode.

In compression tests, Varga et al. [19] concluded that the variation of storage modulus is larger when the mechanical stress and applied magnetic field are parallel. Therefore, to characterise the MREs in compression mode, the equipment was modified to apply an external magnetic field. For that purpose, two solutions have been developed, one using permanent magnets (500 mT) [15, 20, 21] and the other using electromagnets (1T) [1, 22, 23].

According to compression characterisation devices, universal testing machines [22], fatigue machines [23, 24] and dynamic mechanical analysers [1] have been adapted to characterise MREs. However, the maximum characterisation frequency was 25 Hz. To characterise MRE materials at higher frequencies, an electrodynamic shaker were used. Yang et al. [15] characterised MREs in compression mode up to 30 Hz. Nevertheless, larger frequencies up to 1 kHz can be characterised using an electrodynamic shaker [25], up to 1 kHz, although these characterisations were performed in shear mode.

In this work, we developed a new magneto-dynamic compression technique to characterise MREs at high frequencies. The novelty of this work lies in the definition of the LVE region for MREs in compression mode and its subsequent analysis as a function of synthesis and characterisation variables. The compression magneto-viscoelastic properties of isotropic MREs within the linear region are measured at high frequencies. Using an electrodynamic shaker, frequencies from 50 to 200 Hz were characterised, and a magnetic field parallel to the mechanical stress was obtained with an electromagnet. A standard procedure was defined to calculate the viscoelastic properties of MREs using stress–strain diagrams. Two tests were employed, a strain-sweep test to define the LVE region of isotropic MREs in compression mode as a function of particle content and frequency and, using that limit, a frequency-sweep test to analyse magneto-viscoelastic properties

in the linear region.

## 2. Materials

The isotropic MREs studied in this work contain carbonyl iron powder (CIP) as the filler and  
 45 natural rubber (NR) as the matrix. The CIP particles were spherical with an average size of  $1.25 \pm 0.55 \mu\text{m}$ . The particles were supplied by BASF, The Chemical Company. To determine the curing time of the NR, a rubber process analyser (RPA) was used at a frequency of 100 cycles per min at  $150^\circ\text{C}$  and a rotatory angle of  $0.5^\circ$  for 20 min. After 2.14 min 90% of the 0% sample was vulcanised. Therefore, the vulcanisation was done at  $180^\circ\text{C}$  for 10 min. By increasing the  
 50 particle content, the matrix amount and consequently the curing time were reduced.

The mixing of the particles and the matrix was done with a two-roll mixing mill; the particles were added gently to guarantee a homogeneous mix. The mixture was poured into a 10-mm-thick mould (Figure 1) and placed in an oven at  $180^\circ\text{C}$  with a hydraulic pressure of 200 bar for 10 min (indicated with a P in Figure 1). The samples were  $10 \pm 0.1 \text{ mm}$  in diameter and  $10 \pm$   
 55  $0.05 \text{ mm}$  high. Due to particle distribution, two kinds of MREs can be synthesised; in this work, the particles were randomly distributed, resulting in homogeneous and isotropic MREs. Three volumetric particle contents were studied—0%, 15% and 30%. The density of each sample was measured and compared with theoretical densities (Table 1). A Nova Nano SEM 450 scanning electron microscope (SEM) was used to observe the particle distribution (Figure 2). The images  
 60 were taken in low-vacuum conditions with a voltage acceleration of 18 kV.

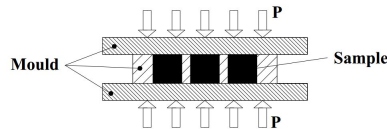


Figure 1: Sketch of the vulcanisation of isotropic MREs.

Table 1: Theoretical and experimental densities of the studied samples.

Particle content	Theoretical [g/cm <sup>3</sup> ]	Experimental [g/cm <sup>3</sup> ]
0%	1.127	$1.122 \pm 0.001$
15%	2.011	$2.077 \pm 0.001$
30%	3.079	$3.013 \pm 0.001$



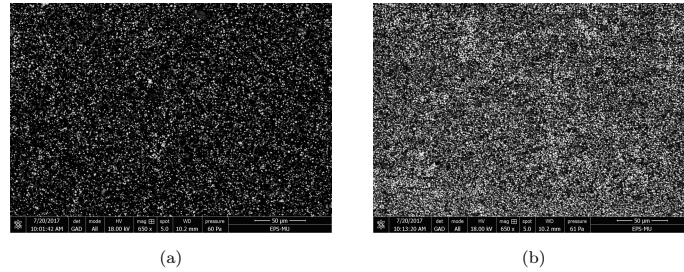


Figure 2: SEM images of (a) 15% and (b) 30% isotropic MRE samples in low-vacuum conditions and with a voltage acceleration of 18 kV.

### 3. Experimental

A new magneto-dynamic compression test device was designed and manufactured (which was fixed to an electrodynamic shaker) to characterise MREs at high frequencies. In this study, the magneto-dynamic response was obtained in the frequency range of 50–200 Hz. The test is detailed in Figure 3. The proposed test is an open-loop test in which a sinusoidal signal is introduced and the output signal is measured. The frequency and the level of the generated signal are defined using the analyser (A). The OROS (OR763) analyser consists of two output channels and four input channels. The analyser (A) generates a sinusoidal signal at a certain frequency that is sent to the electrodynamic shaker (B). The shaker (B) applies a sinusoidal displacement to the testing device, which is measured using an accelerometer (C). The response of the system is measured with a force sensor (D), and the magnetic field density applied to the testing device is regulated with a DC power supply (E). The data acquisition for acceleration and force signals is accomplished using the analyser (A).

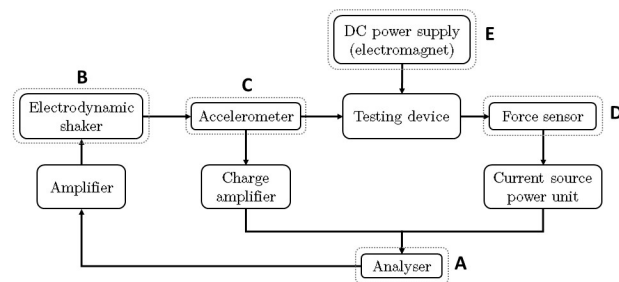


Figure 3: Data acquisition sketch.

After the overall view of the proposed technique is defined, the details of each element, the

75 characterisation procedure and the data processing are explained.

Figure 4(a) shows a photo of the whole testing device and Figure 4(b) shows a close-up of the sample. A harmonic signal was sent to a Ling V406 electrodynamic shaker (1), which applies a harmonic movement at a defined frequency and level conditions. The connection between the testing device and the shaker was made via a ball joint (2), which only transmits a linear displacement to the device. The next element is the translational oscillatory rod (4), which has an accelerometer (Brüel & Kjaer 4371) (3) to measure the input acceleration introduced to the system. That oscillation was applied to the sample (9), and the response was transmitted through the static rod (10) and measured using a Dytran IEPE force sensor 1051v2 (7). The magnetic field was applied with an electromagnet with 2700 turns in the coil (6).

85 Once the sample was placed between the translational oscillatory and static rods, the desired pre-strain was applied with the bolt (11) and measured using a Mitutoyo ABSOLUTE Digimatic Indicator (linear encoder) (8). The accuracy of the encoder is 0.01 mm. The contact between the static and oscillatory rods was guaranteed due to springs (5).

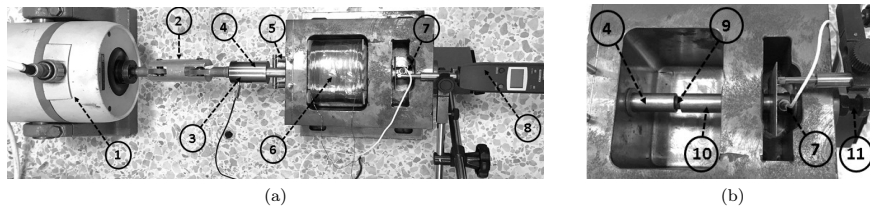


Figure 4: (a) Dynamic compression test and (b) close-up of the sample holding: (1) electrodynamic shaker, (2) ball joint, (3) uniaxial accelerometer (Brüel & Kjaer 4371), (4) translational oscillatory rod, (5) springs, (6) electromagnet, (7) dynamic force sensor (Dytran IEPE force sensor 1051v2), (8) Mitutoyo ABSOLUTE Digimatic Indicator (linear encoder), (9) sample, (10) static rod, and (11) pre-strain bolt and nut.

The two measured signals, the input acceleration and output force, were harmonic (Figure 5) and were acquired in the time domain. In all studied cases and from both signals, 10 oscillations were measured after the first 10 periods has passed (Figure 5(a)); a mean oscillation was obtained for each signal. Next, a sine function was fitted to the mean acceleration using the least square method (Figure 5(b)) and was integrated two times to obtain the oscillatory displacement. At least 50 periods and 125 points per period were measured, and consequently the resolution was different for each frequency.

The stress was determined from the force signal and the cross-section of the sample, and the strain was determined from the displacement, sample's height and pre-strain measured with the linear encoder. As an example, an NR sample was measured at 75 Hz. The stress-strain diagram of the test is shown in Figure 6.

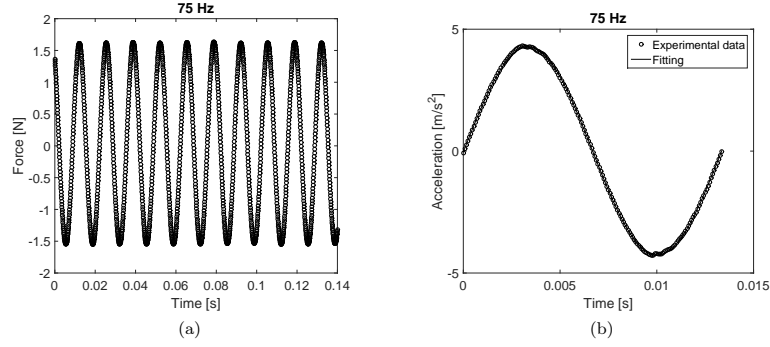


Figure 5: (a) Ten oscillations of the experimental force signal, and (b) 10 experimental oscillations mean acceleration (points) and least square fitting of the sinusoidal function (line).

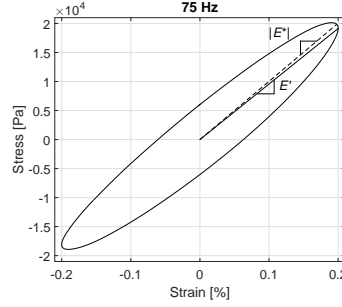


Figure 6: Stress-strain diagram of an NR 30% sample for a strain amplitude of 0.2% at 75 Hz.

100 According to Lakes [26], the complex ( $E^*$ ) and storage modulus ( $E'$ ) and the loss factor ( $\tan \delta$ ) can be obtained from a stress-strain diagram:

$$|E^*| = \frac{\sigma_{\max}}{\varepsilon_{\max}}, \quad (1)$$

$$E' = \frac{\sigma_{\varepsilon_{\max}}}{\varepsilon_{\max}}, \text{ and} \quad (2)$$

$$\tan \delta = \frac{\varepsilon_{\sigma=0}}{\varepsilon_{\sigma_{\max}}}, \quad (3)$$

where  $\sigma_{\max}$  is the maximum stress,  $\varepsilon_{\max}$  is the maximum strain,  $\sigma_{\varepsilon_{\max}}$  is the stress at the maximum strain,  $\varepsilon_{\sigma=0}$  is the strain when the stress is equal to 0 and  $\varepsilon_{\sigma_{\max}}$  is the strain at the maximum stress.

105 Two characterisation tests were performed, a strain-sweep test to define the LVE region of isotropic MREs in compression mode and a frequency-sweep test to study the magneto-viscoelastic properties within the LVE and at high frequencies.

The linear viscoelastic LVE region has to be defined to guarantee the largest MR effect, which is the largest storage modulus variation [4–6]. The LVE region was identified by performing strain-sweep tests. When the response is linear, the stress–strain curve shape is elliptical [27, 28]. The LVE region is determined when the storage modulus deviates 10% [7–10]. In literature for NR in shear mode, the LVE region decreases with particle content and low frequencies [11], while the magnetic field does not restrict the region [9, 11, 12]. Therefore, the studied frequencies were 50, 75, 100, 150 and 200 Hz, and 5 strain amplitudes were analysed for each frequency (Table 2). The influence of the magnetic field was not studied because the most restrictive case is in the absence of the field.

Table 2: Analysed strain amplitudes for each frequency.

Frequency [Hz]	Strain [%]
50	0.3, 0.4, 0.5, 0.6 and 0.7
75	0.2, 0.3, 0.4, 0.5 and 0.6
100	0.1, 0.2, 0.3, 0.4 and 0.5
150	0.1, 0.2, 0.3, 0.4 and 0.5
200	0.1, 0.15, 0.2, 0.25 and 0.3

Next, the LVE region was identified, a strain that guarantees the region was defined and oscillatory tests were performed; the studied frequencies were 50, 75, 100, 150 and 200 Hz. To obtain an adjustable magnetic field, an electromagnet with 2700 turns in the coil was designed, and three currents were applied—0.5, 1 and 1.4 A. The magnetic field density applied to the sample was calculated using Finite Element Method Magnetics (FEMM) software. In Figure 7, a simulation of the magnetic field density is shown, indicating the cross-section area of the testing device. The numbering used in the figure is the same as in Figure 4. Within the electromagnet (6) there is a 20 mm air gap (12) between two iron cores (13) in order to maximise the magnetic field density throughout the sample. In the figure, a homogeneous magnetic field is obtained where the sample is placed. Using the simulations, the three currents (0.5, 1 and 1.4 A) were simulated, and the results showed that the magnetic field densities applied to the samples were 30, 60 and 85 mT, respectively.

The magnetisation of the sample was also proved. To do so, the following test was performed at 100 Hz with the 30% sample. Five magnetic field densities were applied (0-30-0-60-0-85-0 mT); the results are shown in Figure 8.

#### 4. Results and discussion

In this work, the compression magneto-dynamic properties were measured within the LVE region up to 200 Hz. Two tests were performed, a strain-sweep test to determine the LVE region

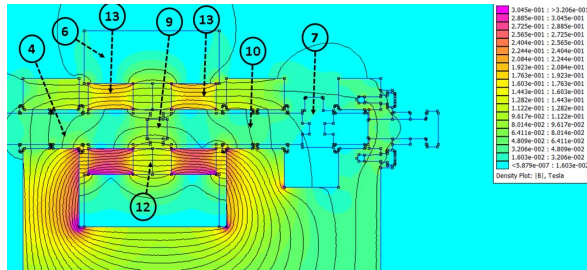


Figure 7: Magnetic field density FEMM simulation for the compression test with a current intensity of 1.4 A. (4) translational oscillatory rod, (6) electromagnet, (7) dynamic force sensor (Dytran IEPE force sensor 1051v2), (9) sample, (10) static rod, (12) 20 mm air gap and (13) iron core.

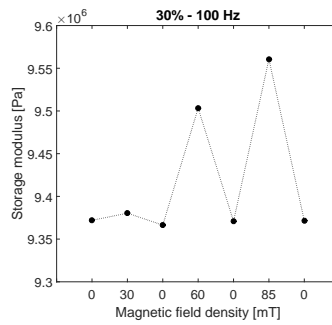


Figure 8: Storage modulus reversibility of the 30% sample at 100 Hz as a function of magnetic field density.

135 and a frequency-sweep test to study the magneto-viscoelastic properties of MREs in compression mode.

The LVE region can be determined with the shape of the stress-strain ellipses [27, 28]. The LVE region decreases with particle content and increases with frequency. The influence of the magnetic field in the LVE region was not studied because the magnetic field does not restrict the LVE region [9, 11, 12]. Using a strain amplitude of 0.3%, the LVE region was guaranteed and frequency-sweep tests were performed to determine the increment of storage modulus due to the particle content and the external magnetic field. All tests were performed at room temperature.

To study the LVE region, stress-strain diagrams were studied. In the diagrams of Figure 9, ellipses at 50 and 200 Hz are shown for 0% and 30% MRE samples. Within the linear region, increasing the strain causes amplitude the ellipses to become larger and wider, and the shape does not change. It can also be seen that for the same strain amplitude, the stress is larger with particle content and frequency. Furthermore, the elliptical shape disappears with strain amplitude for the lower frequency and higher particle content.

To gain a general overview of the influence of the strain amplitude on the magneto-dynamic

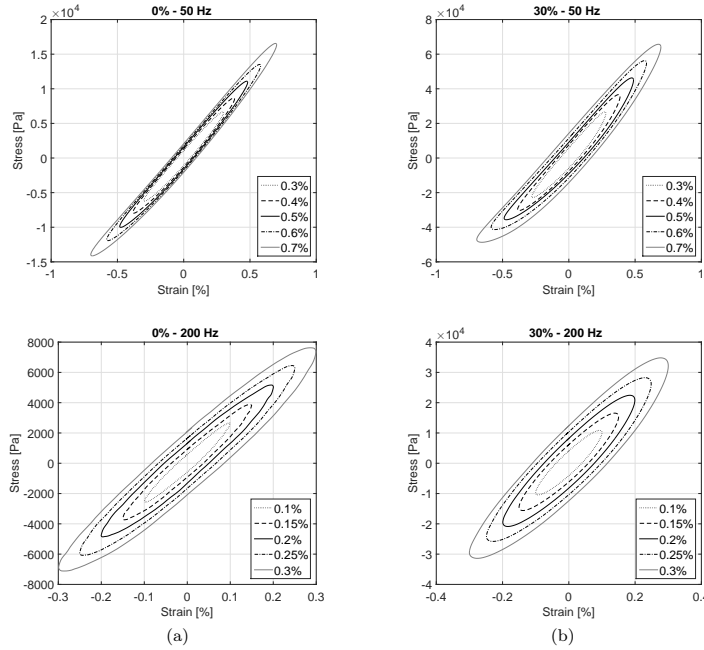


Figure 9: Stress–strain diagrams at 50 and 200 Hz for a particle content of (a) 0% and (b) 30%.

150 properties, the storage modulus is plotted as a function of strain amplitude. As can be seen in Figure 10, the LVE region decreases with particle content and increases with frequency (Figure 10(b) for the 30% sample). These results are in accordance with the literature [8, 11]. Therefore, the LVE region is determined by the 30% sample at a frequency of 50 Hz. Taking into account experimental points of the 30% MRE, the 10% deviation occurs between 0.5% and 0.3% strains.  
 155 The strain that guarantees the LVE region is therefore 0.3%. Comparing these results with the tendencies shown in the literature about the LVE region in shear mode [11], the influence of particle content and frequency are the same, while the LVE region is larger in compression mode.

After the LVE region was defined, frequency-sweep tests were performed to analyse the influence of particle content, frequency and magnetic field on the storage modulus of isotropic MREs  
 160 based on NR within the LVE region. In Figure 11, the influence of frequency is shown for the 15% sample. The elliptical shape remains constant, and the stress is larger with increasing frequency. Furthermore, the ellipse rotates with frequency.

In Figure 12, the influence of particle content and frequency on the viscoelastic properties of isotropic MREs are shown. A maximum 16% increase of the storage modulus for the 30% sample

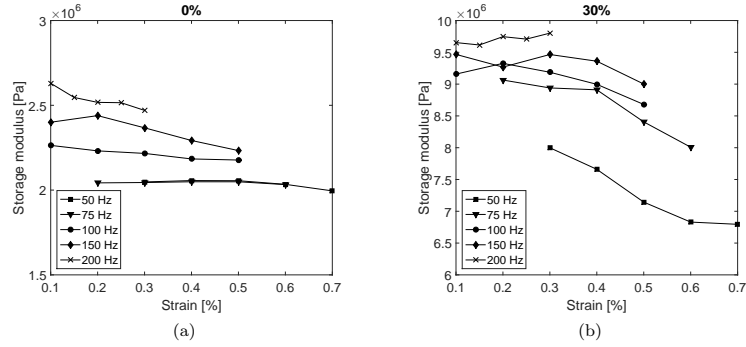


Figure 10: Storage modulus as a function of strain for (a) 0% and (b) 30% MRE samples and different frequencies.

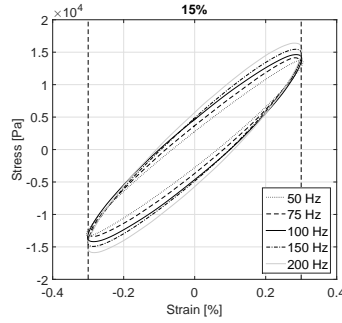


Figure 11: Influence of the frequency in the stress-strain diagrams for the 15% sample with a strain amplitude of 0.3%.

165 is seen, increasing frequency from 50 to 200 Hz (Figure 12(a)). However, the larger frequency influence is seen from 50 to 100 Hz. The particle influence is larger; a 75% increase can be obtained by increasing the particle content from 0% to 30% due to filler reinforcement phenomena [29]. These tendencies are in agreement with the literature for the compression mode [22, 23].

The loss factor also increases with frequency, but the tendency is not so clear (Figure 12(b)),  
 170 which is in accordance with the literature [22, 23]. The influence of particle content seems to increase the loss factor, comparing all contents with the 0% sample. However, comparing the 15% and 30% contents, the loss factor decreases. This can be explained by the damping mechanism. When particles are introduced, internal particle friction and interfacial damping between the particles and the matrix is generated and added to the damping due to the polymer chains [30–  
 175 33]. However, when the particle content is close to the maximum, the polymer chains are smaller and the predominant damping is due to particle friction. This is why the loss factor decreases at

high particle contents.

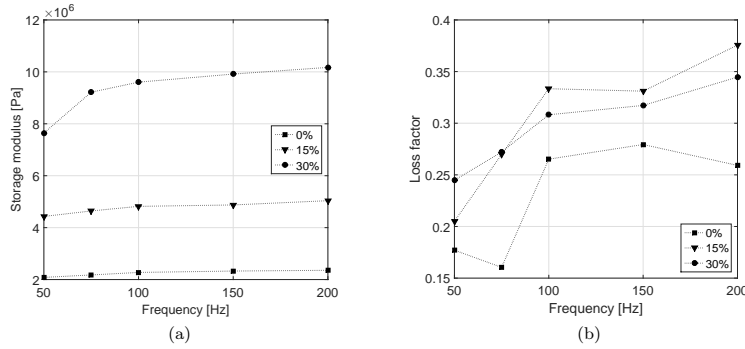


Figure 12: (a) Storage modulus and (b) loss factor as a function of frequency for all studied samples.

The influence of the magnetic field can be seen in Figure 13. As an example, the 30% isotropic MRE is shown. The storage modulus increases with magnetic field (Figure 13(a)), while in the stress-strain diagram it is not evident (Figure 13(b)). The MR effect values (variation of storage modulus due to the magnetic field) are shown in Table 3. The larger MR effect occurs with higher particle content and magnetic field density. However, the values obtained for the MR effect are not as large as in the literature in compression mode [5, 6, 22, 23, 34] due to the low magnetic fields studied in this work. Comparing the compression results with our previous work [35], which investigates the magneto-dynamic properties in shear mode, it can be seen that the MR effect is larger in compression mode.

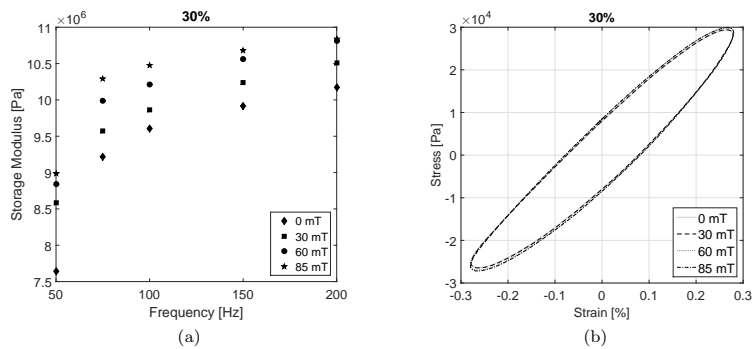


Figure 13: Influence of the magnetic field on the viscoelastic properties of the 30% isotropic MRE sample. (a) Storage modulus variation as a function of frequency and (b) stress-strain diagram at 100 Hz.



Table 3: Mean magnetorheological effect of isotropic MREs.

Particle content	Frequency [Hz]		
	30 mT	60 mT	85 mT
15%	$1.07 \pm 0.73$	$2.76 \pm 0.81$	$4.03 \pm 0.72$
30%	$3.31 \pm 0.47$	$6.89 \pm 1.01$	$8.75 \pm 2.07$

## 5. Conclusions

In this work, a new magneto-dynamic compression technique was developed to characterise MREs at high frequencies. To the best of the author's knowledge, it is the first time the LVE region was determined in compression mode for MREs. This work has analysed the influence of synthesis and characterisation variables on the LVE region, and compression magneto-viscoelastic properties from 50 to 200 Hz were characterised within the LVE region.

Using strain-sweep tests, the linear viscoelastic region was determined for isotropic MREs in compression mode. The LVE region is determined by the storage modulus when the discrepancy is larger than 10%. The LVE region increases with frequency and decreases with particle content. Hence, it is determined by the 30% sample at 50 Hz. However, the LVE region in compression mode is larger than in shear mode.

Magneto-viscoelastic properties were analysed using frequency-sweep tests. The storage modulus and the loss factor increases with particle content and frequency. The largest storage modulus increase of 75% occurs with the particle content, while an increment of 16% is given with frequency. The damping of MREs is also increased with particle content.

The variation of the storage modulus due to magnetic field increases with particle content and magnetic field up to 8%. The MR effect is larger in compression mode than in shear mode.

## Acknowledgement

The authors would like to thank Gorka Aretxaga for helpful discussions in the design of the testing device. Financial support was provided by the Department of Education of the Basque Government for the Research Predoc Grant PRE\_2014\_1\_284 and the PI-2016-1-0026 research project. Financial support for the DPI 2015-71198-R research project was provided by the Spanish Government.

## References

- [1] R. Li, L. Z. Sun, Viscoelastic Responses of Silicone-Rubber-Based Magnetorheological Elastomers Under Compressive and Shear Loadings, *Journal of Engineering Materials and Technology* 135 (2) (2013) 021008. doi:10.1115/1.4023839.

- URL <http://materialstechnology.asmedigitalcollection.asme.org/article.aspx?doi=10.1115/1.4023839>  
 215
- [2] F. S. Bellucci, F. C. Lobato de Almeida, M. A. Lima Nobre, M. A. Rodríguez-Pérez, A. T. Paschoalini, A. E. Job, Magnetic properties of vulcanized natural rubber nanocomposites as a function of the concentration, size and shape of the magnetic fillers, *Composites Part B: Engineering* 85 (2016) 196–206. doi:10.1016/j.compositesb.2015.09.013.  
 220 URL <http://linkinghub.elsevier.com/retrieve/pii/S135983681500548X>
- [3] W. Li, X. Zhang, T. Tian, W. Wen, Fabrication and characterisation of patterned magnetorheological elastomers, in: *AIP Conference Proceedings*, Vol. 1542, 2013, pp. 129–132. doi:10.1063/1.4811884.  
 URL <http://scitation.aip.org/content/aip/proceeding/aipcp/10.1063/1.4811884>  
 225 <http://aip.scitation.org/doi/abs/10.1063/1.4811884>
- [4] M. Lokander, B. Stenberg, Improving the magnetorheological effect in isotropic magnetorheological rubber materials, *Polymer Testing* 22 (6) (2003) 677–680. doi:10.1016/S0142-9418(02)00175-7.  
 URL <http://linkinghub.elsevier.com/retrieve/pii/S0142941802001757>
- 230 [5] G. Schubert, P. Harrison, Large-strain behaviour of Magneto-Rheological Elastomers tested under uniaxial compression and tension, and pure shear deformations, *Polymer Testing* 42 (2015) 122–134. doi:10.1016/j.polymertesting.2015.01.008.  
 URL <http://dx.doi.org/10.1016/j.polymertesting.2015.01.008><http://linkinghub.elsevier.com/retrieve/pii/S0142941815000124>
- 235 [6] H. S. Jung, S. H. Kwon, H. J. Choi, J. H. Jung, Y. G. Kim, Magnetic carbonyl iron/natural rubber composite elastomer and its magnetorheology, *Composite Structures* 136 (2016) 106–112. doi:10.1016/j.compstruct.2015.10.008.  
 URL <http://linkinghub.elsevier.com/retrieve/pii/S0263822315009393>
- [7] N. M. Wereley, A. Chaudhuri, J. H. Yoo, S. John, S. Kotha, A. Suggs, R. Radhakrishnan, B. J. Love, T. S. Sudarshan, Bidisperse Magnetorheological Fluids using Fe Particles at Nanometer and Micron Scale, *Journal of Intelligent Material Systems and Structures* 17 (5) (2006) 393–401. doi:10.1177/1045389X06056953.  
 240 URL <http://jim.sagepub.com/cgi/doi/10.1177/1045389X06056953><http://journals.sagepub.com/doi/10.1177/1045389X06056953>
- 245 [8] I. Agirre-Olabide, J. Berasategui, M. J. Elejabarrieta, M. M. Bou-Ali, Characterization of the linear viscoelastic region of magnetorheological elastomers, *Journal of Intelligent Material*

- Systems and Structures 25 (16) (2014) 2074–2081. doi:10.1177/1045389X13517310.  
URL <http://jim.sagepub.com/cgi/doi/10.1177/1045389X13517310><http://journals.sagepub.com/doi/10.1177/1045389X13517310>
- 250 [9] Ubaidillah, H. J. Choi, S. A. Mazlan, F. Imaduddin, Harjana, Fabrication and viscoelastic characteristics of waste tire rubber based magnetorheological elastomer, *Smart Materials and Structures* 25 (11) (2016) 115026. doi:10.1088/0964-1726/25/11/115026.  
URL <http://dx.doi.org/10.1088/0964-1726/25/11/115026><http://stacks.iop.org/0964-1726/25/i=11/a=115026?key=crossref.0761e19ff6f475189d0136ca9bc71f16>
- 255 [10] A. B. Bonhome-Espinosa, F. Campos, I. A. Rodriguez, V. Carriel, J. A. Marins, A. Zubarev, J. D. G. Duran, M. T. Lopez-Lopez, Effect of particle concentration on the microstructural and macromechanical properties of biocompatible magnetic hydrogels, *Soft Matter* 13 (16) (2017) 2928–2941. doi:10.1039/C7SM00388A.  
URL <http://xlink.rsc.org/?DOI=C7SM00388A>
- 260 [11] I. Agirre-Olabide, M. J. Elejabarrieta, M. M. Bou-Ali, Matrix dependence of the linear viscoelastic region in magnetorheological elastomers, *Journal of Intelligent Material Systems and Structures* 26 (14) (2015) 1880–1886. doi:10.1177/1045389X15580658.  
URL <http://jim.sagepub.com/content/early/2015/04/21/1045389X15580658>.  
abstract<http://journals.sagepub.com/doi/10.1177/1045389X15580658>
- 265 [12] P. Yang, M. Yu, J. Fu, H. Luo, Rheological properties of dimorphic magnetorheological gels mixed dendritic carbonyl iron powder, *Journal of Intelligent Material Systems and Structures* (2017) 1045389X1769205doi:10.1177/1045389X17692050.  
URL <http://journals.sagepub.com/doi/10.1177/1045389X17692050>
- [13] A. A. Lerner, K. Cunefare, Performance of MRE-based Vibration Absorbers, *Journal of Intelligent Material Systems and Structures* 19 (5) (2008) 551–563. doi:10.1177/1045389X07077850.  
270 URL <http://jim.sagepub.com/cgi/doi/10.1177/1045389X07077850><http://journals.sagepub.com/doi/10.1177/1045389X07077850>
- [14] B. Kavlicoglu, B. Wallis, H. Sahin, Y. Liu, Magnetorheological elastomer mount for shock and vibration isolation, in: M. N. Ghasemi-Nejhad (Ed.), *Proc. SPIE 7977, Active and Passive Smart Structures and Integrated Systems*, Vol. 7977, 2011, p. 79770Y.  
275 doi:10.1117/12.881870.  
URL <http://proceedings.spiedigitallibrary.org/proceeding.aspx?articleid=>

- 729230<http://proceedings.spiedigitallibrary.org/proceeding.aspx?doi=10.1117/12.881870>
- 280
- [15] C. Yang, J. Fu, M. Yu, X. Zheng, B. Ju, A new magnetorheological elastomer isolator in shear-compression mixed mode, *Journal of Intelligent Material Systems and Structures* 26 (10) (2015) 1290–1300. doi:10.1177/1045389X14541492.  
URL <http://jim.sagepub.com/cgi/doi/10.1177/1045389X14541492><http://journals.sagepub.com/doi/10.1177/1045389X14541492>
- 285
- [16] S. Sun, J. Yang, H. Deng, H. Du, W. Li, G. Alici, M. Nakano, Horizontal vibration reduction of a seat suspension using negative changing stiffness magnetorheological elastomer isolators, *International Journal of Vehicle Design* 68 (1/2/3) (2015) 104. doi:10.1504/IJVD.2015.071076.  
URL <http://stacks.iop.org/0964-1726/12/i=1/a=316?key=crossref.d53379232b3503d2afee63f7fb80a4ba%5Cnhttp://asa.scitation.org/doi/abs/10.1121/1.4778670%5Cnhttp://stacks.iop.org/0964-1726/13/i=2/a=009?key=crossref.7c75a21e7d1fd4fbafd1b456f31da4d1%5Cnhttp://stacks>
- 290
- [17] I. L. Ladipo, J. Fadly, W. F. Faris, Characterization of Magnetorheological Elastomer (MRE) Engine Mounts, *Materials Today: Proceedings* 3 (2) (2016) 411–418. doi:10.1016/j.matpr.2016.01.029.  
URL <http://dx.doi.org/10.1016/j.matpr.2016.01.029><http://linkinghub.elsevier.com/retrieve/pii/S2214785316000304>
- 295
- [18] T. Komatsuzaki, T. Inoue, Y. Iwata, Experimental Investigation of an Adaptively Tuned Dynamic Absorber Incorporating Magnetorheological Elastomer with Self-Sensing Property, *Experimental Mechanics* 56 (5) (2016) 871–880. doi:10.1007/s11340-016-0137-2.  
URL <http://dx.doi.org/10.1007/s11340-016-0137-2><http://link.springer.com/10.1007/s11340-016-0137-2>
- 300
- [19] Z. Varga, G. Filipcsei, M. Zrínyi, Magnetic field sensitive functional elastomers with tuneable elastic modulus, *Polymer* 47 (1) (2006) 227–233. doi:10.1016/j.polymer.2005.10.139.  
URL <http://linkinghub.elsevier.com/retrieve/pii/S0032386105016125>
- 305
- [20] F. Hiptmair, Z. Major, R. Haflacher, S. Hild, Design and application of permanent magnet flux sources for mechanical testing of magnetoactive elastomers at variable field directions, *Review of Scientific Instruments* 86 (8) (2015) 085107. doi:10.1063/1.4927714.  
URL <http://scitation.aip.org/content/aip/journal/rsi/86/8/10.1063/1.4927714><http://aip.scitation.org/doi/10.1063/1.4927714>
- 310

- [21] H. Vatandoost, M. Norouzi, S. M. S. Alehashem, S. K. Smoukov, A novel phenomenological model for dynamic behavior of magnetorheological elastomers in tension–compression mode, *Smart Materials and Structures* 26 (6) (2017) 065011. doi:10.1088/1361-665X/aa6126.  
315 URL <http://stacks.iop.org/0964-1726/26/i=6/a=065011?key=crossref.7ca190a856b0738ca3c588e17e00bbdc>
- [22] M. Kallio, T. Lindroos, S. Aalto, E. Järvinen, T. Kärnä, T. Meinander, Dynamic compression testing of a tunable spring element consisting of a magnetorheological elastomer, *Smart Materials and Structures* 16 (2) (2007) 506–514. doi:10.1088/0964-1726/16/2/032.  
320 URL <http://stacks.iop.org/0964-1726/16/i=2/a=032?key=crossref.915e591f8565b81af3d733ed36da95b5>
- [23] Ubaidillah, F. Imaduddin, Y. Li, S. A. Mazlan, J. Sutrisno, T. Koga, I. Yahya, S.-B. Choi, A new class of magnetorheological elastomers based on waste tire rubber and the characterization of their properties, *Smart Materials and Structures* 25 (11) (2016) 115002. doi:10.1088/0964-1726/25/11/115002.  
325 URL <http://dx.doi.org/10.1088/0964-1726/25/11/115002>  
<http://stacks.iop.org/0964-1726/25/i=11/a=115002?key=crossref.c79c96e398b6ee0b6c63cf252ba4b662>  
330 <http://stacks.iop.org/0964-1726/25/i=11/a=115002?key=crossref.c79c96e398b6ee0b6c63cf252ba4b662>
- [24] M. Norouzi, S. M. Sajjadi Alehashem, H. Vatandoost, Y. Q. Ni, M. M. Shahmardan, A new approach for modeling of magnetorheological elastomers, *Journal of Intelligent Material Systems and Structures* 27 (8) (2016) 1121–1135. doi:10.1177/1045389X15615966.  
335 URL <http://jim.sagepub.com/content/early/2015/11/17/1045389X15615966.abstract>  
<http://journals.sagepub.com/doi/10.1177/1045389X15615966>
- [25] L. Kari, P. Blom, Magneto-sensitive rubber in a noise reduction context – exploring the potential, *Plastics, Rubber and Composites* 34 (8) (2005) 365–371. doi:10.1179/174328905X59692.  
340 URL <http://www.ingentaconnect.com/content/maney/prc/2005/00000034/00000008/art00005{#}expand/collapse>  
<http://www.tandfonline.com/doi/full/10.1179/174328905X59692>
- [26] R. Lakes, *Viscoelastic Materials*, Cambridge University Press, Cambridge, 2009. doi:10.1017/CB09780511626722.  
URL <http://ebooks.cambridge.org/ref/id/CB09780511626722>

- 345 [27] A. D. Nashif, D. I. G. Jones, J. P. Henderson, *Vibration damping*, John Wiley & Sons, New York, 1985.
- [28] U. R. Poojary, K. V. Gangadharan, Magnetic field and frequency dependent LVE limit characterization of magnetorheological elastomer, *Journal of the Brazilian Society of Mechanical Sciences and Engineering* 39 (4) (2017) 1365–1373. doi:10.1007/s40430-016-0592-9.
- 350 URL <http://link.springer.com/10.1007/s40430-016-0592-9>
- [29] S. Aloui, M. Klüppel, Magneto-rheological response of elastomer composites with hybrid-magnetic fillers, *Smart Materials and Structures* 24 (2) (2015) 025016. doi:10.1088/0964-1726/24/2/025016.
- URL <http://stacks.iop.org/0964-1726/24/i=2/a=025016?key=crossref.f07a589b2b0e8660ce54e220837b0bcb>
- 355 f07a589b2b0e8660ce54e220837b0bcb
- [30] R. K. Shuib, K. L. Pickering, B. R. Mace, Dynamic properties of magnetorheological elastomers based on iron sand and natural rubber, *Journal of Applied Polymer Science* 132 (8) (2015) n/a–n/a. doi:10.1002/app.41506.
- URL <http://doi.wiley.com/10.1002/app.41506>
- 360 [31] B. Ju, R. Tang, D. Zhang, B. Yang, M. Yu, C. Liao, Temperature-dependent dynamic mechanical properties of magnetorheological elastomers under magnetic field, *Journal of Magnetism and Magnetic Materials* 374 (2015) 283–288. doi:10.1016/j.jmmm.2014.08.012.
- URL <http://linkinghub.elsevier.com/retrieve/pii/S0304885314007008>
- [32] S. R. Khimi, K. Pickering, Comparison of dynamic properties of magnetorheological elastomers with existing antivibration rubbers, *Composites Part B: Engineering* 83 (2015) 175–183. doi:10.1016/j.compositesb.2015.08.033.
- 365 URL <http://dx.doi.org/10.1016/j.compositesb.2015.08.033http://linkinghub.elsevier.com/retrieve/pii/S1359836815004631>
- [33] K. Pickering, S. Raa Khimi, S. Ilanko, The effect of silane coupling agent on iron sand for use in magnetorheological elastomers Part 1: Surface chemical modification and characterization, *Composites Part A: Applied Science and Manufacturing* 68 (2015) 377–386. doi:10.1016/j.compositesa.2014.10.005.
- 370 URL <http://linkinghub.elsevier.com/retrieve/pii/S1359835X14003157>
- [34] N. A. Yunus, S. A. Mazlan, Ubaidillah, S.-b. Choi, F. Imaduddin, S. A. Abdul Aziz, M. H. Ahmad Khairi, Rheological properties of isotropic magnetorheological elastomers featuring an epoxidized natural rubber, *Smart Materials and Structures* 25 (10) (2016) 107001.
- 375

doi:10.1088/0964-1726/25/10/107001.

URL <http://dx.doi.org/10.1088/0964-1726/25/10/107001><http://stacks.iop.org/0964-1726/25/i=10/a=107001?key=crossref.261e0ddf4467435ecdf6394b4685951a>

- 380 [35] I. Agirre-Olabide, M. J. Elejabarrieta, Effect of synthesis variables on viscoelastic properties of elastomers filled with carbonyl iron powder, *Journal of Polymer Research* 24 (9) (2017) 139. doi:10.1007/s10965-017-1299-z.  
URL <http://link.springer.com/10.1007/s10965-017-1299-z>





*Find life experiences and swallow them whole. Travel. Meet many people. Go down some dead ends and explore dark alleys. Try everything. Exhaust yourself in the glorious pursuit of life.*

Lawrence K. Fish

# 4

## Magneto-viscoelastic modelling

- I. Agirre-Olabide, and M.J. Elejabarrieta. 2017. A new three-dimensional magneto-viscoelastic model for isotropic magnetorheological elastomers. *Smart Mater. Struct.*, 26(3):035021. doi: 10.1088/1361-665X/26/3/035021
- I. Agirre-Olabide, and M.J. Elejabarrieta. 2016. Maximum attenuation variability of isotropic magnetosensitive elastomers. *Polym. Test.*, 54:104-113. doi: 10.1016/j.polymertesting.2016.06.021
- I. Agirre-Olabide, P. Kuzhir, and M.J. Elejabarrieta. 2018. Linear magneto-viscoelastic model based on magnetic permeability components for anisotropic magnetorheological elastomers. *J. Magn. Magn. Mater.*, 446:155-161. doi: 10.1016/j.jmmm.2017.09.017

In this chapter, the shear magneto-viscoelastic behaviour of isotropic and anisotropic magnetorheological elastomers (MREs) is modelled. The viscoelastic nature of MREs is modelled using a four-parameter fractional derivative model, and the temperature is introduced with the Arrhenius model. Extending both models in the frequency and temperature domain, the maximum attenuation of isotropic MREs is studied. Each parameter of the viscoelastic model is defined as a function of particle content. Furthermore, two models to predict the magneto-induced modulus of isotropic and anisotropic MREs are developed. Finally, the viscoelastic, particle-matrix interaction and magneto-induced modulus models are coupled in a single magneto-viscoelastic model, one for isotropic MREs and another one for anisotropic MREs.

## 4.1 Introduction

The dynamic properties of MREs depend on the matrix ([Hiptmair et al. 2015](#); [Xu et al. 2016](#)), the particle content ([Shuib et al. 2015](#)) and the external magnetic field applied ([Aloui and Klüppel 2015](#)). Hence, each of them has to be modelled to obtain the constitutive model of MREs to predict its dynamic response. Moreover, the properties of MREs are completely dependent on the particle distribution, which is therefore considered an important characteristic of MREs. Isotropic MRE samples are prepared by vulcanisation without an external magnetic field; these samples have a random particle distribution ([Gao and Wang 2016](#)). However, if an external magnetic field is applied during the vulcanisation process, the particles are aligned in the direction of the magnetic field, and consequently, particle chains or thicker chain aggregates are obtained; these samples are called anisotropic MREs ([Aloui and Klüppel 2015](#)).

Due to the viscoelastic matrix, the predominant behaviour of MREs is the viscoelastic one. The modelling of the viscoelasticity of these materials is completed via different constitutive models, such as classical differential models and fractional derivative models.

Combining different rheological elements, classical differential models were developed. For that purpose springs and dashpots were used ([Jones 2001](#)). The

widely used Zener model (Zener 1948) or the standard lineal model is a combination of a Maxwell element and a spring in parallel configuration. In the literature, this model was used by Chen and Jerrams (2011) and Han et al. (2012) to model the viscoelastic behaviour of MREs. However, these materials were also modelled using a different element configuration. Li et al. (2010), Liao et al. (2013) and Behrooz et al. (2014) combined a spring and a Kelvin–Voigt element in serial configuration. To obtain a better fitting, additional material parameters were introduced by Zhu et al. (2015).

Fractional derivative (FD) models containing fewer material parameters can be used to avoid the addition of material parameters. Moreover, the material parameters have a physical interpretation (Pritz 1996). Due to that reason, the viscoelastic behaviour of isotropic (Xu et al. 2016) and anisotropic (Guo et al. 2014; Zhu et al. 2013) MREs have recently been modelled using fractional derivative models. Xu et al. (2016) combined a fractional Kelvin and Maxwell model in the parallel configuration to develop a higher order model (seven material parameters) for isotropic MREs. For anisotropic MREs, two elements were combined: a spring and an Abel dashpot (fractional derivative element); Zhu et al. (2013) combined them in a parallel configuration, while Guo et al. (2014) did so in a serial configuration. Due to the advantages of the fractional derivative models, in this chapter a four-parameter FD model is used to predict the viscoelastic nature of MREs.

In many applications, MREs have been designed to dissipate as much energy as possible. The maximum attenuation (loss factor peak) of these materials occurs at a certain frequency and temperature (Jones 2001), which can be identified via the glass transition temperature  $T_g$  (Pickering et al. 2015).

In order to identify the maximum attenuation conditions, a dynamic mechanical analyser can be used (Tian et al. 2013b). Pickering et al. (2015) and Shuib et al. (2015) studied the variation of the  $T_g$  of magnetorheological elastomers. The maximum attenuation is increased (Robertson et al. 2008; Shuib et al. 2015) and  $T_g$  decreased with particle content (Wu et al. 2009).

Another way to determine the maximum attenuation is extending a fractional derivative model in the frequency domain for rubber (Wollscheid and Lion 2014) or polymer material (Moreira et al. 2010).

The influence of temperature in the viscoelastic properties can be modelled

using the frequency-temperature superposition principle (Ferry 1980). This principle is based on the assumption that the complex modulus measured at any chosen frequency  $f_1$  and at a reference temperature  $T_1$  is identical to that at any other frequency  $f_2$  and a different temperature  $T_2$ . Those conditions are related with a temperature dependent shift factor  $a_T(T)$ , which represents the basic effect of temperature on the viscoelastic properties, and can be described using the equation of Williams-Landel-Ferry (WLF) (Williams et al. 1955) or that of Arrhenius (Jones 2001).

In this thesis, the four-parameter model is coupled with the Arrhenius model, and extend it in the frequency and temperature domain to analyse the maximum attenuation of isotropic MREs.

The embedded particles in MREs modified the viscoelastic behaviour (Lu et al. 2012), and consequently the interaction between the matrix and the filler (particle) have been modelled, also known as filler reinforcement. Based on the viscosity law of Einstein, Guth and Gold (1938) and Guth (1945) modelled the rigidity variation of a rubber matrix. That principle was also used for MREs by Leng et al. (2013). Ray et al. (2002) proposed a two-parameter exponential model to introduce the interaction of surface-treated fillers. However, Chen and Jerrams (2011) used a rheological model, a spring and a Coulomb friction slide, to predict the particle-matrix interaction in MREs.

In order to model the particle-matrix interaction, each parameter of the four-parameter FD model is analysed and modelled as a function of particle content adapting the model proposed for rubber by Mullins and Tobin (1966) to isotropic MREs.

The mechanical properties of isotropic MREs varies with an external magnetic field, which Ivaneyko et al. (2011; 2012) modelled, defining three different lattice models. In addition, they studied the dipole–dipole interaction to model the mechanical properties of isotropic MREs. The same interactions were studied to model the magneto-induced modulus of anisotropic MRE (Davis 1999; Jolly et al. 1996a;b; Shen et al. 2004). Coquelle et al. (2006) developed an effective modulus to represent the magneto-induced modulus of isotropic MREs dependent on the Young modulus and Poisson ratio of the matrix. Therefore, the magneto-induced modulus of isotropic MREs is modelled modifying the model proposed by Jolly

et al. (1996a;b).

Many works developed in the literature for the modelling of the magneto-induced modulus of anisotropic MREs were based on an ideal chain-like structure Davis (1999); Jolly et al. (1996a); Shen et al. (2004). However, López-López et al. (2012) proposed a model for magnetorheological fluids by introducing the influence of aggregates having a body centered tetragonal (BCT) internal structure (a more stable and more realistic structure), and they combined numerical simulations of the composite magnetic permeability with the analytical model predicting the stress–strain relationship. For MREs, Leng et al. (2013) proposed an effective permeability model to estimate the shear storage modulus, and Dong et al. (2013) developed a theoretical model for chains composed of magnetic particles and normal pressure, based on the effective permeability calculated by the Maxwell–Garnett mixing rule. Chen et al. (2007b) proposed a finite-column model to simulate the field-induced shear modulus.

The magnetic permeability of materials can be measured by using different techniques. de Vicente et al. (2002) used a modified force balance method to measure the magnetic permeability of carbonyl iron powder suspension. Bellucci et al. (2016) used vibrating sample magnetometry (VSM) on a magnetic nanocomposite based on natural rubber. Schubert and Harrison (2016) identified the permeability of isotropic and anisotropic MREs using an inverse modelling approach. Furthermore, they calculated the permeabilities of anisotropic MREs in the particle alignment direction and perpendicular to the alignment direction. However, de Vicente et al. (2002) measured the permeability of carbonyl iron powder in a suspension and showed that the permeability decreases with the internal magnetic field.

Using the model proposed by López-López et al. (2012) for MRFs, the magneto-induced modulus of anisotropic MREs is modelled. Furthermore, the magnetic permeability components are measured and modelled in the magnetic field domain.

In the literature, the magneto-viscoelastic models coupling viscoelastic and magnetic interaction models were developed for isotropic and anisotropic MREs. Eem et al. (2012) developed a magneto-viscoelastic model for isotropic MREs using classical differential models. A classical four-parameter magneto-viscoelastic

model have been proposed by [Li et al. \(2010\)](#), and all material parameters were fitted to experimental data for each magnetic field density. The magneto-viscoelastic behaviour using fractional derivatives have been modelled for anisotropic MREs ([Guo et al. 2014](#); [Zhu et al. 2013](#)), and combined in a serial configuration a fractional derivative Maxwell model and a spring, which was dependent on the magnetic field and modelled assuming chain-like structures.

In this thesis, a three magneto-viscoelastic model was developed for MREs, and the proposed two magneto-induced models for isotropic and anisotropic MREs were coupled with the viscoelastic model to predict the shear magneto-viscoelastic behaviour.

## 4.2 Critical review

In the literature, there are some viscoelastic models used to predict the viscoelastic nature of MREs. However, many of them are based on classical differential model where many parameters were used ([Han et al. 2012](#); [Zhu et al. 2015](#)). The fractional derivative model used for isotropic MREs was a high-order fractional derivative model ([Xu et al. 2016](#)), and for anisotropic MREs a three-parameter model ([Guo et al. 2014](#); [Zhu et al. 2013](#)). In the developed works not all parameters have a physical meaning.

The influence of the temperature in the viscoelastic properties of MREs is another important characteristic, because properties are dependent on this variable; and consequently, the operation range of the MRE is different for the applications. The maximum attenuation of MRE materials was characterised using a DMA in the temperature domain ([Khimi and Pickering 2015](#); [Pickering et al. 2015](#)). However, evolution of the attenuation in the frequency domain have not been studied.

According to the influence of filler particles, there are some works in the literature that mainly they focus on the influence in the real part or storage modulus of the MREs ([Guth and Gold 1938](#); [Leng et al. 2013](#)). Therefore, the influence of the particle content in the viscoelastic model parameters is not studied.

The influence of the magnetic field in the mechanical properties of isotropic MREs was modelled by [Ivaneyko et al. \(2011; 2012\)](#). Furthermore, [Coquelle et al.](#)

(2006) developed an effective modulus depending on the Young modulus and Poisson ratio of the matrix, and Eem et al. (2012) proposed a magneto-viscoelastic model based on classical viscoelastic models for isotropic MREs. Nevertheless, the coupling of the influence of matrix, particle content, temperature, frequency and magnetic field in a single model have not been developed.

In the literature, most of the works modelled the magneto-induced modulus for anisotropic MREs, which were based on an ideal chain-like structure (Davis 1999; Shen et al. 2004). However, more realistic and stable structures were developed for MR materials (López-López et al. 2012). Therefore, many works have not analysed the more realistic structures in anisotropic MREs and coupled it with a viscoelastic model.

Therefore, the viscoelastic behaviour is modelled using a four-parameter fractional derivative model, which is extended in the frequency domain to analyse the variability of the maximum attenuation. The influence of temperature is modelled using the Arrhenius model. Furthermore, an external magnetic field is used to analyse the variability of the maximum attenuation conditions. The evolution of each parameter in the function of the particle content is studied and modelled, and particle-matrix interaction is modelled defining a hard phase (particles) and a soft phase (matrix) (Mullins and Tobin 1966). Furthermore, a magneto-induced model is used to predict the evolution of the magnetorheological (MR) effect, a model based on the dipole-dipole interactions for isotropic MREs and another one using the longitudinal and transverse magnetic permeability components for anisotropic MREs. Finally, the proposed constitutive model is a fractional derivative model coupled with particle-matrix interaction and the magneto-induced modulus, which predicts the MR effect of isotropic MREs with different particle contents and magnetic fields. In the same way, a magneto-viscoelastic model is proposed for anisotropic MREs which predicts the influence of magnetic field in the viscoelastic properties of anisotropic MREs.

## 4.3 Aims

The goal of this chapter is to develop two magneto-viscoelastic models to predict the shear magneto-viscoelastic behaviour of isotropic and anisotropic MREs in a wide range of working conditions. The specific objectives are:

- Model the viscoelastic behaviour of MREs and the particle-matrix interaction.
- Model the magneto-induced modulus of isotropic and anisotropic MREs.
- Magneto-viscoelastic modelling of isotropic and anisotropic MREs

## 4.4 Results

In this section, a summary of the results presented in the three papers, to which the chapter refers and include in sec 4.6., are shown. All the models shown in this section are developed for the RTV-SR, and therefore in this chapter all the samples are called MRE. In [Agirre-Olabide et al. \(2017\)](#) the magneto-viscoelastic model for isotropic MREs is developed. Using fractional derivative and Arrhenius models the maximum attenuation of isotropic MREs is analysed in [Agirre-Olabide and Elejabarrieta \(2016\)](#). The magneto-viscoelastic model for anisotropic MREs is proposed in [Agirre-Olabide et al. \(2018\)](#).

In this summary, a viscoelastic model based on a four-parameter fractional derivative model is shown. Besides, the influence of temperature is coupled with the Arrhenius model, and both are extended in the frequency and temperature domain to study the maximum attenuation variability. Moreover, the influence of the filler in the viscoelasticity of isotropic MREs is modelled. The magneto-induced modulus of isotropic and anisotropic MREs is modelled using two different models. Finally, the previously developed models are coupled in a single magneto-viscoelastic model for each type of MRE.



#### 4.4.1 Viscoelastic modelling

Viscoelastic models, such as fractional derivative (FD) models, can be used in the time and frequency domains, and they contain fewer material parameters than classical viscoelastic models, in which each parameter has a physical meaning. A four-parameter fractional derivative model is used in the frequency domain and the shear complex modulus ( $G^*$ ) is,

$$G^* = \frac{G_0 + (G_0 + C)(i\omega\tau)^\alpha}{1 + (i\omega\tau)^\alpha} = G_0 + \frac{C(i\omega\tau)^\alpha}{1 + (i\omega\tau)^\alpha} \quad (4.1)$$

where  $G_0$  is the static shear modulus,  $C$  is the elastic part of the viscoelastic branch of the model,  $\tau$  is the relaxation time,  $\alpha$  is the fractional parameter and  $\omega$  is the angular frequency.

A sketch of equation (4.1) can be seen in Figure 4.1. Two branches are defined: an elastic branch (a spring ( $G_0$ )) and a viscoelastic branch (a spring ( $C$ ), along with an Abel dashpot ( $\alpha$  and  $\tau$ )). The elastic nature of the viscoelastic branch is due to the spring and the viscous nature because of the Abel dashpot. Moreover, a shear strain is defined for each element,  $\gamma$  for the shear strain applied to the model,  $\gamma_v$  for the shear strain of the viscous part and  $\gamma_e$  for the elastic strain of the viscoelastic branch.

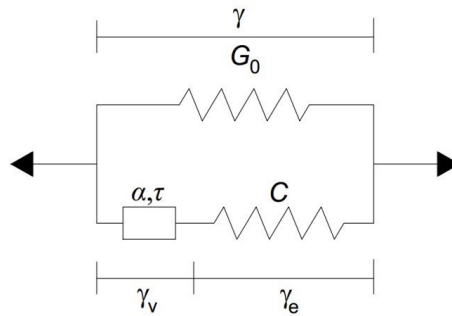


**Figure 4.1** Sketch of the fractional derivative model

Within the viscoelasticity, the influence of the temperature is also analysed. As shown in Figure 2.8, the temperature decreases the storage modulus and loss factor. In order to introduce the temperature dependence to the fractional derivative model, the frequency-temperature superposition principle is used (Ferry 1980).

This principle is based on the assumption that the complex modulus measured at any chosen frequency  $f_1$  and at a reference temperature  $T_1$  is identical to that at any other frequency  $f_2$  and a different temperature  $T_2$ . Those conditions are related with a temperature dependent shift factor  $a_T(T)$ , which represents the basic effect of temperature on the viscoelastic properties and can be described using the equation of Williams-Landel-Ferry (WLF) (Williams et al. 1955) or that of Arrhenius (Jones 2001). The WLF equation is used at temperatures above the glass transition temperature ( $T_g$ ) and under  $T_g + 100$  °C.

The RTV-SR matrix is a polydimethylsiloxane (PDMS)-based silicone rubber, and the glass transition temperature for those polymers is around -125 °C (Fragiadakis and Pissis 2007). Therefore, the Arrhenius model is used to introduce the influence of temperature in the four-parameter fractional derivative model. The Arrhenius shift factor equation describes a lineal relationship between  $\log a_T(T)$  and  $1/T$  based on the molecular kinetic theory of chemical reactions (Equation 4, Agirre-Olabide and Elejabarrieta (2016)).

Coupling the Arrhenius model with the four-parameter FD model, and extend it in the frequency and temperature domain, the evolution of the maximum attenuation in shear mode can be analysed.

In Figure 4.2 the extension in frequency domain for the storage modulus and loss factor is shown. In Figure 4.2a, the storage modulus increases with frequency and particle content. In Figure 4.2b, in terms of shape, the loss factor curves are

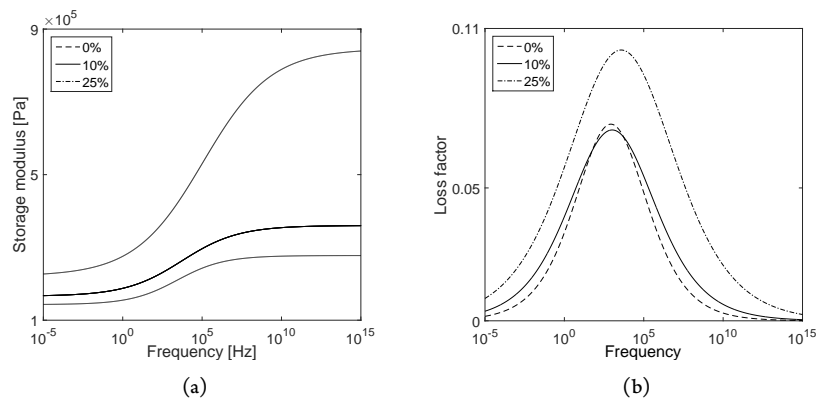


**Figure 4.2** Evolution of the (a) storage modulus ( $G'$ ) and (b) loss factor ( $\tan \delta$ ) of 0%, 10% and 25% isotropic MRE samples as a function of frequency at 25 °C and 0 kA/m

wider with particle content, which indicates that the attenuation is larger over the entire frequency band. In addition, the largest width difference is seen when the maximum particle content is analysed. The maximum attenuation value increases with the particle content, and the maximum increase occurs between the 20% and 25% samples. The frequency at which the loss factor peak occurs also increases with the particle content and, consequently, the loss factor curve is shifted to the right.

In Figure 4.3, the evolution of the peak is shown in the frequency (Figure 4.3(a)) and temperature domains (Figure 4.3(b)) for the 0% isotropic MRE. In frequency domain figures (from  $1e^{-5}$  to  $1e^{15}$  Hz), three temperatures are fixed (-10, 25 and 80 °C), and in the temperature domain (from -200 to 100 °C), the analysed frequencies are 1, 50 and 100 Hz.

The value of the maximum attenuation depends on the particle content and it is constant with frequency and temperature. Specifically, it increases 51% with the particle content from the 5% MRE to the 25% MRE.

In the reduced frequency domain, the frequency at which the maximum attenuation occurs depends on the temperature (Figure 4.3(a)). Therefore, increasing the temperature causes the frequency to increase, which means that the curves are shifted to the right. The same behaviour is observed for storage modulus. Furthermore, the shifting of the storage modulus and loss factor curves is larger with increased particle content (Table 4 Agirre-Olabide and Elejabarrieta (2016)).

On the other hand, the temperature at which the maximum attenuation occurs depends on the frequency (Figure 4.3(b)), which is higher with increased particle content (Pickering et al. 2015). The storage modulus and loss factor curves are shifted to the right, increasing the frequency. Moreover, these increases are larger in the low-frequency range (Figure 4.3(b)), and the variation of the temperature due to frequency is smaller with the increment of particle content (Table 4 Agirre-Olabide and Elejabarrieta (2016)). The shape of the storage modulus and loss factor curves are dependent on frequency.

The influence of the magnetic field in the loss factor of MRE materials is also analysed. The attenuation is larger in the studied frequency band because the shape of the loss factor is wider (Figure 10 Agirre-Olabide and Elejabarrieta (2016)). The maximum attenuation value and frequency are increased with the magnetic

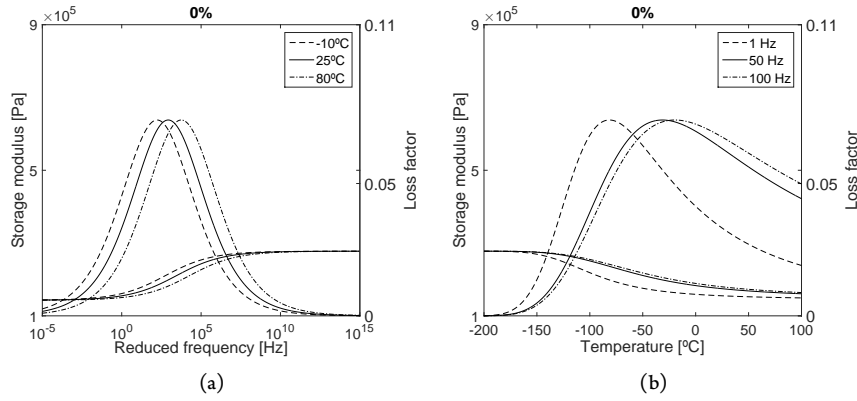


**Figure 4.3** Evolution of the storage modulus ( $G'$ ) and loss factor ( $\tan \delta$ ) as a function of (a) reduced frequency (for -10, 25 and 80 °C), and (b) temperature (for 1, 50 and 100 Hz) for the 0% MRE sample at 0 kA/m

field, except for the maximum particle content (25%). When a MRE sample is under a magnetic field, the relative movement is almost stopped (Ju et al. 2015). Therefore, the damping due to the particle-matrix and particle-particle friction is reduced and, consequently, the maximum attenuation is also reduced.

#### 4.4.2 Fillers

From the analysis of the influence of the particle content in the viscoelastic properties of MREs, was concluded that the storage and loss modulus, and loss factor were increased with particle content in shear mode. Hence, the influence of particle content is modelled for isotropic MREs.

The four-parameters of the fractional derivative model obtained from the fitting of equation (4.1) to the experimental data are shown in Table 4.1. The least square method was used, and the fitting was done using the dynamic complex modulus. The fitting error did not exceed 1% for the storage and loss modulus. In all of the following figures, experimental data are plotted as points and fitted models as lines.

The influence of the particles in the dynamic properties and in each of the model parameters can be seen in Table 4.1. Therefore, the model proposed in equation (4.1) has to be modified to include the influence of the particle content  $G^*(\omega, \varphi)$ . Hence, each parameter is studied one by one, and then, all of them are

**Table 4.1** Fitting parameters of a four-parameter fractional derivative model for the seven isotropic MRE samples (0-25%) at 25 °C and 0 kA/m

	$G_0$ [Pa]	$C$ [Pa]	$\alpha$	$\tau$	$R^2$
0%	120 194	157 127	0.253	$1.525 \times 10^{-5}$	0.997
1%	128 613	190 275	0.257	$6.829 \times 10^{-6}$	0.981
5%	132 241	228 870	0.244	$1.644 \times 10^{-6}$	0.977
10%	135 002	282 801	0.215	$6.594 \times 10^{-7}$	0.994
15%	137 668	337 612	0.177	$3.370 \times 10^{-7}$	0.983
20%	145 884	454 185	0.182	$1.224 \times 10^{-7}$	0.967
25%	151 142	655 889	0.171	$1.719 \times 10^{-7}$	0.984

coupled. In Figure 5 in [Agirre-Olabide et al. \(2017\)](#), the equations and the fitting of each parameter are shown.

Both  $G_0$  and  $C$  increase with particle content due to the filler reinforcement phenomena. The model of those parameters is based on the interaction between rubber and filler developed by [Mullins and Tobin \(1966\)](#). However, the relaxation time ( $\tau$ ) and the fractional parameter ( $\alpha$ ) are reduced with particle content. Therefore, the following four equations are proposed to model de influence of particle content in the viscoelasticity of isotropic MREs,

$$\begin{aligned}
 G_{01}(\varphi) &= G_{01\%} \cdot \sqrt{\frac{1}{1-\varphi}}, \\
 C_1(\varphi) &= C_{1\%} \cdot \left(\frac{1}{1-\varphi}\right)^4, \\
 \tau(\varphi) &= \tau_{25\%} + B_1 \cdot e^{-a_1 \cdot \varphi}, \\
 \alpha(\varphi) &= A_2 + B_2 \cdot e^{-a_2 \cdot \varphi}.
 \end{aligned} \tag{4.2}$$

Hence, this model is dependent on the data of minimum (1%) and maximum (25%) particle content samples. Moreover, eight material parameters ( $G_{01\%}$ ,  $C_{1\%}$ ,  $\tau_{25\%}$ ,  $B_1$ ,  $a_1$ ,  $A_2$ ,  $B_2$ ,  $a_2$ ) are used to determine the evolution of the four key parameters ( $G_{01}(\varphi)$ ,  $C_1(\varphi)$ ,  $\tau(\varphi)$ ,  $\alpha(\varphi)$ ) of the fractional model with the particle content.

In Figure 4.4, the fitting of the proposed FD model coupled with the particle-

matrix interaction model is shown. The proposed equation, includes the particle content variable, and consequently, any particle content between 1% and 25% can be modelled using eight material parameters.

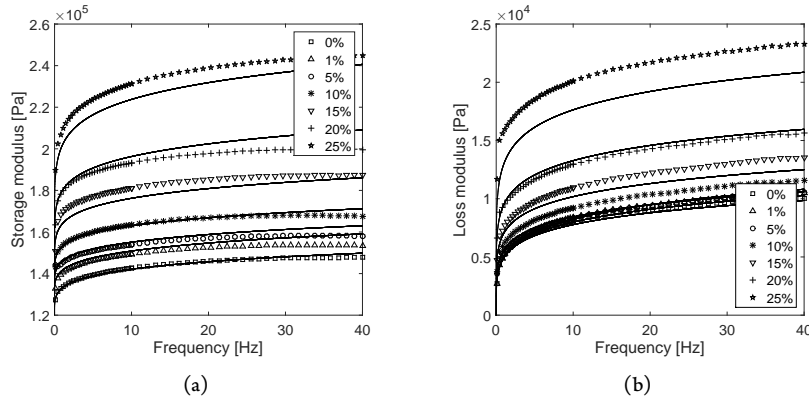


**Figure 4.4** Experimental data (points) and fractional derivative and particle-matrix model (lines) of (a) storage ( $G'$ ) and (b) loss modulus ( $G''$ ) as a function of frequency at 25 °C and 0 kA/m for isotropic MREs and seven particle contents (0%, 1%, 5%, 10%, 15%, 20% and 25%)

#### 4.4.3 Magneto-induced modulus

In this thesis, two magneto-induced modulus models are proposed: one for isotropic MREs and another one for anisotropic MREs. The first one, is based on the model proposed by Jolly et al. (1996a;b) for anisotropic MREs which is modified for isotropic MREs. The second one, is based on a model developed by López-López et al. (2012) for fluids and using magnetic permeability components values. This model is adapted for anisotropic MREs and combine it with experimental permeability values.

Jolly et al. (1996a;b) introduced the influence of magnetic field in the storage modulus for low-strain conditions using the dipole–dipole interaction model. Isotropic MREs are randomly distributed, and consequently, the dipole moment of each particle is not aligned as in the chains of anisotropic MREs.

However, isotropic materials have the same properties in all of the directions. Therefore, Ivaneyko et al. (2011; 2012) defined three particle lattices for isotropic MREs: simple cubic, body-centered cubic (BCC) and hexagonal close-packed lat-

tices. In this chapter, the BCC lattice is used, to define the distance between each particle ( $d$ ).

The magneto-induced modulus and the particle saturation ratio are modified by a correction factor dependent on the particle content due to the randomly distributed dipoles (Lu et al. 2012). A correction factor dependent on the particle content is applied to the magneto-induced modulus,

$$\Delta C_{\text{iso}} = \frac{4\phi J_p^2 R^3}{\mu_1 \mu_0 d_0^3} (1 - \phi) \quad (4.3)$$

where  $\Delta C_{\text{iso}}$  is the magneto-induced modulus due to internal magnetic field for isotropic MREs,  $J_p$  is the induced polarisation of the particles (defined in equation (13) in Agirre-Olabide et al. (2017)),  $R$  is the radius of the particles,  $\mu_1$  is the relative permeability of the medium (matrix),  $\mu_0$  is the vacuum permeability and  $d$  the distance between each particle.

On the other hand, the model proposed for anisotropic MREs is based on the model developed López-López et al. (2012) for MRF. For anisotropic MREs, the magneto-induced modulus variation is called  $\Delta C_{\text{ani}}$ .

The López-López et al. (2012) model was used for magnetorheological fluids in order to introduce the influence of aggregates generated when an external magnetic field was applied. This model assumes bulk-column-like aggregates in the MR sample extended along the applied magnetic field—a more stable and more realistic structure observed in experiments for both MR fluids and MRE. Moreover, the model was analysed for a magnetic field intensity of 18.5 kA/m and a volumetric particle content of 50%. The model is based on the evaluation of the free energy of the sheared MR sample, and the shear stress  $\tau$  is related to the applied strain  $\gamma$ .

MRFs operate within a post-yield continuous shear or flow regime, while MREs operate in the pre-yield region (Carlson and Jolly 2000), which means that the strain amplitudes applied to MREs are smaller. After linearization of the equation proposed López-López et al. (2012), the following expression is developed,

$$\Delta C_{\text{ani}} = \frac{3}{2} \mu_0 \left( \frac{H_0}{\mu_{\parallel}} \right)^2 (\mu_{\parallel} - \mu_{\perp}) \quad (4.4)$$

where  $\Delta C_{\text{ani}}$  is the magneto-induced modulus due to internal magnetic field for

anisotropic MREs,  $H = H_0/\mu_{\parallel}$ ,  $H_0$  is the applied external magnetic field, and  $\mu_{\parallel}$  and  $\mu_{\perp}$  are the longitudinal and transverse components of the magnetic permeability. A vibrating sample magnetometer (VSM) was used to perform magnetisation measurements up to 360 kA/m, and from those experimental data (Sec. 2.3. Agirre-Olabide et al. (2018)), the influence of the magnetic field in the permeability properties was studied. The longitudinal and transverse magnetic permeability components decrease linearly with the external magnetic field (Figure 4.5). The permeability is larger for high particle content and for lower magnetic fields, and the longitudinal one is larger than the transverse one owing to the lower demagnetizing effect in the sample with the aggregates oriented along the applied field. Moreover, the magnetic permeability decrease is larger for the longitudinal component and particle content.

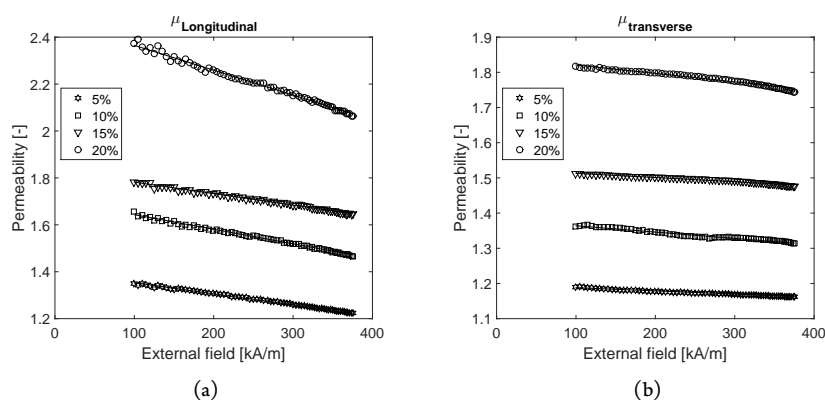


**Figure 4.5** Experimental (points) and numeric data (lines) of (a) longitudinal and (b) transverse components of the magnetic permeability of anisotropic MRE samples (5%, 10%, 15% and 20%) at room temperature as a function of magnetic field density

#### 4.4.4 Magneto-viscoelastic modelling

After the viscoelasticity, particle content and magneto-induced modulus are modelled separately, all of them are coupled in a single magneto-viscoelastic model—one for isotropic MREs and another one for anisotropic MREs.

The introduction of a magnetic field dependent equation in the viscoelastic model is not evident. That is why, the Helmholtz free energy is defined for isotropic



MRE, in order to prove the consistency of the model, which is a tensorial function of the second-order strain tensor and the magnetic field density one-order tensor ( $\mathbf{B}$ ).

As the free energy is an isotropic scalar function, integrity bases of the strain tensor and magnetic field density tensor can be used, based on the isotropic function theory (Kelly 2013). The proposed model is based on the fractional derivative model. Therefore, three parameters are defined dependent on the magnetic field density. The consistency of the fractional derivative model was proved in the literature (Haupt 2002).

$$G_0 = G_0(\varphi, \mathbf{B}), \quad K = K(\varphi, \mathbf{B}) \quad \text{and} \quad C = C(\varphi, \mathbf{B}), \quad (4.5)$$

where  $G_0$  is the static modulus of the model,  $C$  is the modulus of the Maxwell spring (Figure 4.1) and  $K$  is the bulk modulus. The free energy ( $\psi$ ) of the lineal elasticity was defined as  $G_0$  and  $K$  (Haupt 2002). However, the studied case is the magneto-viscoelasticity, and a three-dimensional free energy function is proposed (equation 6, Agirre-Olabide et al. (2017)).

From the proposed three-dimensional model in Agirre-Olabide et al. (2017), the shear one-dimensional case is studied, and the following equation is obtained,

$$G^* = G_0(\varphi, B) + \frac{C(\varphi, B)(i\omega\tau)^\alpha}{1 + (i\omega\tau)^\alpha}. \quad (4.6)$$

Coupling equations 4.2, 4.3 and 4.6, the viscoelastic behaviour of isotropic MREs as a function of frequency, particle content and external magnetic field is modelled, and fit it to the experimental data for the 10% isotropic MRE (Figure 4.6). The fitting is evaluated with the mean error between the experimental data and the approached model. This error does not exceed 4% and occurs at high frequencies. Hence, it is concluded that the fitting error for the particle content is larger than that for the magneto-induced modulus.

For anisotropic MREs, the magneto-induced model (equation 4.4) and the FD model (equation 4.1) are coupled using equation 4.6. From Figure 4.5, the longitudinal and transverse components of magnetic permeability at 150 and 300 kA/m are calculated and substituted in equation 4.4 to model the magneto-induced modulus. As can be seen in Figure 4.7, after including the modelling of

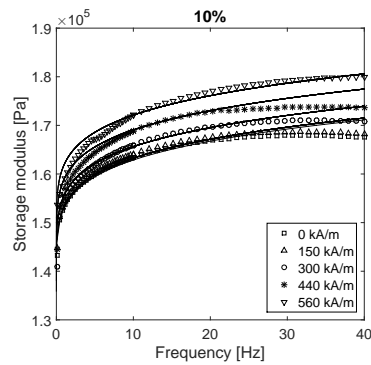


**Figure 4.6** Experimental data (points) and the proposed magneto-viscoelastic model (lines) for the storage modulus ( $G'$ ) of the 10% isotropic MRE sample as a function of frequency at 25 °C and different magnetic field intensities

magnetic permeability components, the predicted behaviour is similar to experimental data—the discrepancy does not exceed 8%.

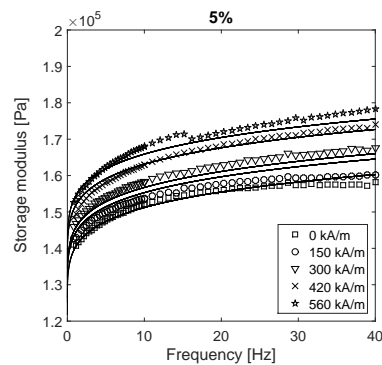


**Figure 4.7** Experimental data (points) and the proposed magneto-viscoelastic model (lines) for the storage modulus ( $G'$ ) of the 5% anisotropic MRE sample as a function of frequency at 25 °C and different magnetic field intensities (150 and 300 kA/m curves are modelled using experimental data, and the 420 and 560 kA/m curves are the extension of the proposed model)

In Figure 4.7, the model develop for anisotropic MREs is extended for 420 and 560 kA/m. For low particle contents, the discrepancy is lower than 7% at high magnetic fields, while at high magnetic field and particle contents does not exceed 10%.

## 4.5 Conclusions

The shear four-parameter fractional derivative viscoelastic model was successfully fitted to experimental data of isotropic and anisotropic MREs samples in the absence of the applied magnetic field. The mean fitting errors did not exceed the 1% for the storage modulus and 6% for the loss modulus.

In order to model the influence of temperature in the dynamic properties, the Arrhenius model was coupled with a four-parameter fractional derivative model. This model was extended in the frequency domain to determine the maximum attenuation of isotropic MREs.

For each particle content and magnetic field, the value of maximum attenuation was unique and occurs at a certain frequency and temperature. The attenuation was larger with increased particle content over the entire frequency band, and the frequency at which the maximum occurs was increased.

The shapes of the loss factor curves were not influenced by temperature, while they were dependent on frequency. The maximum attenuation frequency was reduced with increased temperature and particle content. The maximum attenuation temperature was increased with increased frequency and particle content; this occurred to a greater degree at low frequencies.

With the application of an external magnetic field, the shear maximum attenuation value and frequency were increased, and the loss factor was larger in the studied frequency domain.

The fitting of the particle-matrix and fractional derivative coupled model was successful, although the fitting error was larger for the loss modulus because the influence of the storage modulus in the dynamic complex modulus was larger. In addition, the maximum error for the storage modulus did not exceed 4%, and the loss modulus 13%.

The magneto-induced modulus model of isotropic samples was developed considering anisotropic samples and applying a correction factor to introduce the isotropy. A new three-dimensional magneto-viscoelastic model was developed for isotropic MREs, and the consistency of the model was proved. The proposed magneto-viscoelastic model for isotropic MREs was fitted to experimental data,

and the storage modulus error was less than 4%, which shows that the proposed model was valid.

The viscoelastic model for anisotropic MREs was coupled with the magneto-induced modulus model based on the López-López model. The proposed magnetic model was fed with the longitudinal and transverse components of magnetic permeability of the samples.

The longitudinal and transverse components of magnetic permeability of anisotropic MREs were measured and modelled in the magnetic field domain. The VSM measurements were performed, and experimental data were introduced for the coupled model. The developed new shear model for anisotropic MREs can be extended in the magnetic field domain, in order to overcome VSM limitations (maximum magnetic field intensity of 360 kA/m). The model prediction was compared with rheological measurements, and the discrepancy does not exceed the 7%.

## 4.6 Scientific contribution

# A new three-dimensional magneto-viscoelastic model for isotropic magnetorheological elastomers

*I. Agirre-Olabide<sup>1</sup>, A. Lion<sup>2</sup> and M.J. Elejabarrieta<sup>1</sup>*

<sup>1</sup>Mechanical and Manufacturing Department, Mondragon Unibertsitatea, Loramendi 4,  
20500 Arrasate-Mondragon, Spain

<sup>2</sup>Department of Aerospace Engineering, Institute of Mechanics, Universität der  
Bundeswehr München, Werner-Heisenberg-Weg 39, D-85577 Neubiberg, Germany

Smart Materials and Structures

2017 vol. **26**(3) pag. 035021

DOI: 10.1088/1361-665X/26/3/035021

IF-JCR: 2.909 J. Rank-JCR: 9/58

# A new three-dimensional magneto-viscoelastic model for isotropic magnetorheological elastomers

I Agirre-Olabide<sup>1</sup>, A Lion<sup>2</sup> and M J Elejabarrieta<sup>1</sup>

<sup>1</sup> Mech. & Manuf. Dept., Mondragon Unibertsitatea, E-20500 Arrasate-Mondragon, Spain

<sup>2</sup> Department of Aerospace Engineering, Institute of Mechanics, Universität der Bundeswehr München, Werner-Heisenberg-Weg 39, D-85577 Neubiberg, Germany

E-mail: [mjelejabarrieta@mondragon.edu](mailto:mjelejabarrieta@mondragon.edu)

Received 11 July 2016, revised 26 October 2016

Accepted for publication 16 November 2016

Published 7 February 2017



CrossMark

## Abstract

In this work, a four-parameter fractional derivative viscoelastic model was developed to describe the dynamic shear behaviour of magnetorheological elastomers (MREs) as a function of the matrix, particle content and magnetic field. The material parameters were obtained from experimental data measured with a Physica MCR 501 rheometer from the Anton Paar Company, equipped with a magnetorheological cell. The synthesised isotropic MRE samples were based on room-temperature vulcanising silicone rubber and spherical carbonyl iron powder micro particles as fillers, and seven volumetric particle contents were studied. The influence of particle contents was included in each parameter of the four-parameter fractional derivative model. The dependency of the storage modulus as a function of an external magnetic field (magnetorheological (MR) effect) was studied, and a dipole–dipole interaction model was used. A new three-dimensional magneto-viscoelastic model was developed to couple the viscoelastic model, the particle-matrix interaction and the magneto-induced modulus model, which predicts the influence of the magnetic field and the particle content in the MR effect of isotropic MREs.

Keywords: isotropic magnetorheological elastomers, fractional derivative model, particles, magnetic field

(Some figures may appear in colour only in the online journal)

## 1. Introduction

Magnetorheological elastomers (MRE) are smart materials that exhibit adjustable dynamic properties and consist of magnetisable particles embedded in an elastomeric matrix. Applying an external magnetic field, the properties of MREs vary due to the interaction forces of magnetisable particles. Therefore, these materials are considered smart materials because of their property variability. Due to the damping property variability these materials are used in many applications as dampers [1] and isolators [2, 3].

Depending on the pre-structure process, isotropic MREs or anisotropic MREs can be fabricated. The first ones are cured without any external magnetic field, and the particles are randomly distributed [4]. Anisotropic MREs, however, are

vulcanised under the influence of an external magnetic field obtaining chain-like structures in the direction of the magnetic field [5].

The dynamic properties of isotropic MREs depend on the matrix [6, 7], the particle content [8, 9] and the external magnetic field applied [10]. Hence, each of them has to be modelled to obtain the constitutive model of isotropic MREs to predict its dynamic response.

Due to the viscoelastic matrix, the predominant behaviour of MREs is the viscoelastic one. The modelling of the viscoelasticity of these materials is completed via different constitutive models, such as classical differential models and fractional derivative models.

Combining different rheological elements classical differential models were developed. For it springs and dashpots

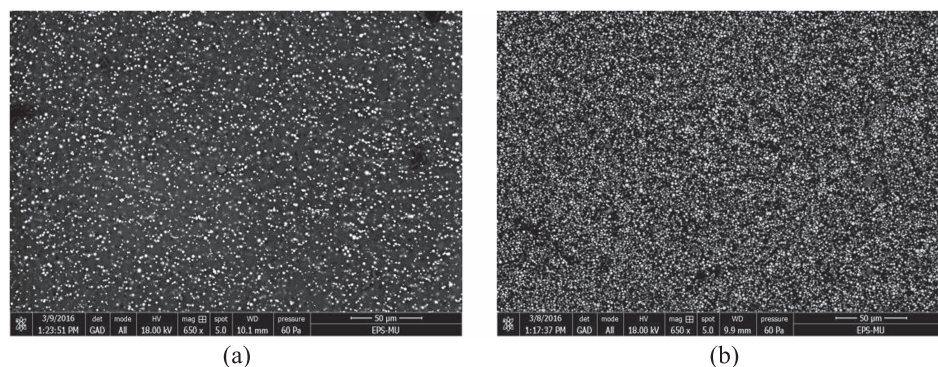


Figure 1. SEM images of (a) 5% and (b) 25% MRE samples in low-vacuum conditions and with a voltage acceleration of 18 kV.

were used [11]. The widely used Zener model [12] or the standard lineal model is a combination of a Maxwell element and a spring in parallel configuration. In literature, this model was used by Chen and Jerrams [13] and Han *et al* [14] to model the viscoelastic behaviour of MREs. However, these materials were also modelled using a different element configuration. Li *et al* [15], Liao *et al* [16] and Behrooz *et al* [17] combined a spring and a Kelvin–Voigt element in serial configuration. To obtain a better fitting, additional material parameters were introduced by Zhu *et al* [18].

Fractional derivative models containing fewer material parameters can be used to avoid the addition of material parameters. Moreover, the material parameters have a physical interpretation [19]. Due to that reason, the viscoelastic behaviour of MREs was modelled using fractional derivative models [20, 21]. In the existing literature, two elements were combined: a spring and an Abel dashpot (fractional derivative element); Zhu *et al* [20] combined them in a parallel configuration, while Guo *et al* [21] did so in a serial configuration. Xu *et al* [22] combined a fractional Maxwell model and a fractional Kelvin model in parallel developing a higher order fractional derivative model (seven material parameters). Hence, the viscoelastic nature of MREs was modelled using three-parameter fractional derivative models.

The embedded particles in MREs modified the viscoelastic behaviour [23], and consequently the interaction between the matrix and the filler (particle) was modelled, also known as filler reinforcement. Based on the viscosity law of Einstein, Guth and Gold [24] and Guth [25] modelled the rigidity variation of a rubber matrix. That principle was also used for MREs by Leng *et al* [26]. Ray *et al* [27] proposed a two-parameter exponential model to introduce the interaction of surface-treated fillers. However, Chen and Jerrams [13] used a rheological model, a spring and a Coulomb friction slide, to predict the matrix-particle interaction in MREs.

An external magnetic field varies the dynamic properties of isotropic MREs, which Ivanenko *et al* [28, 29] modelled, defining three different lattice models. In addition, they studied the dipole–dipole interaction to model the magneto-induced

modulus. However, most of the models used to predict the influence of the magnetic field were used to study anisotropic MREs. The dipole–dipole interaction was used [30, 31], and the interaction energy of two dipoles was formulated to study the magnet-induced modulus. Davis [32] used the dipole–dipole interaction to model the influence of each particle on the other particles of the same chain. Leng *et al* [26] proposed an effective permeability model for anisotropic MREs to estimate the storage modulus in the chain direction.

The aim of this work is to develop a new constitutive model for isotropic MREs based on fractional derivatives, which combines it with particle-matrix interaction and the magneto-induced modulus model. The novelty of this work lies in the development of a three dimensional magneto-viscoelastic model and the coupling of the magnetic field and the fractional derivative viscoelastic model dependent on the particle content, which was developed in [33]. First, shear dynamic properties of isotropic MREs were measured using a rheometer. Secondly, the viscoelastic behaviour was modelled using a four-parameter fractional derivative model, and the evolution of each parameter in the function of the particle content was studied and modelled [33]. Material parameters were obtained from experimental data. Thirdly, matrix-particle interaction was modelled defining a hard phase (particles) and a soft phase (matrix) [34]. Furthermore, the magneto-induced model was used to predict the evolution of the magnetorheological (MR) effect [30]. Finally, the proposed constitutive model is a fractional derivative model coupled with matrix-particle interaction and the magneto-induced modulus, which predicts the MR effect of isotropic MREs with different particle contents and magnetic fields.

## 2. Experimental results

In this work, isotropic MRE samples were used and the random distributed particles were observed using a scanning electron microscope (SEM). The dynamic shear properties of the samples were measured using a rheometer equipped with a magnetorheological device.

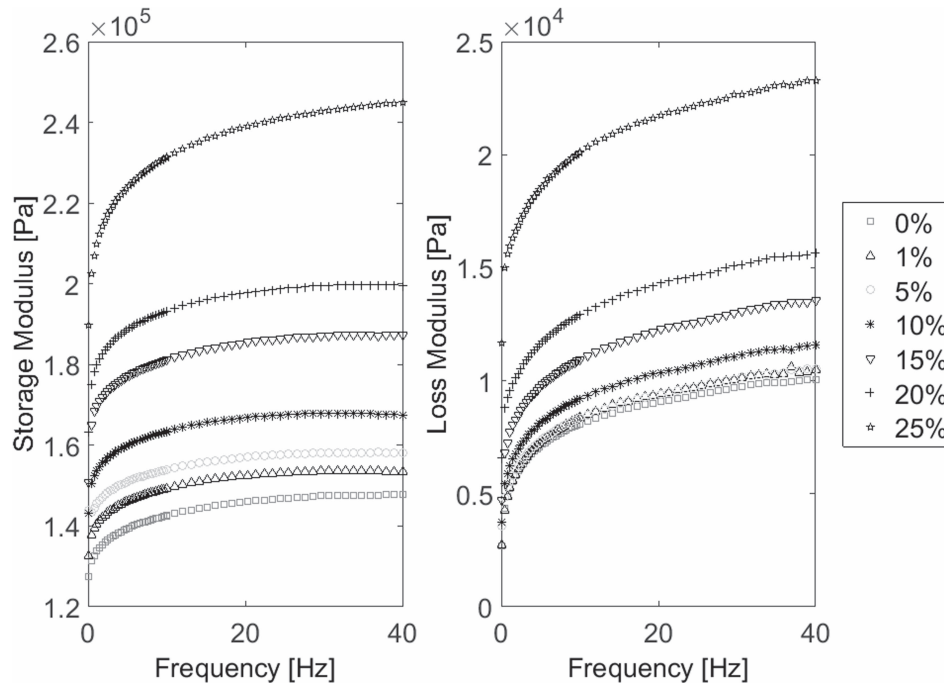


Figure 2. Storage and loss modulus of isotropic MRE samples as a function of frequency.

Table 1. MR effect (%) of the isotropic samples at four magnetic field intensities.

Magnetic field intensity ( $\text{kA m}^{-1}$ )	5%	10%	15%	20%	25%
150	$1.01 \pm 0.98$	$0.41 \pm 0.82$	$0.68 \pm 0.58$	$0.66 \pm 0.39$	$1.26 \pm 0.47$
300	$1.65 \pm 0.50$	$1.43 \pm 0.52$	$1.70 \pm 0.99$	$2.21 \pm 0.42$	$3.10 \pm 0.70$
440	$3.11 \pm 0.84$	$3.07 \pm 0.57$	$3.38 \pm 1.35$	$4.58 \pm 1.08$	$6.36 \pm 1.19$
560	$4.32 \pm 1.15$	$5.45 \pm 1.16$	$6.10 \pm 1.58$	$8.72 \pm 1.67$	$10.90 \pm 1.93$

The isotropic MREs consisted of a silicone rubber WACKER Elastosil<sup>®</sup> M 4644 A and the vulcaniser WACKER Elastosil<sup>®</sup> M 4644 B mixed in a ratio 10:1, respectively, and carbonyl iron powder. The average particle size was  $1.25 \pm 0.55 \mu\text{m}$  supplied by BASF. In this work, seven volumetric particle contents were studied: 0%, 1%, 5%, 10%, 15%, 20% and 25%. Using a SEM, the random distribution of the particles was seen. A Nova NanoSEM 450 microscope was used in low-vacuum conditions and with a voltage acceleration of 18 kV. As an example, in figure 1, the 5% and 25% isotropic MRE samples are shown.

The magneto-dynamic characterisation was performed by an Anton Paar Physica MCR 501 rheometer equipped with a MRD 70/1 T magnetorheological cell and a parallel plate configuration. The diameter of the plate was 20 mm and had a

serrated surface to avoid the slipping between the sample and the plate (PP20/MRD/TI/P2). In order to obtain a higher accuracy in the low frequency range, two steps were defined for the lineal frequency sweep tests. One from 0.1 to 10 Hz and the second one from 10 to 40 Hz. In each step thirty points and 5 s per point were measured [33]. During the characterisation, five external magnetic field intensities were applied: 0, 150, 300, 440 and  $560 \text{ kA m}^{-1}$ . All of the characterisations were made within the lineal viscoelastic region, and for it, a constant strain amplitude of 0.06% was defined [35].

During the tests, the temperature was constant at  $25^\circ\text{C}$  and it was controlled by a water-based heating/cooling system Julabo F-25. A normal force of 3 N was applied to the samples to guarantee a contact avoid the slipping between the sample and plates.



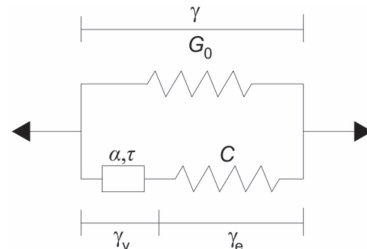


Figure 3. Sketch of the fractional derivative model.

The results of the experimental characterisation are shown in figure 2, where the real part or storage modulus ( $G'$ ) and the imaginary part or loss modulus ( $G''$ ) are plotted as a function of frequency.

The external magnetic field has a large influence on the dynamic properties of isotropic MREs and is evaluated by the MR effect [30]. The MR effect of a sample is defined as the ratio between the change in its storage modulus with and without the magnetic field, and the storage modulus without the magnetic field [36]. Hence, the influence of the magnetic field on the storage modulus was modelled. The experimental MR effect of isotropic MREs is shown in table 1.

### 3. MRE modelling

The viscoelastic modelling of isotropic MRE materials was done in three steps. First, the viscoelastic behaviour was modelled using fractional derivative models. Then, the matrix-particle interactions was modelled and coupled with the viscoelastic model. Finally, the influence of the magnetic field was modelled and coupled with the viscoelastic and matrix-particle interaction models.

#### 3.1. Viscoelastic modelling

Viscoelastic models, such as fractional derivative models, can be used in the time and frequency domains, and they contain fewer material parameters than classical viscoelastic models. In this work, a four-parameter fractional derivative model was used in the frequency domain [33] and dynamic shear modulus ( $G^*$ ) is given as:

$$G^* = \frac{G_0 + (G_0 + C)(i\omega\tau)^\alpha}{1 + (i\omega\tau)^\alpha} = G_0 + \frac{C(i\omega\tau)^\alpha}{1 + (i\omega\tau)^\alpha}, \quad (1)$$

where  $G_0$  is the static shear modulus, the high asymptotic shear modulus is defined as  $G_\infty = G_0 + C$ ,  $C$  is the elastic part of the viscoelastic branch of the model,  $\tau$  is the relaxation time,  $\alpha$  is the fractional parameter and  $\omega$  is the angular frequency. A sketch of equation (1) can be seen in figure 3. Two branches were defined: an elastic branch (a spring ( $G_0$ )) and a viscoelastic branch (a spring ( $C$ ), along with an Abel dashpot ( $\alpha$  and  $\tau$ )).

Table 2. Fitting parameters of a four-parameter fractional derivative model for the seven isotropic MRE samples [33].

	$G_0$ (Pa)	$C$ (Pa)	$\alpha$	$\tau$ (s)
0%	120 194	157 127	0.253	$1.525 \times 10^{-5}$
1%	128 613	190 275	0.257	$6.829 \times 10^{-6}$
5%	132 241	228 870	0.244	$1.644 \times 10^{-6}$
10%	135 002	282 801	0.215	$6.594 \times 10^{-7}$
15%	137 668	337 612	0.177	$3.370 \times 10^{-7}$
20%	145 884	454 185	0.182	$1.224 \times 10^{-7}$
25%	151 142	655 889	0.171	$1.719 \times 10^{-7}$

The elastic nature of the viscoelastic branch is due to the spring and the viscous nature because of the Abel dashpot. Moreover, a shear stress was defined for each element,  $\gamma$  for the shear strain applied to the model,  $\gamma_v$  for the shear strain of the viscous part and  $\gamma_e$  for the elastic strain of the viscoelastic branch.

The four parameters of the fractional derivative model obtained from the fitting of equation (1) to the experimental data (figure 2) are shown in table 2. The least square method was used, and the fitting was done using the dynamic complex modulus. The fitting error did not exceed 1% for the storage and loss modulus. In all of the following figures, experimental data are plotted as points and fitted models as lines. In figure 4, the four-parameter fractional derivative model and experimental data are plotted.

#### 3.2. Particle-matrix interaction model

Once the fractional derivative model was fitted, the influence of the particle content was analysed and modelled. The influence of the particles in the dynamic properties and in each of the model parameters can be seen in figure 4 and table 2, respectively. Therefore, the model proposed in equation (1) had to be modified to include the influence of the particle content  $G^*(\omega, \varphi)$ . Hence, each parameter was studied one by one, and then, all of them were coupled. In figure 5, the equations and the fitting of each parameter is shown.

Both  $G_0$  and  $C$  increase with the particle content due to the filler reinforcement phenomena. The model those parameters was based on the interaction between rubber and filler developed by Mullins and Tobin [34]. They defined a hard phase for the fillers and a soft phase for the rubber and for isotropic MRE samples this approach can also be applied. Particles are the hard phase and matrix the soft phase. With this approach the particle content was introduced using  $1/(1 - \varphi)$  equation type, where additional material parameters were not included [33].

However, the relaxation time ( $\tau$ ) and the fractional parameter ( $\alpha$ ) are reduced  $c$ . Therefore, the following equations was proposed [33] to introduce the particle content influence,

$$A_1 + B_1 \cdot e^{(-a_1 \cdot \varphi)}, \quad (2)$$

where  $A_1$ ,  $B_1$  and  $a_1$  are material parameters. For the relaxation time the parameter was replaced by  $\tau_{25\%}$  [33].

Hence, this model was dependent on the data of minimum (1%) and maximum (25%) particle content samples.

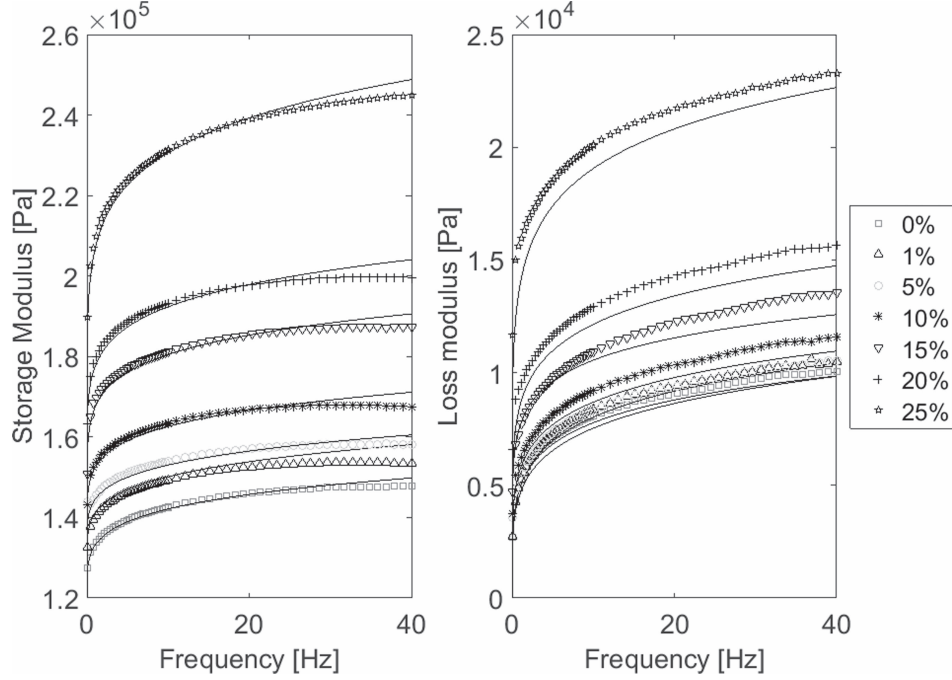


Figure 4. Experimental data and fractional derivative model of storage and loss modulus as a function of frequency.

Moreover, eight material parameters ( $G_{0_{1\%}}$ ,  $C_{1\%}$ ,  $\tau_{25\%}$ ,  $B_1$ ,  $a_1$ ,  $A_2$ ,  $B_2$ ,  $a_2$ ) were used to determine the evolution of the four key parameters ( $G_0(\varphi)$ ,  $C(\varphi)$ ,  $\tau(\varphi)$ ,  $\alpha(\varphi)$ ) of the fractional model with the particle content. All fitting parameters are shown in table 3. Those parameters were used to predict the behaviour of isotropic MRE in the frequency domain, therefore those parameters are constant in this domain.

In equation (3), the shear complex modulus was defined depending on the frequency and the particle content [33]. Moreover, the influence of the particle content in each parameter is also shown.

$$G^*(\omega, \varphi) = \frac{G_0(\varphi) + (G_0(\varphi) + C(\varphi))(i\omega\tau(\varphi))^{\alpha(\varphi)}}{1 + (i\omega\tau(\varphi))^{\alpha(\varphi)}},$$

$$G_0(\varphi) = G_{0_{1\%}} \cdot \sqrt{\frac{1}{1-\varphi}},$$

$$C(\varphi) = C_{1\%} \cdot \left(\frac{1}{1-\varphi}\right)^4,$$

$$\tau(\varphi) = \tau_{25\%} + B_1 \cdot e^{-a_1 \cdot \varphi} \quad \text{and}$$

$$\alpha(\varphi) = A_2 + B_2 \cdot e^{-a_2 \cdot \varphi}.$$

(3)

In figure 6, the fitting of the proposed fractional derivative model coupled with the matrix-particle interaction model (equation (3)) is shown. Comparing figures 4 and 6, the differences of equations (1) and (3) can be seen. The fitting of equation (1) is more accurate, while the values obtained were only valid for the specific conditions of the experimental data. However, equation (3) includes the particle content variable, and consequently, any particle content between 1% and 25% can be modelled using eight material parameters.

### 3.3. Magnetic field model

The influence of the magnetic field is shown in table 1. However, the introduction of a magnetic field dependent equation in the viscoelastic model is not evident. That is why, the Helmholtz free energy ( $\psi$ ) was defined for isotropic MRE, in order to prove the consistency of the model, which is a tensorial function of the second-order strain tensor ( $\boldsymbol{\varepsilon}$ ) and the magnetic field density one-order tensor ( $\mathbf{B}$ ), given by equation (4).

$$\psi(\boldsymbol{\varepsilon}, \mathbf{B}). \quad (4)$$

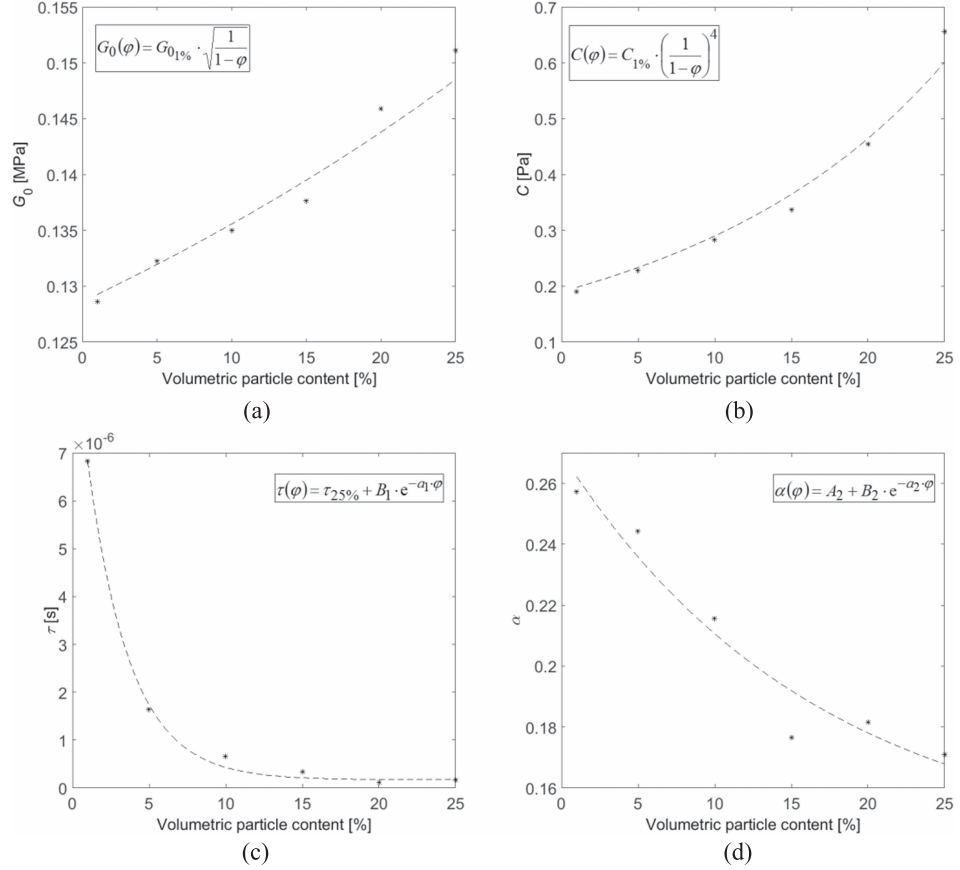


**Figure 5.** Evolution of the (a) static shear modulus, (b) elastic part of the viscoelastic branch, (c) relaxation time and (d) fractional parameter as a function of particle content.

As the free energy is an isotropic scalar function, integrity bases of the strain tensor and magnetic field density tensor can be used, based on the isotropic function theory [37]. The proposed model was based on the fractional derivative model. Therefore, three parameters were defined dependent on the magnetic field density. The consistency of the fractional derivative model was proved in the literature [38].

$$\begin{aligned} G_0 &= G_0(\varphi, |\mathbf{B}|), \\ K &= K(\varphi, |\mathbf{B}|) \text{ and} \\ C &= C(\varphi, |\mathbf{B}|), \end{aligned} \quad (5)$$

where  $G_0$  is the elastic modulus of the model,  $C$  is the modulus of the Maxwell spring (figure 3) and  $K$  is the bulk modulus. The free energy ( $\psi$ ) of the lineal elasticity was defined as  $G_0$  and  $K$  [38]. However, the case studied was the magneto-viscoelasticity, and a three-dimensional free energy

**Table 3.** Fitting material parameters of the isotropic MRE samples for the relaxation time and the fractional parameters.

$G_{0_{\text{res}}}$ (Pa)	$C$ (Pa)	$\tau$ (s)	$\alpha$
128 613	190 275	$\tau_{25\%}$	$A_2$
		$B_1$	$B_2$
		$a_1$	$a_2$
		$1.719 \times 10^{-7}$	0.139
		$9.533 \times 10^{-6}$	0.131
		36.107	5.998

function was proposed,

$$\begin{aligned} \psi &= G_0 \varepsilon^D : \varepsilon^D + \frac{1}{2} K_0 (\text{tr } \varepsilon)^2 + \alpha_{00} \mathbf{B} \cdot \mathbf{B} \\ &+ \alpha_{01} \mathbf{B} \cdot (\varepsilon \mathbf{B}) + \frac{\alpha_{02}}{2} \mathbf{B} \cdot (\varepsilon^2 \mathbf{B}) \\ &+ C \varepsilon_c^D : \varepsilon_c^D + \alpha_{11} \mathbf{B} \cdot (\varepsilon_c \mathbf{B}) + \frac{\alpha_{12}}{2} \mathbf{B} \cdot (\varepsilon_c^2 \mathbf{B}), \end{aligned} \quad (6)$$

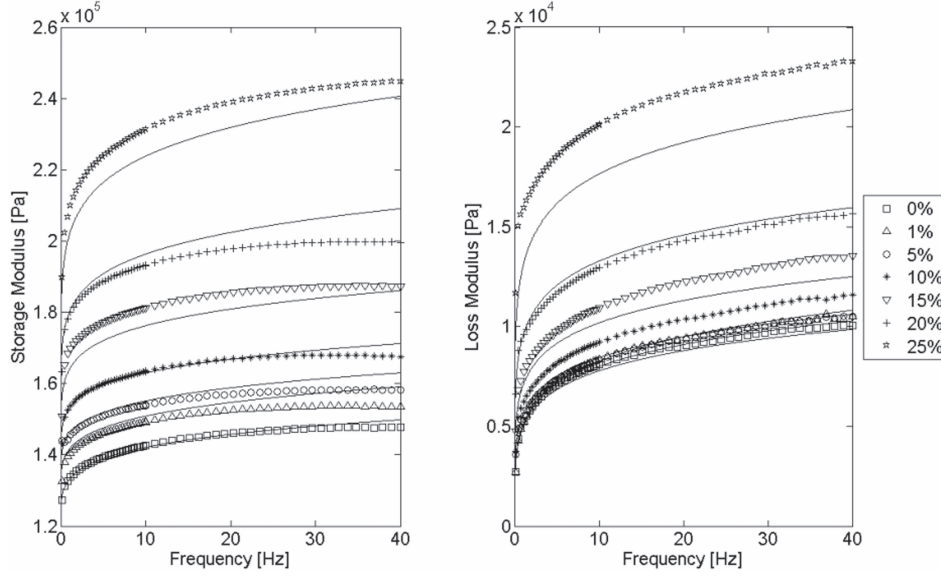


Figure 6. Experimental data and fitting of equation (3) of the storage and loss modulus as a function of frequency.

where  $\varepsilon^D$  is the deviator tensor of the strain tensor,  $\varepsilon_e$  is the strain of the spring of the viscoelastic part ( $C$  spring element (figure 3)) and  $\alpha_{ij}$  are material parameters,  $i = 0$  and  $1$ , and  $j = 0-2$ .

The stress was defined as the partial derivative of the free energy respect to the strain.

$$\sigma = \frac{\partial \psi}{\partial \varepsilon}. \quad (7)$$

Therefore, combining equations (6) and (7), the three-dimensional stress was obtained,

$$\begin{aligned} \sigma = & 2G_0\varepsilon + K(\text{tr } \varepsilon)\mathbf{I} + \alpha_{01}\mathbf{B} \otimes \mathbf{B} + \frac{\alpha_{02}}{2}[\mathbf{B} \otimes (\varepsilon \mathbf{B}) \\ & + (\varepsilon \mathbf{B}) \otimes \mathbf{B}] + 2C(\varepsilon - \varepsilon_v)^D + \alpha_{11}\mathbf{B} \otimes \mathbf{B} \\ & + \frac{\alpha_{12}}{2}[\mathbf{B} \otimes ((\varepsilon - \varepsilon_v)\mathbf{B}) + ((\varepsilon - \varepsilon_v)\mathbf{B}) \otimes \mathbf{B}], \end{aligned} \quad (8)$$

where  $\varepsilon_v$  is the strain corresponding to the Abel dashpot and  $\mathbf{I}$  is the identity second-order tensor.

From the proposed three-dimensional model, equation (8), the shear one-dimensional case was studied. Hence, equation (8) was evaluated for the studied case, and equation (9) was obtained, where  $\gamma$  is the global strain and  $\gamma_v$  is the Abel dashpot strain, figure 3.

$$\tau = G_0\gamma + C(\gamma - \gamma_v). \quad (9)$$

Equation (9) was the same expression as that obtained directly from the fractional derivative sketch, which means that the magneto-viscoelastic model proposed was consistent and the

fractional derivative model is the next one,

$$G^* = \frac{G_0(\varphi, B) + (G_0(\varphi, B) + C(\varphi, B))(i\omega\tau)^\alpha}{1 + (i\omega\tau)^\alpha}, \quad (10)$$

where  $G_0$  and  $C$  are functions of the particle content and magnetic field. Besides, this model took into account the influence of the particle content in the absence of a magnetic field.

$$\begin{aligned} G_0(\varphi, B) &= G_{01}(\varphi) + G_{02}(\varphi, B) \text{ and} \\ C(\varphi, B) &= C_1(\varphi) + C_2(\varphi, B). \end{aligned} \quad (11)$$

After the generalised model was defined, the influence of the magnetic field had to be included in  $G_0$  and  $C$ . Jolly *et al* [30, 31] introduced the influence of the magnetic field on the storage modulus for low-strain conditions using the dipole-dipole interaction model; this is given by equation (12),

$$G_{02}(\varphi, B) = C_2(\varphi, B) = \frac{4\varphi J_p^2 R^3}{\mu_1 \mu_0 d^3}, \quad (12)$$

where  $J_p$  is the induced polarisation of the particle (defined in equation (13)),  $R$  is the radius of the particles,  $\mu_1$  is the relative permeability of the medium (matrix),  $\mu_0$  is the vacuum permeability and  $d$  distance between each particle.

$$J_p = \frac{3}{2}\alpha^3\mu_0 H + (1 - \alpha^3)J_s, \quad (13)$$

where  $J_s$  is the magnetic saturation—for iron particles, it is 2.1 T [31] and  $\alpha_p$  is the saturation ratio of each particle [30, 31].

The isotropic MREs are randomly distributed, and consequently, the dipole moment of each particle is not aligned as

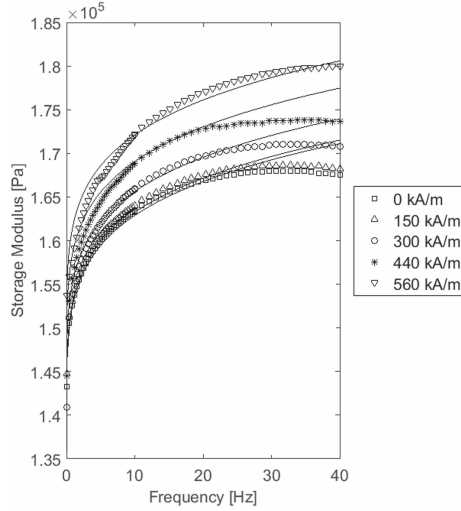


**Figure 7.** Fitting of the proposed magneto-induced modulus coupled with the fractional derivative and particle-matrix model of the 10% MRE sample.

in the chains of anisotropic MREs. However, isotropic materials have the same properties in all of the directions. Therefore, Ivaneyko *et al* [28, 29] defined three particle lattices for isotropic MREs: simple cubic, body-centred cubic (BCC) and hexagonal close-packed lattices. In this work, the BCC lattice was used, and the distance between each particle ( $d$ ) is defined as:

$$d = \sqrt[3]{\frac{4}{v} \frac{\pi R^3}{3}}, \quad v = \begin{cases} 1 \text{ (CC)} \\ 2 \text{ (BCC)} \\ 2\sqrt{2} \text{ (HCP)}, \end{cases} \quad (14)$$

where  $R$  is the radius of the particles, and  $v$  depends on the lattice model. However, the magneto-induced modulus and the particle saturation ratio were modified by a correction factor dependent on the particle content due to the randomly distributed dipoles [23].

A correction factor dependent on the particle content was applied to the magneto-induced modulus. When the particle content is larger, the dipoles' probability of being in the opposite direction of the magnetic field direction is larger, which decreases the magneto-induced modulus. Therefore, equation (12) was modified.

$$G_{02}(\varphi, B) = C_2(\varphi, B) = \frac{4\varphi J_p^2 R^3}{\mu_1 \mu_0 d_0^3} (1 - \varphi). \quad (15)$$

Equation (15) was coupled with equation (3) to obtain the viscoelastic behaviour of isotropic MREs in the functions of the frequency, particle content and external magnetic field

(equation (16)).

$$G^* = \frac{G_0(\varphi, B) + (G_0(\varphi, B) + C(\varphi, B))(i\omega\tau(\varphi))^{\alpha(\varphi)}}{1 + (i\omega\tau(\varphi))^{\alpha(\varphi)}},$$

$$G_0(\varphi, B) = G_{01}(\varphi) + G_{02}(\varphi, B),$$

$$C(\varphi, B) = C_1(\varphi) + C_2(\varphi, B),$$

$$G_{01}(\varphi) = G_{01\%} \cdot \sqrt{\frac{1}{1 - \varphi}},$$

$$C_1(\varphi) = C_{1\%} \cdot \left(\frac{1}{1 - \varphi}\right)^4,$$

$$\tau(\varphi) = \tau_{25\%} + B_1 \cdot e^{-a_1 \cdot \varphi},$$

$$\alpha(\varphi) = A_2 + B_2 \cdot e^{-a_2 \cdot \varphi} \quad \text{and}$$

$$G_{02}(\varphi, B) = C_2(\varphi, B) = \frac{4\varphi J_p^2 R^3}{\mu_1 \mu_0 d^3} (1 - \varphi). \quad (16)$$

The dipole-dipole interaction model was verified with experimental tests. In figure 7, the fractional derivative, particle-matrix interaction and magneto-induced modulus model are coupled (equation (16)) and fit to the experimental data for the 10% isotropic MRE. The fitting was evaluated with the mean error between the experimental data and the approached model. This error does not exceed 4% and occurs at high frequencies. Hence, it was concluded that the fitting error for the particle content was larger than that for the magneto-induced modulus.

#### 4. Conclusions

A new three-dimensional magneto-viscoelastic model was developed for isotropic MREs, and the consistency of the model was proved. The viscoelastic modelling was based on fractional derivatives and it was modified in order to introduce the particle content variable. The fitting of the particle-matrix and fractional derivative coupled model was successful, although the fitting error is larger for the loss modulus because the influence of the storage modulus in the dynamic complex modulus is larger. In addition, the maximum error for the storage modulus does not exceed 4%, and the loss modulus one 13%.

The introduction of an equation dependent on particle content and magnetic field in  $G_0$  and in  $C$  parameters of the fractional viscoelastic model is consistent.

The magneto-induce model of isotropic samples was developed considering anisotropic samples and applying a correction factor to introduce the isotropy. When the fractional derivative, particle-matrix interaction and magneto-induced model were combined, the storage modulus error is less than 4%, which shows that the proposed model is valid.

The new three-dimensional magneto-viscoelastic model predicts the viscoelastic behaviour of isotropic MREs as a function of frequency, matrix, volumetric particle content and magnetic field.

### Acknowledgments

The authors gratefully acknowledge financial support from the Department of Education of the Basque Government for the Research Predoc Grant PRE\_2014\_1\_284, ACTIMAT, IT009-16 and AVISANI (DPI2015-71198-R) research project from the Spanish Government.

### References

- [1] Tu J W, Yu Y, Huang L, Tu B and Xu J Y 2014 Research on new type viscoelastic damper based on MRE smart material: design, experiment and modelling *Mater. Res. Innov.* **18** 243–9
- [2] Xu Z, Suo S and Lu Y 2015 Vibration control of platform structures with magnetorheological elastomer isolators based on an improved SAWS law *Smart Mater. Struct.* **25** 1–11
- [3] Liao G J, Gong X-L, Xuan S H, Kang C J and Zong L H 2012 Development of a real-time tunable stiffness and damping vibration isolator based on magnetorheological elastomer *J. Intell. Mater. Syst. Struct.* **23** 25–33
- [4] Khimi S R and Pickering K L 2015 Comparison of dynamic properties of magnetorheological elastomers with existing antivibration rubbers *Composites B* **83** 175–83
- [5] Schubert G and Harrison P 2015 Large-strain behaviour of magneto-rheological Elastomers tested under uniaxial compression and tension, and pure shear deformations *Polym. Test.* **42** 122–34
- [6] Hiptmair F, Major Z, Haßbacher R and Hild S 2015 Design and application of permanent magnet flux sources for mechanical testing of magnetoactive elastomers at variable field directions *Rev. Sci. Instrum.* **86** 85107
- [7] Kramarenko E Y, Chertovich A V, Stepanov G V, Semisalova A S, Makarova L A, Perov N S and Khokhlov A R 2015 Magnetic and viscoelastic response of elastomers with hard magnetic filler *Smart Mater. Struct.* **24** 35002
- [8] Kruzalak J, Usakova M, Dosoudil R, Hudec I and Sykora R 2014 Microstructure and performance of natural rubber based magnetic composites *Polym. Plast. Technol. Eng.* **53** 1095–104
- [9] Raa Khimi S, Pickering K L and Mace B R 2015 Dynamic properties of magnetorheological elastomers based on iron sand and natural rubber *J. Appl. Polym. Sci.* **132** 41506
- [10] Aloui S and Klüppel M 2015 Magneto-rheological response of elastomer composites with hybrid-magnetic fillers *Smart Mater. Struct.* **24** 25016
- [11] Jones D I G 2001 *Handbook of Viscoelastic Vibration Damping* (Chichester: Wiley)
- [12] Zener C 1948 *Elasticity and Anelasticity of Metals* (Chicago: Chicago University Press)
- [13] Chen L and Jerrams S 2011 A rheological model of the dynamic behaviour of magnetorheological elastomers *J. Appl. Phys.* **110** 013513
- [14] Han Y, Zhang Z, Faidley L E and Hong W 2012 Microstructure-based modeling of magneto-rheological elastomers *Proc. SPIE* **8342** 83421B
- [15] Li W H, Zhou Y and Tian T F 2010 Viscoelastic properties of MR elastomers under harmonic loading *Rheol. Acta* **49** 733–40
- [16] Liao G, Gong X and Xuan S 2013 Magnetic field-induced compressive property of magnetorheological elastomer under high strain rate *Ind. Eng. Chem. Res.* **52** 8445–53
- [17] Behrooz M, Wang X and Gordaninejad F 2014 Modeling of a new semi-active/passive magnetorheological elastomer isolator *Smart Mater. Struct.* **23** 045013
- [18] Zhu G, Xiong Y, Daley S and Shenoi R 2015 Magnetorheological elastomer materials and structures with vibration energy control for marine application *Analysis and Design of Marine Structures V* (Boca Raton, FL: CRC Press) pp 197–204
- [19] Pritz T 1996 Analysis of four-parameter fractional derivative model of real solid materials *J. Sound Vib.* **195** 103–15
- [20] Zhu J, Xu Z and Guo Y 2013 Experimental and modeling study on magnetorheological elastomers with different matrices *J. Mater. Civil Eng.* **25** 1762–71
- [21] Guo F, Du C and Li R 2014 Viscoelastic parameter model of magnetorheological elastomers based on abel dashpot *Adv. Mech. Eng.* **6** 629386
- [22] Xu Z D, Liao Y X, Ge T and Xu C 2016 Experimental and theoretical study of viscoelastic dampers with different matrix rubbers *J. Eng. Mech.* **142** 4016051
- [23] Lu X et al 2012 Mechanical and structural investigation of isotropic and anisotropic thermoplastic magnetorheological elastomer composites based on poly(styrene-*b*-ethylene-co-butylene-*b*-styrene) (SEBS) *Rheol. Acta* **51** 37–50
- [24] Guth E and Gold O 1938 On the hydrodynamical theory of the viscosity of suspensions *Phys. Rev.* **53** 322
- [25] Guth E 1945 Theory of filler reinforcement *J. Appl. Phys.* **16** 20–5
- [26] Leng D, Sun L, Sun J and Lin Y 2013 Derivation of stiffness matrix in constitutive modeling of magnetorheological elastomer *J. Phys.: Conf. Ser.* **412** 12028
- [27] Ray S, Shanmugaraj A M and Bhowmick A K 2002 A new parameter for interpretation of polymer-filler and filler-filler interactions in rubber vulcanizates *J. Mater. Sci. Lett.* **21** 1097–100
- [28] Ivaneyko D, Toshchevikov V P, Saphiannikova M and Heinrich G 2011 Magneto-sensitive elastomers in a homogeneous magnetic field: a regular rectangular lattice model *Macromol. Theory Simul.* **20** 411–24
- [29] Ivaneyko D, Toshchevikov V, Saphiannikova M and Heinrich G 2012 Effects of particle distribution on mechanical properties of magneto-sensitive elastomers in a homogeneous magnetic field *Condens. Matter Phys.* **15** 1–12
- [30] Jolly M R, Carlson J D and Muñoz B C 1999 A model of the behaviour of magnetorheological materials *Smart Mater. Struct.* **5** 607–14
- [31] Jolly M R, Carlson J D, C Muñoz B and Bullions T A 1996 The magnetoviscoelastic response of elastomer composites consisting of ferrous particles embedded in a polymer matrix *J. Intell. Mater. Syst. Struct.* **4** 613–22
- [32] Davis L C 1999 Model of magnetorheological elastomers *J. Appl. Phys.* **85** 3348–51
- [33] Agirre-Olabide I, Elejabarrieta M J and Lion A 2015 Fractional derivative model for magnetorheological elastomers *Constitutive Models for Rubbers IX* (Boca Raton, FL: CRC Press) pp 639–45
- [34] Mullins L and Tobin N R 1966 Stress softening in rubber vulcanizates: I. Use of a strain amplification factor to describe elastic behavior of filler-reinforced vulcanized rubber *J. Appl. Polym. Sci.* **39** 799–813
- [35] Agirre-Olabide I, Berasategui J, Elejabarrieta M J and Bou-Ali M M 2014 Characterization of the linear viscoelastic region of magnetorheological elastomers *J. Intell. Mater. Syst. Struct.* **25** 2074–81
- [36] Lokander M and Stenberg B 2003 Improving the magnetorheological effect in isotropic magnetorheological rubber materials *Polym. Test.* **22** 677–80
- [37] Kelly P 2013 *Solid Mechanics Lecture Notes* (Auckland: The University of Auckland)
- [38] Haupt P 2002 *Continuum Mechanics and Theory of Materials* (Berlin: Springer)

# Maximum attenuation variability of isotropic magneto-sensitive elastomers

*I. Agirre-Olabide and M.J. Elejabarrieta*

Mechanical and Manufacturing Department, Mondragon Unibertsitatea, Loramendi 4,  
20500 Arrasate-Mondragon, Spain

Polymer Testing

2016 vol. **54** pag. 104-113

DOI: 10.1016/j.polymertesting.2016.06.021

IF-JCR: 2.464 J. Rank-JCR: 6/33



Contents lists available at ScienceDirect

Polymer Testing

journal homepage: [www.elsevier.com/locate/polytest](http://www.elsevier.com/locate/polytest)

Material properties

## Maximum attenuation variability of isotropic magnetosensitive elastomers



I. Agirre-Olabide, M.J. Elejabarrieta\*

Mech. &amp; Manuf. Dept., Mondragon Unibertsitatea, 20500, Arrasate-Mondragon, Spain

### ARTICLE INFO

Article history:  
Received 17 May 2016  
Accepted 23 June 2016  
Available online 25 June 2016

Keywords:  
Magnetosensitive  
Maximum attenuation  
Frequency  
Temperature  
Magnetic field

### ABSTRACT

Magnetosensitive elastomers (MSE) are innovative high-tech materials that exhibit changed dynamic properties when an external magnetic field is applied. In this work, the influence of particle content, frequency, temperature and magnetic field on the maximum attenuation of isotropic MSEs was studied. Six particle content types were synthesised using carbonyl iron powder particles embedded in a room-temperature vulcanizing silicone rubber matrix. The characterization of the MSE samples was performed with a Physica MCR 501 rheometer from the Anton Paar Company that is equipped with a magnetorheological cell. All samples were characterized using frequency sweep tests within the lineal viscoelastic region. In addition, a four-parameter fractional derivative model was used and extended over a wide frequency range. The influence of temperature was modelled using the Arrhenius model, coupled with the fractional derivative model. The maximum attenuation is increased with frequency and magnetic field and is independent of temperature.

© 2016 Elsevier Ltd. All rights reserved.

### 1. Introduction

Magnetosensitive elastomers (MSE) are known as smart materials due to their ability to modify their properties depending on an applied external magnetic field. This variability is due to the ferromagnetic particles embedded in a rubber matrix [1].

The dynamic properties of viscoelastic materials, such as MSE, are dependent on the characterization variables [2], such as strain, frequency, temperature and magnetic field. Within the lineal viscoelastic (LVE) region, the variability of the properties is larger than in the non-lineal region or at high strains [3,4]. The dynamic properties, storage modulus and loss factor increase with frequency [5] and magnetic field [6,7], while they decrease with temperature [6,8,9].

In many applications, MSEs are designed to dissipate as much energy as possible. The maximum attenuation (loss factor peak) of these materials is given at a certain frequency and temperature [2], which can be identified via the glass transition temperature  $T_G$  [10].

In order to identify the maximum attenuation conditions, a dynamic mechanical analyser can be used [11]. Pickering et al. [10]

and Raa Khimi and Pickering [12] studied the variation of the  $T_G$  of magnetorheological elastomers. The maximum attenuation for those samples is larger than that defined by a sample without any particle content [12] and it increased with filler content [13]. The glass transition temperature is also modified by the particle content, being decreased with an increase in the content [14].

The maximum attenuation can also be identified by extending a fractional derivative model in the frequency domain for rubber [15] or polymer material [16]. Using such a model, the evolution of the loss factor can be analysed so as to identify the maximum attenuation conditions.

In this work, the variability of the maximum attenuation of isotropic MSEs is analysed. Dynamic characterization was performed in the frequency and temperature domains, and the influences of the magnetic field and particle content on the dynamic properties were studied. Attenuation is defined by the loss factor. In order to determine the maximum attenuation (loss factor peak), a four-parameter fractional derivative model was extended in the frequency domain. The Arrhenius model was used to predict the influence of temperature. Furthermore, an external magnetic field was used to analyse the variability of the maximum attenuation conditions.

\* Corresponding author.

E-mail address: [mjelejabarrieta@mondragon.edu](mailto:mjelejabarrieta@mondragon.edu) (M.J. Elejabarrieta).



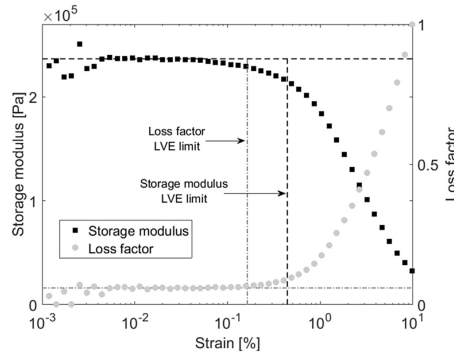


Fig. 1. Storage modulus and loss factor LVE limits of the 25% isotropic MSE at 65 °C, 1 Hz and 616 kA/m.

2. Experimental

2.1. Material

The MSEs analysed in this study were compounded by using a matrix and ferromagnetic particles. The matrix, which has two components, was silicone WACKER Elastosil® M 4644 A, and the vulcanizing agent was WACKER Elastosil® M 4644 B. These were mixed at a 10:1 ratio.

Spherical carbonyl-iron-powder (CIP) ferromagnetic iron particles with an average size of 1.25 ± 0.55 µm were used. These particles were provided by BASF, The Chemical Company. Six volumetric concentrations were analysed: 0%, 5%, 10%, 15%, 20% and 25%.

2.2. Characterization

The characterization was performed with a Physica MCR 501 rheometer from the Anton Paar Company with parallel plate configuration and equipped with a magnetorheological cell MRD

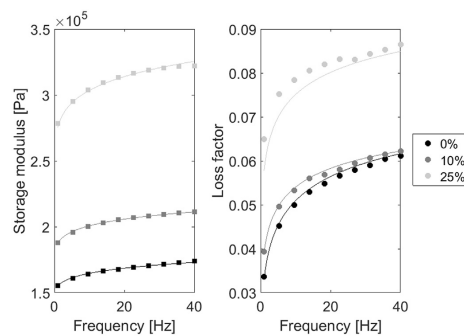


Fig. 2. Experimental data (points) and FD fitting curves (lines) of the storage modulus and loss factor of the 0%, 10% and 25% samples as a function of frequency at 25 °C and 0 kA/m.

70/1T. The plate diameter was 20 mm, and one had a serrated surface (PP20/MRD/TI/P2).

The frequency range analysed in this work extended from 1 Hz to 40 Hz. The studied temperatures ranged from 15 °C to 65 °C, with an increment of 10 °C, and were controlled using a Julabo F-25 water-based heating/cooling system; a normal force of 5 N was applied [17]. Two external magnetic field intensities were studied: 0 kA/m and 616 kA/m. After each characterization, demagnetization cycles were applied.

This work studied the influence of frequency, temperature and magnetic field on the attenuation of MSEs in the lineal viscoelastic (LVE) region because the influence of the magnetic field is larger in this region than at high strains [18]. Within the LVE region, viscoelastic behaviour can be modelled via the complex shear modulus ( $G^*$ ), which is independent of the strain and is defined in Ref. [2] as:

$$G^* = \frac{\tau(t)}{\gamma(t)} = \frac{\tau_{max} \cdot e^{i(\omega t + \delta)}}{\gamma_{max} \cdot e^{i\omega t}} = \frac{\tau_{max}}{\gamma_{max}} (\cos \delta + i \sin \delta), \quad (1)$$

where  $\tau_{max}$  is the amplitude of the shear stress,  $\gamma_{max}$  is the amplitude of the shear strain,  $\delta$  is the phase difference between the strain and stress and  $\omega$  is the frequency in radians per second. The complex shear modulus is compounded by a real part, or the storage modulus ( $G'$ ), and an imaginary part, or the loss modulus ( $G''$ ). The relationship between these is the loss factor ( $\tan \delta$ ).

In order to guarantee that the samples were working within the LVE region, a strain sweep test was performed with the minimum frequency (1 Hz) and the maximum particle content (25%), temperature (65 °C) and magnetic field (616 kA/m) [19]. A logarithmic strain sweep was applied to the 25% isotropic MSE from 0.001 to 10% with 50 points, and 5 s per point were measured. The LVE limit was determined by the loss factor [20] and had a value of 0.01% (Fig. 1).

Frequency sweep tests were performed at a strain of 0.01% (LVE limit) to determine the lineal dynamic mechanical properties of the analysed MSE. For the frequency sweep test, a lineal distribution of 10 frequencies between 1 Hz and 40 Hz was applied. The measured period for each point was 5 s.

2.3. Modelling and analysis

The influence of the frequency, temperature and magnetic field on the maximum attenuation was studied. The evolution of the dynamic properties (storage modulus and loss factor) with the frequency was modelled using a four-parameter fractional derivative model at 25 °C. The constitutive viscoelastic model was extended over the frequency domain in order to identify the maximum attenuation value and frequency. After studying the frequency, the influence of the temperature was analysed. The modelling was performed using the Arrhenius model, and the evolution of the maximum attenuation was studied by varying frequency and temperature. Finally, the influence of the magnetic field on the maximum attenuation amplitude and the frequency at which it occurs were analysed. Although all samples were analysed,

Table 1 The values of the four parameters (Eq. (2)) of isotropic MSE at 25 °C and 0 kA/m.

Sample	$G_0$ [Pa]	$G_{\infty}$ [Pa]	$\tau$ [s]	$\alpha$
0%	142894	277677	5.76 e <sup>-5</sup>	0.281174
5%	155223	311269	6.62 e <sup>-5</sup>	0.245590
10%	165978	360226	2.99 e <sup>-5</sup>	0.235889
15%	181038	430260	1.29 e <sup>-5</sup>	0.218954
20%	208148	591220	4.64 e <sup>-6</sup>	0.205398
25%	220976	845994	1.43 e <sup>-6</sup>	0.198359

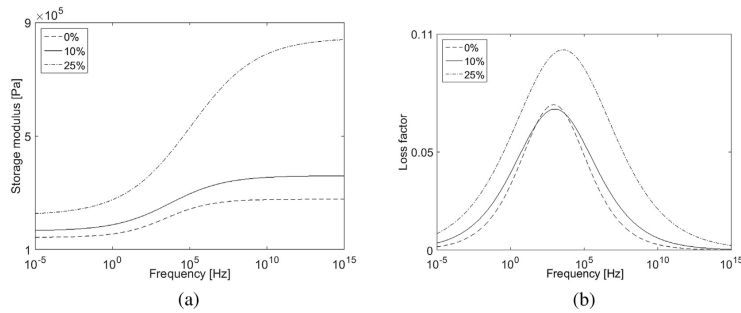


Fig. 3. Evolution of the (a) storage modulus and (b) loss factor of 0%, 10% and 25% MSE samples as a function of frequency at 25 °C and 0 kA/m.

**Table 2**  
Values and frequencies of maximum attenuation for isotropic MSE samples of various particle contents at 25 °C and 0 kA/m.

Sample	Maximum attenuation	Frequency [Hz]
0%	0.0740	847
5%	0.0674	585
10%	0.0718	1018
15%	0.0741	1691
20%	0.0832	2681
25%	0.1019	3703

the 0%, 10% and 25% samples are used as references in order to study the evolution of the studied parameters.

### 3. Results and discussion

#### 3.1. Frequency

The dynamic properties of MSEs are dependent on the frequency. The frequency increases both the storage modulus and loss factor for all studied samples (Fig. 2). The variation of the storage modulus due to the frequency ( $\Delta G'_f = (G'_{40\text{Hz}} - G'_{1\text{Hz}})/G'_{1\text{Hz}}$ ) is larger for MSEs with a high particle contents. On the other hand, the loss factor variation due to the frequency ( $\Delta \tan \delta_f = (\tan \delta_{40\text{Hz}} - \tan \delta_{1\text{Hz}})/\tan \delta_{1\text{Hz}}$ ) decreases with high particle content.

A four-parameter fractional derivative (FD) model was used to

introduce the influence of the frequency on the dynamic properties of MSEs, which is defined as follows:

$$G^* = \frac{G_0 + G_\infty(i\omega\tau)^\alpha}{1 + (i\omega\tau)^\alpha}, \quad (2)$$

where  $G_0$  is the elastic modulus at 0 Hz,  $G_\infty$  is the asymptotic modulus for an infinite frequency,  $\tau$  is the relaxation time and  $\alpha$  is the fractional derivative parameter, which is dimensionless and between 0 and 1 [21].

Once the four-parameter fractional derivative model was defined, it was fitted to all the experimental results at 25 °C. In Fig. 2, the fitting of the 0%, 10% and 25% isotropic samples are shown, and Table 1 summarizes the fittings of the samples without any magnetic field. While  $G_0$  and  $G_\infty$  increase with the particle content,  $\tau$  and  $\alpha$  decrease.

The fractional derivative model was extended in the frequency domain from  $1e^{-5}$  Hz to  $1e^{15}$  Hz in order to observe the evolution of storage modulus and loss factor, and identify the frequency of maximum attenuation. In Fig. 3a, the storage modulus increases with frequency and particle content. In Fig. 3b, the loss factor as a function of frequency is shown. In terms of shape, the loss factor curves are wider with particle content, which indicates that the attenuation is larger over the entire frequency band. In addition, the largest width difference is seen when the maximum particle content is analysed. Table 2 shows the value of the maximum

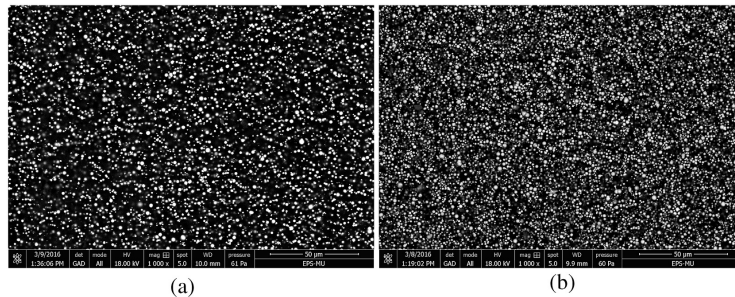


Fig. 4. SEM images of (a) 10% and (b) 25% MSE samples in low vacuum conditions and with a voltage acceleration of 18 kV.

attenuation, loss factor peak and its frequency. The value increases with the particle content, and the maximum increase occurs between the 20% and 25% samples. The frequency at which the loss factor peak occurs also increases with the particle content and, consequently, the loss factor curve is shifted to the right.

In order to detect the difference between samples, scanning electron microscope (SEM) images were used. A Nova NanoSEM 450 microscope was used in low-vacuum conditions and with a

voltage acceleration of 18 kV. As an example, the 10% and 25% MSE samples are shown in Fig. 4. As mentioned by Ju et al. [8] and Raa Khimi et al. [22], the MSE materials have two kinds of damping source, one due to the matrix and the other due to the friction between the matrix and the particles. Therefore, the damping of the MSE is increased with the particle content. However, it can be seen that, in the 25% sample (Fig. 4(b)), the particles are much closer to one another than in the 10% sample (Fig. 4(a)). Therefore,

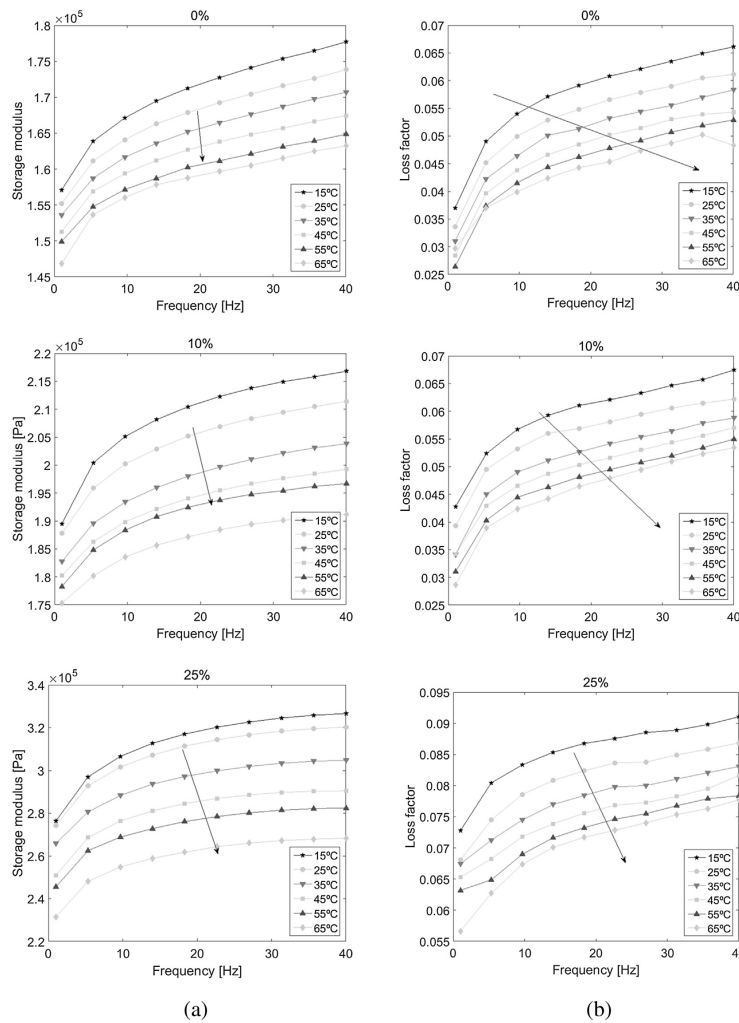


Fig. 5. Evolution of the (a) storage modulus and (b) loss factor of the 0%, 10% and 25% MSEs as a function of frequency, with temperature ranging from 15 °C to 65 °C and 0 kA/m.

there is another damping source related to the friction between the particles, which increases the loss factor of the 25% sample.

### 3.2. Temperature

The storage modulus and loss factor decreased with the increment of temperature for all the studied samples; this represents the inverse of the frequency effect. For the reference samples (0%, 10%

and 25%) in Fig. 5, the influence of temperature (from 15 °C to 65 °C) on the frequency band from 1 Hz to 40 Hz is shown.

The influence of the frequency and temperature depends on the particle content. With the purpose of interpreting the obtained results, arrows are included in Fig. 5. Their inclination with respect to the horizontal represents the influence of frequency, while the length represents the influence of temperature. A larger arrow and inclination means a larger influence of temperature and frequency.

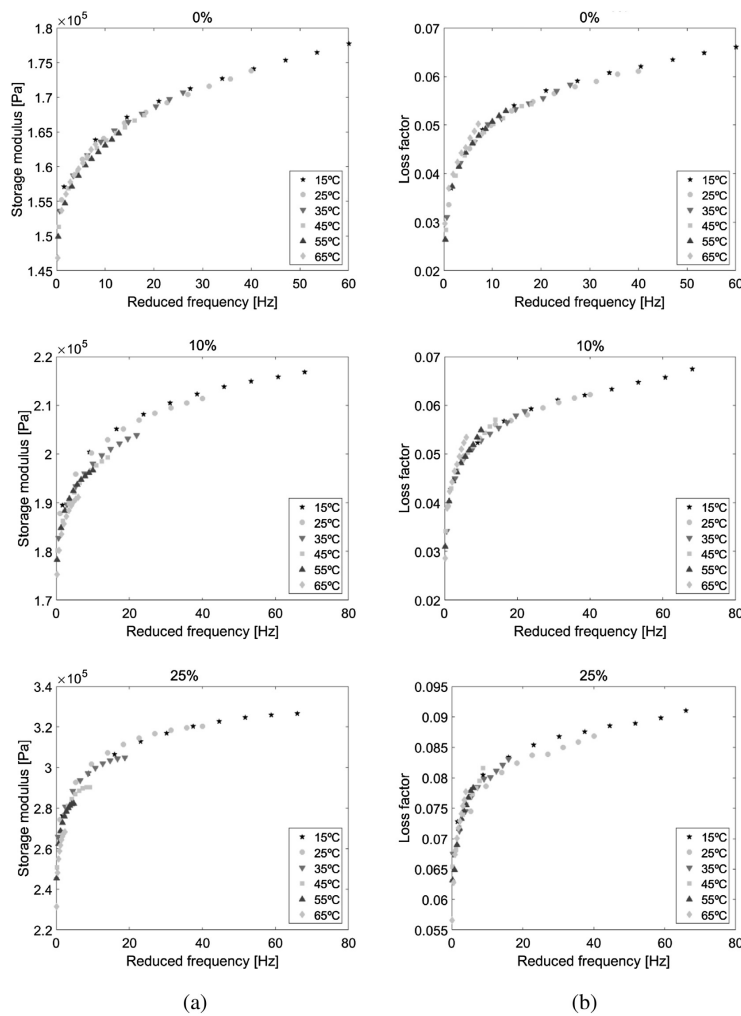


Fig. 6. (a) Storage modulus and (b) loss factor of the 0%, 10% and 25% MSEs as a function of reduced frequency using the temperature-frequency superposition principle with a 0 kA/m magnetic field.

Within the studied temperature and frequency ranges, the influence of frequency and temperature on the storage modulus is larger with the particle content, whereas the influence on the loss factor is decreased.

At low particle content levels, the influence of the frequency on storage modulus is larger than that of temperature. However, at high particle content levels, the influence of temperature on storage modulus is larger than that of frequency. On the other hand, the loss factor of the studied samples is more sensitive to frequency than to temperature.

In order to introduce the temperature dependence to the fractional derivative model, the frequency-temperature superposition principle was used [23]. This principle is based on the assumption that the complex modulus measured at any chosen frequency  $f_1$  and at a reference temperature  $T_1$  is identical to that at any other frequency  $f_2$  and a different temperature  $T_2$ , which must be selected,

$$G^*(f_1, T_1) = G^*(f_2 \alpha_T(T), T_2), \tag{3}$$

where the shift factor  $\alpha_T(T)$  depends on the temperature and the polymer. This principle can be applied by plotting  $[(T_0 \rho_0 / T \rho) \cdot G^*]$  and  $[(T_0 \rho_0 / T \rho) \cdot \tan \delta]$  against the reduced frequency ( $f \alpha_T$ ), where  $T_0$  is the reference temperature, and  $\rho$  and  $\rho_0$  are the density at a certain temperature ( $T$ ) and the density at the reference temperature ( $T_0$ ), respectively [2]. In this work, the reference temperature was 25 °C. These are plotted in Fig. 6, where the 0%, 10% and 25% samples are shown. For this figure, the experimental data are shifted horizontally along the frequency scale [24].

The temperature dependence on the shift factor  $\alpha_T(T)$  represents the basic effect of temperature on the viscoelastic properties and can be described using the equation of Williams-Landel-Ferry (WLF) [25] or that of Arrhenius [2]. The WLF equation is used at temperatures above the glass transition temperature ( $T_g$ ) and under  $T_g + 100$  °C.

The Elastisol matrix is a polydimethylsiloxane (PDMS)-based silicone rubber, and the glass transition temperature for those polymers is around -125 °C [26]. Therefore, the Arrhenius model is used to introduce the influence of temperature on the four-parameter fractional derivative model. The Arrhenius shift factor equation describes a lineal relationship between  $\log \alpha_T(T)$  and  $1/T$  based on the molecular kinetic theory of chemical reactions,

**Table 3**  
Evolution of the fitting parameter of the Arrhenius model,  $T_A$ , for the isotropic MSEs.

Sample	$T_A$ (°C)
0%	1569
5%	1685
10%	2026
15%	2097
20%	2230
25%	2988

$$\log \alpha_T(T) = T_A \left( \frac{1}{T} - \frac{1}{T_0} \right), \tag{4}$$

where  $T_A$  is the slope of the line representing the plot of  $\log \alpha_T(T)$  versus  $1/T$  and  $T_0$  is the reference temperature [2].

An example of the evolution of the  $\log \alpha_T(T)$  with temperature is shown in Fig. 7 for the 0%, 10% and 25% isotropic MSE samples. Moreover, the evolution of  $T_A$  with the studied cases is shown in Table 3;  $T_A$  increased with particle content.

Coupling the Arrhenius model with the four-parameter FD model (Equations (4) and (2)), the evolution of the maximum attenuation was analysed. In Fig. 8, the evolution of the peak is shown in the frequency (Fig. 8(a)) and temperature domains (Fig. 8(b)) for the three reference samples. In the frequency domain figures (from  $1e^{-5}$  Hz to  $1e^{15}$  Hz), three temperatures were fixed (-10 °C, 25 °C and 80 °C), and in the temperature domain (from -200 °C to 100 °C), the analysed frequencies were 1 Hz, 50 Hz and 100 Hz.

The value of the maximum attenuation depends on the particle content and is constant with frequency and temperature. Specifically, it increases 51% with the particle content from 0.0674 (5% MSE) to 0.1019 (25% MSE) (Table 2).

In the reduced frequency domain, the frequency at which the maximum attenuation occurs depends on the temperature (Fig. 8(a)). Therefore, increasing the temperature causes the frequency to increase, which means that the curves are shifted to the right. The same behaviour is observed for storage modulus. Furthermore, the shifting of the storage modulus and loss factor curves is larger with increased particle content (Table 4) due to the dependency on the Arrhenius fitting parameter  $T_A$  (Table 3). Nonetheless, the shapes of storage modulus and loss factor in the frequency domain are independent of temperature.

On the other hand, the temperature at which the maximum attenuation occurs depends on the frequency (Fig. 8(b)), which is

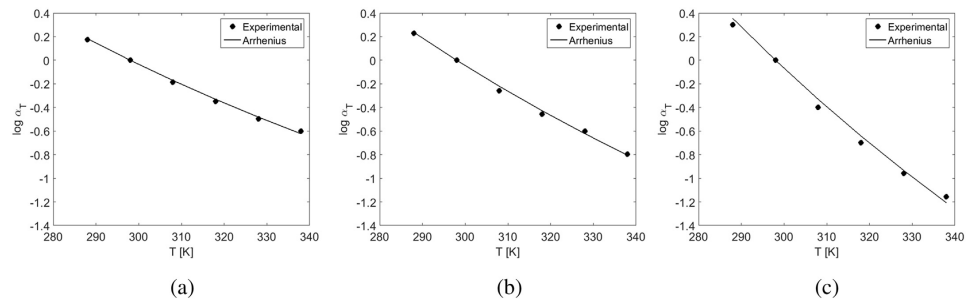
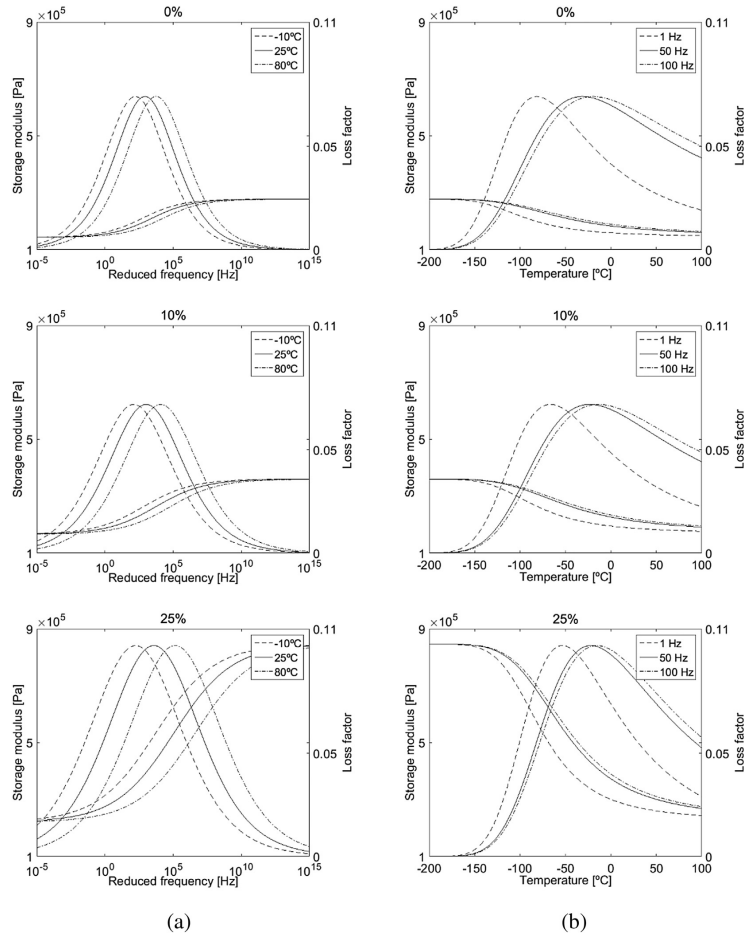


Fig. 7. Shift factor  $\alpha_T$  and Arrhenius model versus temperature for (a) 0%, (b) 10% and (c) 25% samples.



**Fig. 8.** Evolution of the storage modulus and loss factor as a function of (a) reduced frequency (for  $-10\text{ }^{\circ}\text{C}$ ,  $25\text{ }^{\circ}\text{C}$  and  $80\text{ }^{\circ}\text{C}$ ), and (b) temperature (for 1 Hz, 50 Hz and 100 Hz) for the 0%, 10% and 25% MSE samples at 0 kA/m.

higher with increased particle content [10]. The storage modulus and loss factor curves are shifted to the right, increasing the frequency. Moreover, these increases are larger in the low-frequency range (Fig. 8(b)), and the variation of the temperature due to frequency is smaller with increased particle content (Table 4). The shape of the storage modulus and loss factor curves are dependent on frequency.

Therefore, the maximum attenuation can be reached by decreasing the temperature or increasing the frequency; this characteristic behaviour is due to the viscoelastic nature of the matrix.

### 3.3. Magnetic field

The influence of the magnetic field on the attenuation of the 10% and 25% samples is shown in Fig. 9 for a magnetic field of 616 kA/m at  $25\text{ }^{\circ}\text{C}$ . The storage modulus is increased with the magnetic field, while the influence on the loss factor is not evident.

As in the previous frequency and temperature sections, a four-parameter fractional derivative model was fitted to the experimental data of Fig. 9 and extended over the frequency range from  $1\text{e}^{-5}\text{ Hz}$  to  $1\text{e}^{15}\text{ Hz}$ . The influence of the magnetic field on the loss factor of MSE materials can be seen in Fig. 10, and the maximum

**Table 4**  
Values of the maximum attenuation (a) frequency and (b) temperature for all MSE samples and studied conditions.

(a) Frequency			
Sample	Temperature		
	-10 °C	25 °C	80 °C
0%	169	847	5907
5%	102	585	4453
10%	128	1018	11724
15%	167	1691	21347
20%	194	2681	38868
25%	177	3703	141303

(b) Temperature			
Sample	Frequency		
	1 Hz	50 Hz	100 Hz
0%	-81.52	-31.41	-19.68
5%	-72.88	-22.29	-10.53
10%	-66.52	-23.28	-13.65
15%	-68.80	-28.29	-19.38
20%	-68.71	-31.02	-22.86
25%	-53.38	-22.02	-15.51

attenuation values and its frequencies are shown in Table 5. The attenuation is larger in the studied frequency band because

the shape of the loss factor is wider (Fig. 10). The maximum attenuation value and frequency are increased with the magnetic field, except for the maximum particle content (25%) (Table 5). When a MSE sample is under a magnetic field, the relative movement is almost stopped [8]. Therefore, the damping due to the matrix-particle and particle-particle friction is reduced and, consequently, the maximum attenuation is also reduced.

**4. Conclusions**

In this work, the influence of frequency, temperature and a magnetic field on the maximum attenuation of isotropic MSEs was analysed. In order to determine the maximum attenuation (loss factor peak), a four-parameter fractional derivative model was extended in the frequency domain.

For each particle content and magnetic field, the value of maximum attenuation is unique and occurs at a certain frequency and temperature. The attenuation is larger with increased particle content over the entire frequency band, and the frequency at which the maximum occurs is increased.

In order to model the influence of temperature on the dynamic properties, the Arrhenius model was coupled with a four-parameter fractional derivative model. The shapes of the loss factor curves are not influenced by temperature, while they are dependent on frequency. The maximum attenuation frequency is

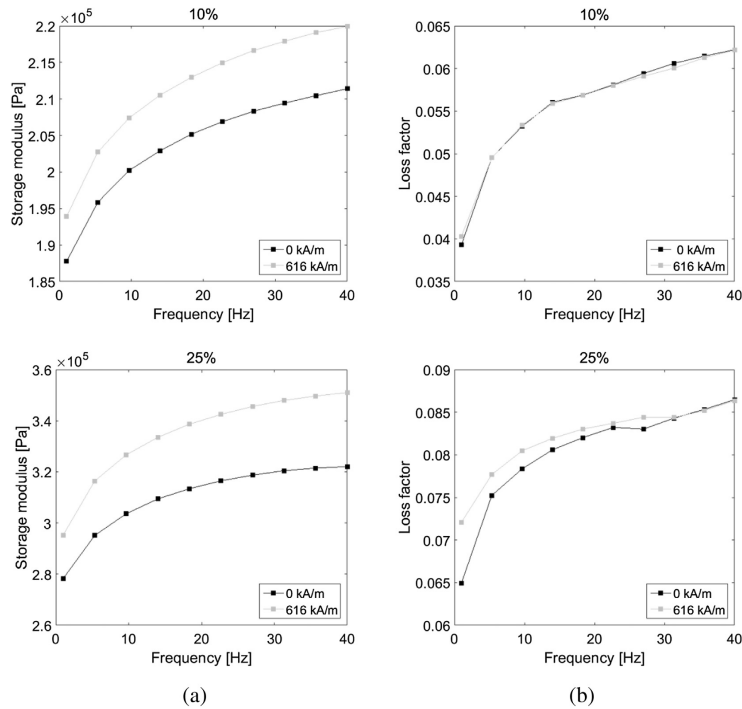


**Fig. 9.** Influence of the magnetic field on the (a) storage modulus and (b) loss factor for the 10% and 25% MSEs as a function of frequency at 25 °C and with 0 kA/m and 616 kA/m.

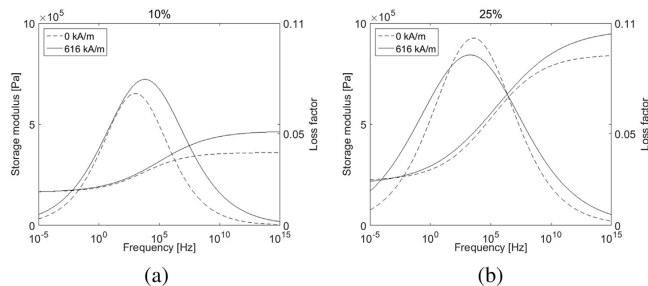


Fig. 10. Influence of the magnetic field on the storage modulus and loss factor of (a) 10% and (b) 25% MSEs as a function of frequency at 25 °C and with 0 kA/m and 616 kA/m.

Table 5

(a) Values and (b) frequencies of maximum attenuation of various particle content isotropic MSE samples under a magnetic field of 0 kA/m and 616 kA/m at 25 °C.

(a) Maximum attenuation		
Sample	Magnetic field	
	0 kA/m	616 kA/m
5%	0.0674	0.0710
10%	0.0718	0.0794
15%	0.0741	0.0769
20%	0.0832	0.0838
25%	0.1019	0.0928

(b) Frequency		
Sample	Magnetic field	
	0 kA/m	616 kA/m
5%	585	2335
10%	1018	6439
15%	1691	9750
20%	2681	12277
25%	3703	1942

reduced with increased temperature and particle content. The maximum attenuation temperature is increased with increased frequency and particle content; this occurs to a greater degree at low frequencies.

With the application of an external magnetic field, the maximum attenuation value and frequency are increased, and the loss factor is larger in the studied frequency domain.

This work illustrates a methodology combining experimental results and theoretical models (fractional derivatives and Arrhenius) in order to predict the frequency, temperature and magnetic field conditions at which the maximum attenuation of isotropic MSEs occurs.

#### Acknowledgements

The authors gratefully acknowledge the financial support received from the Department of Education of the Basque Government for Research Predoc Grant PRE\_2014\_1\_284; ACTIMAT, IT009-16 and the support received for research project AVISANI (DPI2015-71198-R) from the Spanish Government.

#### References

- [1] H.S. Jung, S.H. Kwon, H.J. Choi, J.H. Jung, Y.G. Kim, Magnetic carbonyl iron/natural rubber composite elastomer and its magnetorheology, *Compos. Struct.* 136 (2016) 106–112, <http://dx.doi.org/10.1016/j.compstruct.2015.10.008>.

- [2] D.I.G. Jones, *Handbook of Viscoelastic Vibration Damping*, John Wiley & Sons Ltd, Chichester, 2001.
- [3] M. Lokander, B. Stenberg, Improving the magnetorheological effect in isotropic magnetorheological rubber materials, *Polym. Test.* 22 (2003) 677–680, [http://dx.doi.org/10.1016/S0142-9418\(02\)00175-7](http://dx.doi.org/10.1016/S0142-9418(02)00175-7).
- [4] G. Schubert, P. Harrison, Large-strain behaviour of magneto-rheological elastomers tested under uniaxial compression and tension, and pure shear deformations, *Polym. Test.* 42 (2015) 122–134, <http://dx.doi.org/10.1016/j.polymertesting.2015.01.008>.
- [5] W.H. Li, Y. Zhou, T.F. Tian, Viscoelastic properties of MR elastomers under harmonic loading, *Rheol. Acta* 49 (2010) 733–740, <http://dx.doi.org/10.1007/s00397-010-0446-9>.
- [6] W. Zhang, X. Gong, S. Xuan, W. Jiang, Temperature-dependent mechanical properties and model of magnetorheological elastomers, *Ind. Eng. Chem. Res.* 50 (2011) 6704–6712, <http://dx.doi.org/10.1021/ie200386x>.
- [7] L. Ge, S. Xuan, G. Liao, T. Yin, X. Gong, Stretchable polyurethane sponge reinforced magnetorheological material with enhanced mechanical properties, *Smart Mater. Struct.* 24 (2015) 037001, <http://dx.doi.org/10.1088/0964-1726/24/3/037001>.
- [8] B. Ju, R. Tang, D. Zhang, B. Yang, M. Yu, C. Liao, Temperature-dependent dynamic mechanical properties of magnetorheological elastomers under magnetic field, *J. Magn. Magn. Mater.* 374 (2015) 283–288, <http://dx.doi.org/10.1016/j.jmmm.2014.08.012>.
- [9] X. Gong, Y. Fan, S. Xuan, Y. Xu, C. Peng, Control of the damping properties of magnetorheological elastomers by using polycaprolactone as a temperature-controlling component, *Ind. Eng. Chem. Res.* 51 (2012) 6395–6403, <http://dx.doi.org/10.1021/ie300317b>.
- [10] K.L. Pickering, S. Raa Khimi, S. Ilanko, The effect of silane coupling agent on iron sand for use in magnetorheological elastomers part 1: surface chemical modification and characterization, *Compos. A Appl. Sci. Manuf.* 68 (2015) 377–386, <http://dx.doi.org/10.1016/j.compositesa.2014.10.005>.
- [11] Y. Tian, Y. Liu, M. He, G. Zhao, Y. Sun, High damping properties of magnetic particles doped rubber composites at wide frequency, *Mater. Res. Bull.* 48 (2013) 2002–2005, <http://dx.doi.org/10.1016/j.materresbull.2013.01.035>.
- [12] S.R. Khimi, K.L. Pickering, Comparison of dynamic properties of magnetorheological elastomers with existing antivibration rubbers, *Compos. B Eng.* 83 (2015) 175–183, <http://dx.doi.org/10.1016/j.compositesb.2015.08.033>.
- [13] C.G. Robertson, C.J. Lin, M. Rackaitis, C.M. Roland, Influence of particle size and polymer–filler coupling on viscoelastic glass transition of particle-reinforced polymers, *Macromolecules* 41 (2008) 2727–2731, <http://dx.doi.org/10.1021/ma7022364>.
- [14] J. Wu, X. Gong, L. Chen, H. Xia, Z. Hu, Preparation and characterization of isotropic polyurethane magnetorheological elastomer through in situ polymerization, *J. Appl. Polym. Sci.* 114 (2009) 901–910, <http://dx.doi.org/10.1002/app.30563>.
- [15] D. Wollscheid, A. Lion, The benefit of fractional derivatives in modelling the dynamics of filler-reinforced rubber under large strains: a comparison with the Maxwell-element approach, *Comput. Mech.* 53 (2013) 1015–1031, <http://dx.doi.org/10.1007/s00466-013-0946-4>.
- [16] R.A.S. Moreira, J.D. Corte-Real, J.D. Rodrigues, A generalized frequency-temperature viscoelastic model, *Shock Vib.* 17 (2010) 407–418, <http://dx.doi.org/10.3233/SAV-2010-0536>.
- [17] X. Dong, N. Ma, M. Qi, J. Li, R. Chen, J. Ou, The pressure-dependent MR effect of magnetorheological elastomers, *Smart Mater. Struct.* 21 (2012) 075014, <http://dx.doi.org/10.1088/0964-1726/21/7/075014>.
- [18] M. Lokander, B. Stenberg, Performance of isotropic magnetorheological rubber materials, *Polym. Test.* 22 (2003) 245–251, [http://dx.doi.org/10.1016/S0142-9418\(02\)00043-0](http://dx.doi.org/10.1016/S0142-9418(02)00043-0).
- [19] I. Agirre-Olabide, M.J. Elejabarrieta, M.M. Bou-Ali, Matrix dependence of the



- linear viscoelastic region in magnetorheological elastomers, *J. Intell. Mater. Syst. Struct.* 26 (2015) 1880–1886, <http://dx.doi.org/10.1177/1045389X15580658>.
- [20] I. Agirre-Olabide, J. Berasategui, M.J. Elejabarrieta, M.M. Bou-Ali, Characterization of the linear viscoelastic region of magnetorheological elastomers, *J. Intell. Mater. Syst. Struct.* 25 (2014) 2074–2081, <http://dx.doi.org/10.1177/1045389X13517310>.
- [21] T. Pritz, Analysis of four-parameter fractional derivative model of real solid materials, *J. Sound. Vib.* 195 (1996) 103–115, <http://dx.doi.org/10.1006/jsvi.1996.0406>.
- [22] S. Raa Khimi, K.L. Pickering, B.R. Mace, Dynamic properties of magnetorheological elastomers based on iron sand and natural rubber, *J. Appl. Polym. Sci.* 132 (2015), <http://dx.doi.org/10.1002/app.41506> n/a–n/a.
- [23] J.D. Ferry, *Viscoelastic Properties of Polymers*, third ed., Wiley, New York, 1980.
- [24] A.D. Nashif, D.I.G. Jones, J.P. Henderson, *Vibration Damping*, John Wiley & Sons, New York, 1985.
- [25] M.L. Williams, R.F. Landel, J.D. Ferry, The temperature dependence of relaxation mechanisms in amorphous polymers and other glass-forming liquids, *J. Am. Chem. Soc.* 77 (1955) 3701–3707, <http://dx.doi.org/10.1021/ja01619a008>.
- [26] D. Fragiadakis, P. Pissis, Glass transition and segmental dynamics in poly(dimethylsiloxane)/silica nanocomposites studied by various techniques, *J. Non. Cryst. Solids* 353 (2007) 4344–4352, <http://dx.doi.org/10.1016/j.jnoncrysol.2007.05.183>.



Linear magneto-viscoelastic model based on  
magnetic permeability components for  
anisotropic magnetorheological elastomers

*I. Agirre-Olabide<sup>1</sup>, P. Kuzhir<sup>2</sup> and M.J. Elejabarrieta<sup>1</sup>*

<sup>1</sup>Mechanical and Manufacturing Department, Mondragon Unibertsitatea, Loramendi 4,  
20500 Arrasate-Mondragon, Spain

<sup>2</sup>Univesity Côte d'Azur, CNRS UMR 7010, Institute of Physics of Nice, Parc Valrose,  
06100 Nice, France

Journal of Magnetism and Magnetic Materials

2018 vol. **446** pag. 155-161

DOI: 10.1016/j.jmmm.2017.09.017

IF-JCR: 2.630 J. Rank-JCR: 84/275



Contents lists available at ScienceDirect

Journal of Magnetism and Magnetic Materials

journal homepage: [www.elsevier.com/locate/jmmm](http://www.elsevier.com/locate/jmmm)

Research articles

## Linear magneto-viscoelastic model based on magnetic permeability components for anisotropic magnetorheological elastomers

I. Agirre-Olabide<sup>a</sup>, P. Kuzhir<sup>b</sup>, M.J. Elejabarrieta<sup>a,\*</sup><sup>a</sup> Mech. & Manuf. Dept., Mondragon Unibertsitatea, 20500 Arrasate-Mondragon, Spain<sup>b</sup> University Côte d'Azur, CNRS UMR 7010, Institute of Physics of Nice, Parc Valrose, 06100 Nice, France

## ARTICLE INFO

## Article history:

Received 30 July 2017

Accepted 7 September 2017

Available online 8 September 2017

## Keywords:

Anisotropic magnetorheological elastomers  
 Magnetic permeability components  
 Fractional derivative model  
 Magneto-dynamic properties

## ABSTRACT

A new magneto-viscoelastic model is presented for anisotropic magnetorheological elastomers (MREs), which combines the dynamic behaviour and magnetic permeability components. Five samples were synthesised with different particle contents. Dynamic properties were measured using a rheometer equipped with a magnetorheological cell. A four-parameter fractional derivative model was used to describe MRE viscoelasticity in the absence of a magnetic field. The magnetic permeability of each sample was measured with a vibrating sample magnetometer. From experimental measurements of longitudinal and transverse components of the magnetic permeability, the dependency with magnetic field was modelled. The new magneto-induced modulus model proposed in this work is based on the model developed by López-López et al. [19] for magnetorheological fluids, and was adapted for anisotropic MREs. The proposed model includes the longitudinal and transverse components of magnetic permeability, and it is valid for the linear viscoelastic region of anisotropic MREs. The errors between experimental values and the values predicted by the model do not exceed 10%. Hence, a new linear magneto-viscoelastic model for anisotropic MREs is developed, which predicts the effect of magnetic field on the dynamic shear modulus as a function of magnetic field intensity and frequency.

© 2017 Elsevier B.V. All rights reserved.

## 1. Introduction

Magnetorheological elastomers (MRE) consist of ferromagnetic particles embedded in an elastomeric matrix [1]. When an external magnetic field is applied to these materials, their mechanical properties are modified; and they are referred to as smart materials.

The properties of MREs are completely dependent on the particle distribution, which is therefore considered an important characteristic of MREs. Isotropic MRE samples are prepared by vulcanisation without an external magnetic field; these samples have a random particle distribution [2,3]. However, if an external magnetic field is applied during the vulcanisation process, the particles are aligned in the direction of the magnetic field, and consequently, particle chains or thicker chain aggregates are obtained; these samples are called anisotropic MREs [4,5].

Dynamic properties of anisotropic MREs are dependent on the matrix, particle content, and magnetic field. The predominant behaviour is the viscoelasticity, owing to the nature of the main component of these materials: silicone rubber or natural rubber [6,7]. This behaviour has been modelled for MRE materials by com-

binning different elements such as dashpots and springs in different configurations [8,9]. To obtain a better fit to experimental data, more elements have been introduced by increasing the number of fitting parameters [10].

The fractional derivative model can be used to decrease the number of material parameters, and these parameters have a physical significance [11]. By using these advantages, the viscoelastic behaviour of isotropic [7,12] and anisotropic [13,14] MREs have recently been modelled using fractional derivative models. Agirre-Olabide et al. [12] used four material parameters to simulate the viscoelastic behaviour of isotropic MREs, and Xu et al. [7] combined a fractional Kelvin and Maxwell model in the parallel configuration to develop a higher order model (seven material parameters). Guo et al. [13] combined an Abel dashpot (fractional derivative element) and a spring in a series configuration, while Zhu et al. [14] employed a parallel configuration. Hence, three material parameters were used to predict the viscoelastic behaviour of anisotropic MREs.

The effect of the magnetic field on the properties of anisotropic MREs has been widely studied. Many models have assumed that perfectly aligned chains are created during the vulcanisation process. Jolly et al. [15,16] analysed the interaction of two particles by using dipole–dipole moments, while Davis [17] and Shen

\* Corresponding author.

E-mail address: [mjelejabarrieta@mondragon.edu](mailto:mjelejabarrieta@mondragon.edu) (M.J. Elejabarrieta).<http://dx.doi.org/10.1016/j.jmmm.2017.09.017>

0304-8853/© 2017 Elsevier B.V. All rights reserved.

et al. [18] studied the interaction of each particle in the whole chain of particles. Bica et al. [4] used a dipolar magnetic moment approach and the ideal elastic body model.

López-López et al. [19] proposed a model for magnetorheological fluids by introducing the influence of aggregates having a body centered tetragonal (bct) internal structure (a more stable and more realistic structure), and they combined numerical simulations of the composite magnetic permeability with the analytical model predicting the stress–strain relationship. For MREs, Leng et al. [20] proposed an effective permeability model to estimate the shear storage modulus, and Dong et al. [21] developed a theoretical model for chains composed of magnetic particles and normal pressure, based on the effective permeability calculated by the Maxwell–Garnett mixing rule. Chen et al. [22] proposed a finite-column model to simulate the field-induced shear modulus.

The magnetic permeability of materials can be measured by using different techniques. De Vicente et al. [23] used a modified force balance method to measure the magnetic permeability of carbonyl iron powder suspension. Bellucci et al. [24] used vibrating sample magnetometry on a magnetic nanocomposite based on natural rubber. Schubert and Harrison [25] identified the permeability of isotropic and anisotropic MREs using an inverse modelling approach. Furthermore, they calculated the permeabilities of anisotropic MREs in the particle alignment direction and perpendicular to the alignment direction. However, de Vicente et al. [23] measured the permeability of carbonyl iron powder in a suspension and showed that the permeability decreases with the internal magnetic field.

A few magneto-viscoelastic models have been developed by coupling viscoelastic and magnetic interaction models. A classical four parameter magneto-viscoelastic model has been proposed by Li et al. [26], and all material parameters were fitted to experimental data for each magnetic field density. The magneto-viscoelastic behaviour using fractional derivatives has been modelled for isotropic [27] and anisotropic [13,14] MREs. Agirre-Olabide et al. [27] proposed a three-dimensional magneto-viscoelastic model within the linear viscoelastic region for isotropic MREs, by coupling a fractional-derivative-based viscoelastic model with a magnetic-field-dependant model. Conversely, the magneto-viscoelastic model proposed in [13,14] for anisotropic MREs is composed of a serial configuration a fractional derivative Maxwell model and a spring, which is dependent on the magnetic field and is modelled assuming chain-like structures. The strain amplitudes applied were 0.1% in [13] and 25% in [14], and the maximum magnetic field intensity was 300 mT.

In this work, we developed a new linear magneto-viscoelastic model for anisotropic MREs based on the longitudinal and transverse components of magnetic permeability. We modified the model developed by López-López et al. [19] for magnetorheological fluids, and we adapted it for anisotropic MREs. The new model assumes bulk column-like aggregates in the MR samples, and coupled it with the viscoelastic model. The viscoelastic model is based in a four-parameter fractional derivative model. We studied the influence of the magnetic field on the longitudinal and transverse components of the magnetic permeability of anisotropic MREs. We proposed a model to predict the evolution of the permeability components as a function of the external magnetic field (100–360 kA/m) and extend it for higher magnetic fields. The proposed new linear magneto-viscoelastic model was validated with experimental data, and can be extended to larger magnetic field and frequency conditions.

## 2. Experimental

In this work, anisotropic magnetorheological elastomers were synthesised using a room-temperature-vulcanising silicone rubber

and soft magnetic particles; five particle contents were analysed. Two different characterisation techniques were performed; the dynamic behaviour was measured using a rheometer equipped with a magnetorheological device, and the magnetic properties were measured using a vibrating sample magnetometer (VSM).

### 2.1. Preparation of anisotropic samples

In this study, we used two components based on room-temperature-vulcanising vulcanised silicone rubber (RTV-SR): the main matrix WACKER Elastosil® M 4644A and the vulcaniser WACKER Elastosil® M 4644B mixed in a 10:1 ratio. The embedded soft magnetic spherical particles were carbonyl iron particles HS (BASF The Chemical Company, Germany) with a particle size of  $1.25 \pm 0.55 \mu\text{m}$ . Samples of five different particle volume fractions were prepared: 0%, 5%, 10%, 15%, and 20%.

The main matrix (Elastosil® M 4644A) and particles were mixed at the mentioned contents, and when a homogeneous mixture was obtained, the vulcaniser (Elastosil® M 4644B) was added. Every time a component was added, vacuum cycles for 30 min were applied to remove air bubbles generated during the mixing. Finally, the homogenous mixture was poured into a 1-mm-thick mould.

During the vulcanisation process, a magnetic field was applied in the thickness direction to obtain a chain alignment of the particles in the direction perpendicular to the shear strain applied during the rheometric experiments (Fig. 1). A magnetic field of a flux density of 130 mT was applied using a pair of permanent magnets placed on the both sides of the mould.

A Nova Nano SEM 450 scanning electron microscope (SEM) was used to observe the particle alignment and distribution (Fig. 2). The images were taken in a low vacuum condition with an acceleration voltage of 18 kV.

### 2.2. Magnetorheology

The dynamic properties of anisotropic MRE were measured using an Anton Paar Physica MCR 501 rheometer equipped with a MRD 70/1T magnetorheological cell, and a parallel plate configuration was used. To avoid slipping between the sample and plates, one of the plates had a serrated surface (PP20/MRD/TI/P2); a normal compressive force of 5 N was applied to the sample in order to increase the contact of the sample to the rheometer plates [28]. The sample's diameter and thickness were 20 mm and 1 mm, respectively. To check the reproducibility, three samples were studied for each particle content.

The samples were subjected to torsional deformation generated by a periodic oscillatory rotation of the upper rheometer plate. A strain amplitude of 0.01% was used in the frequency sweep tests to guarantee that all tests were performed in the linear viscoelastic

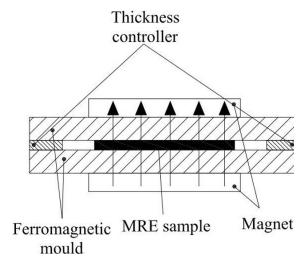


Fig. 1. Sketch of the anisotropic MRE sample vulcanisation device.

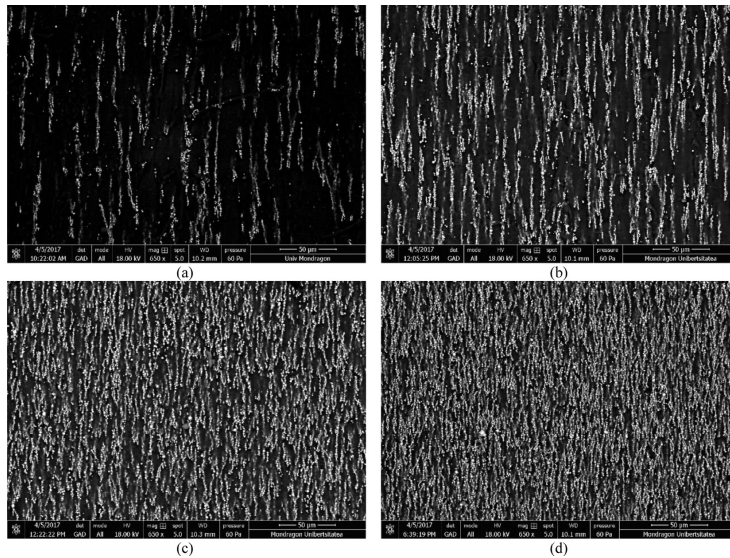


Fig. 2. SEM image of (a) 5%, (b) 10%, (c) 15%, and (d) 20% anisotropic RTV-SR MRE samples in low-vacuum conditions and with a voltage acceleration of 18 kV.

(LVE) region [29,30]. The frequency range of 0.1–40 Hz was analysed and divided into two steps: the first one from 0.1 to 10 Hz, and the second one from 10 to 40 Hz. In each step, 30 points were measured, while the acquisition time was fixed to 5 s per point. The temperature was controlled at 25 °C using the Julabo F-25 water-based heating/cooling system. Three magnetic field intensities were used: 0, 150, and 300 kA/m.

### 2.3. Vibrating sample magnetometer

The magnetostatic properties of the anisotropic MRE samples were investigated using a vibrating sample magnetometer (VSM, 4500 EG&G Princeton Applied Research). This technique consists of vibrating a sample at a frequency of 85 Hz in the direction per-

pendicular to a permanent and nearly homogeneous external magnetic field (Fig. 3). When a magnetic sample is introduced, it is magnetised and it consequently generates its own magnetic field around the sample. Periodic vibrations of the sample produce periodic variation of the magnetic field induced by the sample in the laboratory reference frame related to fixed electromagnets. According to Faraday's induction law, this change produces an electromotive force in the pick-up coils, which is measured and directly related to the sample magnetization.

All measurements were performed at room temperature in the field range of  $\pm 360$  kA/m. The aim of this characterisation was to measure the magnetic susceptibility of the sample in the direction parallel and perpendicular to the particle chains. For measurements of the longitudinal magnetic permeability, a sample with

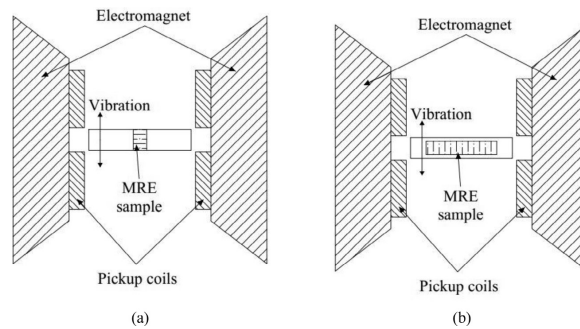


Fig. 3. VSM sketch for particles chains aligned in the (a) parallel and (b) perpendicular direction to the external magnetic field.

the chains oriented along the electromagnet axis and having a diameter of 3 mm and thickness of  $1.08 \pm 0.12$  mm was used (Fig. 3(a)). For measurements of the transverse magnetic permeability, a sample with the chains oriented perpendicularly to the electromagnet axis and having a rectangular shape with a length of  $10.48 \pm 0.82$  mm and thickness of 1 mm was used (Fig. 3(b)). These samples were held in an  $\text{Ø}3 \times 20$  mm container. One measurement was performed for each particle content.

From the VSM measurements, the longitudinal and transverse magnetic permeability of each sample was calculated for external fields from 100 to 360 kA/m.

### 3. Anisotropic MRE modelling

A four-parameter fractional derivative model was used, and the material parameters were identified using the dynamic properties measured by the rheometer. The influence of the magnetic field was introduced by using an empirical magneto-viscoelastic model [27] with the magnetic field contribution to the elastic modulus calculated using a variation of the model developed by López-López et al. [19] for magnetorheological fluids.

#### 3.1. Fractional derivative model for MRE in the absence of the magnetic field

The generalised Zener model in the frequency domain written with fractional derivatives contains four parameters,

$$G^* = \frac{G_0 + (G_0 + C)(i\omega\tau)^\alpha}{1 + (i\omega\tau)^\alpha} = G_0 + \frac{C(i\omega\tau)^\alpha}{1 + (i\omega\tau)^\alpha}, \quad (1)$$

where  $G_0$  is the static elastic modulus,  $G_\infty = G_0 + C$  is the high frequency limit value of the dynamic modulus,  $\tau$  is the relaxation time, and  $\alpha$  is the fractional parameter [11,27], whose value varies between 0 and 1.

This model is applied to MRE samples in the absence of the field. In Fig. 4, experimental dynamic properties are shown as a function of frequency, and the error does not exceed the 5%. All samples show the same behaviour – both moduli increase with frequency and particle content.

After fitting Eq. (1) to the experimental data of each sample (Fig. 4), the four parameters of the fractional derivative model were obtained (Table 1). The fitting was done using the least square method, and the minimised error was calculated for the shear complex modulus. The  $R^2$  parameter is shown in order to evaluate the accuracy of the fitting.

**Table 1**  
Fitting parameters of a four-parameter fractional derivative model for the anisotropic MRE samples and the  $R^2$  parameter.

	$G_0$ (MPa)	$C$ (MPa)	$\tau$ (s) [1 0 –7]	$\alpha$	$R^2$
0%	0.120	0.157	152.1	0.253	0.997
5%	0.121	0.198	95.23	0.229	0.971
10%	0.131	0.212	51.72	0.224	0.993
15%	0.138	0.379	5.919	0.180	0.965
20%	0.148	0.467	6.863	0.172	0.987

Fig. 4 shows the fitting and the experimental results. The fitting is accurate for all contents in the studied frequency band. However, the fitting is better for the storage modulus than for the loss modulus because the storage modulus is one order of magnitude higher than the loss modulus, and consequently, its influence on the complex modulus is larger. The larger mean relative error does not exceed 0.5% for the storage modulus and 6% for the loss modulus.

#### 3.2. Magnetic field effect

The dynamic properties of anisotropic MREs increase with magnetic field intensity (Fig. 5), and a larger increase was measured with a larger magnetic field.

In this study, we assumed that the magnetic field only modifies  $G_0$  and  $C$  parameters (Eq. (1)). Consistency of this assumption has been proved in [27]. These parameters are supposed to depend on the magnetic field density ( $H$ ) and the volumetric particle content ( $\phi$ ), as follows:

$$G_0(\phi, H) = G_0 + \Delta C(\phi, H) \quad \text{and} \quad C(\phi, H) = \Delta C(\phi, H), \quad (2)$$

where  $G_0$  and  $C$  corresponds to the fitting values of each particle content (Table 1), and  $\Delta C$  is the elastic modulus variation due to the external magnetic field. The magnetic field ( $\Delta C$ ) and the viscoelastic model were coupled as follows:

$$G^* = (G_0 + \Delta C) + \frac{(C + \Delta C)(i\omega\tau)^\alpha}{1 + (i\omega\tau)^\alpha}. \quad (3)$$

The López-López et al. model [19] was used for magnetorheological fluids in order to introduce the influence of aggregates generated when an external magnetic field was applied. This model assumes bulk-column-like aggregates in the MR sample extended along the applied magnetic field – a more stable and more realistic structure observed in experiments for both MR fluids and MRE. Moreover, the model was analysed for a magnetic field intensity

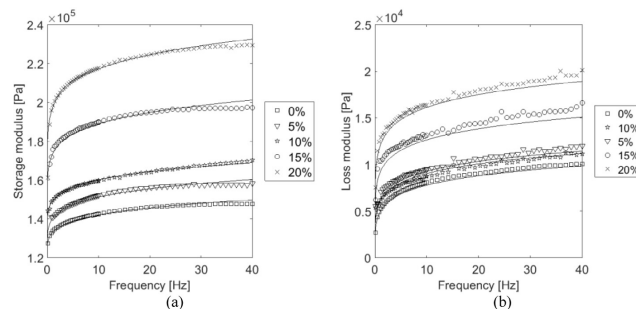


**Fig. 4.** Dynamic properties of anisotropic MRE samples as a function of frequency, (a) storage and (b) loss modulus. Experimental data are represented as points, and the lines correspond to the fitting of Eq. (1).

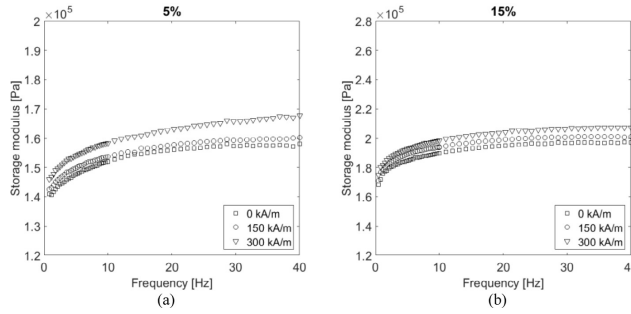


Fig. 5. Influence of the magnetic field on the MRE storage modulus for (a) 5% and (b) 15% anisotropic MRE samples as a function of frequency.

of 18.5 kA/m and a volumetric particle content of 50%. The model is based on the evaluation of the free energy of the sheared MR sample, and the shear stress  $\sigma$  is related to the applied strain  $\gamma$ , as follows:

$$\sigma = \mu_0 H^2 (\mu_{\parallel} - \mu_{\perp}) \frac{\gamma}{(1 + \gamma^2)} - \frac{1}{2} \mu_0 H^2 \left[ \frac{\partial \mu_{\parallel}}{\partial \gamma} \cdot \frac{1}{1 + \gamma^2} + \frac{\partial \mu_{\perp}}{\partial \gamma} \cdot \frac{\gamma^2}{1 + \gamma^2} \right] + \frac{1}{2} \mu_0 H^2 (\mu_{\parallel} - \mu_{\perp}) \times \frac{\gamma}{1 + \gamma^2} \quad (4)$$

where  $H$  is the magnetic field intensity within the samples, and  $\mu_{\parallel}$  and  $\mu_{\perp}$  are the longitudinal and transverse components of the magnetic permeability; the second term containing magnetic permeability derivatives appears to be negligible at strong magnetic fields used in our rheological experiments, so it is neglected. Moreover, MR fluids operate within a post-yield continuous shear or flow regime, while MREs operate in the pre-yield region [31], which means that the strain amplitudes applied to MREs are smaller. After linearization of Eq. (4), the following expression was developed,

$$\Delta C = \frac{3}{2} \mu_0 \left( \frac{H_0}{\mu_i} \right) \mu_{\parallel} - \mu_{\perp}, \quad (5)$$

where  $\Delta C$  is the increment of the zero-frequency storage modulus due to internal magnetic field,  $H = H_0 / \mu_i$ , and  $H_0$  is the applied

external magnetic field. From the magnetization measurements (Section 2.3), the influence of the magnetic field on the permeability properties was studied. The longitudinal and transverse magnetic permeability components decrease linearly with the external magnetic field (Fig. 6). The permeability is larger for high particle content and for lower magnetic fields, and the longitudinal one is larger than the transverse one owing to the lower demagnetizing effect in the sample with the aggregates oriented along the applied field. Moreover, the magnetic permeability decrease is larger for the longitudinal component and particle content. Therefore, we propose to use a linear equation (Eq. (6)) fitting for each component and particle content, which are shown in Fig. 6, and the  $R^2$  was higher than 0.963 for all the cases,

$$\begin{aligned} \mu_{\parallel}(H, \phi) &= -a_{\parallel, \phi} (H - 100) + \mu_{\parallel, \phi} \\ \mu_{\perp}(H, \phi) &= -a_{\perp, \phi} (H - 100) + \mu_{\perp, \phi} \end{aligned} \quad (6)$$

where  $a_{\parallel, \phi}$  and  $a_{\perp, \phi}$  are the slope values of permeability components for each particle content,  $\mu_{\parallel, \phi}$  and  $\mu_{\perp, \phi}$  are the permeability components at 100 kA/m for each particle content, and  $H$  is in kA/m. As an example,  $a_{\parallel, 5\%}$  corresponds to the slope of longitudinal component of the 5% sample and  $\mu_{\perp, 5\%}$  to the transverse component of the 5% sample at 100 kA/m.

From Fig. 6, the longitudinal and transverse components of magnetic permeability at 150 and 300 kA/m are substituted in Eqs. (5) and (6), and introduced in (3). As can be seen in Fig. 7, after including the modelling of magnetic permeability components, the

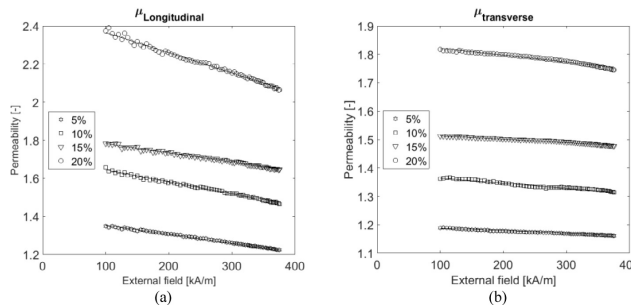


Fig. 6. (a) Longitudinal and (b) transverse components of the magnetic permeability of anisotropic MRE samples. Experimental data are represented as points, and the lines correspond to the fitting.



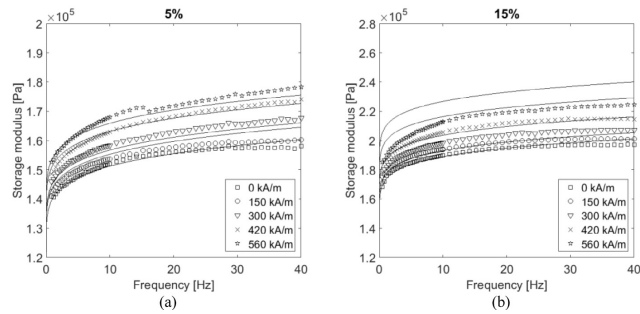


Fig. 7. Influence of magnetic field for (a) 5% and (b) 15% anisotropic MRE samples as a function of frequency for the coupling of Eqs. (3), (5), and (6). 150 and 300 kA/m curves are modelled using experimental data, and the 420 and 560 kA/m curves are the extension of the proposed model.

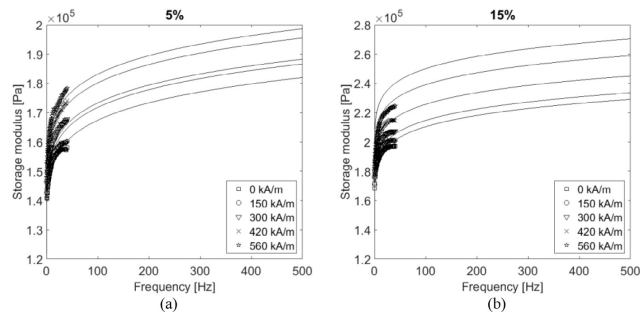


Fig. 8. Extension of the proposed new model in the frequency domain. Storage modulus of (a) 5% and (b) 15% anisotropic MRE samples.

predicted behaviour is similar – the discrepancy does not exceed 8%.

Magnetic permeability components are modelled as a function of external magnetic field, and consequently magnetic field higher than experimental ones can be predicted. In Fig. 7, we extended the model developed in this work for 420 and 560 kA/m. For low particle contents, the discrepancy is lower than 7% at high magnetic fields, while at high magnetic field and particle contents, it does not exceed 10%. Furthermore, the proposed model can also be modelled in the frequency domain, as shown in Fig. 8, which does not affect the error.

#### 4. Conclusions

In this work, a new magneto-viscoelastic model is proposed for anisotropic MREs within the lineal viscoelastic region, which can be extended in the frequency and magnetic field domain. The four-parameter fractional derivative viscoelastic model was successfully fitted to experimental data of anisotropic MREs samples in the absence of the applied field. The mean fitting errors does not exceed the 1% for the storage modulus and 6% for the loss modulus.

The viscoelastic model for anisotropic MREs was coupled with the magneto-induced modulus model (based on the López-López model). The proposed magnetic model was fed with the longitudi-

nal and transverse components of magnetic permeability of the samples.

The longitudinal and transverse components of magnetic permeability of anisotropic MREs has been measured and modelled in the magnetic field domain. The VSM measurements were performed, and experimental data were introduced for the coupled model. The model prediction was compared with rheological measurements, and the discrepancy does not exceed the 7%. Both components decrease with magnetic field, and the decreases are larger with particle content and longitudinal component. Moreover, the permeability values increase with particle content.

The new model can be extended in the magnetic field domain, in order to overcome VSM limitations (maximum magnetic field intensity of 360 kA/m). The model was extended for 420 and 560 kA/m fields, while the discrepancy is smaller than 10%.

Hence, a new magneto-viscoelastic model for anisotropic MREs is proposed by coupling a four-parameter fractional derivative model with the magnetic model, including the components of magnetic permeability. Moreover, the model can be extended in the frequency and magnetic field domain, which overcomes the experimental limitations, 40 Hz and 360 kA/m.

#### Acknowledgements

The authors gratefully acknowledge the financial support from the Department of Education of the Basque Government for the

Research Predoc Grant PRE\_2014\_1\_284 and PI-2016-1-0026 research project; and DPI 2015-71198-R research project from the Spanish Government.

#### Appendix A. Supplementary data

Supplementary data associated with this article can be found in the online version, at <http://dx.doi.org/10.1016/j.jmmm.2017.09.017>.

#### References

- [1] L.A. Makarova, Y.A. Alekhina, N.S. Perov, Peculiarities of magnetic properties of magnetoactive elastomers with hard magnetic filler in crossed magnetic fields, *J. Magn. Magn. Mater.* (2016), <http://dx.doi.org/10.1016/j.jmmm.2016.12.095>.
- [2] N.A. Yunus, S.A. Mazlan, S. Ubaidillah, F. Imaduddin Choi, S.A. Abdul Aziz, et al., Rheological properties of isotropic magnetorheological elastomers featuring an epoxidized natural rubber, *Smart Mater. Struct.* 25 (2016) 107001, <http://dx.doi.org/10.1088/0964-1726/25/10/107001>.
- [3] W. Gao, X. Wang, Steady shear characteristic and behavior of magneto-thermo-elasticity of isotropic MR elastomers, *Smart Mater. Struct.* 25 (2016) 25026, <http://dx.doi.org/10.1088/0964-1726/25/2/025026>.
- [4] I. Bica, M. Balasoiu, A.I. Kuklin, Anisotropic silicone rubber based magnetorheological elastomer with oil silicone and iron microparticles, *Solid State Phenom.* 190 (2012) 645–648, <http://dx.doi.org/10.4028/www.scientific.net/SSP.190.645>.
- [5] S. Aloui, M. Klüppel, Magneto-rheological response of elastomer composites with hybrid-magnetic fillers, *Smart Mater. Struct.* 24 (2015) 25016, <http://dx.doi.org/10.1088/0964-1726/24/2/025016>.
- [6] H.S. Jung, S.H. Kwon, H.J. Choi, J.H. Jung, Y.G. Kim, Magnetic carbonyl iron/natural rubber composite elastomer and its magnetorheology, *Compos. Struct.* 136 (2016) 106–112, <http://dx.doi.org/10.1016/j.compstruct.2015.10.008>.
- [7] Z.D. Xu, Y.X. Liao, T. Ge, C. Xu, Experimental and theoretical study of viscoelastic dampers with different matrix rubbers, *J. Eng. Mech.* 142 (2016) 4016051, [http://dx.doi.org/10.1061/\(ASCE\)EM.1943-7889.0001101](http://dx.doi.org/10.1061/(ASCE)EM.1943-7889.0001101).
- [8] L. Chen, S. Jerrams, A rheological model of the dynamic behaviour of magnetorheological elastomers, *J. Appl. Phys.* 13513 (2011) 1–9, <http://dx.doi.org/10.1063/1.3603052>.
- [9] M. Behrooz, X. Wang, F. Gordaninejad, Modeling of a new semi-active/passive magnetorheological elastomer isolator, *Smart Mater. Struct.* 23 (2014) 45013, <http://dx.doi.org/10.1088/0964-1726/23/4/045013>.
- [10] G. Zhu, Y. Xiong, S. Daley, R. Shenoi, Magnetorheological elastomer materials and structures with vibration energy control for marine application, in: *Anal. Des. Mar. Struct.*, V. CRC Press, 2015, pp. 197–204, <http://dx.doi.org/10.1201/b18179-27>.
- [11] T. Pritz, Analysis of four-parameter fractional derivative model of real solid materials, *J. Sound Vib.* 195 (1996) 103–115, <http://dx.doi.org/10.1006/jsvi.1996.0406>.
- [12] I. Agirre-Olabide, M.J. Elejabarrieta, Maximum attenuation variability of isotropic magnetosensitive elastomers, *Polym. Test.* 54 (2016) 104–113, <http://dx.doi.org/10.1016/j.polymertesting.2016.06.021>.
- [13] F. Guo, C.-b. Du, R.-p. Li, Viscoelastic parameter model of magnetorheological elastomers based on Abel Dashpot, *Adv Mech. Eng.* 6 (2015), <http://dx.doi.org/10.1155/2014/629386>, 629386–629386.
- [14] J. Zhu, Z. Xu, Y. Guo, Experimental and modeling study on magnetorheological elastomers with different matrices, *J. Mater. Civ. Eng.* 25 (2013) 1762–1771, [http://dx.doi.org/10.1061/\(ASCE\)MT.1943-5533.0000727](http://dx.doi.org/10.1061/(ASCE)MT.1943-5533.0000727).
- [15] M.R. Jolly, J.D. Carlson, B.C. Muñoz, T.A. Bullions, The magnetoviscoelastic response of elastomer composites consisting of ferrous particles embedded in a polymer matrix, *J. Intell. Mater. Syst. Struct.* 4 (1996) 613–622, <http://dx.doi.org/10.1177/1045389X9600700601>.
- [16] M.R. Jolly, J.D. Carlson, B.C. Muñoz, A model of the behaviour of magnetorheological materials, *Smart Mater. Struct.* 5 (1999) 607–614, <http://dx.doi.org/10.1088/0964-1726/5/5/009>.
- [17] L.C. Davis, Model of magnetorheological elastomers, *J. Appl. Phys.* 85 (1999) 3348–3351, <http://dx.doi.org/10.1063/1.369682>.
- [18] Y. Shen, M.F. Golnaraghi, G.R. Heppler, Experimental research and modeling of magnetorheological elastomers, *J. Intell. Mater. Syst. Struct.* 15 (2004) 27–35, <http://dx.doi.org/10.1177/1045389X04039264>.
- [19] M.T. López-López, P. Kuzhir, J. Caballero-Hernández, L. Rodríguez-Arco, J.D.G. Duran, G. Bossis, Yield stress in magnetorheological suspensions near the limit of maximum-packing fraction, *J. Rheol.* 56 (2012) 1209, <http://dx.doi.org/10.1122/1.4731659>.
- [20] D. Leng, L. Sun, J. Sun, Y. Lin, Derivation of stiffness matrix in constitutive modeling of magnetorheological elastomer, *J. Phys. Conf. Ser.* 412 (2013) 12028, <http://dx.doi.org/10.1088/1742-6596/412/1/012028>.
- [21] X. Dong, N. Ma, J. Ou, M. Qi, Predicting magnetorheological effect of magnetorheological elastomers under normal pressure, *J. Phys. Conf. Ser.* 412 (2013) 12035, <http://dx.doi.org/10.1088/1742-6596/412/1/012035>.
- [22] L. Chen, X.L. Gong, W.H. Li, Microstructures and viscoelastic properties of anisotropic magnetorheological elastomers, *Smart Mater. Struct.* 16 (2007) 2645–2650, <http://dx.doi.org/10.1088/0964-1726/16/6/069>.
- [23] J. de Vicente, G. Bossis, S. Laci, M. Guyot, Permeability measurements in cobalt ferrite and carbonyl iron powders and suspensions, *J. Magn. Magn. Mater.* 251 (2002) 100–108, [http://dx.doi.org/10.1016/S0304-8853\(02\)00484-5](http://dx.doi.org/10.1016/S0304-8853(02)00484-5).
- [24] F.S. Bellucci, F.C. Lobato de Almeida, M.A. Lima Nobre, M.A. Rodríguez-Pérez, A. T. Paschoalini, A.E. Job, Magnetic properties of vulcanized natural rubber nanocomposites as a function of the concentration, size and shape of the magnetic fillers, *Compos. Part B Eng.* 85 (2016) 196–206, <http://dx.doi.org/10.1016/j.compositesb.2015.09.013>.
- [25] G. Schubert, P. Harrison, Magnetic induction measurements and identification of the permeability of magneto-rheological elastomers using finite element simulations, *J. Magn. Magn. Mater.* 404 (2016) 205–214, <http://dx.doi.org/10.1016/j.jmmm.2015.12.003>.
- [26] W.H. Li, Y. Zhou, T.F. Tian, Viscoelastic properties of MR elastomers under harmonic loading, *Rheol. Acta* 49 (2010) 733–740, <http://dx.doi.org/10.1007/s00397-010-0446-9>.
- [27] I. Agirre-Olabide, A. Lion, M.J. Elejabarrieta, A new three-dimensional magneto-viscoelastic model for isotropic magnetorheological elastomers, *Smart Mater. Struct.* 26 (2017) 35021, <http://dx.doi.org/10.1088/1361-665X/26/3/035021>.
- [28] X. Dong, N. Ma, M. Qi, J. Li, R. Chen, J. Ou, The pressure-dependent MR effect of magnetorheological elastomers, *Smart Mater. Struct.* 21 (2012) 75014, <http://dx.doi.org/10.1088/0964-1726/21/7/075014>.
- [29] I. Agirre-Olabide, J. Berasategui, M.J. Elejabarrieta, M.M. Bou-Ali, Characterization of the linear viscoelastic region of magnetorheological elastomers, *J. Intell. Mater. Syst. Struct.* 25 (2014) 2074–2081, <http://dx.doi.org/10.1177/1045389X13517310>.
- [30] I. Agirre-Olabide, M.J. Elejabarrieta, M.M. Bou-Ali, Matrix dependence of the linear viscoelastic region in magnetorheological elastomers, *J. Intell. Mater. Syst. Struct.* 26 (2015) 1880–1886, <http://dx.doi.org/10.1177/1045389X15580658>.
- [31] J.D. Carlson, M.R. Jolly, MR fluid, foam and elastomer devices, *Mechatronics* 10 (2000) 555–569, [http://dx.doi.org/10.1016/S0957-4158\(99\)00064-1](http://dx.doi.org/10.1016/S0957-4158(99)00064-1).

*Sometimes you will never know the value of a moment until it  
becomes a memory*

Theodor Seuss Geisel

# 5

## Conclusions and future work

In this chapter the outcomes of the project are summarized and proposals for further work are given.

## 5.1 Conclusions

The main goal of the present thesis has been to analyse the magneto-thermo-dynamic behaviour of magnetorheological elastomers. The most relevant conclusions obtained to the objectives listed in this thesis are:

- **Implement an experimental shear procedure to analyse the shear magneto-thermo-dynamic properties of isotropic and anisotropic MREs within the linear viscoelastic region**

A new standard procedure to determine the LVE region of MREs was defined, which included the analysis of storage modulus and loss factor. Besides, with that procedure, the influence of synthesis (matrix, particle content and pre-structure) and characterisation parameters (frequency, temperature and magnetic field) in the shear LVE region was studied. From the storage modulus and loss factor analysis, it was observed that the most restrictive dynamic property to define the LVE region was the loss factor.

The matrix is a key synthesis parameter to determine the LVE limit of the MRE. The softer the matrix, the larger the LVE region of the MRE. Moreover, the LVE region is reduced with the increment of particle content.

Characterisation variables also determined the LVE region of MREs. Frequency increased the LVE region of the MREs in all the analysed working conditions. Furthermore, the magnetic field and the temperature influence depended on the matrix.

The shear magneto-viscoelastic properties of the synthesised MREs were obtained in the LVE region. The storage and loss modulus increased with frequency, while decreased with temperature; this is a typical behaviour of viscoelastic material within the rubbery region.

The storage and loss modulus increased with the particle content for all the studied matrices in shear mode. However, the influence on each matrix was differ-

ent. At high particle content levels, the influence of temperature in storage modulus was larger than that of frequency. On the other hand, the loss factor of the studied samples was more sensitive to frequency than to temperature.

The MR effect was dependent on the viscoelastic nature of the matrix. Larger MR effects occurs when the matrix was softer. In this thesis, RTV-SR was the softer matrix, and it showed maximum storage and loss modulus MR effect. Therefore, the influence of particle content and external magnetic field in the storage and loss modulus were completely dependent on the matrix.

To maximise the storage and loss modulus MR effect, anisotropic MREs were synthesised with the softer matrix (RTV-SR). Anisotropic samples showed a larger shear storage and loss modulus than isotropic ones. Both were increased when a magnetic field was applied owing to larger particle-particle interaction forces, 30% MR effect and 21% loss modulus MR effect.

**► Develop an experimental compression technique to analyse the compression magneto-viscoelastic properties of isotropic MREs within the linear viscoelastic region**

A new magneto-dynamic compression technique was developed to characterise MREs at high frequencies. To the best of the author's knowledge, it is the first time the LVE region was determined in compression mode for MREs. This dissertation has analysed the influence of synthesis and characterisation variables on the LVE region, and compression magneto-viscoelastic properties from 50 to 200 Hz were characterised within the LVE region.

Using strain sweep tests, the linear viscoelastic region was determined for isotropic MREs in compression mode. The LVE region was defined by the storage modulus when the discrepancy was larger than 10%. The LVE region increased with frequency and decreased with particle content. Hence, it was determined by the 30% sample at 50 Hz. However, the LVE region in compression mode was larger than in shear mode.

Magneto-viscoelastic properties were analysed using frequency sweep tests. The storage modulus and the loss factor increased with particle content and frequency. The largest storage modulus increase of 75% occurred with the particle

content, while an increment of 16% was generated with frequency. The damping of MREs was also increased with particle content.

The variation of the storage modulus due to magnetic field increased with particle content and magnetic field up to 8%. The MR effect was larger in compression mode than in shear mode.

► **Develop two magneto-viscoelastic models to predict the shear magneto-viscoelastic behaviour of isotropic and anisotropic MREs in a wide range of working conditions**

The shear four-parameter fractional derivative viscoelastic model was successfully fitted to experimental data of isotropic and anisotropic MREs samples in the absence of the applied magnetic field. The mean fitting errors did not exceed the 1% for the storage modulus and 6% for the loss modulus.

In order to model the influence of temperature in the dynamic properties, the Arrhenius model was coupled with a four-parameter fractional derivative model. This model was extended in the frequency domain to determine the maximum attenuation of isotropic MREs.

For each particle content and magnetic field, the value of maximum attenuation was unique and occurs at a certain frequency and temperature. The attenuation was larger with increased particle content over the entire frequency band, and the frequency at which the maximum occurs was increased.

The shapes of the loss factor curves were not influenced by temperature, while they were dependent on frequency. The maximum attenuation frequency was reduced with increased temperature and particle content. The maximum attenuation temperature was increased with increased frequency and particle content; this occurred to a greater degree at low frequencies.

With the application of an external magnetic field, the shear maximum attenuation value and frequency were increased, and the loss factor was larger in the studied frequency domain.

The fitting of the particle-matrix and fractional derivative coupled model was successful, although the fitting error was larger for the loss modulus because the influence of the storage modulus in the dynamic complex modulus was larger. In

addition, the maximum error for the storage modulus did not exceed 4%, and the loss modulus 13%.

The magneto-induced modulus model of isotropic samples was developed considering anisotropic samples and applying a correction factor to introduce the isotropy. A new three-dimensional magneto-viscoelastic model was developed for isotropic MREs, and the consistency of the model was proved. The proposed magneto-viscoelastic model for isotropic MREs was fitted to experimental data, and the storage modulus error was less than 4%, which shows that the proposed model was valid.

The viscoelastic model for anisotropic MREs was coupled with the magneto-induced modulus model based on the López-López model. The proposed magnetic model was fed with the longitudinal and transverse components of magnetic permeability of the samples.

The longitudinal and transverse components of magnetic permeability of anisotropic MREs were measured and modelled in the magnetic field domain. The VSM measurements were performed, and experimental data were introduced for the coupled model. The developed new shear model for anisotropic MREs can be extended in the magnetic field domain, in order to overcome VSM limitations (maximum magnetic field intensity of 360 kA/m). The model prediction was compared with rheological measurements, and the discrepancy does not exceed the 7%.

## 5.2 Future work

In the presented dissertation the magneto-viscoelastic behaviour of MREs was analysed in shear and compression modes, while new interesting issues and starting points for new research paths are created.

The shear magneto-viscoelastic properties were characterised in the linear viscoelastic region, and the influence of synthesis and characterisation variables in the LVE region and in the magneto-viscoelastic properties were analysed. It would be therefore of great interest to study the influence of temperature in the magneto-viscoelasticity of anisotropic MREs, which seems that it would increase the MR

effect of the samples.

According to compression magneto-dynamic test, the first step was fixed. A high frequency test was designed and a standard procedure was defined to determine the compression magneto-viscoelastic properties of MREs at high frequencies. However, the magnetic field obtained with the electromagnet is not as high as in the literature. It is therefore interesting to redesign the electromagnet or research in a new system to generate a larger magnetic field, up to 300 mT.

The compression magneto-viscoelastic properties were analysed for a NR matrix and isotropic samples. Nevertheless, it would be of interest to study the influence of synthesis (matrix, more particle contents and pre-structure) in the LVE region. Furthermore, the analysis of the magneto-viscoelastic properties of anisotropic MREs in compression mode at high frequencies would be interesting.

Once isotropic and anisotropic MREs are characterised in similar shear and compression characterisation conditions, it would be interesting to determine the Poisson coefficient, and analyse the evolution of the Poisson coefficient as a function of matrix, particle content, pre-structure, frequency and external magnetic field.

The magneto-viscoelastic behaviour of isotropic MREs was successfully fitted to experimental data, while for anisotropic MREs the model developed does not take into account the influence of particle content in the viscoelastic properties. Hence, a new path would be to introduce the influence of particle content in each of the parameter of the viscoelastic model.

Finally, the maximum attenuation of isotropic MREs was determined extending the FD model in the frequency and temperature domain. Therefore, would be interesting to extent the this analysis to anisotropic MREs.



## References

- Agirre-Olabide, I. and Elejabarrieta, M. J. 2016. Maximum attenuation variability of isotropic magnetosensitive elastomers. *Polymer Testing*, 54:104–113. doi: 10.1016/j.polymertesting.2016.06.021.
- Agirre-Olabide, I. and Elejabarrieta, M. J. 2017. Effect of synthesis variables on viscoelastic properties of elastomers filled with carbonyl iron powder. *Journal of Polymer Research*, 24(9):139. doi: 10.1007/s10965-017-1299-z.
- Agirre-Olabide, I., Berasategui, J., Elejabarrieta, M. J., and Bou-Ali, M. M. 2014. Characterization of the linear viscoelastic region of magnetorheological elastomers. *Journal of Intelligent Material Systems and Structures*, 25(16):2074–2081. doi: 10.1177/1045389X13517310.
- Agirre-Olabide, I., Elejabarrieta, M. J., and Bou-Ali, M. M. 2015. Matrix dependence of the linear viscoelastic region in magnetorheological elastomers. *Journal of Intelligent Material Systems and Structures*, 26(14):1880–1886. doi: 10.1177/1045389X15580658.
- Agirre-Olabide, I., Lion, A., and Elejabarrieta, M. J. 2017. A new three-dimensional magneto-viscoelastic model for isotropic magnetorheological elastomers. *Smart Materials and Structures*, 26(3):035021. doi: 10.1088/1361-665X/26/3/035021.
- Agirre-Olabide, I., Kuzhir, P., and Elejabarrieta, M. J. 2018. Linear magneto-viscoelastic model based on magnetic permeability components for anisotropic magnetorheological elastomers. *Journal of Magnetism and Magnetic Materials*, 446:155–161. doi: 10.1016/j.jmmm.2017.09.017.

- Airey, G. D. and Rahimzadeh, B. 2004. Combined bituminous binder and mixture linear rheological properties. *Construction and Building Materials*, 18(7):535–548. doi: 10.1016/j.conbuildmat.2004.04.008.
- Aloui, S. and Klüppel, M. 2015. Magneto-rheological response of elastomer composites with hybrid-magnetic fillers. *Smart Materials and Structures*, 24(2):025016. doi: 10.1088/0964-1726/24/2/025016.
- Arenz, R. 1998. Nonlinear Shear Behavior of Poly(vinyl acetate) Material. *Mechanics of Time-Dependent Materials*, 2(4):287–305. doi: 10.1023/A:1009827310712.
- Behrooz, M., Wang, X., and Gordaninejad, F. 2014. Modeling of a new semi-active/passive magnetorheological elastomer isolator. *Smart Materials and Structures*, 23(4):045013. doi: 10.1088/0964-1726/23/4/045013.
- Bellan, C. and Bossis, G. 2002. Field dependence of viscoelastic properties of MR elastomers. In *Electrorheological Fluids and Magnetorheological Suspensions*, pages 507–513. WORLD SCIENTIFIC. doi: 10.1142/9789812777546\_0075.
- Bellucci, F. S., Lobato de Almeida, F. C., Lima Nobre, M. A., Rodríguez-Pérez, M. A., Paschoalini, A. T., and Job, A. E. 2016. Magnetic properties of vulcanized natural rubber nanocomposites as a function of the concentration, size and shape of the magnetic fillers. *Composites Part B: Engineering*, 85:196–206. doi: 10.1016/j.compositesb.2015.09.013.
- Blom, P. and Kari, L. 2005. Amplitude and frequency dependence of magneto-sensitive rubber in a wide frequency range. *Polymer Testing*, 24(5):656–662. doi: 10.1016/j.polymertesting.2005.04.001.
- Bonhome-Espinosa, A. B., Campos, F., Rodriguez, I. A., Carriel, V., Marins, J. A., Zubarev, A., Duran, J. D. G., and Lopez-Lopez, M. T. 2017. Effect of particle concentration on the microstructural and macromechanical properties of biocompatible magnetic hydrogels. *Soft Matter*, 13(16):2928–2941. doi: 10.1039/C7SM00388A.

- Carlson, J. and Jolly, M. R. 2000. MR fluid, foam and elastomer devices. *Mechanics*, 10(4-5):555–569. doi: 10.1016/S0957-4158(99)00064-1.
- Chen, L. and Jerrams, S. 2011. A rheological model of the dynamic behavior of magnetorheological elastomers. *Journal of Applied Physics*, 110(1):013513. doi: 10.1063/1.3603052.
- Chen, L., Gong, X.-l., Jiang, W.-q., Yao, J.-j., Deng, H.-x., and Li, W.-h. 2007a. Investigation on magnetorheological elastomers based on natural rubber. *Journal of Materials Science*, 42(14):5483–5489. doi: 10.1007/s10853-006-0975-x.
- Chen, L., Gong, X. L., and Li, W. H. 2007b. Microstructures and viscoelastic properties of anisotropic magnetorheological elastomers. *Smart Materials and Structures*, 16(6):2645–2650. doi: 10.1088/0964-1726/16/6/069.
- Chen, L., Gong, X., and Li, W. 2008a. Effect of carbon black on the mechanical performances of magnetorheological elastomers. *Polymer Testing*, 27(3):340–345. doi: 10.1016/j.polymertesting.2007.12.003.
- Chen, L., Gong, X.-l., and Li, W.-h. 2008b. Damping of Magnetorheological Elastomers. *Chinese Journal of Chemical Physics*, 21(6):581–585. doi: 10.1088/1674-0068/21/06/581-585.
- Coquelle, E., Bossis, G., Szabo, D., and Giulieri, F. 2006. Micromechanical analysis of an elastomer filled with particles organized in chain-like structure. *Journal of Materials Science*, 41(18):5941–5953. doi: 10.1007/s10853-006-0329-8.
- Danas, K., Kankanala, S., and Triantafyllidis, N. 2012. Experiments and modeling of iron-particle-filled magnetorheological elastomers. *Journal of the Mechanics and Physics of Solids*, 60(1):120–138. doi: 10.1016/j.jmps.2011.09.006.
- Davis, L. C. 1999. Model of magnetorheological elastomers. *Journal of Applied Physics*, 85(6):3348–3351. doi: 10.1063/1.369682.
- de Vicente, J., Bossis, G., Lacis, S., and Guyot, M. 2002. Permeability measurements in cobalt ferrite and carbonyl iron powders and suspensions. *Journal of Magnetism and Magnetic Materials*, 251(1):100–108. doi: 10.1016/S0304-8853(02)00484-5.

- Dong, X., Ma, N., Qi, M., Li, J., Chen, R., and Ou, J. 2012. The pressure-dependent MR effect of magnetorheological elastomers. *Smart Materials and Structures*, 21(7):075014. doi: 10.1088/0964-1726/21/7/075014.
- Dong, X., Ma, N., Ou, J., and Qi, M. 2013. Predicating magnetorheological effect of magnetorheological elastomers under normal pressure. *Journal of Physics: Conference Series*, 412:012035. doi: 10.1088/1742-6596/412/1/012035.
- Eem, S.-H., Jung, H.-J., and Koo, J.-H. 2012. Modeling of Magneto-Rheological Elastomers for Harmonic Shear Deformation. *IEEE Transactions on Magnetics*, 48(11):3080–3083. doi: 10.1109/TMAG.2012.2205140.
- Fan, Y., Gong, X., Xuan, S., Zhang, W., Zheng, J., and Jiang, W. 2011. Interfacial friction damping properties in magnetorheological elastomers. *Smart Materials and Structures*, 20(3):035007. doi: 10.1088/0964-1726/20/3/035007.
- Feng, J., Xuan, S., Liu, T., Ge, L., Yan, L., Zhou, H., and Gong, X. 2015. The prestress-dependent mechanical response of magnetorheological elastomers. *Smart Materials and Structures*, 24(8):085032. doi: 10.1088/0964-1726/24/8/085032.
- Ferry, J. D. 1980. *Viscoelastic Properties of Polymers*. Wiley, New York, 3 edition.
- Fragiadakis, D. and Pissis, P. 2007. Glass transition and segmental dynamics in poly(dimethylsiloxane)/silica nanocomposites studied by various techniques. *Journal of Non-Crystalline Solids*, 353(47-51):4344–4352. doi: 10.1016/j.jnoncrysol.2007.05.183.
- Gao, W. and Wang, X. 2016. Steady shear characteristic and behavior of magneto-thermo-elasticity of isotropic MR elastomers. *Smart Materials and Structures*, 25(2):025026. doi: 10.1088/0964-1726/25/2/025026.
- Ge, L., Gong, X., Fan, Y., and Xuan, S. 2013. Preparation and mechanical properties of the magnetorheological elastomer based on natural rubber/rosin glycerin hybrid matrix. *Smart Materials and Structures*, 22(11):115029. doi: 10.1088/0964-1726/22/11/115029.

- Ginder, J. M., Clark, S. M., Schlotter, W., and Nichols, M. 2002. Magnetostrictive phenomena in magnetorheological elastomers. *International Journal of Modern Physics B*, 16(17n18):2412–2418. doi: 10.1142/S021797920201244X.
- Gordaninejad, F., Wang, X., and Mysore, P. 2012. Behavior of thick magnetorheological elastomers. *Journal of Intelligent Material Systems and Structures*, 23(9): 1033–1039. doi: 10.1177/1045389X12448286.
- Guo, F., Du, C.-b., and Li, R.-p. 2014. Viscoelastic Parameter Model of Magnetorheological Elastomers Based on Abel Dashpot. *Advances in Mechanical Engineering*, 6:629386. doi: 10.1155/2014/629386.
- Guth, E. 1945. Theory of filler reinforcement. *Journal of Applied Physics*, 16(1): 20–25. doi: 10.1063/1.1707495.
- Guth, E. and Gold, O. 1938. On the hydrodynamical theory of the viscosity of suspensions. *Physical Review*, 53:322.
- Han, Y., Zhang, Z., Faidley, L. E., and Hong, W. 2012. Microstructure-based modeling of magneto-rheological elastomers. In Goulbourne, N. C. and Ounaies, Z., editors, *Proc. SPIE 8342, Behavior and Mechanics of Multifunctional Materials and Composites*, volume 8342, page 83421B. doi: 10.1117/12.925492.
- Haupt, P. 2002. *Continuum Mechanics and Theory of Materials*. Advanced Texts in Physics. Springer Berlin Heidelberg, Berlin, Heidelberg, 2 edition. doi: 10.1007/978-3-662-04775-0.
- Hiptmair, F., Major, Z., Haßlacher, R., and Hild, S. 2015. Design and application of permanent magnet flux sources for mechanical testing of magnetoactive elastomers at variable field directions. *Review of Scientific Instruments*, 86(8): 085107. doi: 10.1063/1.4927714.
- Hu, Y., Wang, Y., Gong, X., Gong, X., Zhang, X., Jiang, W., Zhang, P., and Chen, Z. 2005. New magnetorheological elastomers based on polyurethane/Si-rubber hybrid. *Polymer Testing*, 24(3):324–329. doi: 10.1016/j.polymertesting.2004.11.003.

- Ivaneyko, D., Toshchevnikov, V. P., Saphiannikova, M., and Heinrich, G. 2011. Magneto-sensitive Elastomers in a Homogeneous Magnetic Field: A Regular Rectangular Lattice Model. *Macromolecular Theory and Simulations*, 20(6): 411–424. doi: 10.1002/mats.201100018.
- Ivaneyko, D., Toshchevnikov, V. P., Saphiannikova, M., and Heinrich, G. 2012. Effects of particle distribution on mechanical properties of magneto-sensitive elastomers in a homogeneous magnetic field. *Condensed Matter Physics*, 15(3): 33601. doi: 10.5488/CMP.15.33601.
- Jolly, M. R., Carlson, J. D., and Muñoz, B. C. 1996a. A model of the behaviour of magnetorheological materials. *Smart Materials and Structures*, 5(5):607–614. doi: 10.1088/0964-1726/5/5/009.
- Jolly, M. R., Carlson, J. D., Muñoz, B. C., and Bullions, T. A. 1996b. The Magneto-viscoelastic Response of Elastomer Composites Consisting of Ferrous Particles Embedded in a Polymer Matrix. *Journal of Intelligent Material Systems and Structures*, 7(6):613–622. doi: 10.1177/1045389X9600700601.
- Jones, D. I. G. 2001. *Handbook of viscoelastic vibration damping*. John Wiley & Sons Ltd, Chichester.
- Ju, B., Tang, R., Zhang, D., Yang, B., Yu, M., and Liao, C. 2015. Temperature-dependent dynamic mechanical properties of magnetorheological elastomers under magnetic field. *Journal of Magnetism and Magnetic Materials*, 374:283–288. doi: 10.1016/j.jmmm.2014.08.012.
- Ju, B. X., Yu, M., Fu, J., Yang, Q., Liu, X. Q., and Zheng, X. 2012. A novel porous magnetorheological elastomer: preparation and evaluation. *Smart Materials and Structures*, 21(3):035001. doi: 10.1088/0964-1726/21/3/035001.
- Jung, H. S., Kwon, S. H., Choi, H. J., Jung, J. H., and Kim, Y. G. 2016. Magnetic carbonyl iron/natural rubber composite elastomer and its magnetorheology. *Composite Structures*, 136:106–112. doi: 10.1016/j.compstruct.2015.10.008.
- Kallio, M., Lindroos, T., Aalto, S., Järvinen, E., Kärnä, T., and Meinander, T. 2007. Dynamic compression testing of a tunable spring element consisting of a mag-

- netorheological elastomer. *Smart Materials and Structures*, 16(2):506–514. doi: 10.1088/0964-1726/16/2/032.
- Kari, L. and Blom, P. 2005. Magneto-sensitive rubber in a noise reduction context – exploring the potential. *Plastics, Rubber and Composites*, 34(8):365–371. doi: 10.1179/174328905X59692.
- Kavlicoglu, B., Wallis, B., Sahin, H., and Liu, Y. 2011. Magnetorheological elastomer mount for shock and vibration isolation. In Ghasemi-Nejhad, M. N., editor, *Proc. SPIE 7977, Active and Passive Smart Structures and Integrated Systems*, volume 7977, page 79770Y. doi: 10.1117/12.881870.
- Kelly, P. 2013. *Solid Mechanics Lecture Notes*. The University of Auckland 2013, Auckland.
- Khimi, S. R. and Pickering, K. 2015. Comparison of dynamic properties of magnetorheological elastomers with existing antivibration rubbers. *Composites Part B: Engineering*, 83:175–183. doi: 10.1016/j.compositesb.2015.08.033.
- Komatsuzaki, T., Inoue, T., and Iwata, Y. 2016. Experimental Investigation of an Adaptively Tuned Dynamic Absorber Incorporating Magnetorheological Elastomer with Self-Sensing Property. *Experimental Mechanics*, 56(5):871–880. doi: 10.1007/s11340-016-0137-2.
- Ladipo, I. L., Fadly, J., and Faris, W. F. 2016. Characterization of Magnetorheological Elastomer (MRE) Engine Mounts. *Materials Today: Proceedings*, 3(2): 411–418. doi: 10.1016/j.matpr.2016.01.029.
- Lakes, R. 2009. *Viscoelastic Materials*. Cambridge University Press, Cambridge. doi: 10.1017/CBO9780511626722.
- Leblanc, J. L. 2012. Effect of temperature on dynamic rheological properties of uncured rubber materials in both the linear and the nonlinear viscoelastic domains. *Journal of Applied Polymer Science*, 126(2):408–422. doi: 10.1002/app.37006.
- Lejon, J. and Kari, L. 2013. Measurements on the Temperature, Dynamic Strain Amplitude and Magnetic Field Strength Dependence of the Dynamic Shear

- Modulus of Magneto-sensitive Elastomers in a Wide Frequency Range. *Journal of Vibration and Acoustics*, 135(6):064506. doi: 10.1115/1.4025063.
- Leng, D., Sun, L., Sun, J., and Lin, Y. 2013. Derivation of stiffness matrix in constitutive modeling of magnetorheological elastomer. *Journal of Physics: Conference Series*, 412:012028. doi: 10.1088/1742-6596/412/1/012028.
- Lerner, A. A. and Cunefare, K. 2008. Performance of MRE-based Vibration Absorbers. *Journal of Intelligent Material Systems and Structures*, 19(5):551–563. doi: 10.1177/1045389X07077850.
- Li, R. and Sun, L. Z. 2013. Viscoelastic Responses of Silicone-Rubber-Based Magnetorheological Elastomers Under Compressive and Shear Loadings. *Journal of Engineering Materials and Technology*, 135(2):021008. doi: 10.1115/1.4023839.
- Li, W., Zhang, X., and Du, H. 2012. Development and simulation evaluation of a magnetorheological elastomer isolator for seat vibration control. *Journal of Intelligent Material Systems and Structures*, 23(9):1041–1048. doi: 10.1177/1045389X11435431.
- Li, W. H. and Nakano, M. 2013. Fabrication and characterization of PDMS based magnetorheological elastomers. *Smart Materials and Structures*, 22(5):055035. doi: 10.1088/0964-1726/22/5/055035.
- Li, W. H., Zhou, Y., and Tian, T. F. 2010. Viscoelastic properties of MR elastomers under harmonic loading. *Rheologica Acta*, 49(7):733–740. doi: 10.1007/s00397-010-0446-9.
- Liao, G., Gong, X., and Xuan, S. 2013. Magnetic Field-Induced Compressive Property of Magnetorheological Elastomer under High Strain Rate. *Industrial & Engineering Chemistry Research*, 52(25):8445–8453. doi: 10.1021/ie400864d.
- Liao, G. J., Gong, X.-L., Xuan, S. H., Kang, C. J., and Zong, L. H. 2012. Development of a real-time tunable stiffness and damping vibration isolator based on magnetorheological elastomer. *Journal of Intelligent Material Systems and Structures*, 23(1):25–33. doi: 10.1177/1045389X11429853.



- Lokander, M. and Stenberg, B. 2003a. Performance of isotropic magnetorheological rubber materials. *Polymer Testing*, 22(3):245–251. doi: 10.1016/S0142-9418(02)00043-0.
- Lokander, M. and Stenberg, B. 2003b. Improving the magnetorheological effect in isotropic magnetorheological rubber materials. *Polymer Testing*, 22(6):677–680. doi: 10.1016/S0142-9418(02)00175-7.
- López-López, M. T., Kuzhir, P., Caballero-Hernández, J., Rodríguez-Arco, L., Duran, J. D. G., and Bossis, G. 2012. Yield stress in magnetorheological suspensions near the limit of maximum-packing fraction. *Journal of Rheology*, 56(5): 1209. doi: 10.1122/1.4731659.
- Lu, X., Qiao, X., Watanabe, H., Gong, X., Yang, T., Li, W., Sun, K., Li, M., Yang, K., Xie, H., Yin, Q., Wang, D., and Chen, X. 2012. Mechanical and structural investigation of isotropic and anisotropic thermoplastic magnetorheological elastomer composites based on poly(styrene-*b*-ethylene-co-butylene-*b*-styrene) (SEBS). *Rheologica Acta*, 51(1):37–50. doi: 10.1007/s00397-011-0582-x.
- Moreira, R. A. S., Corte-Real, J. D., and Rodrigues, J. D. 2010. A generalized frequency-temperature viscoelastic model. *Shock and Vibration*, 17(4-5):407–418. doi: 10.3233/SAV-2010-0536.
- Mullins, L. and Tobin, N. R. 1966. Stress Softening in Rubber Vulcanizates. Part I. Use of a Strain Amplification Factor to Describe Elastic Behavior of Filler-Reinforced Vulcanized Rubber. *Rubber Chemistry and Technology*, 39(4):799–813. doi: 10.5254/1.3547144.
- Nashif, A. D., Jones, D. I. G., and Henderson, J. P. 1985. *Vibration damping*. John Wiley & Sons, New York.
- Norouzi, M., Sajjadi Alehashem, S. M., Vatandoost, H., Ni, Y. Q., and Shahmardan, M. M. 2016. A new approach for modeling of magnetorheological elastomers. *Journal of Intelligent Material Systems and Structures*, 27(8):1121–1135. doi: 10.1177/1045389X15615966.

- Payne, A. R. 1962. The dynamic properties of carbon black-loaded natural rubber vulcanizates. Part I. *Journal of Applied Polymer Science*, 6(19):57–63. doi: 10.1002/app.1962.070061906.
- Phewthongin, N., Saeoui, P., and Sirisinha, C. 2006. Rheological behavior of CPE/NR blends filled with precipitated silica. *Journal of Applied Polymer Science*, 100(4):2565–2571. doi: 10.1002/app.22550.
- Pickering, K., Raa Khimi, S., and Ilanko, S. 2015. The effect of silane coupling agent on iron sand for use in magnetorheological elastomers Part 1: Surface chemical modification and characterization. *Composites Part A: Applied Science and Manufacturing*, 68:377–386. doi: 10.1016/j.compositesa.2014.10.005.
- Poojary, U. R. and Gangadharan, K. V. 2017. Magnetic field and frequency dependent LVE limit characterization of magnetorheological elastomer. *Journal of the Brazilian Society of Mechanical Sciences and Engineering*, 39(4):1365–1373. doi: 10.1007/s40430-016-0592-9.
- Pritz, T. 1996. Analysis of four-parameter fractional derivative model of real solid materials. *Journal of Sound and Vibration*, 195(1):103–115. doi: 10.1006/jsvi.1996.0406.
- Qiao, X., Lu, X., Li, W., Chen, J., Gong, X., Yang, T., Li, W., Sun, K., and Chen, X. 2012. Microstructure and magnetorheological properties of the thermoplastic magnetorheological elastomer composites containing modified carbonyl iron particles and poly(styrene-*b*-ethylene-ethylenepropylene-*b*-styrene) matrix. *Smart Materials and Structures*, 21(11):115028. doi: 10.1088/0964-1726/21/11/115028.
- Raa Khimi, S. and Pickering, K. 2016. The effect of silane coupling agent on the dynamic mechanical properties of iron sand/ natural rubber magnetorheological elastomers. *Composites Part B: Engineering*, 90:115–125. doi: 10.1016/j.compositesb.2015.11.042.
- Rabinow, J. 1948. The Magnetic Fluid Clutch. *Transactions of the American Institute of Electrical Engineers*, 67(2):1308–1315. doi: 10.1109/T-AIEE.1948.5059821.

- Ray, S., Shanmugaraj, a. M., and Bhowmick, a. K. 2002. A new parameter for interpretation of polymer-filler and filler-filler interactions in rubber vulcanizates. *Journal of Materials Science Letters*, 21(14):1097–1100. doi: 10.1023/A:1016506532606.
- Robertson, C. G., Lin, C. J., Rackaitis, M., and Roland, C. M. 2008. Influence of Particle Size and Polymer–Filler Coupling on Viscoelastic Glass Transition of Particle-Reinforced Polymers. *Macromolecules*, 41(7):2727–2731. doi: 10.1021/ma7022364.
- Schubert, G. and Harrison, P. 2015. Large-strain behaviour of Magneto-Rheological Elastomers tested under uniaxial compression and tension, and pure shear deformations. *Polymer Testing*, 42:122–134. doi: 10.1016/j.polymertesting.2015.01.008.
- Schubert, G. and Harrison, P. 2016. Magnetic induction measurements and identification of the permeability of Magneto-Rheological Elastomers using finite element simulations. *Journal of Magnetism and Magnetic Materials*, 404:205–214. doi: 10.1016/j.jmmm.2015.12.003.
- Shen, Y., Golnaraghi, M. F., and Heppler, G. R. 2004. Experimental Research and Modeling of Magnetorheological Elastomers. *Journal of Intelligent Material Systems and Structures*, 15(1):27–35. doi: 10.1177/1045389X04039264.
- Shuib, R. K., Pickering, K. L., and Mace, B. R. 2015. Dynamic properties of magnetorheological elastomers based on iron sand and natural rubber. *Journal of Applied Polymer Science*, 132(8):n/a–n/a. doi: 10.1002/app.41506.
- Starkova, O. and Aniskevich, A. 2007. Limits of linear viscoelastic behavior of polymers. *Mechanics of Time-Dependent Materials*, 11(2):111–126. doi: 10.1007/s11043-007-9036-3.
- Stepanov, G., Abramchuk, S., Grishin, D., Nikitin, L., Kramarenko, E., and Khokhlov, A. 2007. Effect of a homogeneous magnetic field on the viscoelastic behavior of magnetic elastomers. *Polymer*, 48(2):488–495. doi: 10.1016/j.polymer.2006.11.044.

- Sun, S., Yang, J., Deng, H., Du, H., Li, W., Alici, G., and Nakano, M. 2015. Horizontal vibration reduction of a seat suspension using negative changing stiffness magnetorheological elastomer isolators. *International Journal of Vehicle Design*, 68(1/2/3):104. doi: 10.1504/IJVD.2015.071076.
- Sun, T., Gong, X., Jiang, W., Li, J., Xu, Z., and Li, W. 2008. Study on the damping properties of magnetorheological elastomers based on cis-polybutadiene rubber. *Polymer Testing*, 27(4):520–526. doi: 10.1016/j.polymertesting.2008.02.008.
- Tian, T. F., Zhang, X. Z., Li, W. H., Alici, G., and Ding, J. 2013a. Study of PDMS based magnetorheological elastomers. *Journal of Physics: Conference Series*, 412: 012038. doi: 10.1088/1742-6596/412/1/012038.
- Tian, Y., Liu, Y., He, M., Zhao, G., and Sun, Y. 2013b. High damping properties of magnetic particles doped rubber composites at wide frequency. *Materials Research Bulletin*, 48(5):2002–2005. doi: 10.1016/j.materresbull.2013.01.035.
- Tu, J. W., Yu, Y., Huang, L., Tu, B., and Xu, J. Y. 2014. Research on new type viscoelastic damper based on MRE smart material: design, experiment and modelling. *Materials Research Innovations*, 18(sup2):S2–243–S2–249. doi: 10.1179/1432891714Z.000000000455.
- Ubaidillah, Choi, H. J., Mazlan, S. A., Imaduddin, F., and Harjana. 2016a. Fabrication and viscoelastic characteristics of waste tire rubber based magnetorheological elastomer. *Smart Materials and Structures*, 25(11):115026. doi: 10.1088/0964-1726/25/11/115026.
- Ubaidillah, Imaduddin, F., Li, Y., Mazlan, S. A., Sutrisno, J., Koga, T., Yahya, I., and Choi, S.-B. 2016b. A new class of magnetorheological elastomers based on waste tire rubber and the characterization of their properties. *Smart Materials and Structures*, 25(11):115002. doi: 10.1088/0964-1726/25/11/115002.
- Varga, Z., Filipcsei, G., and Zrínyi, M. 2006. Magnetic field sensitive functional elastomers with tuneable elastic modulus. *Polymer*, 47(1):227–233. doi: 10.1016/j.polymer.2005.10.139.

- Vatandoost, H., Norouzi, M., Alehashem, S. M. S., and Smoukov, S. K. 2017. A novel phenomenological model for dynamic behavior of magnetorheological elastomers in tension–compression mode. *Smart Materials and Structures*, 26(6):065011. doi: 10.1088/1361-665X/aa6126.
- Wang, X., Ge, H. Y., and Liu, H. S. 2011. Study on Epoxy Based Magnetorheological Elastomers. *Advanced Materials Research*, 306-307:852–856. doi: 10.4028/www.scientific.net/AMR.306-307.852.
- Wang, Y., Zhang, X., Oh, J., and Chung, K. 2015. Fabrication and properties of magnetorheological elastomers based on CR/ENR self-crosslinking blends. *Smart Materials and Structures*, 24(9):095006. doi: 10.1088/0964-1726/24/9/095006.
- Wereley, N. M., Chaudhuri, A., Yoo, J. H., John, S., Kotha, S., Suggs, A., Radhakrishnan, R., Love, B. J., and Sudarshan, T. S. 2006. Bidisperse Magnetorheological Fluids using Fe Particles at Nanometer and Micron Scale. *Journal of Intelligent Material Systems and Structures*, 17(5):393–401. doi: 10.1177/1045389X06056953.
- Williams, M. L., Landel, R. F., and Ferry, J. D. 1955. The Temperature Dependence of Relaxation Mechanisms in Amorphous Polymers and Other Glass-forming Liquids. *Journal of the American Chemical Society*, 77(14):3701–3707. doi: 10.1021/ja01619a008.
- Wollscheid, D. and Lion, A. 2014. The benefit of fractional derivatives in modelling the dynamics of filler-reinforced rubber under large strains: a comparison with the Maxwell-element approach. *Computational Mechanics*, 53(5):1015–1031. doi: 10.1007/s00466-013-0946-4.
- Wu, J., Gong, X., Chen, L., Xia, H., and Hu, Z. 2009. Preparation and characterization of isotropic polyurethane magnetorheological elastomer through in situ polymerization. *Journal of Applied Polymer Science*, 114(2):901–910. doi: 10.1002/app.30563.

- Xu, Z. D., Liao, Y. X., Ge, T., and Xu, C. 2016. Experimental and Theoretical Study of Viscoelastic Dampers with Different Matrix Rubbers. *Journal of Engineering Mechanics*, 142(8):04016051. doi: 10.1061/(ASCE)EM.1943-7889.0001101.
- Yang, C., Fu, J., Yu, M., Zheng, X., and Ju, B. 2015. A new magnetorheological elastomer isolator in shear-compression mixed mode. *Journal of Intelligent Material Systems and Structures*, 26(10):1290–1300. doi: 10.1177/1045389X14541492.
- Yang, P., Yu, M., Fu, J., and Luo, H. 2017. Rheological properties of dimorphic magnetorheological gels mixed dendritic carbonyl iron powder. *Journal of Intelligent Material Systems and Structures*, page 1045389X1769205. doi: 10.1177/1045389X17692050.
- Yu, W. X. and Yang, S. C. 2012. Study on Dynamic Properties of Semi-Active Seism Isolator for Building. *Advanced Materials Research*, 598:299–302. doi: 10.4028/www.scientific.net/AMR.598.299.
- Yunus, N. A., Mazlan, S. A., Ubaidillah, Choi, S.-b., Imaduddin, F., Abdul Aziz, S. A., and Ahmad Khairi, M. H. 2016. Rheological properties of isotropic magnetorheological elastomers featuring an epoxidized natural rubber. *Smart Materials and Structures*, 25(10):107001. doi: 10.1088/0964-1726/25/10/107001.
- Zener, C. 1948. *Elasticity and anelasticity of metals*. Chicago University Press, Chicago.
- Zhu, G., Xiong, Y., Daley, S., and Sheno, R. 2015. Magnetorheological elastomer materials and structures with vibration energy control for marine application. In *Analysis and Design of Marine Structures V*, pages 197–204. CRC Press. doi: 10.1201/b18179-27.
- Zhu, J.-t., Xu, Z.-d., and Guo, Y.-q. 2013. Experimental and Modeling Study on Magnetorheological Elastomers with Different Matrices. *Journal of Materials in Civil Engineering*, 25(11):1762–1771. doi: 10.1061/(ASCE)MT.1943-5533.0000727.